NCHRP
REPORT 543

NATIONAL COOPERATIVE HIGHWAY RESEARCH PROGRAM

Effective Slab Width for Composite Steel Bridge Members

TRANSPORTATION RESEARCH BOARD
OF THE NATIONAL ACADEMIES

NATIONAL COOPERATIVE HIGHWAY RESEARCH PROGRAM

NCHRP REPORT 543

Effective Slab Width for Composite Steel Bridge Members

S.S. Chen, A.J. Aref, I.–S. Ahn, M. Chiewanichakorn
J.A. Carpenter, A. Nottis, and I. Kalpakidis
Department of Civil, Structural and Environmental Engineering
State University of New York at Buffalo
Buffalo, NY

Subject Areas
Bridges, Other Structures, and Hydraulics and Hydrology

Research Sponsored by the American Association of State Highway and Transportation Officials
in Cooperation with the Federal Highway Administration

TRANSPORTATION RESEARCH BOARD

WASHINGTON, D.C.
2005
www.TRB.org

NATIONAL COOPERATIVE HIGHWAY RESEARCH PROGRAM

Systematic, well-designed research provides the most effective approach to the solution of many problems facing highway administrators and engineers. Often, highway problems are of local interest and can best be studied by highway departments individually or in cooperation with their state universities and others. However, the accelerating growth of highway transportation develops increasingly complex problems of wide interest to highway authorities. These problems are best studied through a coordinated program of cooperative research.

In recognition of these needs, the highway administrators of the American Association of State Highway and Transportation Officials initiated in 1962 an objective national highway research program employing modern scientific techniques. This program is supported on a continuing basis by funds from participating member states of the Association and it receives the full cooperation and support of the Federal Highway Administration, United States Department of Transportation.

The Transportation Research Board of the National Academies was requested by the Association to administer the research program because of the Board's recognized objectivity and understanding of modern research practices. The Board is uniquely suited for this purpose as it maintains an extensive committee structure from which authorities on any highway transportation subject may be drawn; it possesses avenues of communications and cooperation with federal, state and local governmental agencies, universities, and industry; its relationship to the National Research Council is an insurance of objectivity; it maintains a full-time research correlation staff of specialists in highway transportation matters to bring the findings of research directly to those who are in a position to use them.

The program is developed on the basis of research needs identified by chief administrators of the highway and transportation departments and by committees of AASHTO. Each year, specific areas of research needs to be included in the program are proposed to the National Research Council and the Board by the American Association of State Highway and Transportation Officials. Research projects to fulfill these needs are defined by the Board, and qualified research agencies are selected from those that have submitted proposals. Administration and surveillance of research contracts are the responsibilities of the National Research Council and the Transportation Research Board.

The needs for highway research are many, and the National Cooperative Highway Research Program can make significant contributions to the solution of highway transportation problems of mutual concern to many responsible groups. The program, however, is intended to complement rather than to substitute for or duplicate other highway research programs.

Note: The Transportation Research Board of the National Academies, the National Research Council, the Federal Highway Administration, the American Association of State Highway and Transportation Officials, and the individual states participating in the National Cooperative Highway Research Program do not endorse products or manufacturers. Trade or manufacturers' names appear herein solely because they are considered essential to the object of this report.

NCHRP REPORT 543

Project 12-58

ISSN 0077-5614

ISBN 0-309-08834-8

Library of Congress Control Number 2005906168

Price $37.00

NOTICE

The project that is the subject of this report was a part of the National Cooperative Highway Research Program conducted by the Transportation Research Board with the approval of the Governing Board of the National Research Council. Such approval reflects the Governing Board's judgment that the program concerned is of national importance and appropriate with respect to both the purposes and resources of the National Research Council.

The members of the technical committee selected to monitor this project and to review this report were chosen for recognized scholarly competence and with due consideration for the balance of disciplines appropriate to the project. The opinions and conclusions expressed or implied are those of the research agency that performed the research, and, while they have been accepted as appropriate by the technical committee, they are not necessarily those of the Transportation Research Board, the National Research Council, the American Association of State Highway and Transportation Officials, or the Federal Highway Administration, U.S. Department of Transportation.

Each report is reviewed and accepted for publication by the technical committee according to procedures established and monitored by the Transportation Research Board Executive Committee and the Governing Board of the National Research Council.

Published reports of the

NATIONAL COOPERATIVE HIGHWAY RESEARCH PROGRAM

are available from:

Transportation Research Board
Business Office
500 Fifth Street, NW
Washington, DC 20001

and can be ordered through the Internet at:

http://www.national-academies.org/trb/bookstore

Printed in the United States of America

THE NATIONAL ACADEMIES

Advisers to the Nation on Science, Engineering, and Medicine

The **National Academy of Sciences** is a private, nonprofit, self-perpetuating society of distinguished scholars engaged in scientific and engineering research, dedicated to the furtherance of science and technology and to their use for the general welfare. On the authority of the charter granted to it by the Congress in 1863, the Academy has a mandate that requires it to advise the federal government on scientific and technical matters. Dr. Ralph J. Cicerone is president of the National Academy of Sciences.

The **National Academy of Engineering** was established in 1964, under the charter of the National Academy of Sciences, as a parallel organization of outstanding engineers. It is autonomous in its administration and in the selection of its members, sharing with the National Academy of Sciences the responsibility for advising the federal government. The National Academy of Engineering also sponsors engineering programs aimed at meeting national needs, encourages education and research, and recognizes the superior achievements of engineers. Dr. William A. Wulf is president of the National Academy of Engineering.

The **Institute of Medicine** was established in 1970 by the National Academy of Sciences to secure the services of eminent members of appropriate professions in the examination of policy matters pertaining to the health of the public. The Institute acts under the responsibility given to the National Academy of Sciences by its congressional charter to be an adviser to the federal government and, on its own initiative, to identify issues of medical care, research, and education. Dr. Harvey V. Fineberg is president of the Institute of Medicine.

The **National Research Council** was organized by the National Academy of Sciences in 1916 to associate the broad community of science and technology with the Academy's purposes of furthering knowledge and advising the federal government. Functioning in accordance with general policies determined by the Academy, the Council has become the principal operating agency of both the National Academy of Sciences and the National Academy of Engineering in providing services to the government, the public, and the scientific and engineering communities. The Council is administered jointly by both the Academies and the Institute of Medicine. Dr. Ralph J. Cicerone and Dr. William A. Wulf are chair and vice chair, respectively, of the National Research Council.

The **Transportation Research Board** is a division of the National Research Council, which serves the National Academy of Sciences and the National Academy of Engineering. The Board's mission is to promote innovation and progress in transportation through research. In an objective and interdisciplinary setting, the Board facilitates the sharing of information on transportation practice and policy by researchers and practitioners; stimulates research and offers research management services that promote technical excellence; provides expert advice on transportation policy and programs; and disseminates research results broadly and encourages their implementation. The Board's varied activities annually engage more than 5,000 engineers, scientists, and other transportation researchers and practitioners from the public and private sectors and academia, all of whom contribute their expertise in the public interest. The program is supported by state transportation departments, federal agencies including the component administrations of the U.S. Department of Transportation, and other organizations and individuals interested in the development of transportation. **www.TRB.org**

www.national-academies.org

COOPERATIVE RESEARCH PROGRAMS STAFF FOR NCHRP REPORT 543

ROBERT J. REILLY, *Director, Cooperative Research Programs*
CRAWFORD F. JENCKS, *Manager, NCHRP*
DAVID B. BEAL, *Senior Program Officer*
EILEEN P. DELANEY, *Director of Publications*
HILARY FREER, *Editor*
ANDREA BRIERE, *Editor*

NCHRP PROJECT 12-58 PANEL
Field of Design—Area of Bridges

EDWARD P. WASSERMAN, *Tennessee DOT* (Chair)
SCOT BECKER, *Wisconsin DOT*
NATHAN S. BROWN, *Washington State DOT*
THOMAS DOMAGALSKI, *Illinois DOT*
LIAN DUAN, *California DOT*
DACIO MARIN, III, *Texas DOT*
JOHN O'FALLON, *FHWA Liaison*
STEPHEN F. MAHER, *TRB Liaison*

AUTHOR ACKNOWLEDGMENTS

The research reported herein was performed under NCHRP Project 12-58 by the Department of Civil, Structural and Environmental Engineering at the University at Buffalo (UB), State University of New York (SUNY). UB was the contractor for this study, with the Research Foundation of SUNY serving as Fiscal Administrator.

Dr. Stuart S. Chen, P.E., Associate Professor of Civil Engineering at UB, was the Project Director and co-Principal Investigator. The other authors of this report are Dr. Amjad J. Aref, Associate Professor of Civil Engineering at UB and co-Principal Investigator; Il–Sang Ahn, Research Assistant and Ph.D. Candidate at UB; Methee Chiewanichakorn, Research Assistant and Ph.D. Candidate at UB; and Aaron Nottis, Jeffrey Carpenter, and Ioannis Kalpakidis, Research Assistants and M.S. Candidates at UB. The work was done under the general supervision of Professors Chen and Aref at UB.

Others assisting in contributing or pointing to material used in this report, all of whose assistance is gratefully acknowledged, include the following:

- Various state bridge engineers and TRB representatives who responded to a survey seeking information relevant to the present study;
- Mr. Arun Shirole of Arora and Associates, Mr. Ayaz Malik of the New York State Department of Transportation, and Mr. Peter Stapf of the New York State Thruway Authority, who served as members of the Industry Advisory Panel;
- Dr. Y. Kitane, a former Ph.D. Candidate at UB, and Dr. S. Unjoh of the Public Works Research Institute of Japan, who provided an English translation of the effective width criteria found in the Japanese code and information about girder spacing practices in Japan, respectively;
- Mr. G. Booth, Dr. J-P. Lebet, and Mr. Joel Raoul, who provided information about British, Swiss/Eurocode, and French effective width practices, respectively;
- Dr. H. Gil of the Korea Highway Corporation, who provided information about recent effective width studies on a cable-stayed bridge in Korea;
- Dr. R.Q. Bridge of University of Western Sydney, who provided information about Australian effective width practices;
- Mr. I. Savage of Parsons Transportation Group, who provided information about a recent effective width study on a major box girder crossing;
- Dr. David Byers of HNTB and Mr. Michael Abrahams of Parsons Brinckerhoff and Palmetto Bridge Constructors for providing access to material and geometric property data used in modeling and analysis of selected cable-stayed bridges for effective width;
- Technical staff (Scot Weinreber, Duane Kozlowski, Mark Pitman, Chris Budd) in the SEESL (Structural Engineering and Earthquake Simulation Laboratory), of which A. Reinhorn and M. Constantinou are Co-Directors in the Department of Civil, Structural and Environmental Engineering at UB; and
- Technical assistance in the laboratory provided by Guarav Shringarpure, William Lane, and Chad Liddell.

FOREWORD

By David B. Beal
Staff Officer
Transportation Research Board

This report contains the findings of research performed to develop expressions for the effective slab width of composite steel bridge members. Recommended specifications and commentary and examples illustrating the application of the specifications were also developed. The material in this report will be of immediate interest to bridge designers.

The determination of the section properties of composite steel bridge members is influenced by the effective slab width assumed in their calculation. These section properties include the stiffness, which is used to determine the distribution of forces in the structure, and the section modulus, which is used to determine the stresses induced in the member by these forces. As such, the determination of effective slab width directly affects the computed moments, shears, torques, and deflections for the composite section and also affects the proportions of the steel section and the number of shear connectors required. The effective slab width is particularly important for serviceability checks, which often can govern the design.

In AASHTO bridge design specifications, the slab width effective for composite action for all types of bridge superstructures, except for segmental concrete structures, is specified as the least of (1) 12 times the least thickness of the deck plus one-half the top flange width, (2) one-fourth the span length of the girder, or (3) the girder spacing. For girder spacings 8 feet or less, the effective width computed according to this provision generally includes all of the deck. With the ever-increasing use of wider girder spacing, the contribution of the additional width of deck is not fully recognized. The *AASHTO Guide Specifications for Segmental Concrete Bridges* recognize the entire deck width to be effective unless shear lag adjustments become necessary. Field measurements of modern composite steel bridges indicate that recognition of more of the concrete deck often is necessary to better correlate actual with calculated deflections.

The objective of this research was to develop recommended revisions to the AASHTO specifications for the effective slab width of composite steel bridge members. The recommended specifications are applicable to all types of composite steel bridge superstructures and are suitable for design office use. This research was performed by the State University of New York at Buffalo. The report fully documents the research leading to the recommendations to increase the effective slab width estimates for composite steel bridge members. Accompanying *CRP-CD-56* contains extensive supporting information, including the recommended specifications and design examples. AASHTO is expected to consider these recommendations for adoption in 2006.

CONTENTS

EFFECTIVE SLAB WIDTH FOR COMPOSITE STEEL BRIDGE MEMBERS

SUMMARY

The objectives of this work were to (1) propose criteria for effective width and recommended specifications and commentary for effective width and (2) provide worked examples illustrating the use of those proposed new criteria. The principal focus was common slab-on-girder configurations.

A new definition for effective width that accounts for the variation of bending stresses through the deck thickness has been needed. A finite element modeling approach was developed, corroborated with experimental data by others and by the authors, and applied to a suite of bridges designed according to industry guidelines. Effective widths according to the new definition were extracted from this finite element parametric study of the suite of bridges. Principal findings from the parametric study were as follows: (1) full width was typically acting "at cross sections where it is most needed," i.e., where moments and hence performance ratios would be highest, and (2) where the effective width was less than full width at such cross sections, that cross section had considerable excess flexural capacity.

Draft criteria for effective width were developed by applying regression approaches in order to account for different subsets of the parameters varied in the extensive parametric study of bridge finite element models. The effects of those criteria were assessed using the Rating Factor (RF) as the measure of impact. Based on the impact assessment, draft criteria based on using the full physical slab width were recommended and illustrated in the context of positive and negative moment region worked examples.

CHAPTER 1

INTRODUCTION AND RESEARCH APPROACH

1.1 PROBLEM STATEMENT AND PROJECT OBJECTIVES

The phenomenon of shear lag is shown in Figure 1a. Shear lag can result in underestimating the deflections and stresses at the web-flange intersections of a girder in calculations based on line-girder analysis and the elementary theory of bending, which assumes that plane cross sections remain plane. It is traditional to obtain correct values of maximum deflection or stress from the elementary theory by using an effective slab width concept in which the actual width of each flange is replaced by an appropriate reduced ("effective") width (Moffatt and Dowling, 1978; ASCE, 1979; Garcia and Daniels, 1971), labeled b_{eff} in Figure 1b. The determination of effective slab width directly affects the computed moments, shears, torques, and deflections for the composite section and also affects the proportions of the steel section and the number of shear connectors required. The effective slab width is thought to be particularly important for serviceability checks (e.g., fatigue, overload, and deflection), which can often govern the design.

Figure 2 summarizes the various influences that the effective width b_{eff} has in the design and rating of a composite beam. Both sides of the basic LRFD methodology, $\Sigma\eta_i\gamma_i Q_i \leq \phi R_n$, are influenced by the effective width for all limit states involving flexure of a slab-on-girder composite beam. Thus it is not possible by inspection to determine the net effect of any proposed change to effective width for a given bridge, let alone for a suite of bridges. A systematic parametric study is necessary. Just such a study is at the heart of the research results presented herein.

In AASHTO bridge design specifications (AASHTO, 2004), the effective slab width for interior girders of all types of composite bridge superstructures, except for orthotropic deck and segmental concrete structures, is specified as the least of the following: (1) one-quarter of the effective span length, (2) 12.0 times the average depth of the slab plus the greater of web thickness or one-half the top flange width, and (3) the average spacing of adjacent beams. These criteria currently apply to all types of composite interior and exterior steel bridge members with any combination of the following:

- Conventional or High-Performance Steel Girder System:
  - Tub-girder
  - Two-girder system
  - Conventional multi-girder system
- Deck System:
  - Conventional Cast-in-Place
    - Conventional concrete (e.g., $f'_c = 21$ MPa or 28 MPa)
    - High-Performance Concrete (HPC)
  - Prestressed, either constant depth or variable depth, and often prestressed longitudinally as well as transversely, on potentially very wide girder spacings
- Alignment:
  - Right
  - Skew
- Span Location:
  - Positive Moment Region
  - Negative Moment Regions considered composite where sufficient shear studs and longitudinal reinforcing steel are supplied
- Applicable Limit State, e.g.,
  - Service II and Fatigue (elastic), and
  - Strength I and perhaps Strength II (possibly inelastic).

For girder spacings 2.4 m (8 ft) or less, the effective width computed according to the current AASHTO provisions generally includes all of the deck. With the increasing use of wider girder spacing, however, the contribution of the additional width of deck is not fully recognized by the current criteria. The *AASHTO Guide Specifications for Segmental Concrete Bridges* recognize the entire deck width to be effective, unless shear lag adjustments become necessary. Field measurements of modern composite steel bridges indicate that recognition of more of the concrete deck is often necessary to better correlate actual with calculated deflections.

The above criteria apply to all types of composite interior and exterior steel bridge members. In addition to their common use on multi-girder bridges, composite deck systems can participate structurally with tied arches or cable-stayed bridges. Thus, the effective width of the slab may well differ among some of these cases from more conventional multi-stringer I-girder bridges. The effective width of decks using high-strength concrete may also be affected by the larger elastic and shear moduli of the concrete. Distinctions for the effective width of slab to be used may be needed

- In positive and negative bending,
- At the AASHTO serviceability and strength limit states,

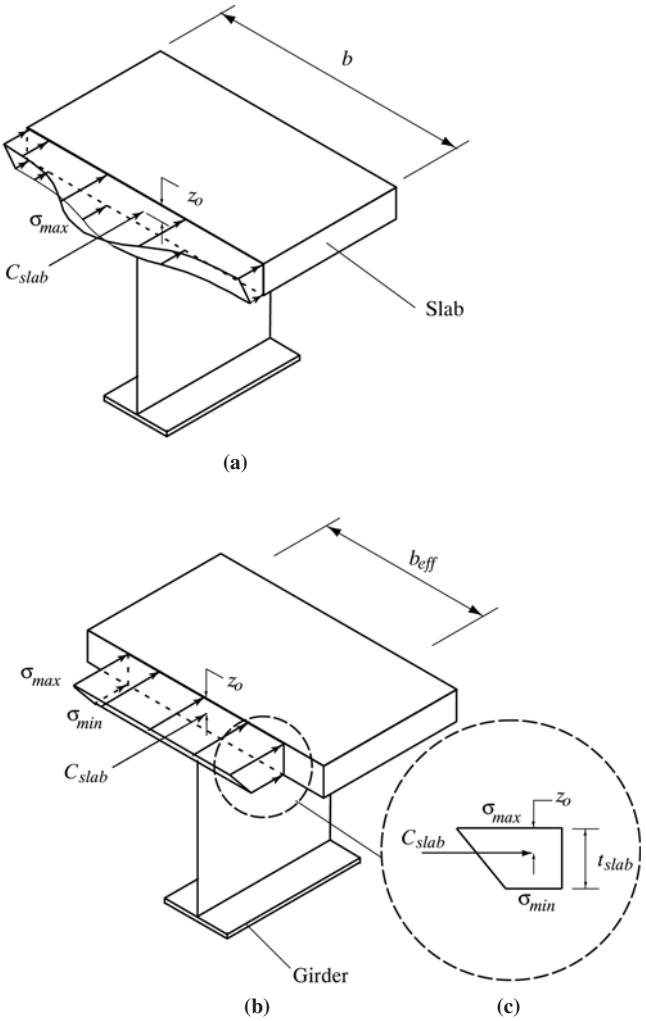

Figure 1. Effective width for the positive moment section.

- Considering both conventionally reinforced and prestressed decks.

In accordance with the NCHRP 12-58 Project Statement, the objectives of the research undertaken were to investigate both new and existing approaches for effective slab width and to develop and validate the most promising of these. The research products consist of criteria, recommended specifications and commentary, and worked examples addressing applicable AASHTO LRFD limit states in AASHTO LRFD format.

1.2 RESEARCH TASKS

The set of research tasks in the original solicitation for the NCHRP Project 12-58 investigation was augmented to incorporate the following:

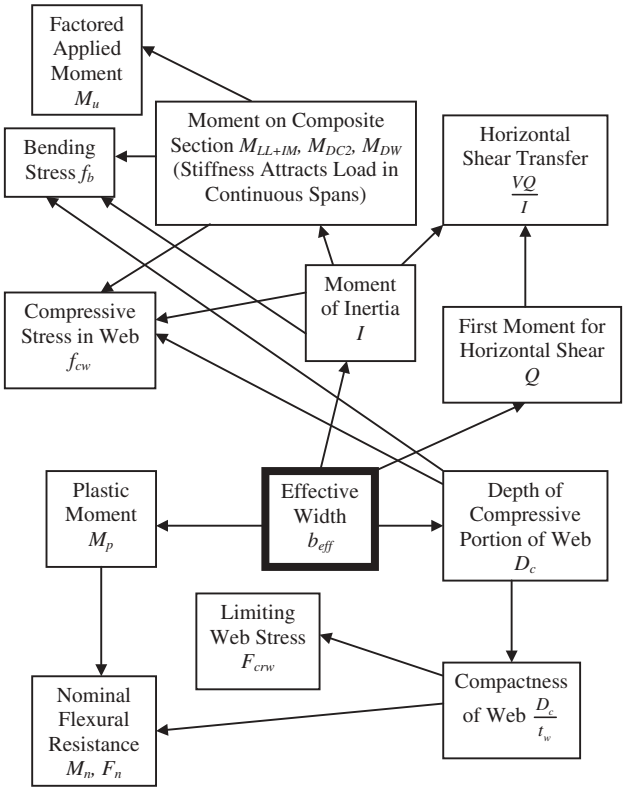

Figure 2. Design parameters influenced by effective width.

- Conduct experimental investigations of scale-model slab-on-girder bridge structures to complement the finite element-based parametric study,
- Conduct several analysis cases of cable-stayed bridges,
- Explore impacts of proposed changes to effective width code provisions ("Process 12-50"),
- Analyze additional cases required by the DOE (Design of Experiments) approach that were not contained in the original scope of work,
- Analyze a few prestressed concrete girder cases to investigate whether changes proposed for effective slab width in composite steel bridge members could reasonably be applied to bridges supported by prestressed concrete girders, and
- Revise the MathCad worksheets developed for use in presenting illustrative design examples to reflect the substantive changes to S6.10 and S6.11 in the 3rd Edition AASHTO LRFD code, published in 2004.

The resulting amended task descriptions were as follows:

Task 1. Review domestic and foreign field and laboratory test results, analytical studies, and specifications regarding the effective slab widths for all types of steel and concrete composite structures.

Task 2. Using the findings from Task 1, summarize applicable methodologies for determining the effective slab width

for different types of composite steel bridge superstructures typical of those in use today. As a minimum, I-girder and tub-girder cross-sections should be considered. Both interior and exterior girders should be considered. Composite floor systems that participate structurally with tied arches, cable-stayed bridges, and deck or through trusses should also be considered, along with variable- or constant-depth composite, precast post-tensioned decks. Consider the effects of the larger elastic and shear moduli of high-strength deck concrete on the computed effective width.

Task 3. Prepare an interim report documenting the findings from Tasks 1 and 2. Provide practical recommendations for promising methodologies to determine effective slab width that can be further developed and validated. Prepare an expanded work plan for the remainder of the project describing the type of investigations needed to develop and validate the recommended methodologies.

Task 4. Develop and validate the methodologies for determining effective slab width using finite element analysis.

Task 5. Verify the finite element analysis through a program of laboratory testing of reduced scale structures as approved by the project panel.

Task 6. Perform parametric studies of different composite steel-bridge superstructure configurations using the current provisions of the *AASHTO LRFD Bridge Design Specifications* and the proposed effective-width criteria. At least 100 cases shall be considered. In addition, a limited set of concrete girders should be investigated to determine the applicability of the criteria and several cable-stayed bridges designed by others shall be investigated for axial and flexural effective width.

Task 7. Propose recommended revisions to the specifications and provide design examples demonstrating their use. For each case considered, develop suggested general guidelines for designing the slab reinforcement and shear connectors to transfer the calculated shear forces effectively between the girder and slab at each limit state. The design examples shall conform to the provisions of the 2004 AASHTO LRFD Specifications.

Task 8. Perform impact testing to compare rating factors resulting from the recommended revisions with those of the LRFD Specifications. The method for impact testing developed in NCHRP Project 12-50 is recommended.

Task 9. Submit a final report documenting the entire research effort. The recommended specifications shall be provided in an appendix to the report and must be in a format suitable for consideration by the AASHTO Highway Subcommittee on Bridges and Structures.

1.3 RESEARCH APPROACH

Key specific aspects of the above research tasks are further described below. Tasks 1 through 3 involved not only an extensive literature review of both analytical and experimental explorations of effective slab width and associated slab-on-girder bridge studies but also a survey of effective slab width criteria and maximum girder spacings used by the various states, documented in Appendix A (provided on the accompanying CD-ROM). In addition, international practice was surveyed and the various effective width provisions compared. The literature review is contained in Appendix B (provided on the accompanying CD-ROM).

Task 4 involved an implementation of finite element modeling techniques at an appropriate level of detail to predict both linear and nonlinear (post-cracking and post-yielding) behavior of composite steel bridge member superstructures. In order to determine what level of detail was appropriate, an extensive review of the shear lag phenomenon and effective width definitions was conducted along with new definitions for effective width b_{eff} developed herein. The details of this review and the new definitions are contained in Appendix C (provided on the accompanying CD-ROM), while the finite element modeling and the verifications thereof are described in detail in Appendix D (provided on the accompanying CD-ROM).

Task 5, laboratory testing, was conducted of a two-span continuous one-quarter-scale slab-on-girder bridge structure and is documented in Appendix E (provided on the accompanying CD-ROM). Testing of two one-half-scale subassemblages of the negative moment region portion of such structures is documented in Appendix F (provided on the accompanying CD-ROM). These experiments were used to help establish the credibility of the finite element modeling approaches developed in Task 4 so that these approaches could be used for parametric studies of various bridge configurations in Task 6.

Task 6 pursued a systematic set of analyses of finite element models representing bridges with various span lengths (15 m to 60 m), girder spacings (2.4 m to 4.8 m), skew angles (0 to 60 deg), and (in the cases of continuous bridges) span length ratios (from 1.0 to 1.5). Both single-span and three-span continuous configurations were the focus of the systematic set. The set was assembled using "design of experiments" (DOE) concepts (Montgomery, 2001). Effective width according to the new definitions developed in Task 4 was extracted from the finite element analysis results considering both interior and exterior girders, service and strength limit states, positive and negative moment regions, and both right and skew alignments. Details of the "design of experiments" background, the finite element modeling, and the suite of bridges analyzed in the parametric study along with the analysis results are presented in Appendix G (provided on the accompanying CD-ROM). The bridges modeled in this parametric investigation needed to be designed first. Industry guidelines were carefully followed in the design of these bridges. These guidelines and the resulting bridge parameters (e.g., girder sizes) are described in further detail in Appendix H (provided on the accompanying CD-ROM).

In addition to the parametric study set of bridges, various bridge configurations that go beyond the parametric limits were investigated. These included some of cable-stayed bridges, described in Appendix I (provided on the accompanying

CD-ROM). Other bridges beyond the parametric limits include a limited number of prestressed-concrete bridges, two-girder bridges with girders spaced as widely as 7.6 m, tub-girder, hybrid, and prestressed-slab bridges. Finite element analysis results for these "validation cases" are documented in Appendix J (provided on the accompanying CD-ROM).

Task 7 involved the development of curve-fit expressions for predicting effective width based on the results of the finite element analyses. Development and comparison of various such curve-fit expressions are documented in Appendix K (provided on the accompanying CD-ROM).

Task 8 addressed evaluating the impact of these candidate b_{eff} expressions as compared with the current AASHTO provisions. The basis for this evaluation of impact was taken to be the Rating Factor, considering both service and strength limit states, and was documented in Appendix L (provided on the accompanying CD-ROM). The culmination of this effort was the draft code and commentary language for proposed new effective width provisions, which were documented along with their underlying rationale in Appendix M (provided in print herein and on the accompanying CD-ROM).

Appendix N (provided on the accompanying CD-ROM) contains information about the finite element modeling of the prestressed girder bridge structures investigated in this study, while Appendix O (provided in print herein and on the accompanying CD-ROM) presents worked design examples illustrating the use of the new proposed provisions for effective slab width.

The scope of the investigation excludes consideration of the following:

- Horizontally curved bridges, for which a system analysis is recommended instead of a line-girder approach for which effective width is traditionally applied;
- Segmental bridges; and
- Tied-arch bridges, with net tension added to flexure on the cross section.

1.4 ORGANIZATION OF THIS REPORT

This report consists of four chapters as well as the aforementioned appendixes (provided on *CRP-CD-56*). This chapter provides the introduction and research approach, describes the research objectives, and outlines the scope of the study. Chapter 2 describes the findings of the survey and literature review, new definitions for effective width, verifications of the FEM (Finite Element Method) modeling approaches employed, highlights of results from the FEM-based parametric study, and insights from the experiments performed. Chapter 3 summarizes the development of candidate design criteria and impact assessment of these criteria using a straightforward application of Process 12-50 to show that the subtle differences among the various possible curve-fit expressions are, for all practical purposes, negligible. This observation leads to a recommendation of simplified design criteria for effective width. Highlights of the worked example illustrating the use of these simplified design criteria are summarized. Chapter 4 then summarizes the conclusions of this study and presents suggestions for future research.

CHAPTER 2

FINDINGS

This chapter is organized as follows. The survey sent to gather information from various bridge-owning jurisdictions is described. Insights from the literature review that are particularly relevant to study of effective width are summarized, including comparison of several codes in use on the international scene. New definitions of effective width developed in this research are summarized, as are verifications of the finite element modeling approach employed. The Finite Element Method (FEM) based parametric study is at the heart of the research conducted herein, and its principal features and results are summarized along with those of "special case" bridges, which are beyond the limits of the parametric study. Key experimental results and their role in corroborating the FEM-based parametric study are provided as well.

2.1 SURVEY AND LITERATURE REVIEW FINDINGS

2.1.1 Survey Results

A survey was distributed in the summer of 2001 to the state bridge engineers and TRB representatives in all 50 states. Replies were received from approximately 40 of these states. The replies are tallied in Appendix A along with a copy of the survey form itself. Replies indicate no leads regarding other studies investigating effective slab width. A few replies indicate a few recently constructed bridges with large girder spacings. Where maximum girder spacing policies are explicitly stated, they are generally conservative, with a 3 to 3.6 m (10 to 12 ft) limit being common. In some cases, the stated reason for this limit is to facilitate eventual deck replacement. Where more liberal limits are stated, those limits are based on, for example, maximum spans of stay-in-place forms (approximately 4.6 m = 15 ft) or maximum girder spacings allowed for the use of empirical deck design (4.1 m = 13.5 ft).

Personal contacts in Europe (Switzerland, France, and the U.K.) and Japan were consulted. European and Japanese limits on girder spacing are more liberal than those in the United States, as described later in this chapter. In Japan, for example, girder spacings are permitted up to 6 m when supporting prestressed decks (although no known field test results on bridges with girder spacings larger than 3 m are available).

The literature review confirmed the need to examine negative moment regions specifically, given the little previous research on the subject. Criteria originally developed for the positive moment region were co-opted for use in the negative moment region without explicit study of the unique aspects of negative moment region behavior as regards effective width. This is a key reason for the negative moment region subassemblage experiments described later in this chapter and in Appendix F.

2.1.2 Comparisons of International Code Provisions for Effective Width

Other findings of interest from the literature review concerned the various codes and specifications for effective width in use internationally (Ahn et al., 2004). Figure 3 shows a comparison of various international codes in graph form, while Table 1 provides a complementary view of the similarities and differences of these codes. Most have a limitation on effective width based on span length. Given that a span length parameter is present, the notion of "effective span length" was invented to enable such criteria originally developed for positive moment regions to be co-opted for application in negative moment regions. This redefinition of span length is one example of issues that have arisen in applying positive moment criteria to a region where those criteria were not originally even intended to apply. Figure 4 shows how several international codes define the notion of "effective span length."

The historical review presented in Appendix B and Appendix C indicates that the 12t limitation in the AASHTO effective width formulation (AASHTO LRFD S4.6.2.6, AASHTO Standard Specs 10.38.3.1) has been in AASHTO (then AASHO) since the 1940s, the early days of composite beams. Even that formulation is based on empirical research published in the World War I era—long predating composite beams. That research was for reinforced concrete T-beams, not steel beams with composite concrete decks. Also in those days, highway vehicle loads were small, bridge decks were not mandated to be a minimum of 175 mm (7 in.) thick, and bridge floor systems had closely spaced longitudinal stringers. Design and construction practices obviously have changed significantly since then. For example, almost all international

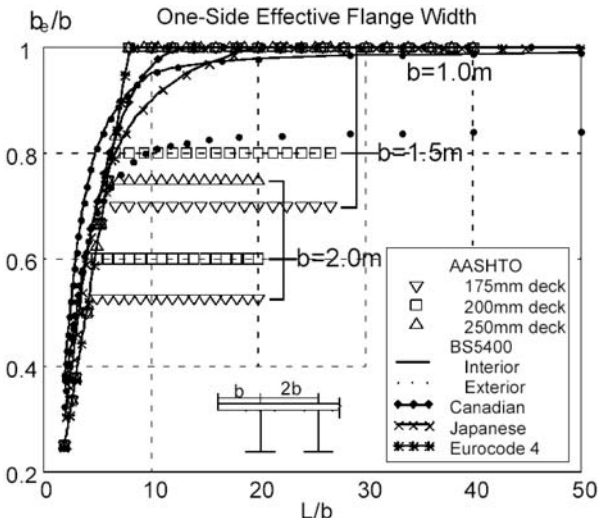

Figure 3. Effective flange width of simply-supported span.

building and bridge codes for steel-concrete composite beam members in the last few decades have departed from any kind of thickness limitation in their effective slab width formulations. These various considerations taken together suggest that the 12t limitation in the current AASHTO provisions for effective width can be liberalized.

The research team is not advocating a blind copycat approach. The background for the various international code provisions typically consists primarily of parametric analytical work that most recently is finite element based. Little companion experimental work is cited by these codes to accompany the analytical background. The limited test data points to the desirability of experimental verification of analytical results.

Table 1 highlights the various parameters that have some influence on effective width. In general, there is a tradeoff between accuracy and simplicity. For example, the value of effective width depends on whether the applied loading is distributed or concentrated—but only the British and Japanese codes recognize this distinction. Another example is whether distinct values of effective width are to be used depending on whether service or ultimate loading is applied—here only the British code and Eurocode recognize the distinction.

The review of design criteria presented above brought to light several distinct philosophies underlying the various effective width code formulations being used internationally, ranging from simple (e.g., Canada, which presumes line-girder analysis) to relatively complex (e.g., the British BS 5400, which does not presume line-girder analysis and which also distinguishes between point loads and distributed loads). As one might expect, there is a tradeoff between simplicity and accuracy—especially when the full spectrum of possibilities must be accommodated even within the context of line-girder analysis (e.g., interior and exterior girders, positive and negative moment regions, linear and nonlinear realms of behavior, box and I-girders, and absence or presence of axial load, the latter being the case for cable-stayed and tied-arch structures).

2.1.3 Other Aspects of the Literature Review

Detailed description of the literature review is provided in Appendix B. Much of the classical literature in this area

TABLE 1 Comparison of provisions

b_e Provisions	AASHTO	BS 5400	Canadian	Japanese	Eurocode 4
Distinguish UDL vs. Point Load	N	Y[a]	N	Y[b]	N
Distinguish Exterior vs. Interior Girder	Y	Y	N	N	N
Expressed as One-Sided	N	Y	Y[c]	Y	Y[c]
Distinguish M(+) region from M(-) region	N	Y	N	Y	N
Distinguish I Girder from Box Girder	Y[d]	N	N	NA	NA
Distinguish Strength (Ultimate) vs. Service	N	Y[e]	N	N	Y[f]
Value Modified at Supports	N	Y	N	N	Y
Value Modified for Concrete Cracking	N	Y	N	N	Y

Y : considered N : not considered NA : not applicable

[a] use UDL (Uniformly Distributed Load) case for highway bridges
[b] use PL case especially for internal supports of continuous girders
[c] effective flange width is divided into central part and side parts
[d] use different provisions for concrete segmental box girder bridges
[e] use effective flange width for service limit state, use full width for ultimate limit state
[f] use effective flange width for service limit state

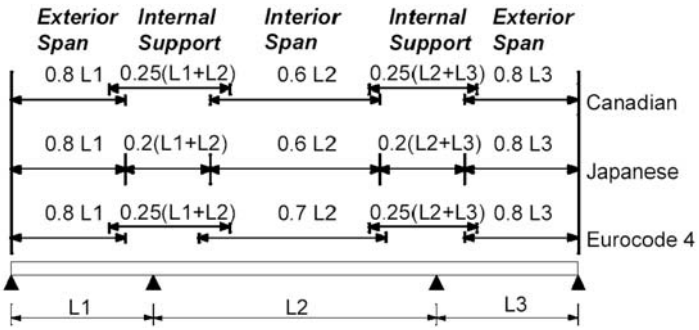

Figure 4. Effective span length ratios.

predates modern computer analysis. Assumptions need to be made in order to make the closed-form analytical problem tractable. With modern day approaches such as the Finite Element Method, however, many of those classical assumptions do not need to be made. Nor do the same classical definitions of effective flange width need to be used.

2.2 NEW DEFINITION FOR EFFECTIVE WIDTH

The review of literature revealed that the classical definition of effective width was more suited to a stiffened plate than to a composite girder-deck system undergoing flexure. In the latter, the deck (plate) is sufficiently thick for stress variation through the thickness to be an important consideration. Thus, a new definition of effective width was developed. The new definition (Chiewanichakorn et al., 2004) enforced two conditions that the traditional definition does not:

- Enforce the same moment in the idealized Bernoulli-Euler line girder as in the 3-D FEM slab-girder system (the classical definition requires only the same force), and
- Enforce moment equilibrium as well as force equilibrium.

This new definition is applied according to the following procedure in a positive moment section.

Step 1: Calculate total compressive force in the slab

Compute the total or resultant compressive force in the slab by summing up all element forces in the slab using Equation 1.

$$C_{slab} = \sum_{i=1}^{n} \sigma_i \cdot Area_i \qquad \text{Equation 1}$$

where

C_{slab} = total or resultant compressive force in the slab
σ = element longitudinal stress
$Area$ = element cross-sectional area
i = element number

Step 2: Define the centroidal location of the total compressive force in the slab

Determine the vertical location of the resultant compressive force using statics. The distance from the top of the slab to this centroidal location is defined as z_o (see Figure 1).

In order to enforce both assumptions, both C_{slab} and z_o must remain unchanged.

Step 3: Determination of maximum longitudinal stress in the slab

Extract the maximum longitudinal stress (σ_{max}) in the slab directly from the finite element analysis results. For instance, the maximum slab longitudinal stress is located at the extreme compression fiber in the elastic response (see Figure 1).

Step 4: Calculate minimum longitudinal stress of the slab

The term "minimum longitudinal stress (σ_{min})" of the slab in Figure 1 can also be described as an equivalent longitudinal stress at the bottom of the slab. Because of a linear variation in the strain profile, simple beam theory assumes a linear variation in the stress profile for the elastic response, that is, a trapezoidal shape.

In order to satisfy the two assumptions, the centroidal location of the resultant compressive force must be the same for both finite element analysis and simple beam theory. With the pre-determined values of σ_{max} and z_o, compute the minimum longitudinal stress (σ_{min}) of the slab such that the conditions of total force and resultant location are similar to those obtained from finite element analysis.

Step 5: Computation of "effective slab width"

After the value of σ_{min} is obtained from Step 4, calculate the equivalent compressive block (area of the trapezoid) and determine the effective slab width using Equation 2:

$$b_{eff} = \frac{C_{slab}}{A} = \frac{C_{slab}}{0.5 \cdot t_{slab} \cdot \left(\sigma_{\max} + \sigma_{\min}\right)} \qquad \text{Equation 2}$$

where

b_{eff} = effective slab width

C_{slab} = total or resultant compressive force of the slab from Equation 1
A = area of an equivalent compressive block for simple beam theory
t_{slab} = total structural slab thickness
σ_{max} = maximum compressive stress at the extreme compression fiber of slab
σ_{min} = minimum compressive stress at the bottom of the slab

Elastic section properties such as second moment of inertia (I_{xx}) and elastic section modulus (S) can be determined using the effective slab width (b_{eff}). The maximum compressive stress at the extreme compression fiber can be calculated by simple beam theory using the total bending moment for the specific section obtained from the finite element analysis as shown in Equation 3:

$$\sigma_{\max,\text{°}BeamTheory} = \frac{M_{FEM}}{S_{top,\text{°}BeamTheory}} \qquad \text{Equation 3}$$

where

$\sigma_{max,\text{°}Beam\ Theory}$ = maximum compressive stress at extreme compression fiber
M_{FEM} = bending moment at the specific section (Condition #1 holds)
$S_{top,\ Beam\ Theory}$ = elastic section modulus for the extreme compression fiber

This procedure can require an iterative process, unless the values of the maximum compressive stress at the extreme compression fiber obtained from the simple beam theory (Equation 3) are comparatively close to the extreme fiber stresses resulting from the finite element analysis.

Initially developed with the positive moment region in mind as shown in Figure 1 and illustrated above, the same principles were applied to the negative moment region as shown in Figure 5. Further details of the derivation and resulting expressions for effective width are provided in Appendix C. The new definitions exploit the expressive power afforded by the use of four layers of three-dimensional (3-D) brick finite elements through the deck thickness and "smeared" modeling of the top and bottom mats of rebar in the deck.

2.3 FINITE ELEMENT MODELING AND VERIFICATION

2.3.1 Finite Element Modeling

A suitable finite element modeling methodology was systematically established for use during the parametric study.

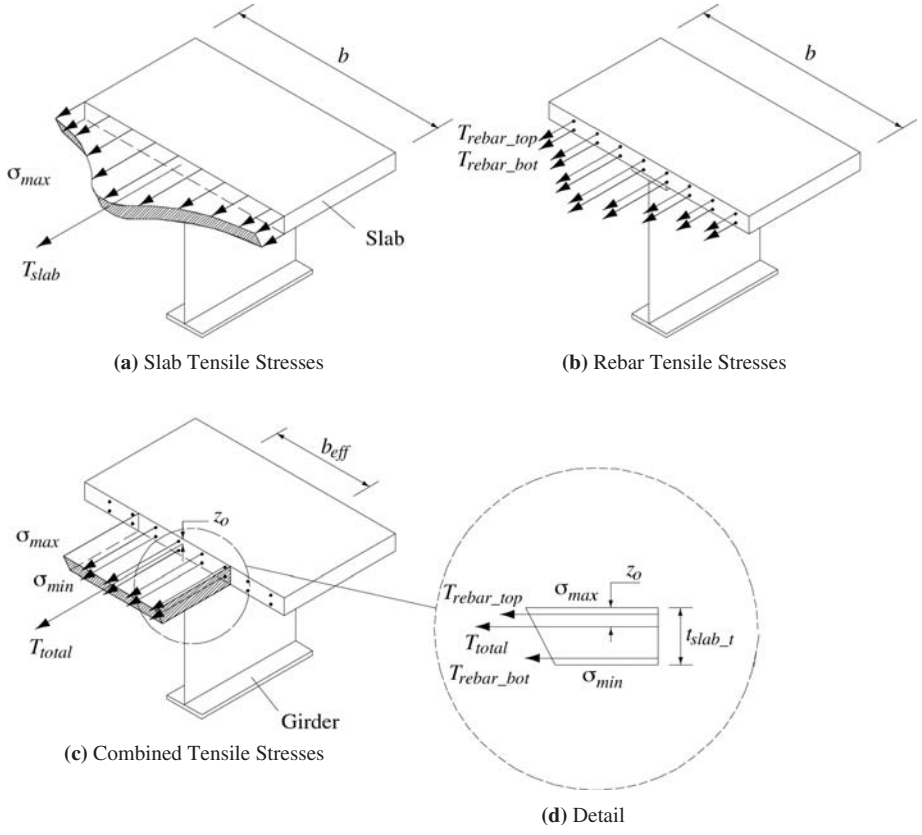

Figure 5. Effective width for the negative moment section.

This methodology is outlined briefly in this section and documented more fully in Appendix D.

2.3.1.1 Structural Element Modeling

Solid (also known as continuum) elements were used in ABAQUS to model both steel girder and concrete slab in this research. The element type used is a 3-D eight-noded element with a reduced integration formulation (element C3D8R). Reduced integration provides accurate results while significantly reducing computation time. Steel reinforcing bars in the deck slab are modeled using the *REBAR function as a smeared property in ABAQUS. The rebars in the 3-D continuum elements are thus defined as layers lying in surfaces with respect to the isoparametrically mapped cube of the 3-D elements. The stiffness of the reinforcement layer is superposed onto the stiffness of the continuum element in which the rebar resides.

The stud shear connector is modeled using a type of connector element called a "Flexible Joint Element" or JOINTC element. The JOINTC elements are composed of translational and rotational springs and parallel dashpots in a local, rotational coordinate system. This type of element was used to model the interaction between two nodes that are (almost) coincident geometrically so that the second node of the joint can displace and rotate slightly with respect to the first node. The JOINTC elements that represent the stud shear connectors consist of three nonlinear springs in each of the translational coordinate directions.

Figure 6 shows the finite element modeling scheme employed.

2.3.1.2 Material Models

Concrete. The concrete model employed in this investigation is based on classical 3-D plasticity (ANATECH, 1997).

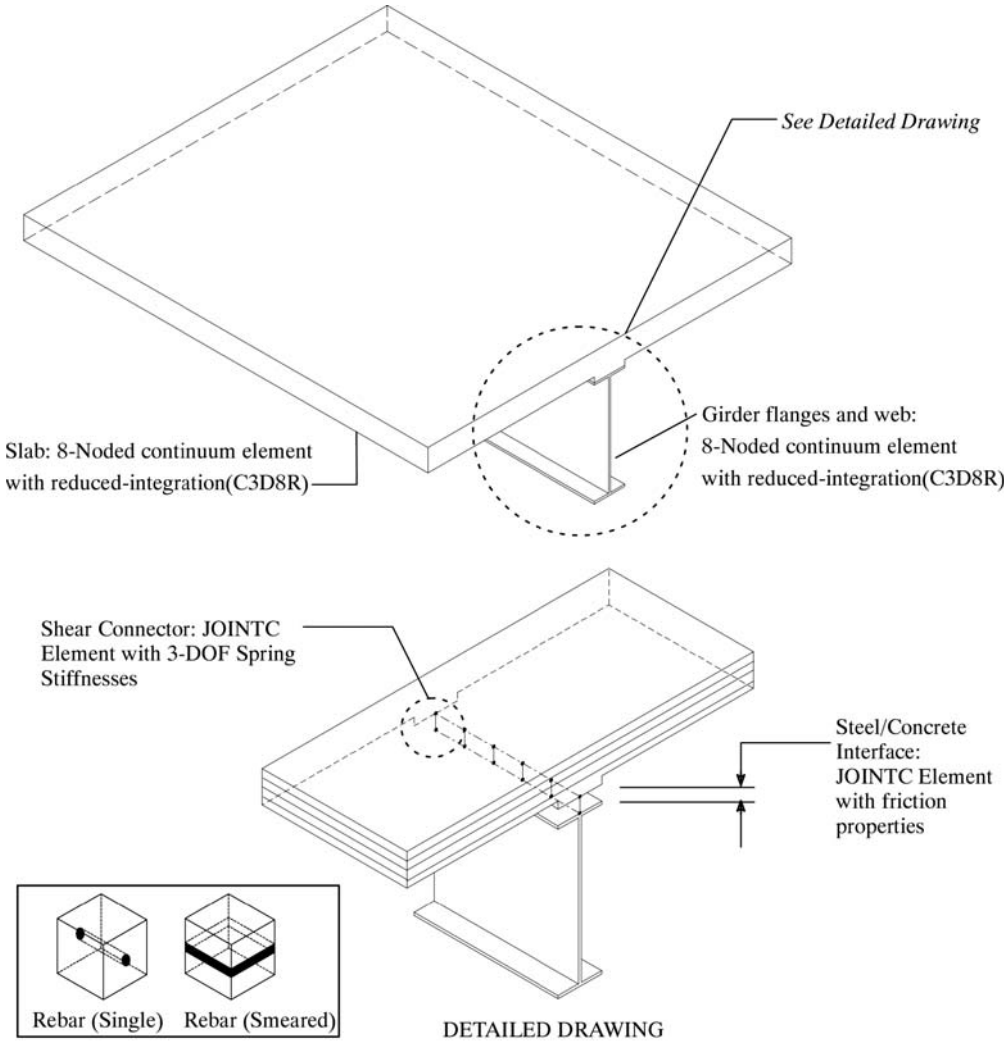

Figure 6. Element modeling scheme employed.

An advanced concrete model called ANAMAT takes into consideration many critical aspects of concrete material behavior. The ANAMAT concrete constitutive model is based on the smearedcracking methodology developed by Rashid (1968) and a Drucker-Prager modified J_2-plasticity theory.

In the ANAMAT concrete model, a crack is a mechanism that transforms the material behavior from isotropic to orthotropic, where the material stiffness normal to the crack surface becomes zero while the full stiffness parallel to the crack is maintained. The cracks can follow independent histories. In this smeared-crack model, a smooth crack should close and all the material stiffness in the normal direction is recovered.

Given that crack surfaces are typically rough and irregular, ANAMAT takes into consideration the mechanism of shear transfer in cracked concrete by retaining a reduced shear modulus in the stress-strain matrix. Tension stiffening of cracked concrete, which is the ability of cracked concrete to share the tensile load with the reinforcement, is also considered in the ANAMAT concrete model. The addition of tension stiffening to the smeared-crack model improves the numerical stability of the solution. The ANAMAT concrete material model was implemented using the UMAT subroutine available in the general-purpose finite element program ABAQUS.

Steel. The steel constitutive model used in the girders is based on the incremental theory of plasticity in which the total plastic strain is obtained by summing the plastic strain increments. Ordinary reinforcing bars are modeled as elastic-perfectly plastic. A bilinear stress-strain relationship is used. Because of the monotonic nature of the loading, the reduction in the yield stress of the steel due to cyclic loading, that is, the Bauschinger effect, is not considered.

Steel-Concrete Interface (Shear Connectors). The shear connection is modeled based on Oehlers and Coughlan (1986), which proposed a simple mathematical formulation that incorporates the beneficial effects of friction. The shear connection is modeled using two orthogonal spring elements to simulate the shear stiffness of stud shear connectors between the steel-concrete interface and the stiffness normal to the interface. A bilinear rigid-elastic relationship is used to model the steel-concrete interfacial behaviors of the composite bridge girders, as described further in Appendix G.

2.3.1.3 Management of the Parametric Study

The pre-processing package called MSC/PATRAN is employed with this modeling procedure. Hence, every model will have the same level of consistency and accuracy in terms of

- Node numbering,
- Element numbering and orientation, and
- Reinforcing steel location.

A procedure for post-processing was prepared in such a way that all relevant information can be systematically extracted from a large data file (.dat file from ABAQUS) and post-processed in order to achieve the following:

- Comparing FEM and lab experimental results and
- Formulating the "Effective Flange Width" criteria.

For extracting the data from the .dat file, FORTRAN 77 routines were developed for the different data groups (i.e., Load vs. Displacement, Load vs. Girder Strain, Load vs. Concrete Strain, and Load vs. Rebar Strains).

Before starting the parametric study, systematic studies were performed to verify the correctness of the behavior of the material models, geometric and boundary condition modeling in both the linear (elastic) and nonlinear (inelastic-cracking and crushing) realms of material behavior. Initially, other researchers' results on steel-concrete composite bridges were used for this purpose, as documented in further detail in Appendix D. Appendix D also includes further specifics about the material models and other aspects of the finite element formulations and modeling.

2.3.1.4 A Question about Barriers

Another FEM modeling question that arises regards barriers that may be cast with the deck. A study of the barrier effect under the applied load on the exterior girder was divided into three parts: (1) load-displacement, (2) strain profile, and (3) effective slab width. The purpose of this study was to evaluate the significance of the barrier on the structural behavior and to determine whether it can be ignored. Three different barrier-modeling schemes were considered:

- Beam element,
- Solid element, and
- No-barrier.

A typical "New Jersey Barrier" used in the OPIS software was used. Section properties of the barrier were computed and used in the finite element modeling.

From this investigation, it was concluded that the barriers in the parametric study cases can be ignored for the following reasons:

- By not considering barriers, shear-lag would be more pronounced. Hence, the effective slab width would be smaller, which is more conservative.
- Practically, barriers are sometimes placed after the concrete is poured and cured without connecting to the slab or with expansion joints that eliminate full continuity. Therefore, they should not always be considered as structural components for design and rating purposes. It is for these purposes, after all, that effective width will be used.

2.3.2 Verification Based on Experiments by Others

The finite element modeling scheme described above was verified for use in conducting the parametric study by comparing the results obtained from ABAQUS/ANAMAT with those of full-scale and model-scale laboratory experimental results by others. These included a full-scale concrete deck on steel superstructure bridge experiment conducted by the Nebraska Department of Roads (Kathol et al., 1995) and a continuous composite beam test conducted at Lehigh University (Daniels and Fisher, 1967).

As documented further in Appendix D, suitable agreement was found between those experiments and the FEM-based predictions, even well into the nonlinear range of behavior.

2.3.3 Verification Based on Experiments by the Authors

The literature survey produced little information related specifically to experimental investigation of the negative moment regions of multi-girder bridge specimens. Much of the research has focused on composite beams alone and not necessarily on bridge superstructure systems. Also, many of the bridge experiments encountered in the review focus on positive moment region alone or do not provide strain data in the negative moment region. There is little detail to be found in the literature about deck instrumentation methods for those that included instrumentation in the negative moment region. Furthermore, very little presentation of composite behavior is not explicitly intentional (i.e., composite behavior in the negative moment region due to friction and interface bond or due to longitudinal deck rebar anchored at the ends but without shear connectors along the length). This lack of data motivates the experimental research discussed in this report, which is documented more fully in Appendixes E and F.

The experiments performed as part of the NCHRP Project 12-58 work provided an additional source of verification data for the FEM-based parametric study. The specimens built were based on a prototype bridge.

2.3.3.1 Prototype Description

The prototype bridge on which the laboratory specimens are based is a two-span continuous plate-girder bridge with a cast-in-place reinforced concrete deck. The *AASHTO LRFD Bridge Design Specifications* (1998, with Interims through 2001) were used to design the prototype bridge in accordance with the HL-93 notional live load. Material properties used for the design are shown in Table 2. The bridge is 13.68 m (45 ft) wide, and each span has a length of 24.4 m (80 ft). As seen in Figure 7, the four girders are spaced at 3.8 m (12 ft, 5½ in.), and there is a deck overhang of 1.14 m (3 ft, 9 in.) at the exterior girders. An elevation view of a typical girder is illustrated in Figure 8, and Figure 9 shows the framing plan. The Traditional method (Section 5.7.3 of The Code) was used to design the reinforced concrete deck, and the reinforcement details are provided in Figure 10 in addition to Figure 7. Shear studs are used to connect the concrete deck to the steel girders thus forming an intentionally composite structure. The shear stud pitch of the intentionally composite prototype is designed according to Section 9.7.3 of The Code and is shown in Figure 11.

This prototype bridge served as the basis for experimental studies carried out as part of the NCHRP Project 12-58 effort. The quarter-scale two-span continuous specimen is called 4GQTCOM. The two half-scale negative moment region subassemblage specimens are called 4GHFCOM and 4GHFNON. In these specimens, instrumentation is placed with a number of factors considered. Such factors include providing insight regarding specimen behavior and furnishing a practical data

TABLE 2 Prototype material properties

Components		f_y in MPa [ksi]	f'_c in MPa [ksi]
Girder	Flanges	345 [50]	
	Web	345 [50]	
Stiffeners (transverse)	Bearing	345 [50]	
	Intermediate	345 [50]	
Stud Connector		345 [50]	
Weld		*550 [80ksi]	
Reinforcement		420 [60ksi]	
Concrete			28 [4ksi]

*f_u

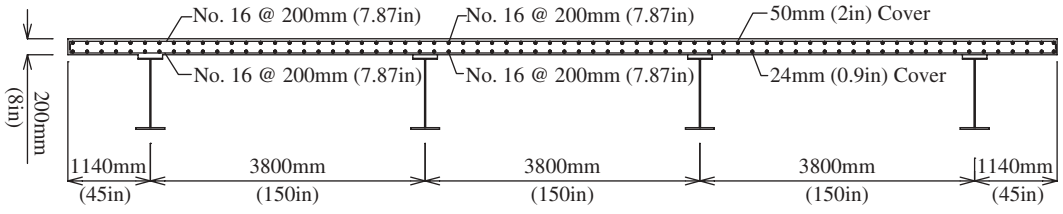

REINFORCEMENT DETAIL

Figure 7. Cross section of prototype bridge.

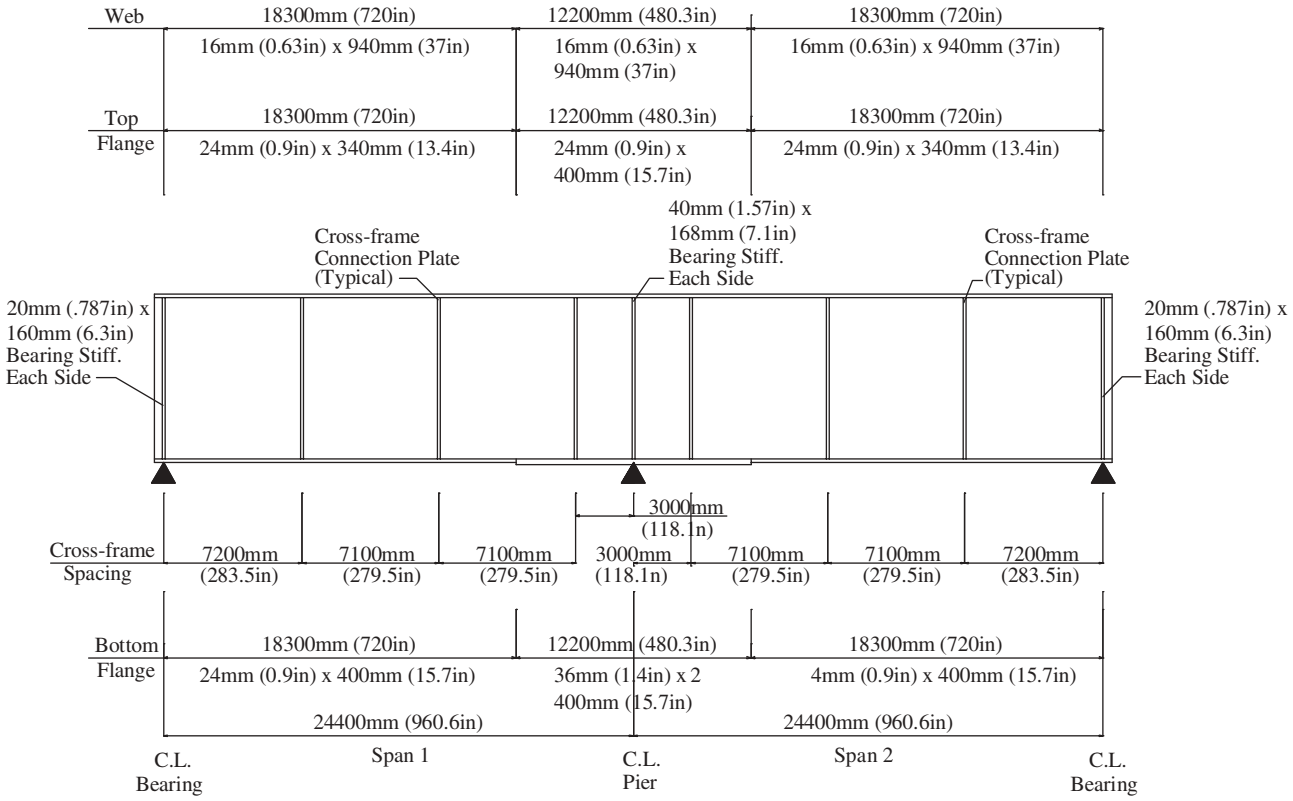

Figure 8. Girder elevation of four-girder prototype.

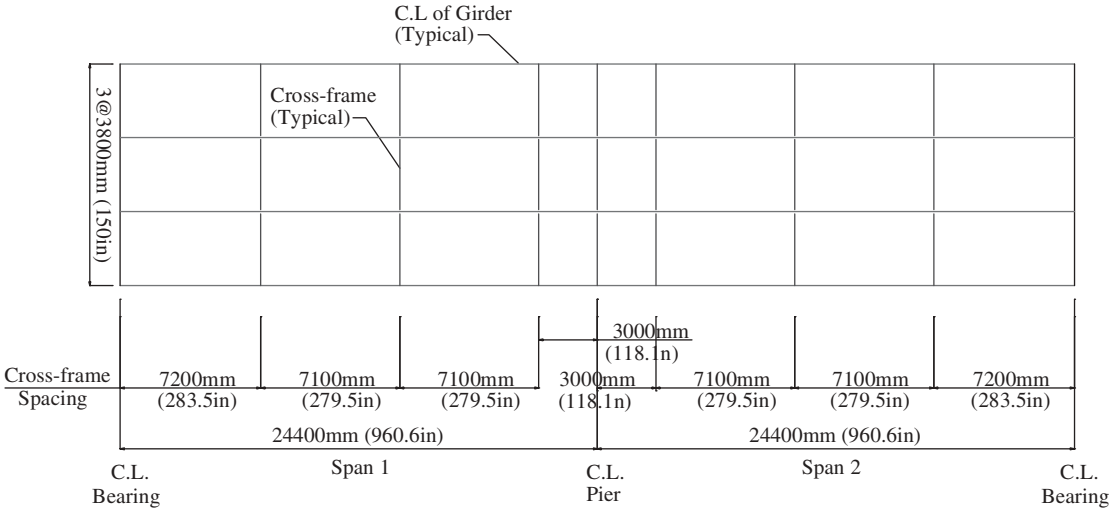

Figure 9. Framing plan of four-girder prototype.

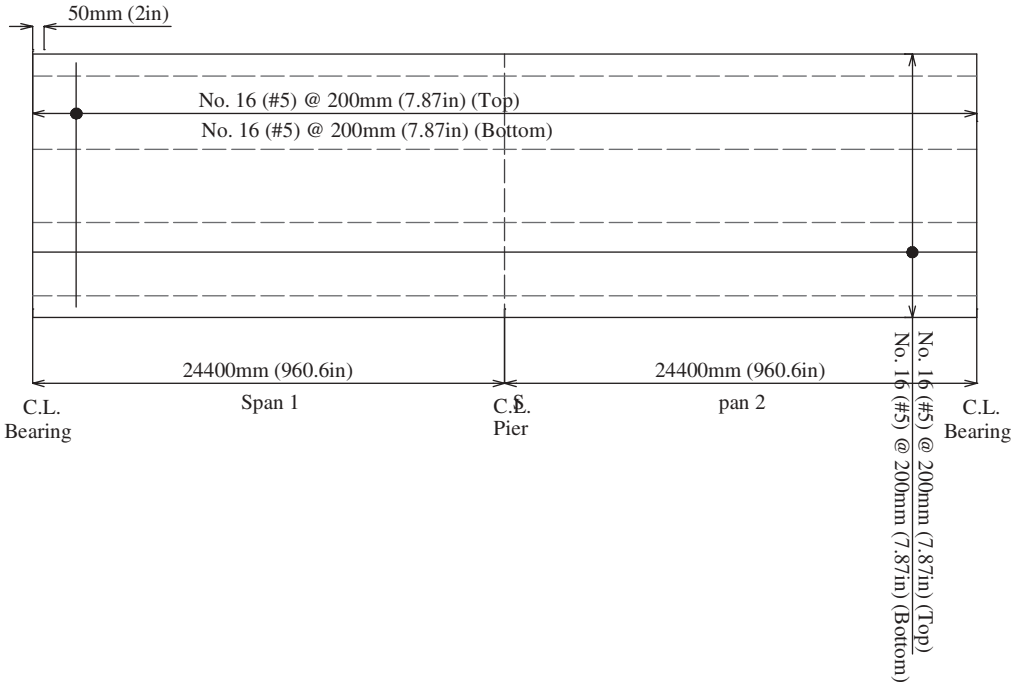

Figure 10. Deck reinforcement plan in prototype.

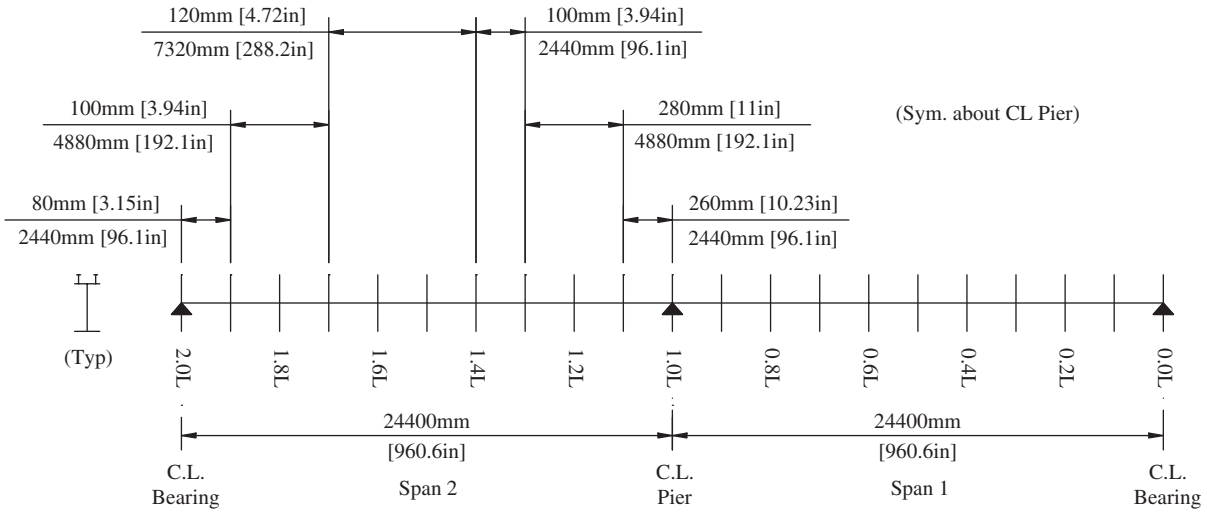

Figure 11. Prototype shear stud pitch.

set for comparing experimental test results with the FEM analysis. Findings from these studies are described next.

2.3.3.2 Quarter-Scale Specimen and Instrumentation

The four-girder, quarter-scale composite I-beam specimen consists of two continuous 6.1 m (20 ft) spans. Girder spacing is 0.95 m (3 ft, 1 in.), transversely connected by cross-frames along the span length. The geometric parameters of the composite specimen are shown in Figures 12 and 13. The specimen was designed to enable study of the behavior within the positive and negative moment regions of continuous span bridge girders. The girders were designed using Grade 345 (50 ksi) steel, with compact flanges to develop full plastic moment capacity and lateral bracing close enough to avoid lateral buckling. Webs were designed to be compact

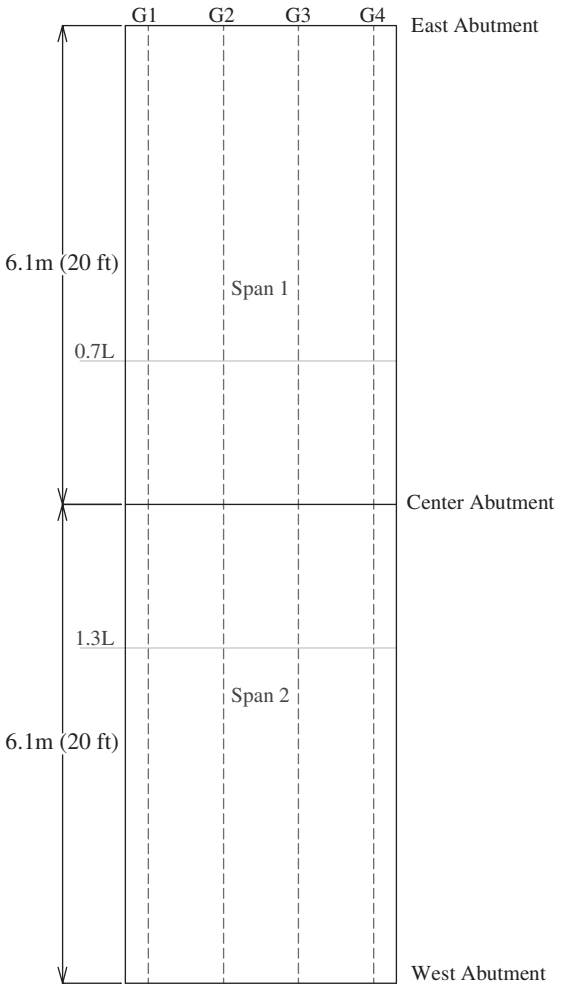

Figure 12. Plan view of four-girder specimen.

and unstiffened. Typical cross sections through the positive and negative moment regions can be seen in Figure 14.

The maximum aggregate size was chosen as 9.5 mm ($^3/_8$ in.) to prevent any large voids in the deck. The slab reinforcement was isotropically laid out in the reinforced concrete deck with a thickness of 50 mm (2 in.) and the double-layers of 4 mm (.157 in.) diameter reinforcing steel placed at 50 mm (2 in.) spacing, transversely and longitudinally.

A modified design truck was recommended for the experimental study. Two different loading conditions were considered: (1) complete 6-wheel design truck portion of the HL-93 loading and (2) 4-wheel loading representing the two rear axles of the design truck. Analysis results using SAP2000 show variations less than 1 percent in the high-stress regions and less then 10 percent in the low-stress regions. Based on this observation, a two rear-axle loading configuration was applied to the test specimen.

For the service limit state, five loading positions were used to test the positive moment region and eight loading positions were used to test the negative moment region. Positive moment tests were performed at 0.4L and negative moment tests performed at 0.6L. The design truck was located at 0.4L and 0.6L for the positive and negative moment tests, respectively. For the ultimate loading tests, a re-configuration of the design truck was used which allowed loads to be applied over each girder line. For the negative strength test, each girder was loaded at 0.6L on Spans 1 and 2 until failure.

Strain and deflection measurements were recorded during the testing process. Displacement transducers were used for the deflection measurements along the bridge.

2.3.3.3 Selected Experimental Results from the Quarter-Scale Specimen

The purpose of the experiments was to establish a basis for confidence in the finite element modeling scheme employed in the parametric studies of this research. Two experimental loading cases were the focus of the results presented herein for the experiments conducted on the four-girder, quarter-scale, two-span continuous slab-on-girder bridge specimen:

- The "Positive Service Yield Case," loading one span to just reach yield of the bottom flanges in the positive moment region, and
- The "Negative Strength Case," loading both spans to maximize negative moment at the support and form a plastic collapse mechanism in the specimen.

Positive Service Yield Case Results. Primarily positive moment region results are presented here because the negative-moment region subassemblages reported in the following sections and Appendix F provided much better negative moment region data, with strain-gaged longitudinal rebars, etc. Sufficient agreement was obtained between experimental results and FEM predictions that the originally planned fourth experimental specimen (2GQTCOM) was deleted from the scope of work for this project.

Figure 15 shows the position of loading for the Positive Service Yield Case. Deflections of an exterior (G1) and interior (G2) girder were compared with FEM results. Figure 16 compares recorded deflections of exterior girder G1 and interior girder G2 versus FEM results and line girder (LG) predictions. Line girder deflections were computed using predicted values

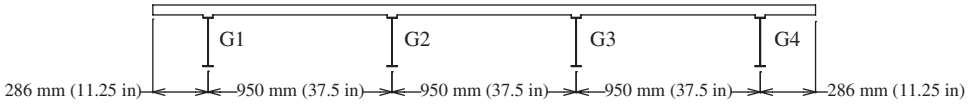

Figure 13. Cross-section view of four-girder specimen.

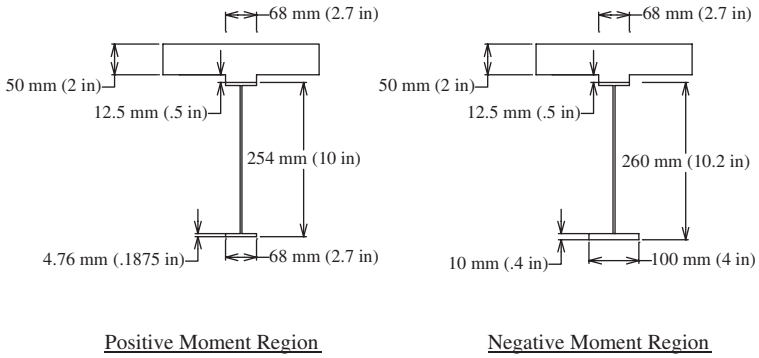

Figure 14. Typical cross sections in quarter-scale specimen.

of b_{eff}, which included full width ($b_{eff} = S$) in the positive moment region and 0.9 ∗ full width ($b_{eff} = 0.9 * S$) in the negative moment region. The FEM used the value of the load cell to provide the direct comparison noted earlier. The values having box symbols on the graph correspond to problematic gages. Clamps were placed at the end supports of Span 2 to prevent the bridge from any lift-off that might have otherwise occurred during testing. This clamping process introduced unintended rotational restraint, which affected the deflection of G1 (Figure 16) at a distance of 10,800 mm (425 in.) from the end where a slight reverse in curvature is evident. G2 (Figure 16) and FEM show a good correlation in Span 1 and 2.

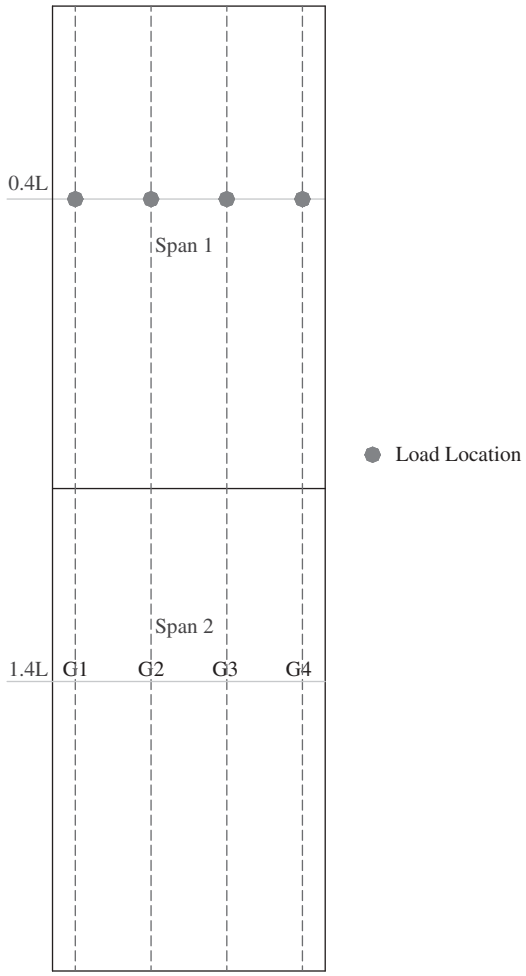

Figure 15. General layout and load location for positive service yield case.

The Positive Service Yield Case was designed to capture the elastic response of the experimental model at yield load levels for comparison with FEM. The various comparative plots show reasonable accuracy in the positive moment region. The experimental results (i.e., deflections and strains) were consistent throughout the test. Deflections that exceeded FEM values were accompanied by corresponding high strain values. Strains through the depth of the cross section remained plane throughout the test for nearly all the specified locations (neglecting problematic gages). The FEM adequately predicted the observed behavior of the experimental specimen throughout the Positive Service Yield Case. Further testing was performed beyond yield and is presented next.

Negative Strength Case Results. Figure 17 identifies the points of load application during the Negative Strength Case. Next, Figure 18 shows values at two loading stages, one at 360kN (81kips) and the other at 453kN (102kips), the maximum loading achieved. Figure 18 compares the experimental and FEM-predicted deflections of G1 and G2. Under both loading conditions, the experimental results were consistent with the FEM results.

The Negative Strength Case showed significant cracking in the negative moment region, as was to be expected with the continuous specimen. Although the results between the FEM and experimental specimen differed slightly, the results were generally consistent and thus verified FEM results for the positive moment region.

Discussion of Test Results. These experiments consisted of various serviceability level loads followed by tests to failure. The major cracking occurred in the negative moment region, which was expected and can be seen in Figure 19. The cracks shown in Figure 19 carried across the specimen transversely.

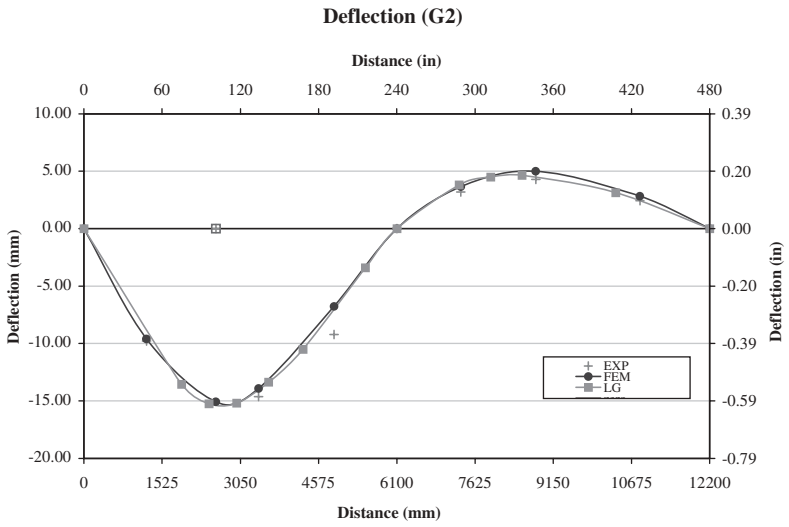

Figure 16. G1 and G2 deflection for positive yield case.

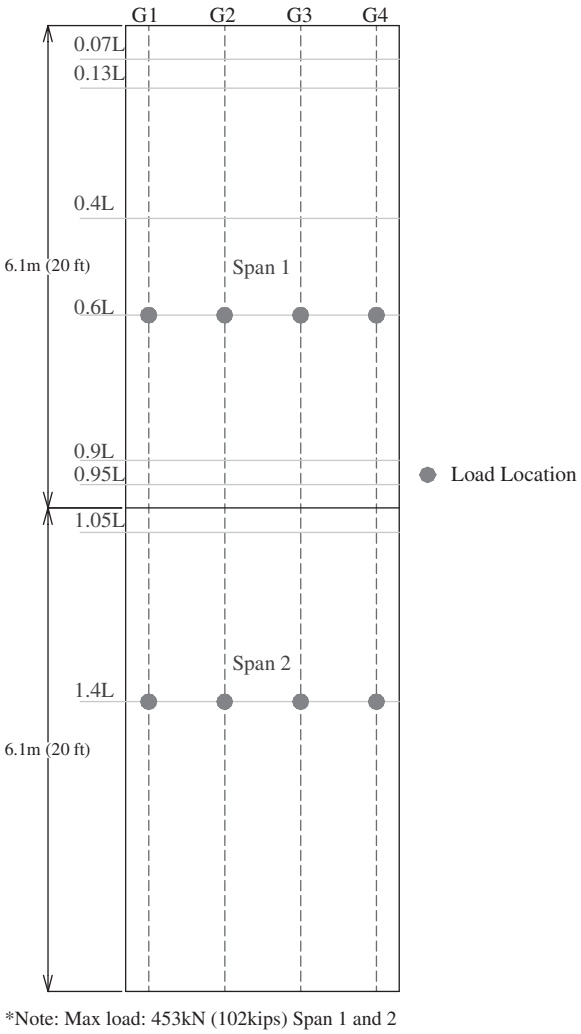

*Note: Max load: 453kN (102kips) Span 1 and 2

Figure 17. General layout and load location for negative strength case.

Figure 20 shows the specimen after the testing was completed. At 0.6L, after the positive strength case, a significant amount of rotation occurred along with a permanent displacement confirming a high level of ductile behavior from the specimen. The other service and strength cases demonstrated that the FEM and experimental behavior were consistent and accurate in the positive moment region. The experimental behavior was predicted reasonably accurately by FEM.

As mentioned above, a crack check was performed after each test, and each crack was outlined and dated. This provided enough information to create the drawings shown in Figures 21 and 22. Many of the gages in the negative moment region on the concrete deck were lost because of severe cracking as shown in Figure 22.

2.3.3.4 Half-Scale Specimens and Instrumentation

Two half-scale bridge specimens were produced based on the negative moment region of the prototype bridge described in Section 2.3.3.1. The specimens represented a portion of the prototype that included two of the four girders and ranged from 0.70L to 1.3L, where the parameter L represented one span length. Figure 23 illustrates the portion of the prototype that was represented by the specimens. Additional cross-frames are shown within the specimen portion of the bridge at 0.75L and 1.25L. Although these additional cross-frames were not in the prototype, they were required for stability because the specimens were loaded at those locations. Tie-down and loading at 0.75L and 1.25L (respectively) simulated shear forces at the permanent load inflection points of the prototype while the pier of the prototype was directly represented by a central support in the specimen at 1.0L.

The bridge specimens were composed of two continuous homogeneous girders 7220 mm (284 in.) long and a 110-mm (4.375-in.) thick reinforced concrete deck. The girders were

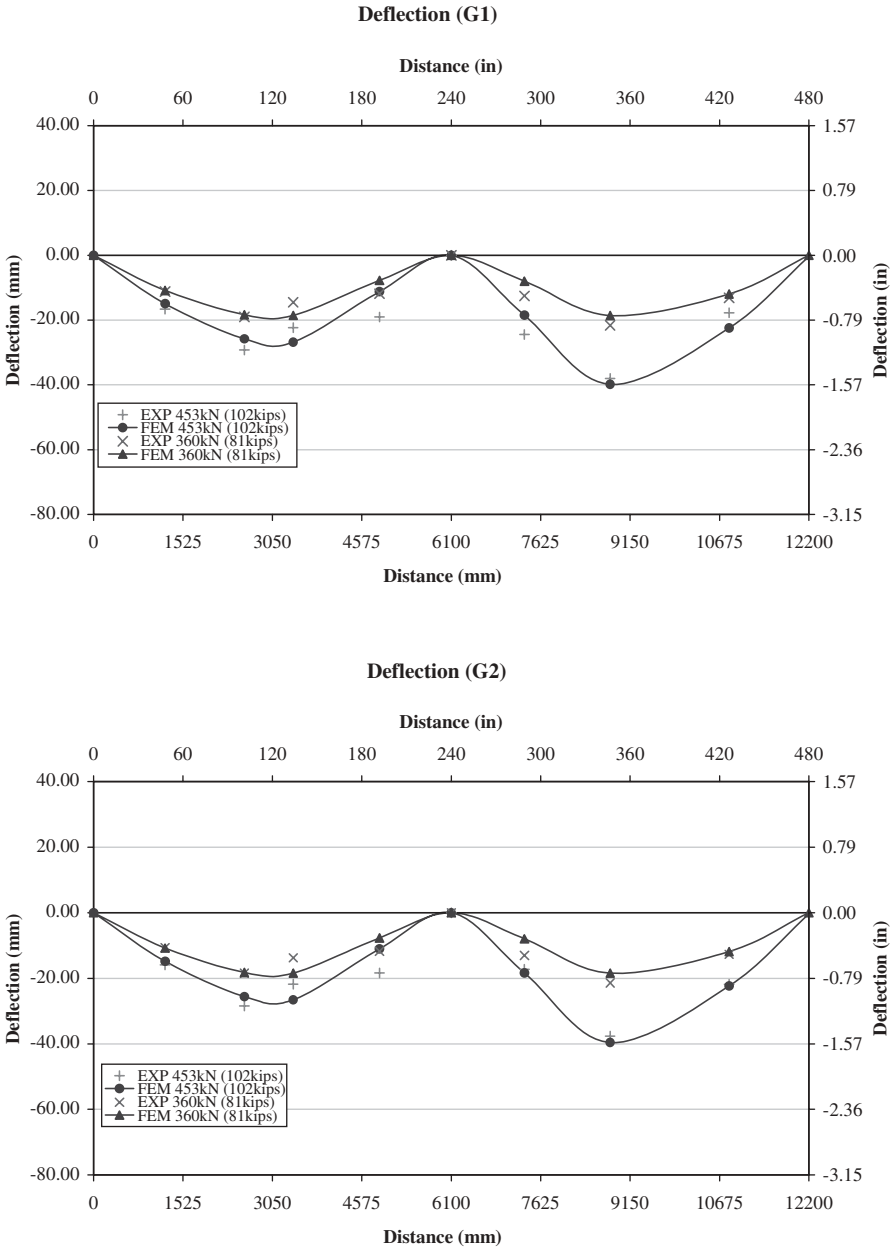

Figure 18. G1 and G2 deflection for negative strength case.

490 mm (19.25 in.) deep and had a spacing of 1900 mm (75 in.), while the overhang was 570 mm (22.5 in.). Cross-frames were constructed from L3 × 3 × 3/8 stock and welded in place in an X configuration. Specimen geometry is depicted in Figures 24 through 27.

The main difference between the two bridge specimens was the layout of the shear connectors. Many states use shear connectors in the negative moment region of composite bridges while for others it is less common. Effective width criteria are based on composite behavior. Composite behavior that is unintentional (i.e., which results only from friction and steel-to-concrete interface bond strength and not the presence of discrete mechanical connectors) is not something that designers typically will rely on. Furthermore, the *AASHTO LRFD Bridge Design Specifications* appear to be inconsistent with regard to composite action in the negative moment region. "Article S6.10.7.4.3 states that 'Where composite girders are noncomposite for negative flexure, additional shear connectors shall be provided in the region of points of permanent load contraflexure'. However, the commentary to that article states that 'The purpose of the additional connectors is to develop the reinforcing bars used as part of the negative flexural composite section.' Is it composite or noncomposite?—the code is confusing on this point" (Chen et al., 2001). In any event, *AASHTO LRFD Bridge Design Specifications* were used to design the shear connectors for both specimens.

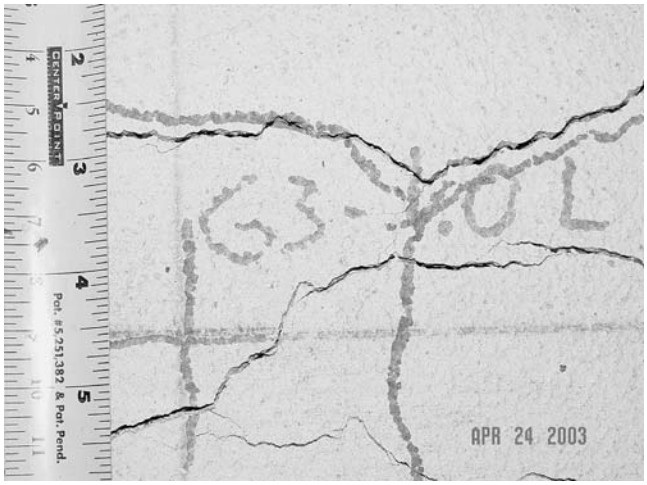

Figure 19. Cracking at G3 over the center support.

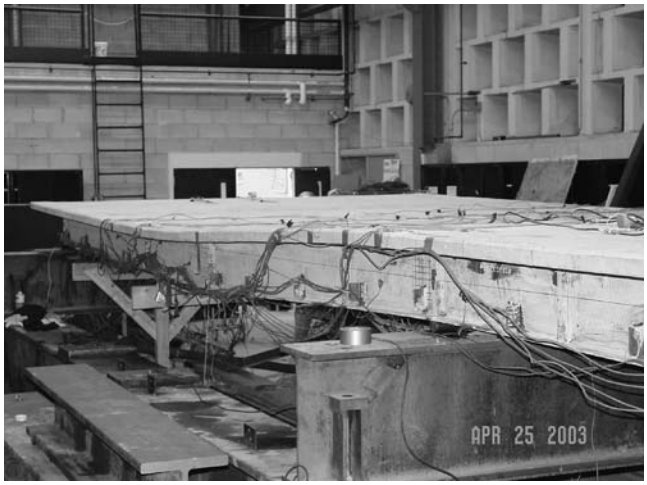

Figure 20. Final curvature after testing.

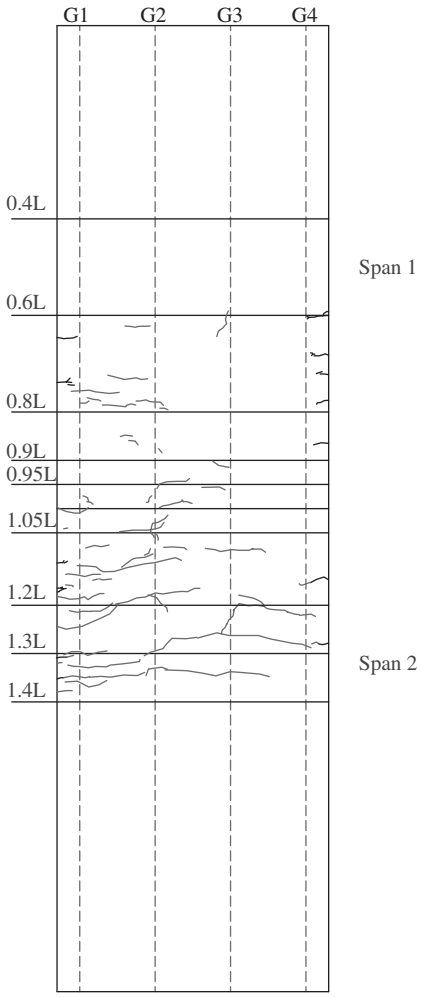

Figure 21. Cracking due to service loading.

The intentionally composite bridge was designated as 4GHFCOM because it was based on a four-girder prototype at half scale. Similarly, the noncomposite specimen was designated as 4GHFNON. The shear studs used for both specimens are 10 mm [$^3/_8$ in.] in diameter and have a length of 80 mm [3.1 in.]. As shown in Figure 25, studs are placed in two rows at 75 mm [3 in.] in the vicinity of the permanent load inflection point and at 300 mm [12 in.] elsewhere on 4GHFCOM, resulting in 128 shear connectors per beam. The 'noncomposite' specimen, 4GHFNON, has clusters of shear studs in the vicinity of the permanent load inflection point to develop longitudinal rebar as The Code specifies.

Instrumentation was placed not only for the reasons listed above but also to generate data that might be useful in comparing the intentionally composite behavior of specimen 4GHFCOM with the behavior of specimen 4GHFCOM, which was noncomposite but had longitudinal rebar anchored at the ends. Strain gages were placed on the rebar embedded in concrete as well as on the deck and girders. In addition to direct strain measurements, displacement transducers such as Temposonics, Linear Variable Displacement Transducers (LVDTs), and potentiometers were used to measure quantities such as displacement, slip, plastic hinge rotation, and smeared values of strain.

The strain gages placed on the rebar included regular and backup gages placed on both longitudinal layers (top and bottom) of rebar. A significant number of gages were placed near the pier because one objective of this experiment was to investigate behavior near the interior support. A denser concentration of gages near the pier might be desired but was not fully provided because of equipment limitations and because protective coating and wires in the vicinity of the gage might slightly reduce the volume of concrete and, therefore, the amount of concrete in contact with the bars in the immediate vicinity of the gages. This reduction of concrete volume and contact area was not expected to be significant, however, given that the gages were reasonably spaced across the width of the deck. A significant number of gages were placed along Girder 1 as well in order to provide information for comparing

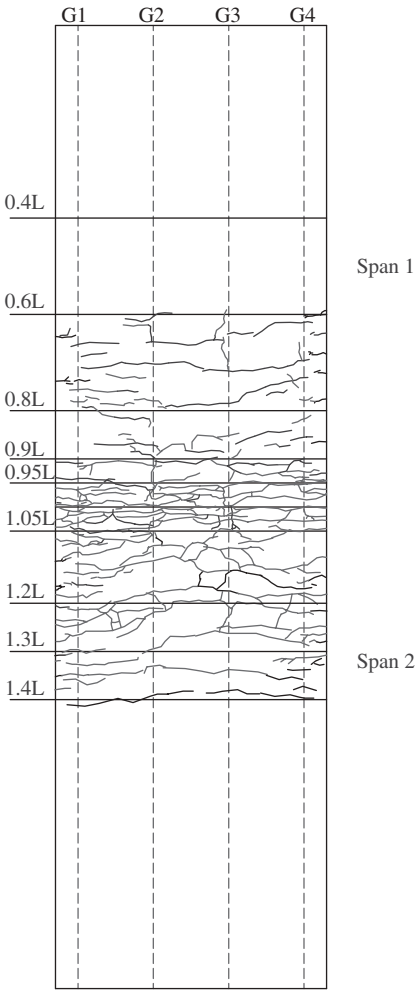

Figure 22. Cracking due to ultimate loading.

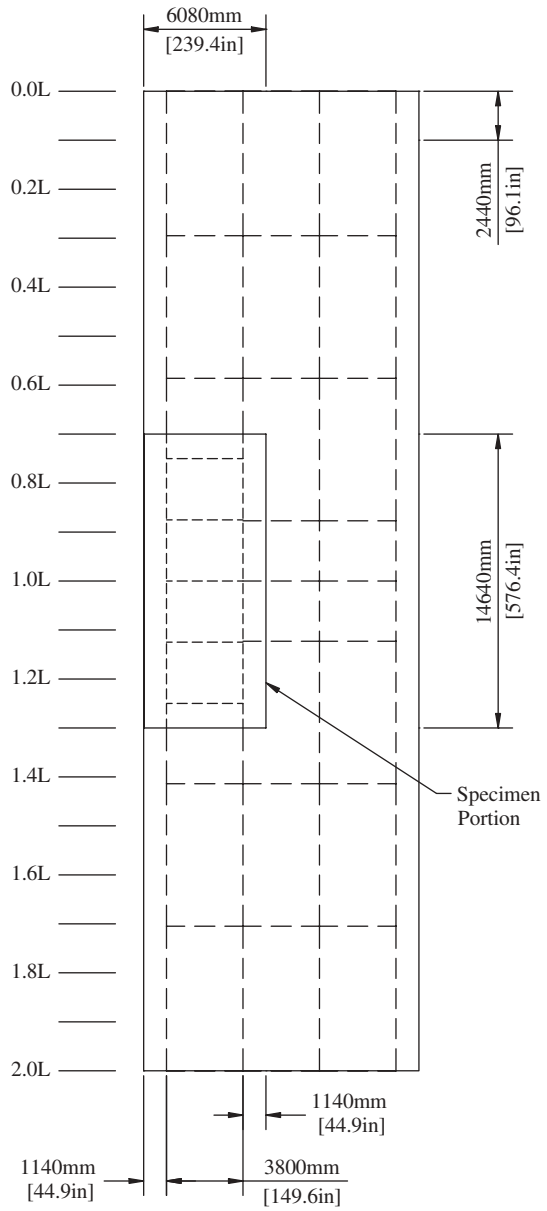

Figure 23. Specimen portion of prototype.

the composite action of 4GHFCOM with that of 4GHFNON. In addition to those near the pier, another transverse line of rebar strain gages was placed along 0.85L. This location was chosen because it was expected to be far enough away from the point of loading (0.75L) such that local effects from the loading were not a concern. Other rebar gages were placed to provide data points to plot the strain profile through the composite section. Backup gages were provided in case some gages were damaged during deck casting. The line of backup gages on Bar 10 was supplied to replace the gages along Bar 8 if the state of stress near the shear studs was complex enough to corrupt the readings along Bar 8. They also served as backup for other gages in their vicinity.

Strain gages on the girders and on the concrete deck girder line were positioned to give information about the strain profile within a section. These gages corresponded to the rebar gages mentioned earlier for the same purpose. Other concrete deck gages were placed to provide information about the strain variation in plan across the width of the deck.

Further information about instrumentation is provided in Appendix F.

2.3.3.5 Selected Experimental Results: Half-Scale Specimens

Figures 28 and 29 show deck cracking results for the 0.95 ∗ yield case and the post-yield case, respectively. Figure 30 shows the force displacement relationships for both 4GHFCOM and 4GHFNON on the same plot. The load levels used for FEM comparison are also depicted. The 4GHFNON specimen deviated from the FEM curve sooner than the 4GHFCOM specimen. This was probably the result of at least partial loss of composite action. The plots indicate that the forces were similar in the ultimate limit state, thus indicating that overall behavior of the noncomposite specimen with developed longitudinal rebar was similar to that of the

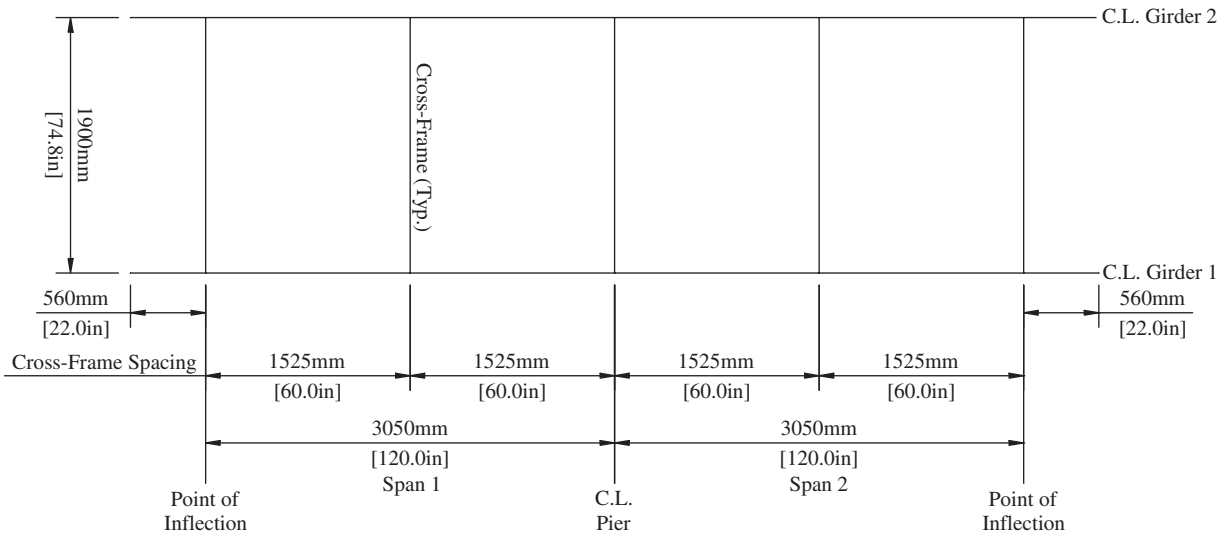

Figure 24. Specimen framing plan.

intentionally composite one. Comparative deflection profiles shown in Figure 31 generally confirmed this behavior as well, although deviation from linear behavior began slightly sooner for the noncomposite specimen.

The findings from the negative moment region subassemblage experiments may be summarized as follows:

1. There is a good correlation between the FEM and line-girder (LG) predicted results for much of the experimental data. Before the specimens' girders buckled, their load displacement curves followed very near the FEM curve. These specimens were designed to have barely compact webs (based on the current 12t-limited

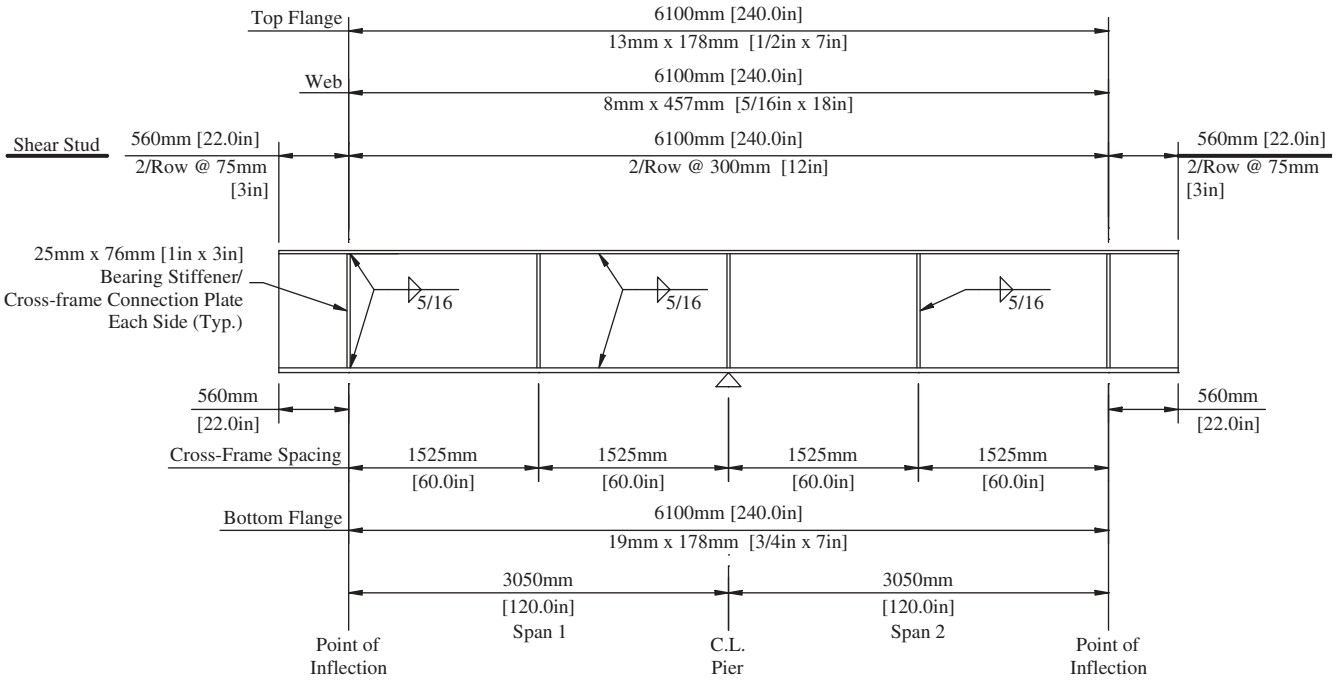

Figure 25. 4GHFCOM girder elevation.

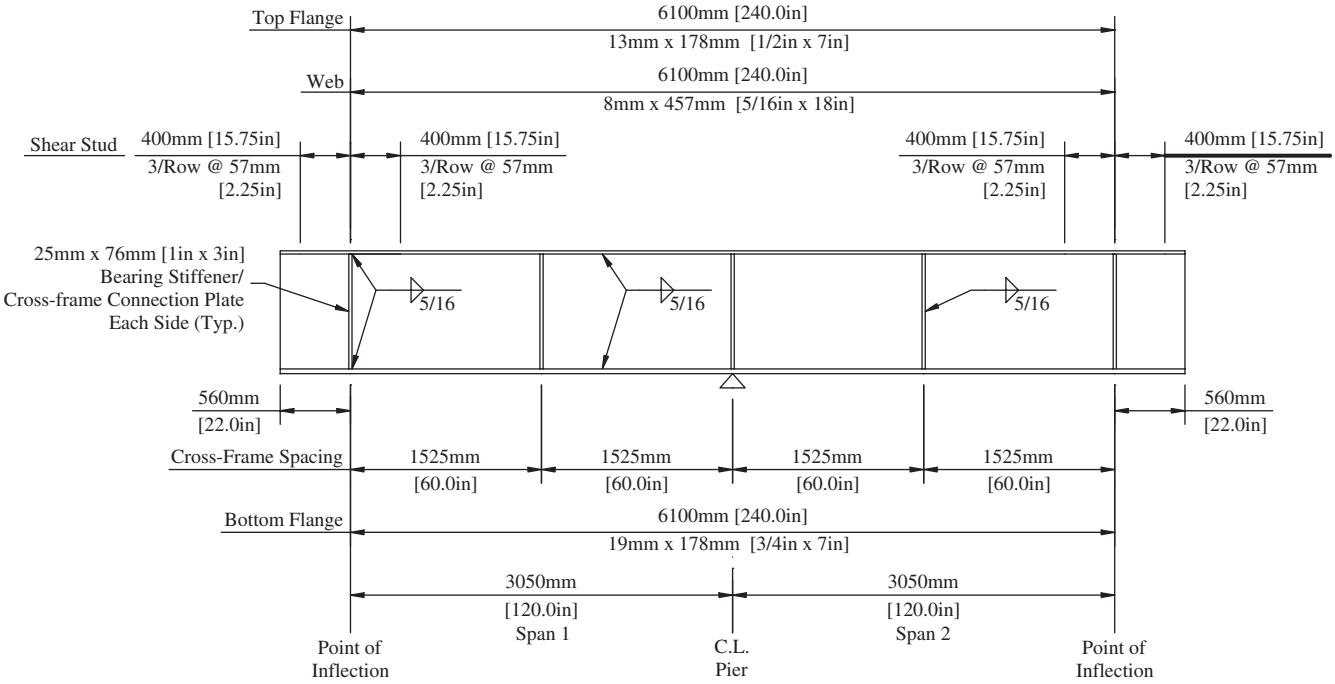

Figure 26. 4GHFNON girder elevation.

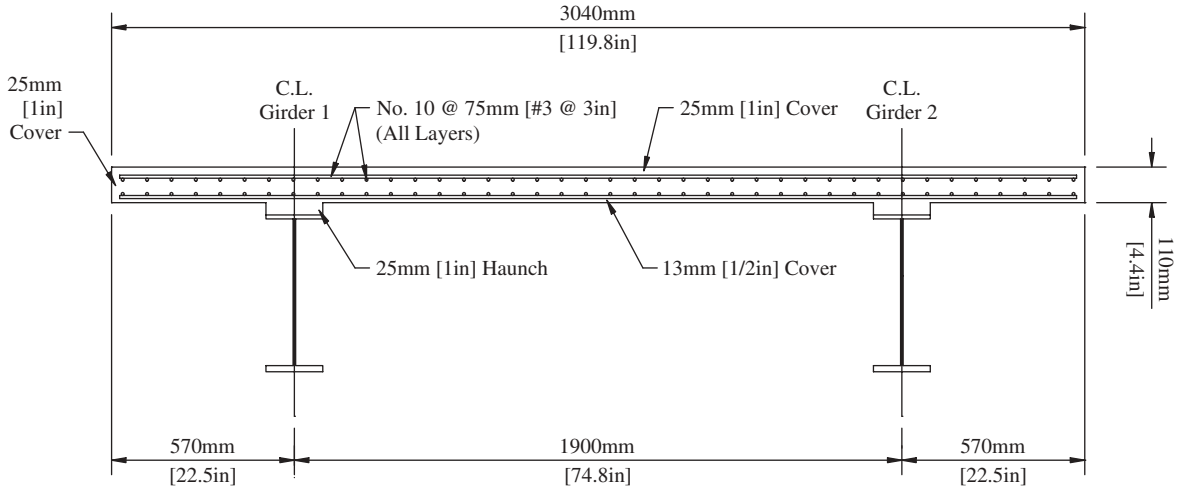

Figure 27. Specimen section.

definition of effective width) in order to develop a plastic hinge and investigate experimentally the cracked-deck effective width at plastic hinge conditions. But in doing so, it was overlooked that full (not 12t-limited) effective width would raise the neutral axis, thereby rendering the web noncompact. Such a web would be expected to buckle before full plastification, which is precisely what occurred in the experiment. Attempts to model the geometric nonlinearity of web buckling combined with the material nonlinearity of yielding in the FEM model were unsuccessful. Thus, the plotted FEM model results neglected web buckling. Even after buckling, however, the general shape of the load displacement curve mimics the shape of that predicted by FEM modeling. It is therefore reasonable to assume that, had the section been fully compact, it might have continued

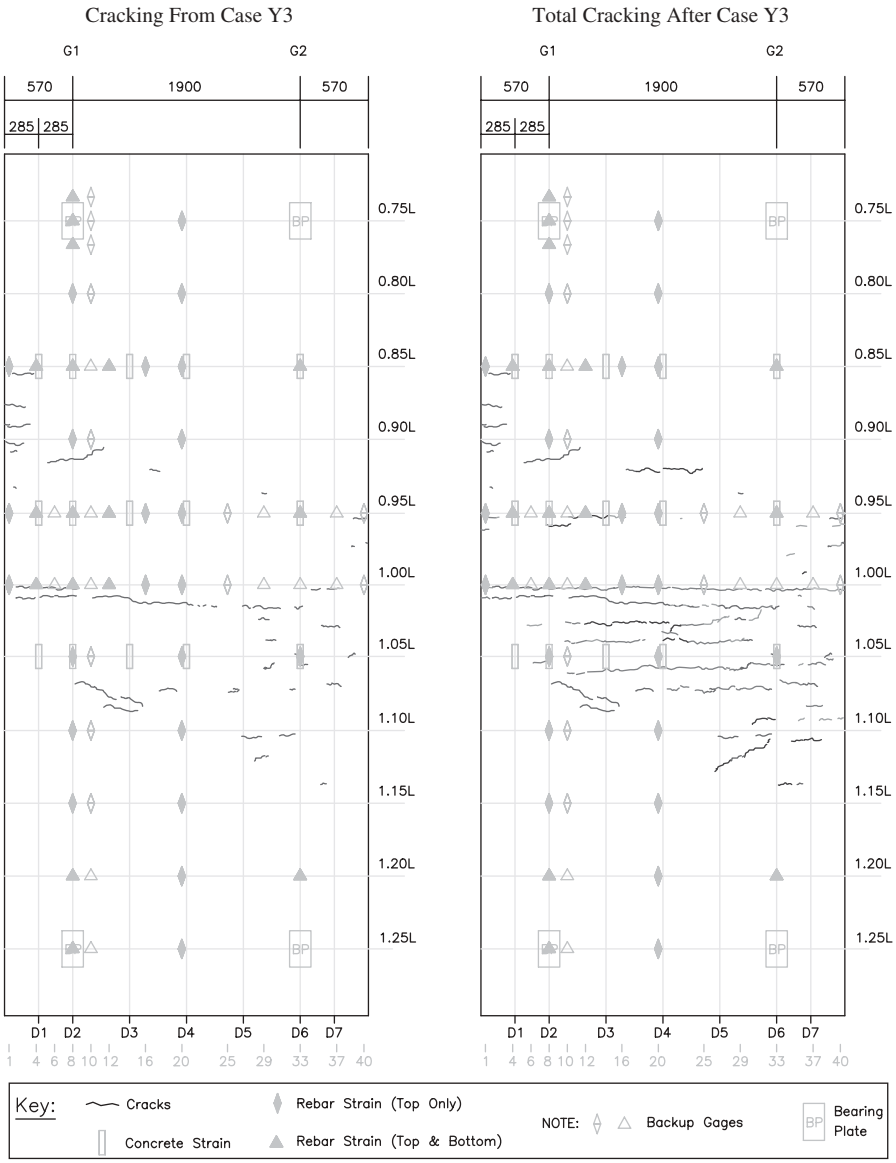

Figure 28. 4GHFCOM Case Y3 cracking.

close to the FEM curve. That it was not compact itself is evidence of full effective width, given that, on the basis of current AASHTO provisions for effective width, it would have been compact. Deflection profiles were also predicted reasonably well by the FEM model up to the onset of buckling.

2. Girder strains obtained from the experiment also compared well with FEM-predicted values. There were some discrepancies near the boundary conditions (i.e., loading and tie-down points) but this was to be expected.
3. Strain readings associated with the deck were generally unreliable for the composite specimen, and most of them were questionable for the noncomposite one as well. Unfortunately, deck surface gage results were the most unreliable. Some of the rebar-mounted strain gages on the second specimen did, however, yield reasonable results. This favorable outcome is believed to be due to the introduction of epoxy as the protective coating. The general unreliability of deck-related strain gages because of deck cracking makes it difficult, if not impossible, to extract effective width values directly from experimental results. That most of the other data correlated well with FEM, however, was considered sufficient to conclude that FEM results were reasonable. The reader may wish to refer to the dissertation by Chiewanichakorn (2005) for more information regarding the validity of FEM relating to evaluation of composite bridges.
4. The global behavior of the 4GHFNON specimen (noncomposite but with developed rebar) was similar to that of the 4GHFCOM (intentionally composite) specimen,

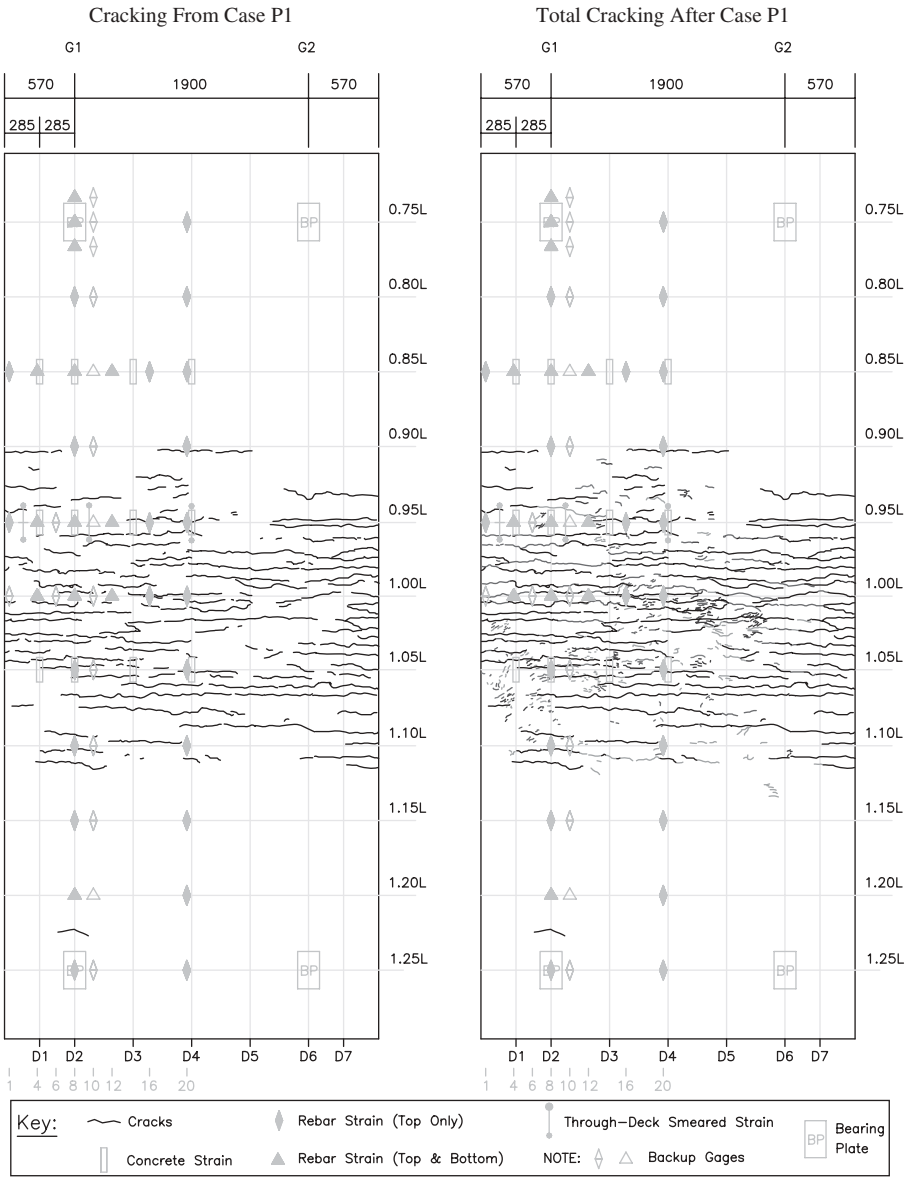

Figure 29. 4GHFNON Case P1 cracking.

especially at the ultimate limit state. Local behavior (i.e., slippage and separation of the concrete deck from the steel girder), however, would normally be used to classify the girder as noncomposite.

5. Despite the problems encountered with deck gages
   a. There was good correlation of deck strains with FEM strains before cracking,
   b. Overall load-deflection prediction was good,
   c. Existence and extent of cracking was reasonably well predicted by the smeared cracking approach used in the FEM herein,
   d. Steel strains correlated well with FEM predictions pre-buckling,
   e. Those strain profiles confirmed the upward movement of the neutral axis consistent with the full effective width predicted by FEM for the experiment, and
   f. That the web flexural buckling was observed provides additional confirmation that the neutral axis had moved up—consistent with a full effective width.

Thus, the principal insights from the experiments were that the FEM methodology employed was reasonably trustworthy for extracting effective width and that full width is consistent with those experimental results. Further details on the experiments conducted are provided in Appendixes E and F.

2.4 FEM PARAMETRIC STUDY

In the parametric study of the effective slab width project (NCHRP Project 12-58), design of experiment (DOE) concepts described in Appendix G were employed to ensure

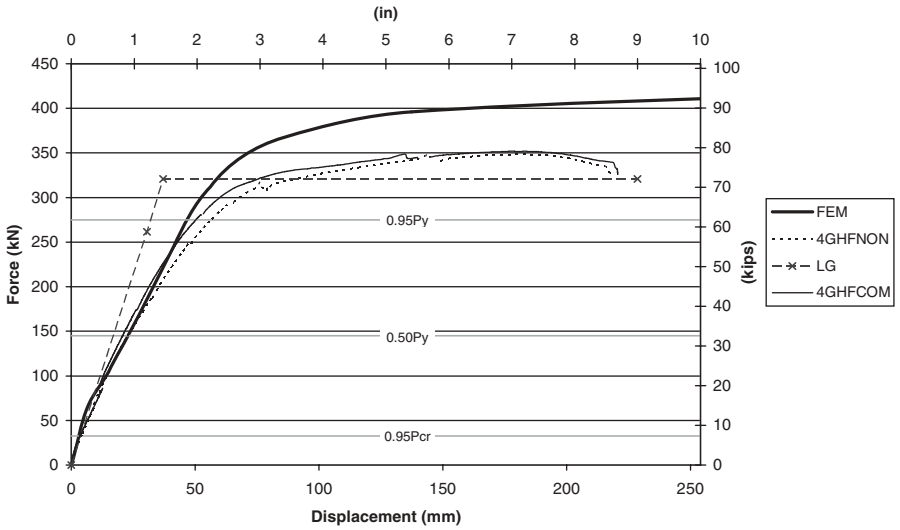

Figure 30. Comparative force versus displacement at 1.20L.

that both common and extreme cases were covered. In addition, curve-fitted equations were derived considering the effects from each parameter. Various cases were considered:

- Simple-span right bridge (non-skewed),
- Simple-span with skewed supports,
- Multiple-span continuous right bridge (non-skewed), and
- Multiple-span continuous with skewed supports.

By using DOE, all cases for both simple-span and multiple-span continuous bridges are illustrated in Tables 3 and 4, respectively.

For simple-span cases, the main parameters are

- Girder spacing (S) 2.4 m to 4.8 m,
- Span length (L) from 15 m to 60 m, and
- Skew angle (θ) from 0 degree to 60 degrees.

For multiple-span continuous cases, the main parameters are

- Girder spacing (S) 2.4 m to 4.8 m,
- Exterior span length (L_1) from 20 m to 60 m,
- Interior-to-exterior span ratio (L_2/L_1) from 1 to 1.5, and
- Skew angle (θ) from 0 degree to 60 degrees.

2.4.1 Bridge Designs for Parametric Study

All bridges in the parametric study were designed according to a common set of industry guidelines for economical design of slab-on-steel girder-type structures. These guidelines are as follows.

Strength I, Service II, and Fatigue and Fracture limit states were considered in the designs, as was the construction stage assuming conventional unshored construction. Load effects were calculated using the QConBridge software. Bridges were designed for these load effects using MathCad Worksheets developed for that purpose. Bridges so designed were checked using the OPIS 5.0 software. Line girder analysis with the current 12t-limited effective slab width was used for each of the designs. Details of deck and girder design considerations are summarized below.

2.4.1.1 Deck Design

The thinnest practicable deck was used in order to maximize shear lag behavior. The deck thickness depended on the girder spacing. The following thicknesses were used:

Girder Spacing	Deck Thickness	S/t	Design Method
2.4m	175mm	13.7	Empirical Design
3.6m	200mm	18.0	Empirical Design
4.8m	240mm	20.0	Conventional

Overhang width was assumed as 0.4S for every bridge design based on an investigation of overhang width on several bridges to produce the same exterior girder as used for the interior girder, with similar structural efficiency, i.e., performance ratio.

Skewed Deck. Two skew angles were considered in the designs: 30 and 60 degrees. The reinforcement in both directions was doubled in the end zones of the deck and placed perpendicular to the main supporting components as specified in Article 9.7 of the AASHTO LRFD code.

Negative Moment Regions. The total cross-sectional area of the longitudinal reinforcement should not be less than 1 percent of the total cross-sectional area of the slab. The

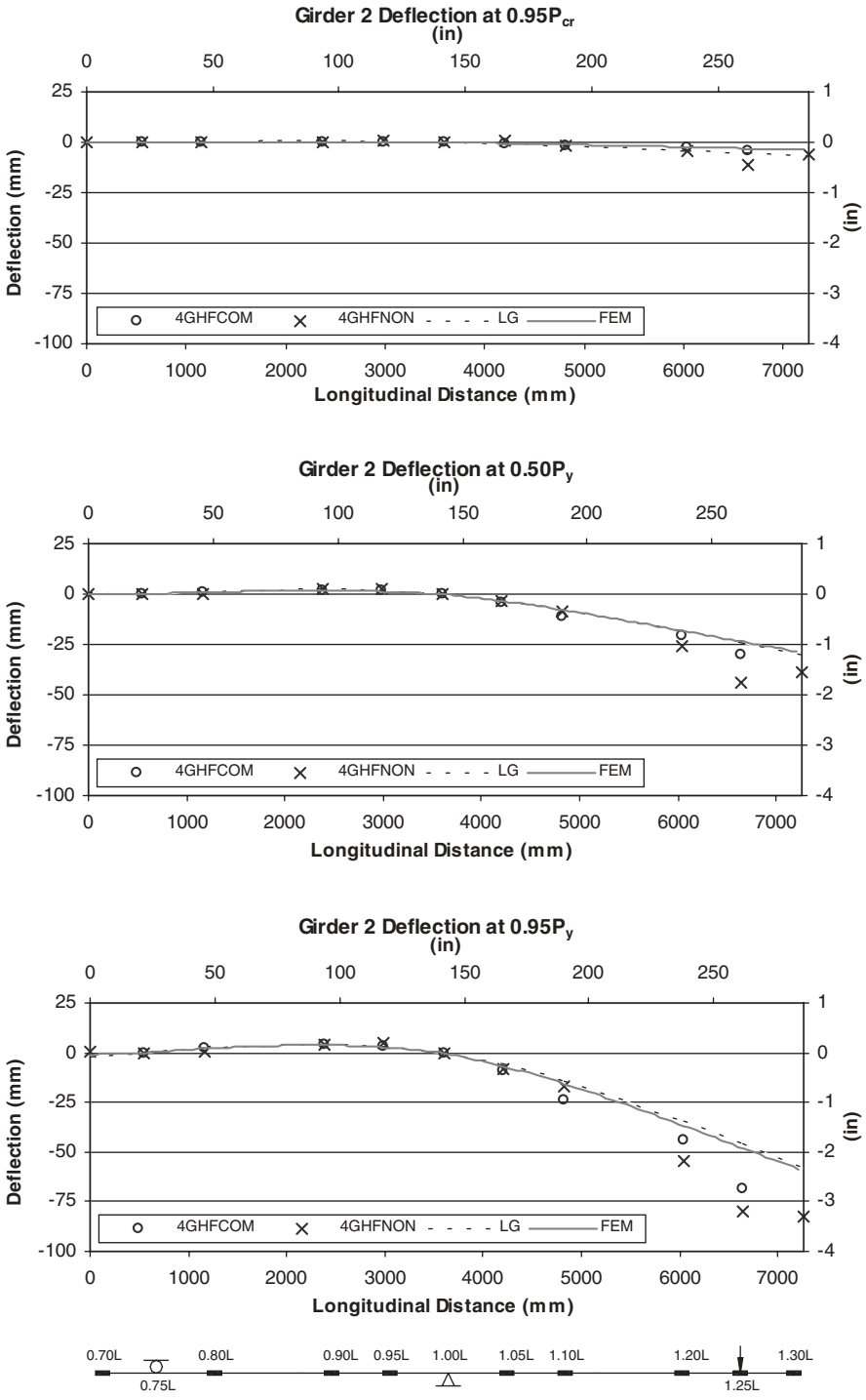

Figure 31. Comparative deflection profiles.

minimum yield strength of reinforcement should not be less than 420 MPa and a size not exceeding #19 (metric, #6 English) bars.

Prestressed deck should be considered when $S/t \geq 20$, which corresponds to the 4.8 m girder spacing. Prestressed deck was not considered as part of the basic parametric study but was considered as one of the special cases.

2.4.1.2 Girder Design

Guidelines employed for the girder design included the following:

- The minimum web plate thickness was assumed as 11 mm.

TABLE 3 Simple-span parametric study cases

Bridge ID	Parameter			L/S
	S (m)	L (m)	θ (degrees)	
SS-01	2.4	15	0	6.25
SS-03	4.8	15	0	3.125
SS-07	2.4	60	0	25
SS-09	4.8	60	0	12.5
SS-19	2.4	15	60	6.25
SS-21	4.8	15	60	3.125
SS-25	2.4	60	60	25
SS-27	4.8	60	60	12.5

TABLE 4 Multiple-span continuous parametric study cases

Bridge ID	Parameter				L_1/S
	S (m)	L_1 (m)	L_2/L_1	θ (degrees)	
CS-01	2.4	20	1.0	0	8.33
CS-03	4.8	20	1.0	0	4.17
CS-07	2.4	60	1.0	0	25
CS-09	4.8	60	1.0	0	12.5
CS-19	2.4	20	1.5	0	8.33
CS-21	4.8	20	1.5	0	4.17
CS-25	2.4	60	1.5	0	25
CS-27	4.8	60	1.5	0	12.5
CS-55	2.4	20	1.0	60	8.33
CS-57	4.8	20	1.0	60	4.17
CS-61	2.4	60	1.0	60	25
CS-63	4.8	60	1.0	60	12.5
CS-73	2.4	20	1.5	60	8.33
CS-75	4.8	20	1.5	60	4.17
CS-79	2.4	60	1.5	60	25
CS-81	4.8	60	1.5	60	12.5

- The minimum flange size was assumed as 19 mm × 300 mm.
- The Traditional Minimum Depth requirement was applied [AASHTO LRFD Table 2.5.2.6.3-1].
- Uniform depth was assumed for web design throughout the length of a bridge.
- The web was designed as partially stiffened, if applicable.
- For simply supported girders, girder transitions were located at 0.2L and 0.8L. For continuous girders, girder transitions were located approximately at 0.7L, 1.2L, 1.8L, and 2.3L.
- The top flange width was fixed for every design; heavier flange requirements were accommodated by varying thickness. The bottom flange width was changed only in negative moment regions.
- For positive moment regions, most of the girder sections were compact. For negative moment regions, noncompact sections (noncompact web) were used if applicable.
- Designs were fine-tuned to have the maximum performance ratio for the most critical limit state exceed 95 percent (except in some cases where the aforementioned minimum flange size of 19 mm × 300 mm was used).
- For skewed bridges, intermediate cross frames were oriented normal to the main members. Cross frames may be staggered or discontinuous across the bridge. Displacement-induced fatigue considerations should be investigated in such cases, but those considerations were not the focus of the present study.
- For shear in skewed bridges, the same web thickness was used for both right and skewed bridges sharing the same span lengths and girder spacings to avoid deviation of flexural effects if possible. Shear effects in any two such comparable bridges are not the same, however, because of the shear correction applied to the distribution factor for skewed bridges.

More details on the specifics of the industry guidelines and rules of thumb used to design the suite of bridges in the parametric study set, along with resulting girder section sizes and governing limit states, are provided in Appendix H.

2.4.2 Simple-Span Bridges

Finite element analyses of eight simple-span bridge configurations were conducted using the general-purpose finite element analysis software, ABAQUS. Configurations of all simple-span bridges are illustrated in Table 3. Bridges ranged from 15 to 60 m in span length, 2.4 to 4.8 m in girder spacing, and 0 to 60 degrees in skew angle at the supports. Most bridges were designed to have two flange transition points at $0.2L$ and $0.8L$, where L is the span length. Material properties are summarized in Table 5.

TABLE 5 Material properties for parametric study cases

Material	Description	Value
Steel	Elastic modulus, E_s	200 GPa
	Yield strength, F_y	345 MPa
Concrete	Elastic modulus, E_c	24.4 GPa
	Compressive strength, f'_c	28 MPa
Reinforcement	Elastic modulus, E_{rebar}	200 GPa
	Yield strength, f_y	420 MPa
Shear Connector	Elastic modulus, E_{sc}	200 GPa
	Yield strength, $f_{y,sc}$	345 MPa
	Ultimate strength, $f_{u,sc}$	420 MPa

All bridges were subjected to the nominal live load, which consists of HL-93 trucks and lane load, including impact effects. Both truck and lane loads were applied at the specific location to simulate the maximum positive moment condition. Longitudinally, the middle axle of the truck was located at mid-span of the bridge, while the trucks were placed transversely across the width to maximize the bending moment in either interior or exterior girders, whichever was the focus of interest.

Each simple-span bridge analysis can be subdivided into two categories at the Service II limit state:

- Interior girder, and
- Exterior girder.

Truck configurations are illustrated in Figure 32 for the interior girder loading and Figure 33 for the exterior girder loading. Distances between the front-to-middle axles and rear-to-middle axles were chosen to have the minimum of 4.3 m based on the code and the influence line principle for simple-spans. Additionally, lane load configurations are illustrated in Figures 34 and 35 for the interior girder and exterior girder loading, respectively. For the purpose of the parametric study, all bridges were analyzed up to the serviceability limit state (SERVICE II), which has the load combination of 1.0(DC1 & DC2 & DW) + 1.3(LL & IM). A limited number of Strength limit state cases were chosen randomly to verify that the serviceability limit states always governed the effective slab width values.

Effective Slab Width Variation Along the Span. The effective slab width values were computed along the span using the proposed definition for positive moment section. The results are summarized in Table 6. Figures 36 and 37 illustrate the effective slab width ratio variation (b_{eff}/b) and associated bending moment diagrams versus normalized span length (x/L) for simple-span bridges for interior and exterior girders, respectively. The values were determined based on the finite-element analysis results taken between a half width on one side and the other half width on the other side of the girder (interior) or the overhang width (exterior). The ending moments were calculated from element stresses and cross-sectional area. The circles on the plots represent the data points and were connected by straight lines. The series of numbers after the bridge ID contain the bridge configuration information. The three numbers are

- Girder spacing (m),
- Span length (m), and
- Skew angle (degree).

Thus, for bridge SS-19: 2.4/15/60 represents a bridge with 2.4-m-girder spacing, 15 m long, and 60-deg skew angle. Truck placement location is indicated in the diagram of each plot of b_{eff}/b.

The results show that a full slab width can be used as the effective slab width for all investigated right bridges. These encompass a L/S range of 3.125 to 25.

The SS-07 bridge has the highest L/S value among the four right bridges, hence the most flexural dominated structural behavior. Likewise, SS-09, with the second highest L/S value, exhibits similar behavior with the b_{eff}/b of 1.0 across the entire span length.

In the region close to the abutments, the support boundary conditions influenced the effective slab width ratio. The closer the section was to the end support, the smaller the effective slab width ratio tended to be. In most practical situations, there is significant excess flexural capacity as well near end supports. Thus the reduction in b_{eff}/b should not be of concern in such regions. The support effect becomes more prominent as the L/S values get smaller. For instance, the interior girder effective slab width ratios of the SS-03 bridge reduced below 1.0 further away from the supports than SS-01.

For the interior girder and highly skewed cases, three out of four bridges exhibited an effective slab width ratio of less than 1.0. The exception was the SS-25 bridge, which had a high L/S of 25 (see Figure 36). But where $b_{eff}/b < 1$ near midspan, the bending moment diagrams of short-span skewed bridges SS-19 and SS-21 extracted from FEM do not have the shape or magnitude used in the girder design based on line girder analysis. FEM-extracted moments in these bridges, as shown in Figure 36, were less than the moments that full truck axle loads produce in a line-girder analysis.

Table 7 compares the extreme fiber stresses with Service II Live Load (LL+IM), as computed by line-girder analysis (OPIS) and FEM, for comparable right and skewed configurations. As shown in the table, the line girder analysis significantly overestimated the girder flange stresses in the skewed bridges. This overestimation provided a source of conservatism in the very situations where a full effective width was not attained.

For short-span skewed bridges, the computed effective slab width ratios varied erratically along the span length. The effective slab width ratios at midspan of these short-span skewed bridges, the SS-19 and SS-21 bridges, were 0.90 and 0.93, respectively. These short bridges also had their flange sizes governed by the minimum flange size guideline rather

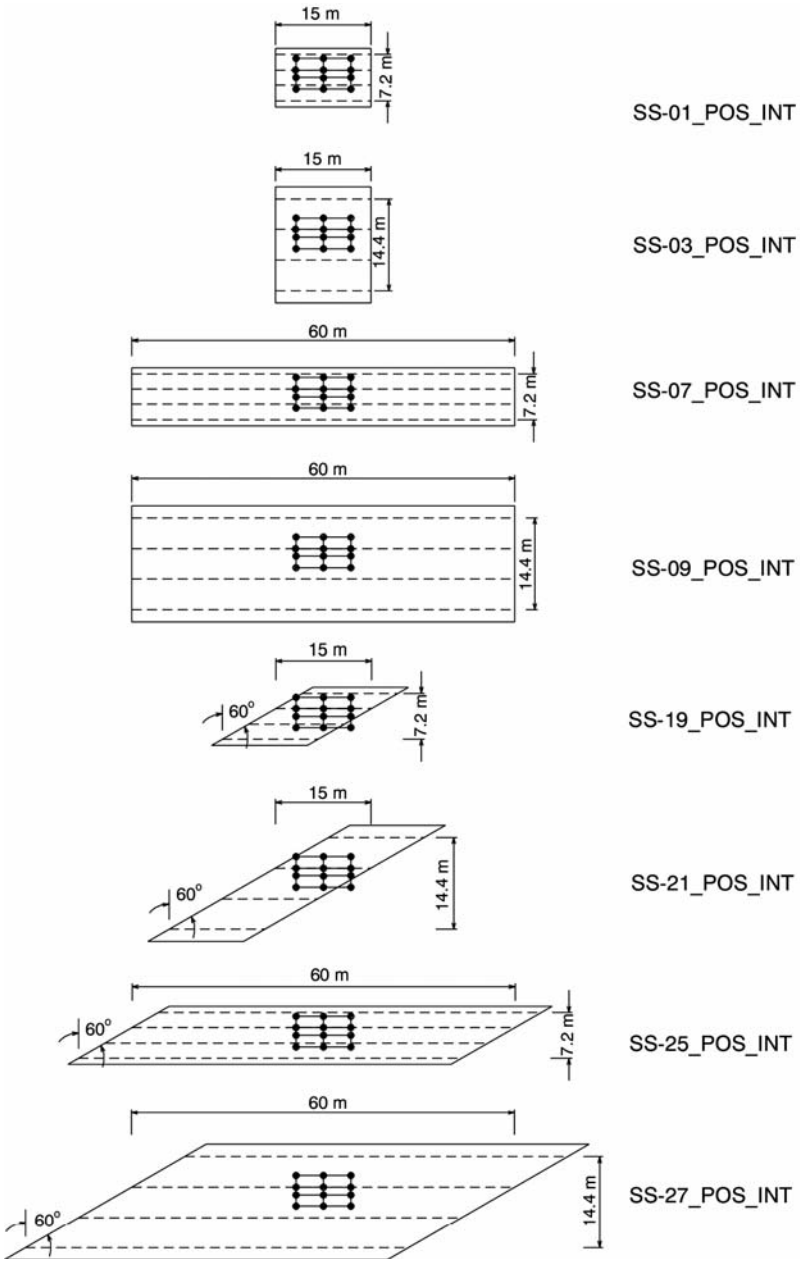

Figure 32. HL-93 truck configurations, simple span, interior girder, positive moment.

than by Service II or Strength I, as documented further in Appendix H.

For exterior girders, all four skewed bridges experienced the effective slab width slightly smaller than the full width (see Figure 37). Of these, however, SS-25 had the highest effective slab width ratio as expected because of flexural dominated behavior.

The results presented here are for Service II conditions. At Strength I loading levels, effective widths were always found from the FEM results to be equal or greater than the Service II effective widths, as expected. Representative results of this nature are provided in Appendix G.

2.4.3 Continuous Span Bridges

A total of 16 multiple-span continuous bridges, providing 64 subcases, were analyzed using ABAQUS. All these bridges are composed of four three-span continuous steel girders with conventional reinforced concrete slab. Bridge configurations

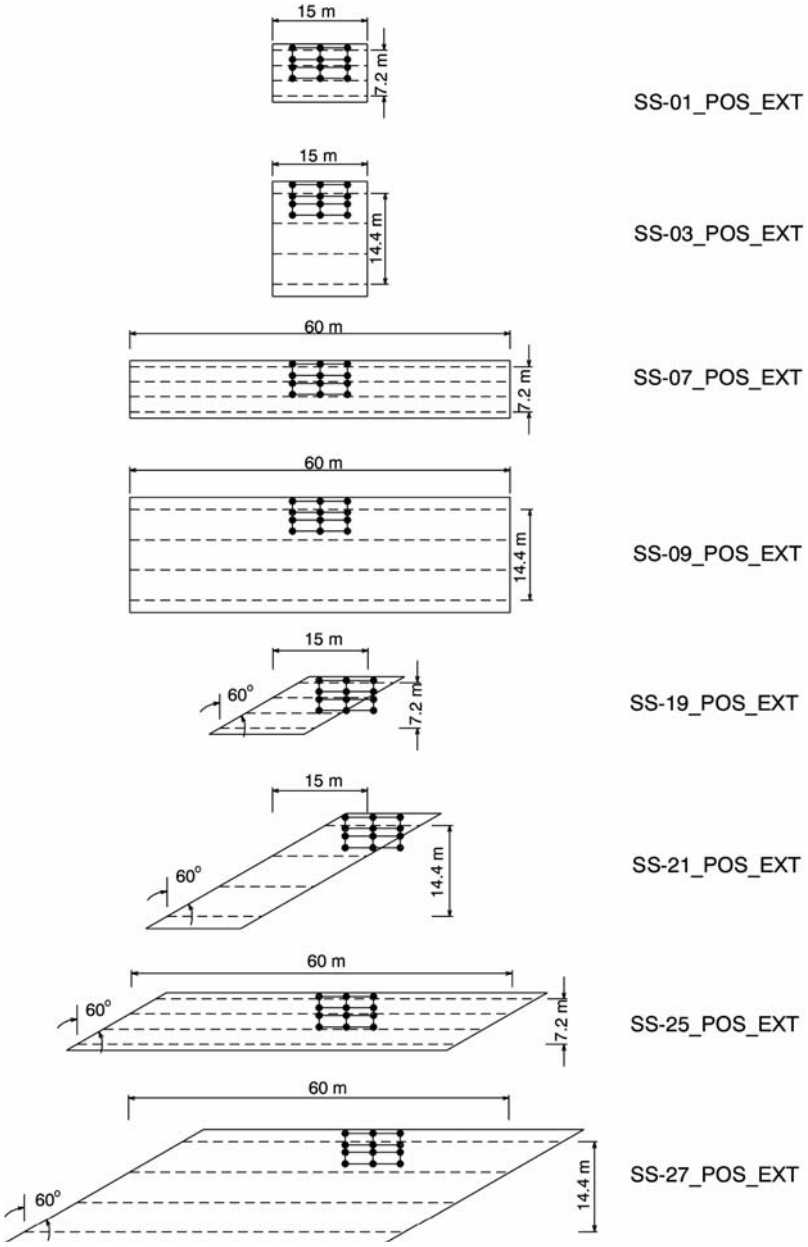

Figure 33. HL-93 truck configurations, simple span, exterior girder, positive moment.

are summarized in Table 4 with four different parameters—girder spacing (S), exterior span length (L_1), interior-to-exterior span ratio (L_2/L_1), and skew angle of the support (θ). Parameters range from 2.4 m to 4.8 m for girder spacing, 20 m to 60 m for exterior span length, 1.0 to 1.5 for interior-to-exterior span ratio, and 0 deg to 60 deg for skew angle. Each bridge analysis consisted of four subcases at the Service II limit state:

- Positive Moment, Interior girder;
- Positive Moment, Exterior girder;
- Negative Moment, Interior girder; and
- Negative Moment, Exterior girder.

For the positive moment loading, the truck middle axles were placed at $0.4L_1$ where L_1 was the exterior span length, with the rear axle facing the closest abutment (see Figures 38 through 41). Lane load for the positive moment loading cases was applied only on the exterior span where the trucks were located. In addition, selected bridges were loaded in the middle span only and subjected to the truck loading at $0.5L_2$ where L_2 was the interior span length. This was to simulate

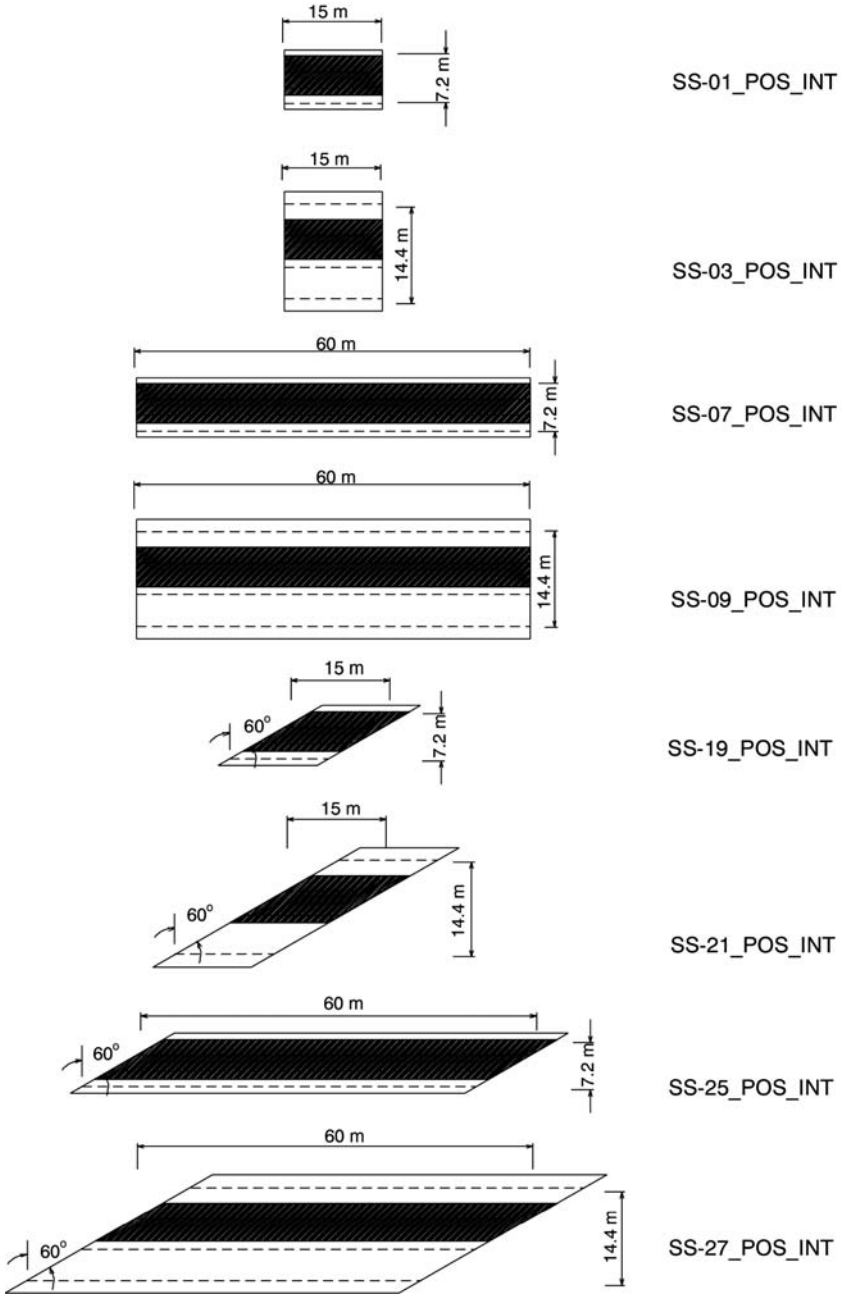

Figure 34. Lane load configurations, simple span, interior girder, positive moment.

the positive moment condition on Span 2. These cases were used for validating the results obtained by loading on Span 1.

For the negative moment loading, two truck middle axles were placed on the exterior span at $0.6L_1$ and the other two truck middle axles were placed at $1.4L_2$, where L_1 and L_2 were the exterior and interior span lengths, respectively. These locations were systematically chosen based on influence line concepts to maximize the negative bending moment at the interior support. All trucks' rear axles were facing the closest abutment as described for the positive moment loading. Truck configurations are illustrated in Figures 42 to 45. Similarly, lane load was applied on both spans where the trucks were located, that is Spans 1 and 2.

2.4.3.1 Positive Moment Section

Effective Slab Width Variation Along the Span. For positive moment loading on the exterior span (Span 1), some sections along the bridge experienced negative bending moment,

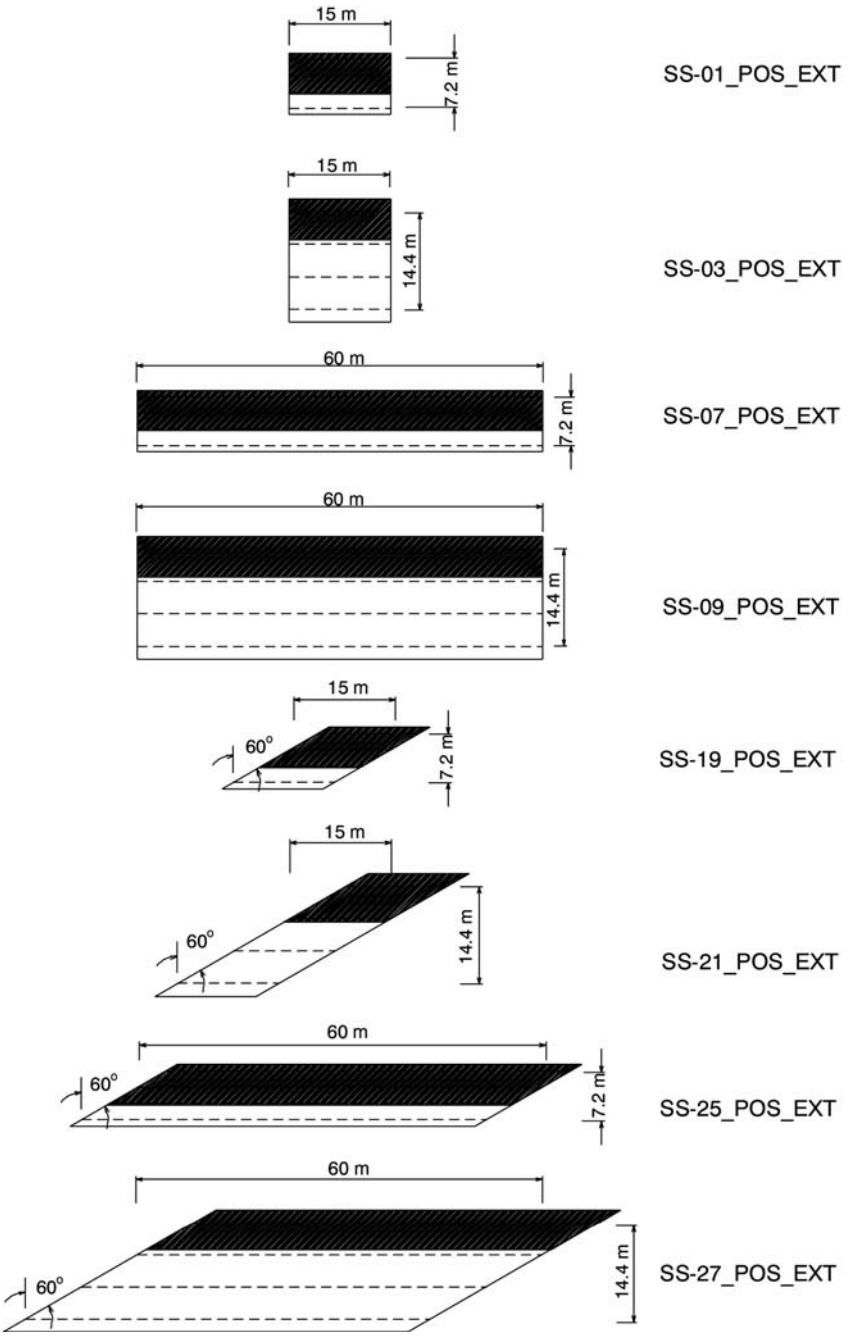

Figure 35. Lane load configurations, simple span, exterior girder, positive moment.

TABLE 6 Effective slab width ratio (b_{eff}/b) for simple-span bridges

Bridge ID	Interior Girder					Exterior Girder				
	0.40*L*	0.45 *L*	0.50 *L*	0.55 *L*	0.60 *L*	0.40 *L*	0.45 *L*	0.50 *L*	0.55 *L*	0.60 *L*
SS-01	1.00	1.00	1.00	1.00	1.00	1.00	1.00	1.00	1.00	1.00
SS-03	1.00	1.00	1.00	1.00	1.00	1.00	1.00	1.00	1.00	1.00
SS-07	1.00	1.00	1.00	1.00	1.00	1.00	1.00	1.00	1.00	1.00
SS-09	1.00	1.00	1.00	1.00	1.00	1.00	1.00	1.00	1.00	1.00
SS-14	1.00	1.00	1.00	1.00	1.00	0.98	0.97	0.95	0.97	0.98
SS-19	1.00	0.80	0.90	0.84	0.88	0.83	0.89	0.88	0.86	0.85
SS-21	0.85	0.80	0.93	0.81	0.81	0.80	0.75	0.80	0.78	0.78
SS-25	1.00	1.00	1.00	1.00	1.00	0.93	0.96	0.96	0.95	0.93
SS-27	0.95	0.92	0.94	0.94	0.94	0.80	0.81	0.92	0.83	0.80

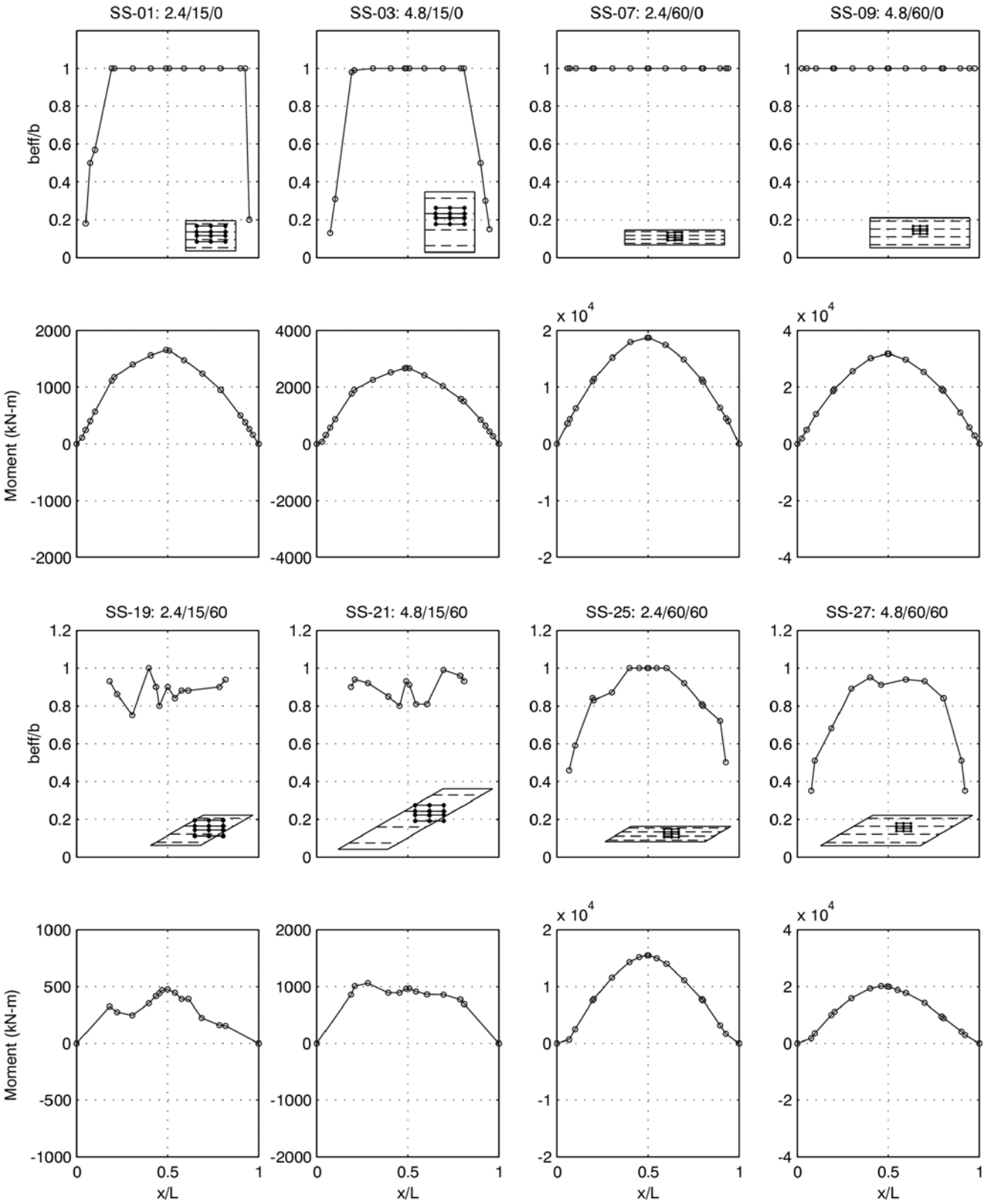

Figure 36. b_{eff}/b and bending moment versus x/L, simple span, interior girder, positive moment.

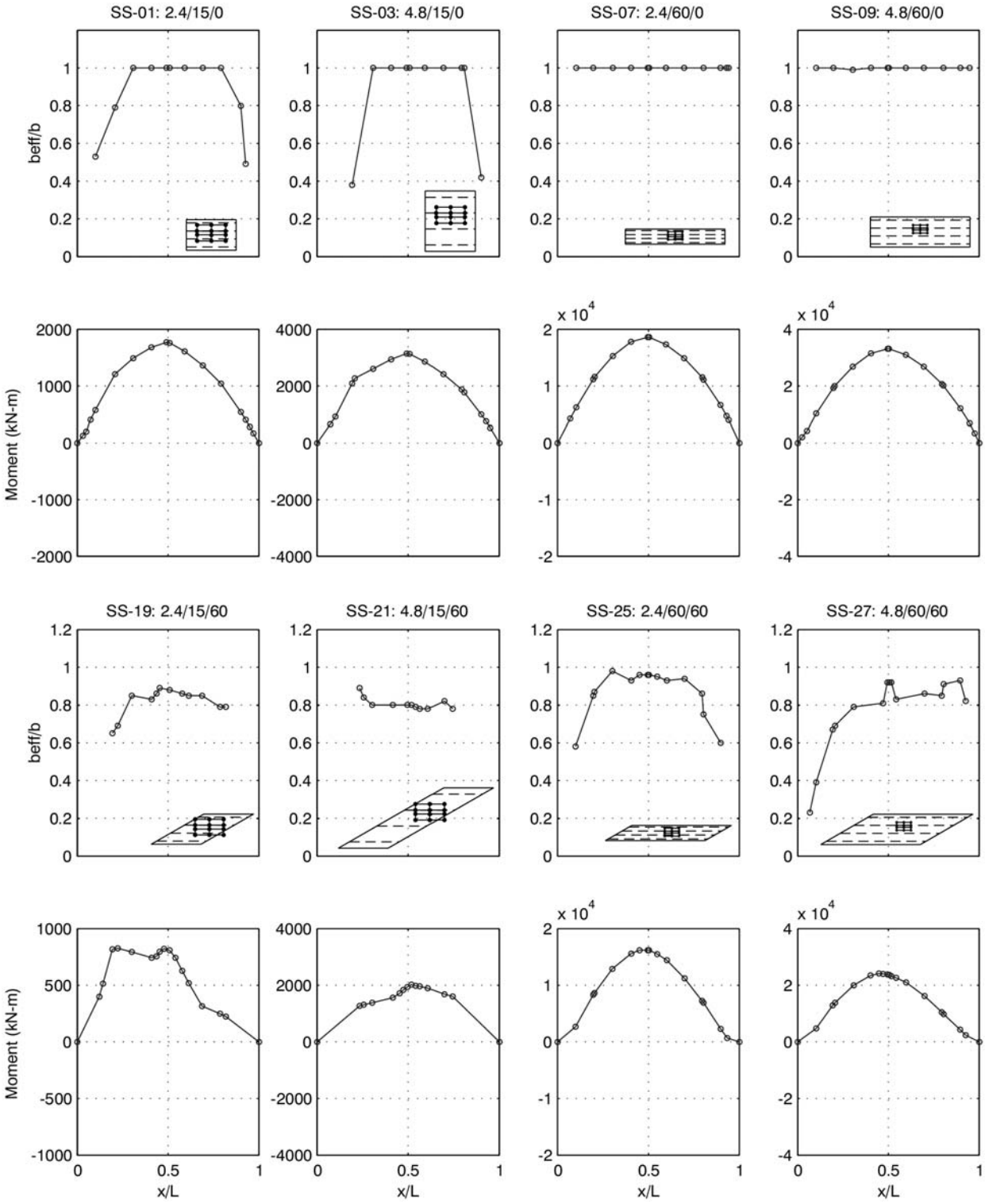

Figure 37. b_{eff}/b and bending moment versus x/L, simple span, exterior girder, positive moment.

TABLE 7 Comparison of 1.3(LL+IM) stresses in the bottom flange at 0.5L

Bridge	L (m)	S (m)	θ	Flange Stress in OPIS (MPa)	RF	Flange Stress in FEM (MPa)
SS-01	15	2.4	0	180.3	1.116	150
SS-09	60	4.8	0	86.8	1.423	60
SS-19	15	2.4	60	164.4	1.089	71
SS-27	60	4.8	60	93.23	1.171	48

especially the region near the interior pier. Hence, the effective slab width values were computed based on the proposed definitions for the positive and negative moments accordingly. In this section, the main focus will be on the positive moment section where the maximum positive bending moments take place. The variations of effective slab width ratio were plotted along the normalized span length between $0L_1$ and $1.1L_2$ in Figures 46 and 47 for the interior girder of right and skewed bridges, respectively. Similar plots for the exterior girders are illustrated in Figures 48 and 49. The associated bending moment diagrams are plotted. Numerical results are summarized in Table 8.

All right bridge results indicate that the full width can be used as the effective slab width for the critical positive moment

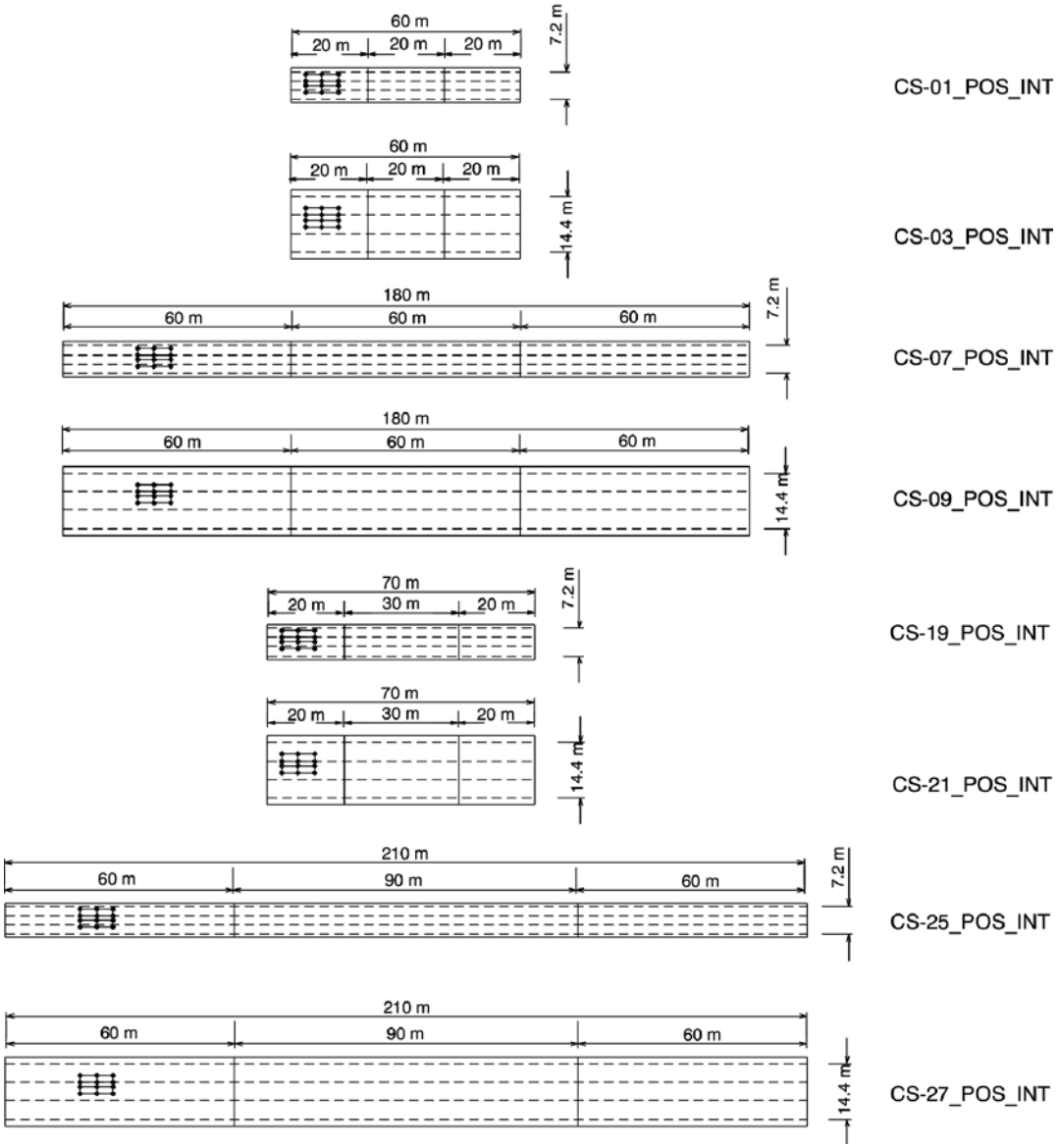

Figure 38. HL-93 truck configurations of the multiple-span continuous cases (right bridges, interior girder, positive moment).

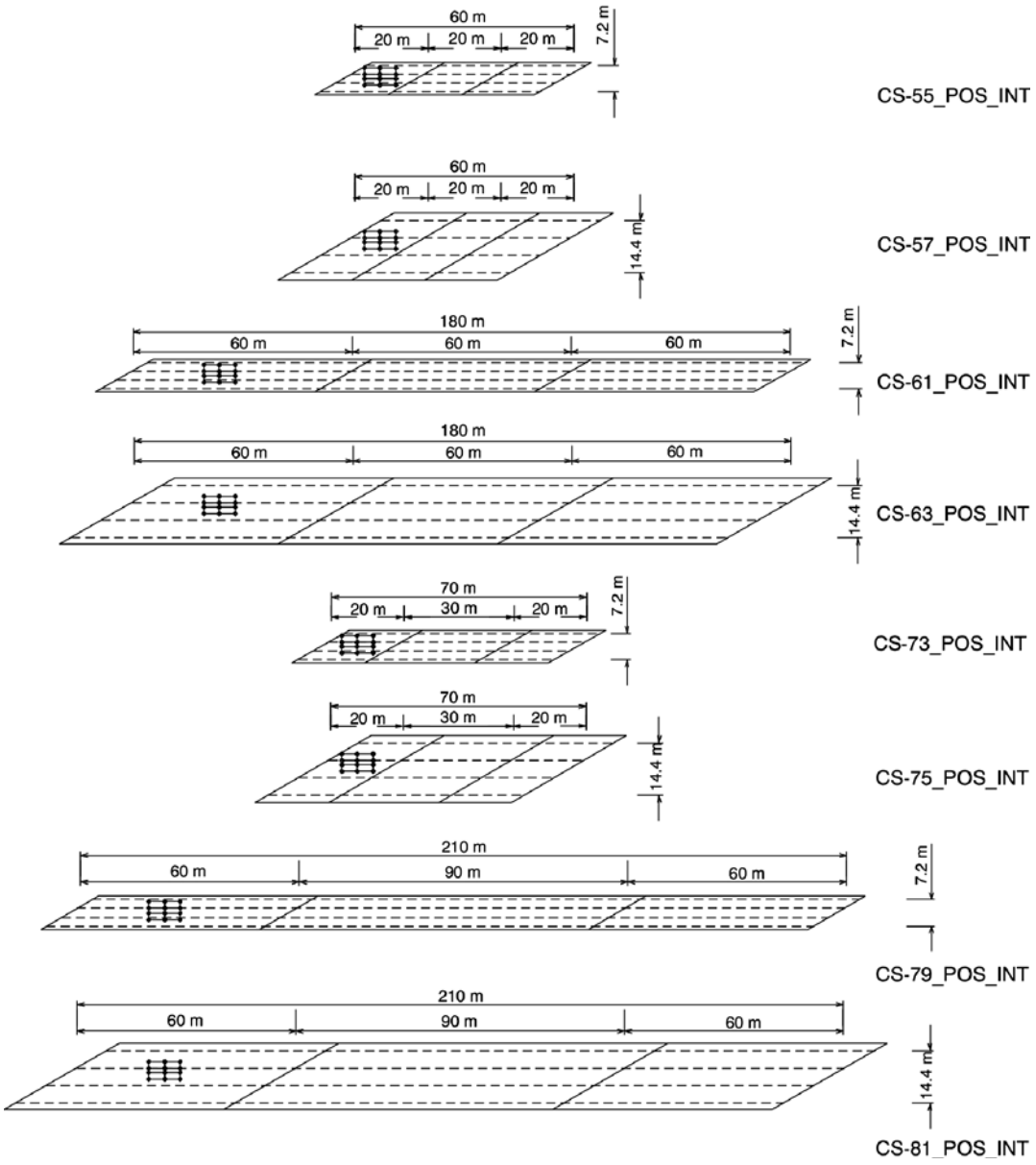

Figure 39. HL-93 truck configurations of the multiple-span continuous cases (skewed bridges, interior girder, positive moment).

section, at approximately $0.4L_1$ (see Figure 46). The reduction of the effective slab width occurs at the point of contraflexure where the transition of bending moment from positive to negative takes place. This phenomenon will be addressed more fully in the negative moment section discussion.

The variations of effective slab width ratio for the highly skewed bridges were rather chaotic. However, the effective slab width value associated with the maximum positive moment section was relatively close to 1.0. The exterior girders had more or less the same behavior as the interior girders in terms of effective slab width ratio (see Figures 48 and 49).

The case of loading on the interior span (Span 2) was also investigated. Eight selected cases were analyzed by subjecting the interior span to the live load that maximizes the positive bending moment of the interior girder. Figure 50 illustrates the effective slab width ratio variation along the normalized span length of all eight of these cases, i.e. CS-03, CS-07, CS-21, CS-25, CS-57, CS-61, CS-75 and CS-79. These cases were chosen to ensure all the extreme cases in terms of L_1/S were covered. All bridges experienced a full width as the effective slab width for positive moment in the middle span, except for CS-75. The result was very consistent with the exterior span loading case (see Figure G.48).

Bridge CS-75, like SS-19 and SS-21, had not only high skew but also short spans such that the flange sizes in the positive moment region were governed by the minimum flange

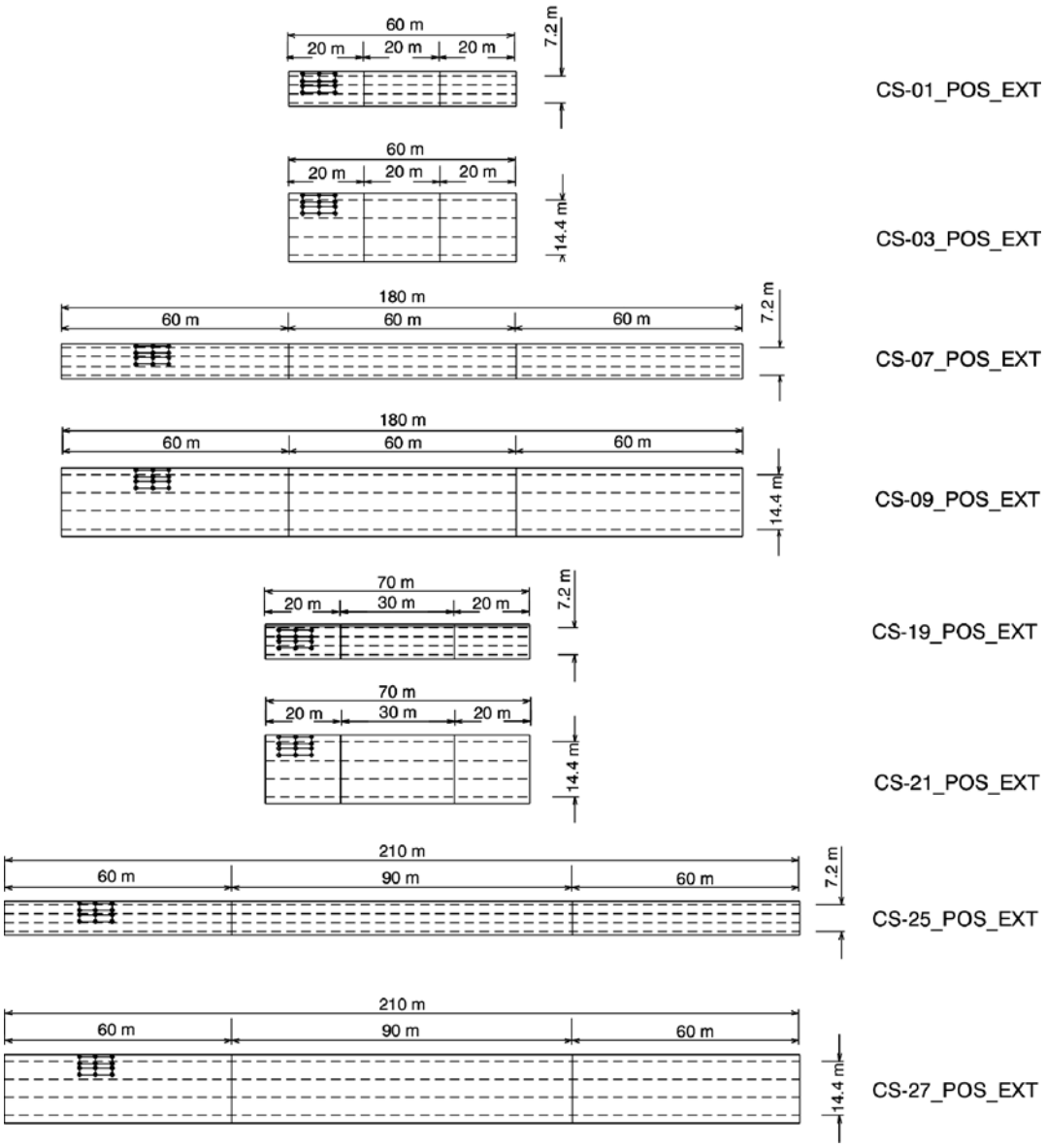

Figure 40. HL-93 truck configurations of the multiple-span continuous cases (right bridges, exterior girder, positive moment).

size guideline rather than by Service II or Strength I, as documented further in Appendix H.

2.4.3.2 Negative Moment Section

This section focuses on the region close to the interior pier where the negative moment is maximized. Many issues arise under the investigation of the negative moment section and will be explored more fully as the discussion progresses.

Effective Slab Width Variation Along the Span. Figures 51 and 52 demonstrate how the effective slab width ratios of the interior girder varied in the region close to the interior pier, $1.0L_1$. Almost every right bridge experienced full width as the effective slab width. The sole exception was the CS-03 bridge. For skewed bridges, a few cases had the effective slab width smaller than 1.0. In addition, the bending moment diagrams associated with these skewed bridges deviated from the line-girder analysis results as with skewed simple-span bridges. Moments extracted from FEM in such cases were considerably less than those obtained from line-girder analysis. The location of truck placement could have had a major influence on the computed effective slab width ratios, especially in the short and high skewed bridge (see Figure 52). Similar plots of the exterior girder are illustrated in Figures 53 and 54. All exterior girder cases, except the CS-03 bridge, experienced a full width as the effective slab width. Numerical results are summarized in Table 9.

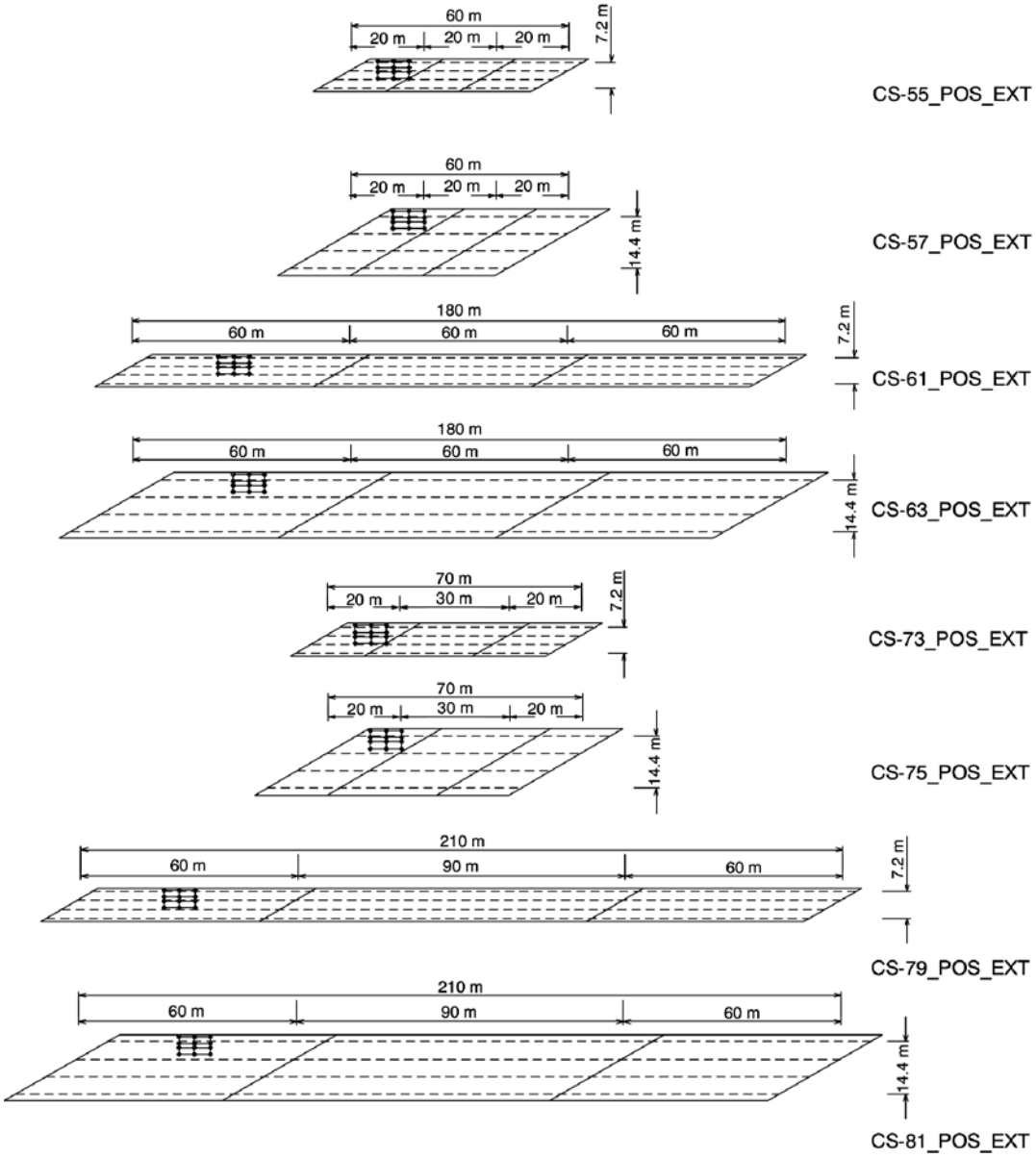

Figure 41. HL-93 truck configurations of the multiple-span continuous cases (skewed bridges, exterior girder, positive moment).

Uncracked Versus Cracked Sections. From the result of the investigation using the new effective slab width definition for the negative moment section, the concrete slab can be divided into two categories: uncracked and cracked. There are major distinctions between the two slab types, which in turn affect how much of the slab contributes to resisting tensile stresses.

An uncracked slab section is an intact condition of the concrete slab that is subjected to tensile stresses below the concrete tensile strength. Both concrete and rebars are working together and sharing tensile forces accordingly. At low stress levels, this gives a smaller effective slab width. Once cracks initiate, tensile stresses would be redistributed in the uncracked portion of the slab and result in the larger effective slab width. As soon as the entire slab reaches the concrete tensile strength, the slab becomes a cracked section. Forces start to transfer from slab to rebars, which pushes the effective slab width wider until the full slab width is reached.

As for the positive moment region, the results presented here are for Service II conditions. At Strength I loading levels, effective widths were always found from the FEM results to be equal to or greater than the Service II effective widths, as expected. Representative results of this are provided in Appendix G.

2.4.4 Summary of FEM Parametric Study

FEM results showed the following:

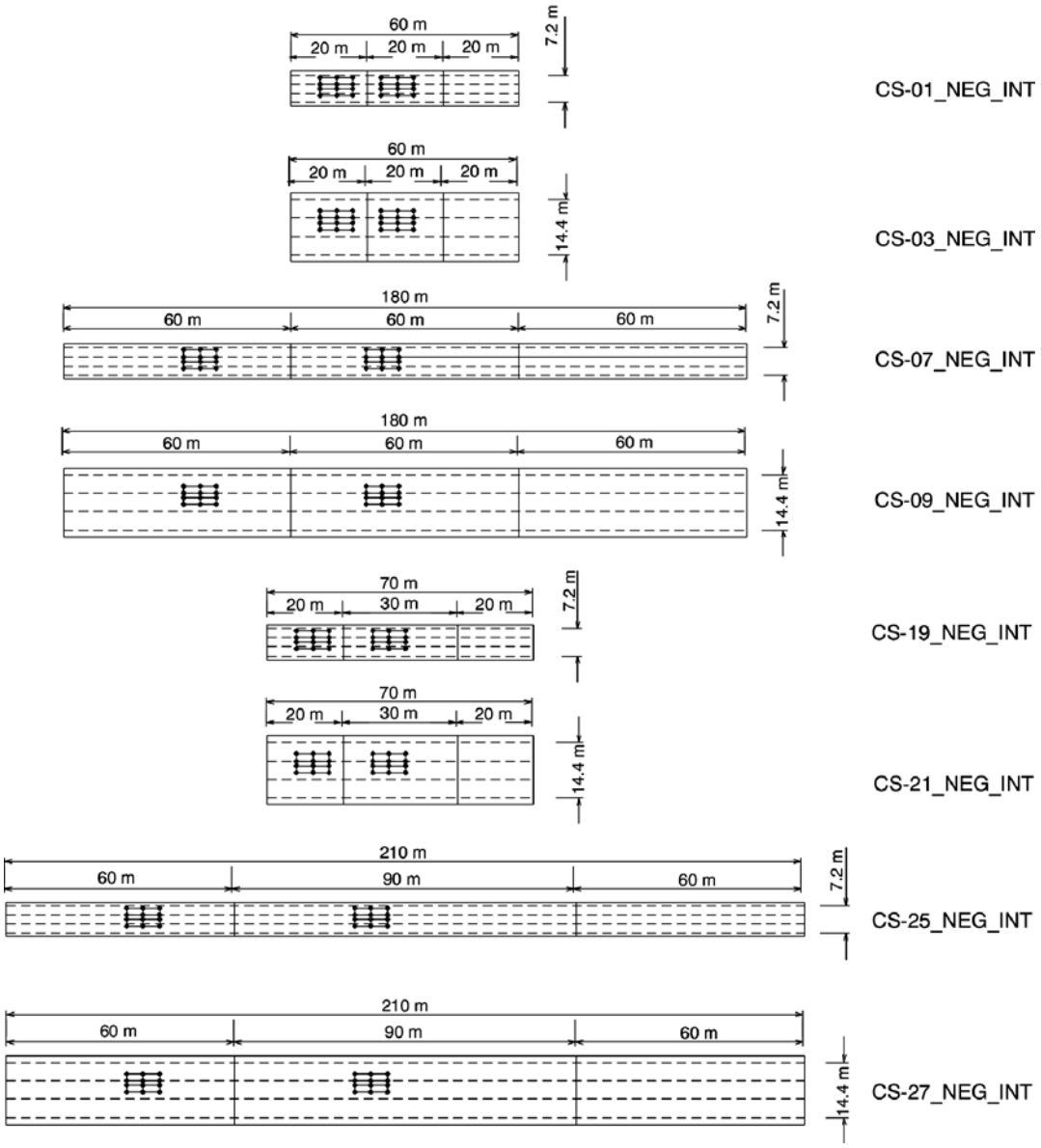

Figure 42. HL-93 truck configurations of the multiple-span continuous cases (right bridges, interior girder, negative moment).

- Full width was typically acting at cross sections where it was most needed, i.e., where moments and hence performance ratios would be highest.
- Where the effective width was less than full width at such cross sections, those cross sections had considerable excess flexural capacity.

2.5 SPECIAL CASE BRIDGES

Special cases such as cable-stayed and prestressed girder bridges typically confirmed the trends observed in the parametric study reported above, although girder spacings wider than 4.8 m were beyond the realm of the parametric study. For the purpose of this study, special case bridges were divided into Cable-Stayed Bridges and Validation Cases.

2.5.1 Cable-Stayed Bridge Investigation

This section summarizes the investigation of effective slab width in cable-stayed bridges. Further detail on the cable-stayed investigation is provided in Appendix I.

2.5.1.1 Cable-Stayed Bridges Investigated

Five cable-stayed bridges were investigated, four of them having been analyzed previously by Byers (1999). The fifth

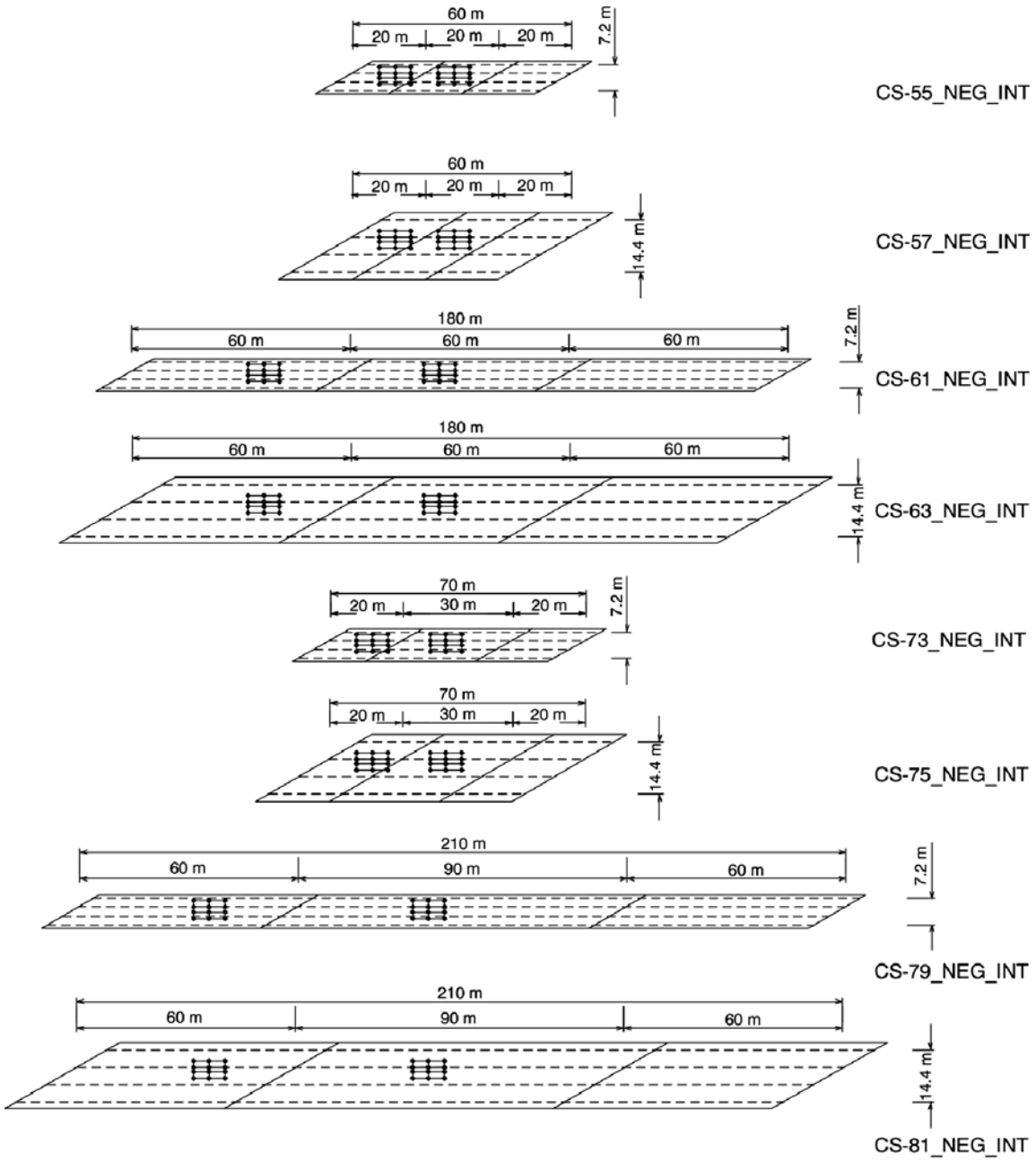

Figure 43. HL-93 truck configurations of the multiple-span continuous cases (skewed bridges, interior girder, negative moment).

bridge analyzed was the Cooper River Bridge. All had two edge girders on a cross section, two pylons, and a semi-harp cable configuration with two planes of cables. Table 10 and Figure 55 summarize principal dimensional differences among the bridges investigated.

The first number in the bridge designation (e.g., "8" in "8_15") indicates the number of cables on each side of the tower. The second number indicates the distance from the centerline (CL) of the slab to the centerline of the edge girder in meters.

2.5.1.2 Two-Level Modeling Scheme

Each structure was modeled on a "global" and a "substructure" or "local" level. The former takes into account the behavior of the bridge as a whole, while the latter focuses on parts of the structure with a more detailed model and assesses how the bridge performs under the loads considered.

There were four global models, one for each bridge. The solution obtained for the global model was used as input to the local model of the structure where a part of the bridge

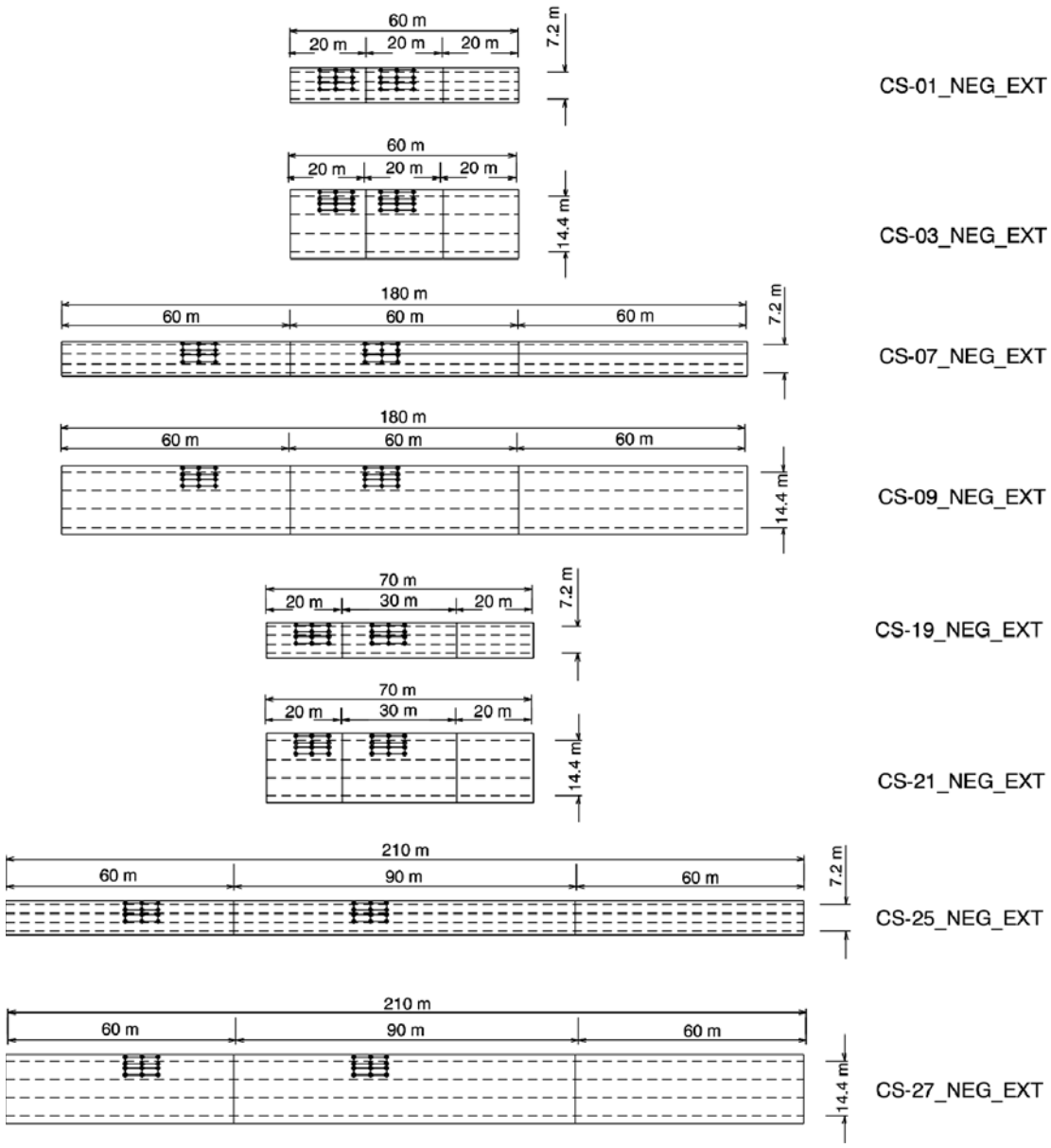

Figure 44. HL-93 truck configurations of the multiple-span continuous cases (right bridges, exterior girder, negative moment).

between two cables was modeled in greater detail. In this way the stresses in the composite cross-section could be obtained, and the effective width could be computed. Only dead load was applied.

Global Models. Figure 55 shows the element types used in the global models. All materials were considered linear-elastic. The structural elements were modeled as follows. The deck was modeled as a thick plate (each element had width and length not significantly higher than the thickness) at the level of its mid-surface. The cables were modeled as truss elements. The beams (floor beams and girders) and the towers were discretized into 3-D beam elements along their centroidal axes. There were "rigid" beam link elements connecting the deck to the floor beams; two edge girders and no middle girder existed in each model.

The cable areas were such that they all provided approximately the same vertical stiffness. The towers were considered to be fixed at their bases. Each linear element (e.g., beam or tower) was located at the equivalent member's centroidal axis. The concept of rigid linear elements was used to ensure that members that were connected shared common displacements. Part of a global bridge model (8_8) is shown in Figure 56.

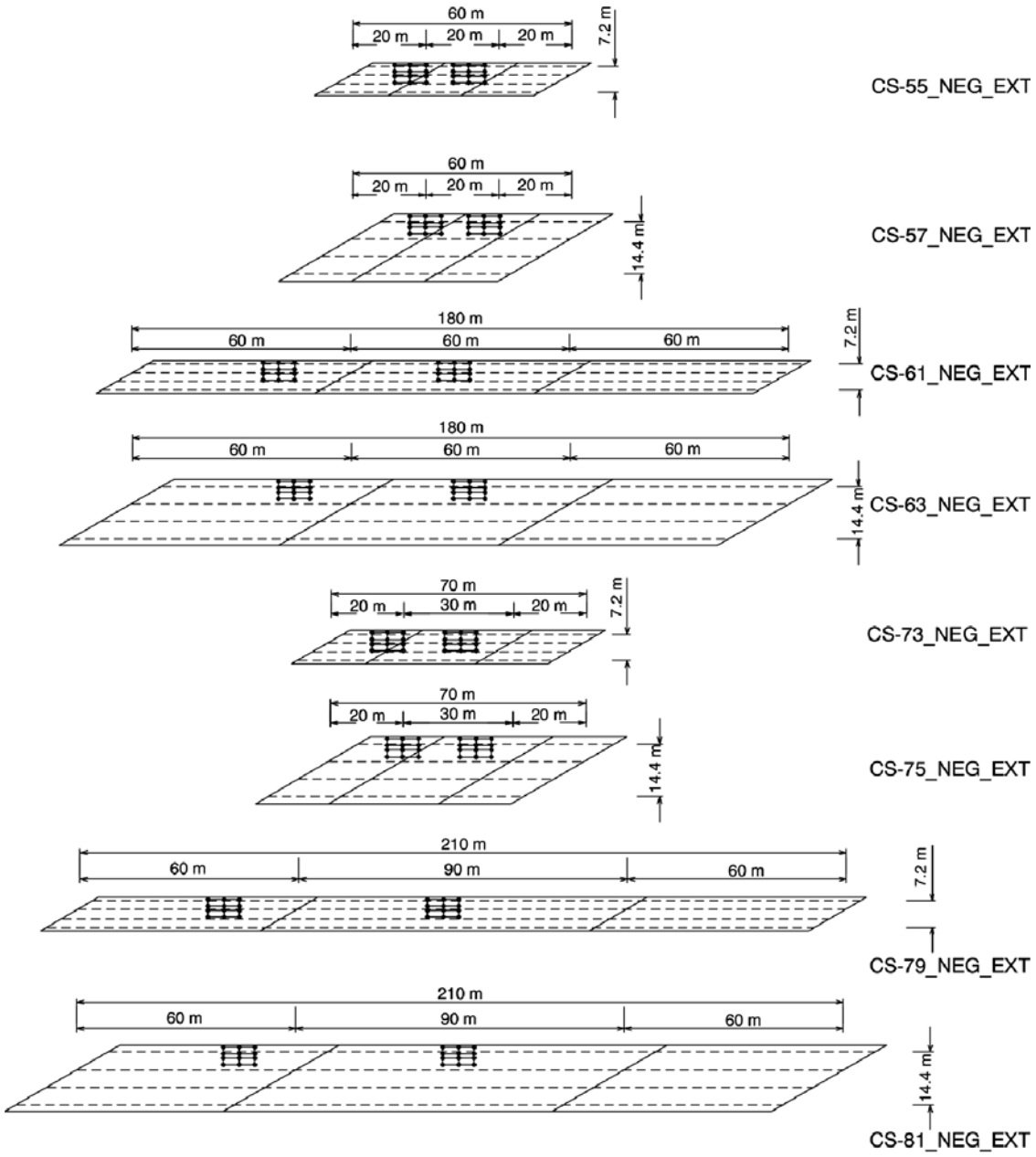

Figure 45. HL-93 truck configurations of the multiple-span continuous cases (skewed bridges, exterior girder, negative moment).

Local Models. Each local model represented the part of the structure lying between two adjacent cables. The floor beams and the girders shared common nodes at the points where they met given that those points were connected and should have had the same displacements. The cable-stayed local models had the same level of detail as the models used in the parametric study, except that deck rebar was neglected. The slab, for example, was divided into four layers.

The material properties and beam dimensions were the same as those given in the description of the global models. All the elements were 3-D eight-noded solid elements (C3D8 in ABAQUS notation). Concrete was used for the slab. Steel was used for the beams.

2.5.1.3 Cable-Stayed Bridge Results

Results were categorized on the basis of which of three regions along the bridge they were in:

- Type I (positive moment and low axial force regions close to the center of the main span),

(*text continued on p. 47*)

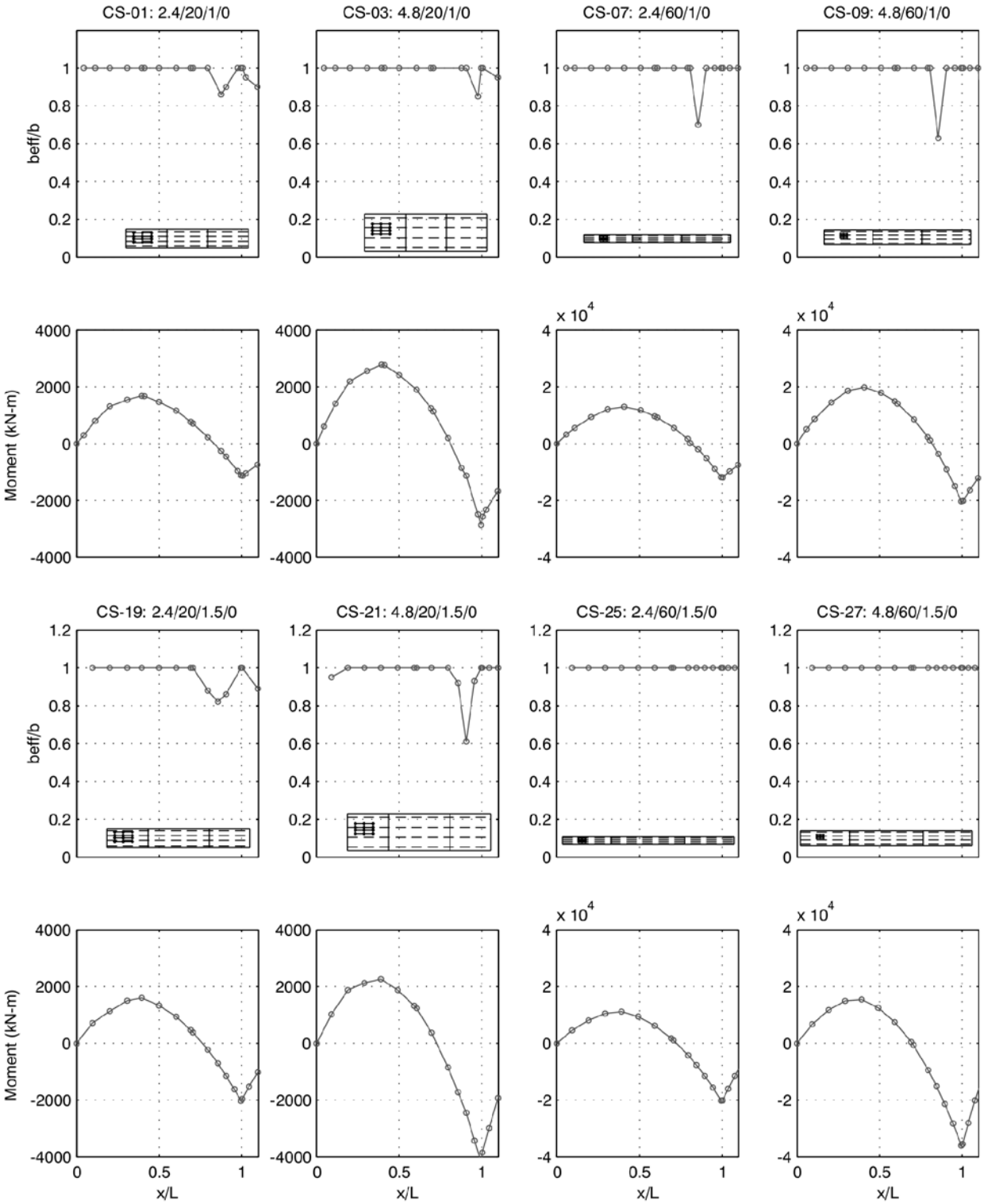

Figure 46. b_{eff}/b and bending moment versus x/L for the multiple-span continuous cases (right bridges, interior girder, positive moment, Service II).

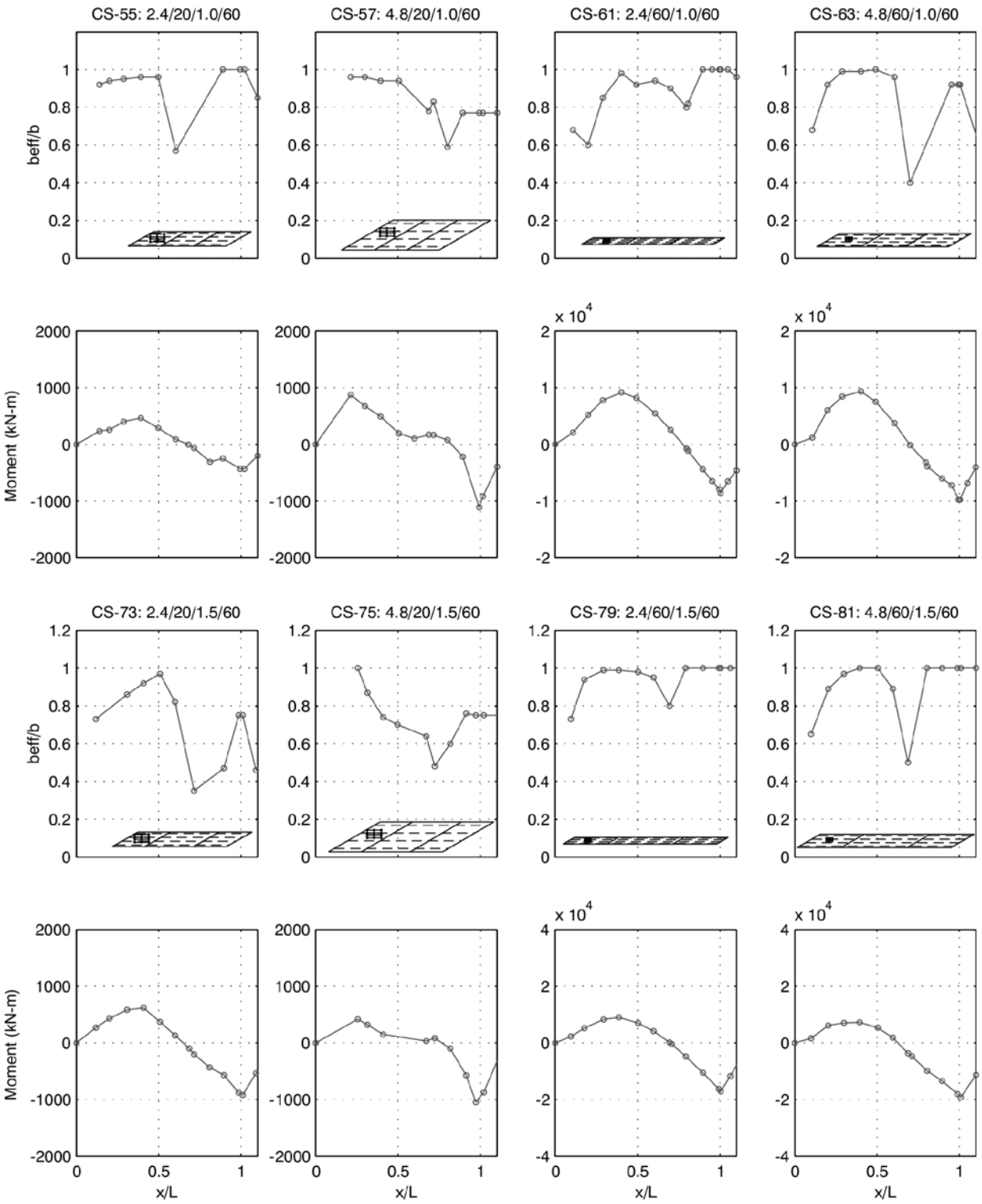

Figure 47. b_{eff}/b and bending moment versus x/L for the multiple-span continuous cases (skewed bridges, interior girder, positive moment, Service II).

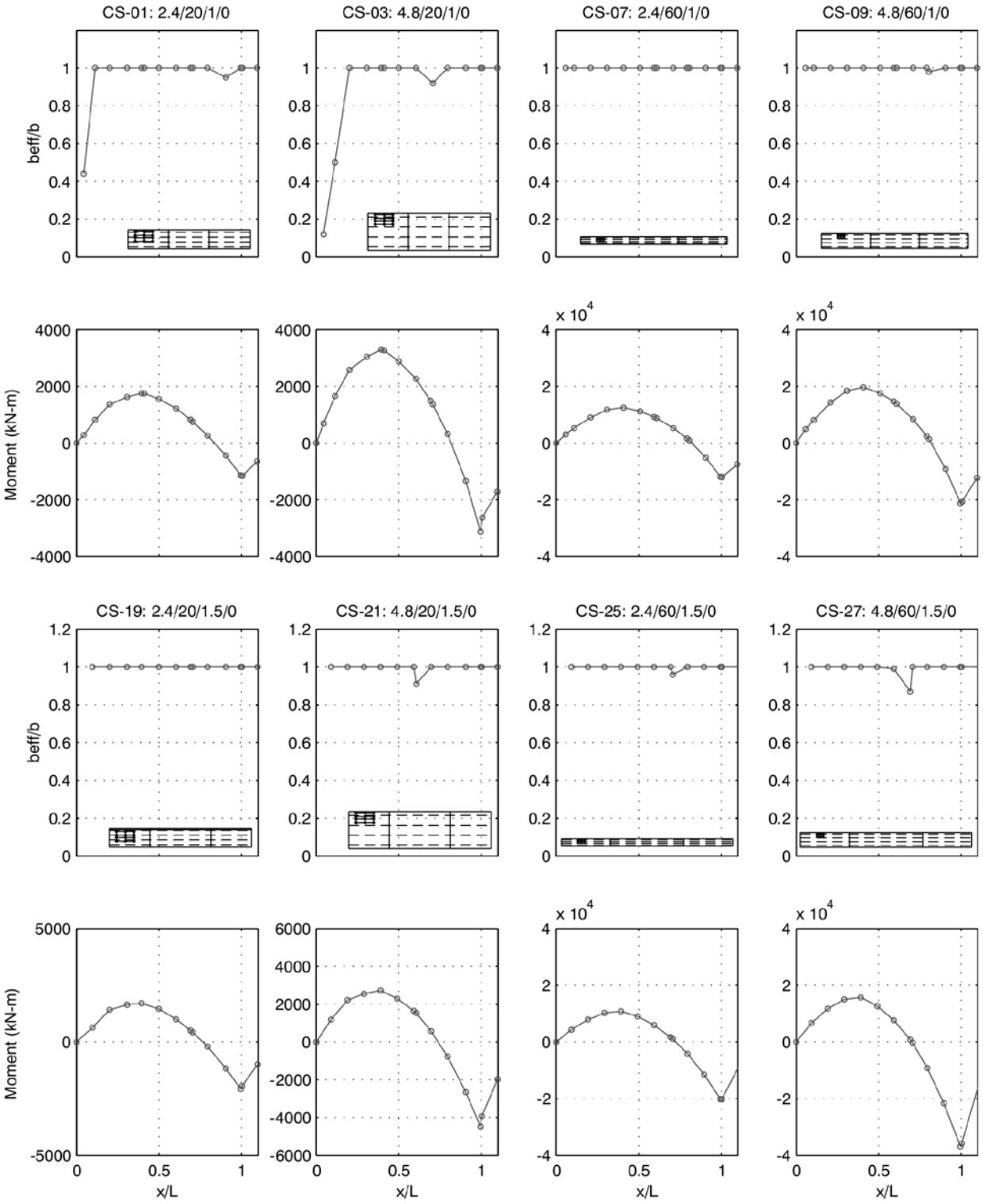

Figure 48. b_{eff}/b and bending moment versus x/L for the multiple-span continuous cases (right bridges, exterior girder, positive moment, Service II).

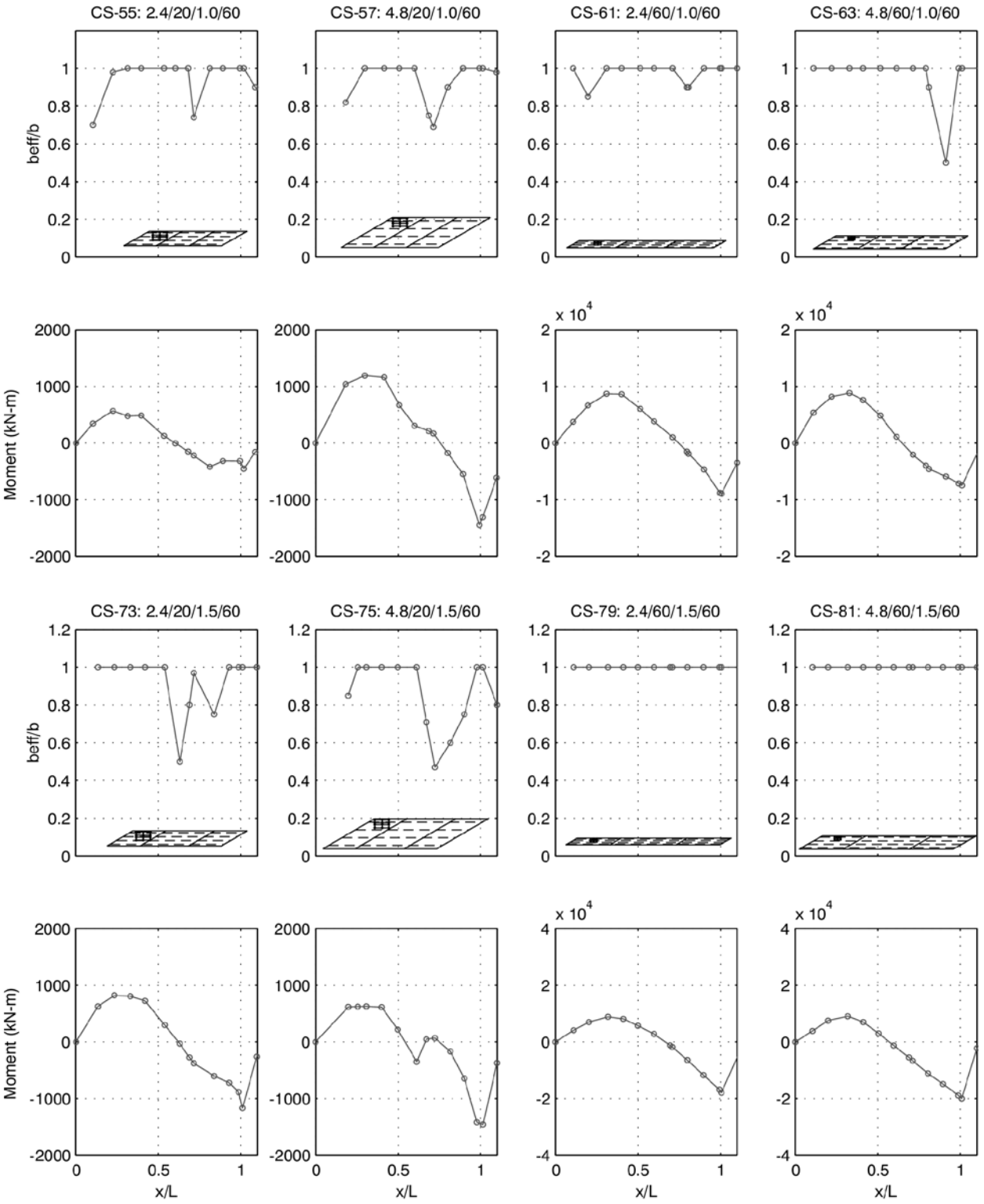

Figure 49. b_{eff}/b and bending moment versus x/L for the multiple-span continuous cases (skewed bridges, exterior girder, positive moment, Service II).

TABLE 8 Effective slab width ratio (b_{eff}/b) for multiple-span continuous bridges (positive moment)

Bridge ID	Interior Girder					Exterior Girder				
	$0.3L_1$	$0.35\ L_1$	$0.4\ L_1$	$0.45\ L_1$	$0.5\ L_1$	$0.3L_1$	$0.35\ L_1$	$0.4\ L_1$	$0.45\ L_1$	$0.5\ L_1$
CS-01	1.00	1.00	1.00	1.00	1.00	1.00	1.00	1.00	1.00	1.00
CS-03	1.00	1.00	1.00	1.00	1.00	1.00	1.00	1.00	1.00	1.00
CS-07	1.00	1.00	1.00	1.00	1.00	1.00	1.00	1.00	1.00	1.00
CS-09	1.00	1.00	1.00	1.00	1.00	1.00	1.00	1.00	1.00	1.00
CS-19	1.00	1.00	1.00	1.00	1.00	1.00	1.00	1.00	1.00	1.00
CS-21	1.00	1.00	1.00	1.00	1.00	1.00	1.00	1.00	1.00	1.00
CS-25	1.00	1.00	1.00	1.00	1.00	1.00	1.00	1.00	1.00	1.00
CS-27	1.00	1.00	1.00	1.00	1.00	1.00	1.00	1.00	1.00	1.00
CS-41	1.00	1.00	1.00	1.00	1.00	1.00	1.00	1.00	1.00	1.00
CS-55	0.95	0.95	0.96	0.96	0.96	1.00	1.00	1.00	1.00	1.00
CS-57	0.96	0.95	0.94	0.94	0.94	1.00	1.00	1.00	1.00	1.00
CS-61	0.85	0.92	0.98	0.95	0.92	1.00	1.00	1.00	1.00	1.00
CS-63	0.99	0.99	0.99	0.99	1.00	1.00	1.00	1.00	1.00	1.00
CS-73	0.86	0.89	0.92	0.95	0.97	1.00	1.00	1.00	1.00	1.00
CS-75	0.87	0.81	0.74	0.72	0.70	1.00	1.00	1.00	1.00	1.00
CS-79	0.94	0.95	0.96	0.95	0.98	1.00	1.00	1.00	1.00	1.00
CS-81	0.97	0.99	1.00	1.00	1.00	1.00	1.00	1.00	1.00	1.00

- Type II (positive moment and high axial force regions close to the support of the main span), and
- Type III (negative moment and high axial force regions very close to the tower).

Figure 57 shows the transverse distribution of normal slab stresses in a Type I region, while Figures 58 and 59 show slab stresses in Type II and Type III regions, respectively. These were for the 8_15 and 12_15 bridges. Analogous distributions were also observed for the Cooper River Bridge, as shown in Figures 60 and 61. Some shear lag was evident in these figures, but substantial effective widths were realized anyway—considerably beyond the 4.8-m girder spacing maximum investigated in the parametric study presented earlier.

Table 11 summarizes the values of effective width extracted from all three regions of all five cable-stayed bridges analyzed. As in the main parametric study, the short wide bridge (Bridge 8_15) had the smallest effective width.

Figures 62 through 72 show the variation of effective width ratio b_{eff}/b along the length in representative regions of the first four bridges. Figure 73 shows the variation of effective width ratio along the length of the main span in the Cooper River Bridge. Results from Cooper River were similar to those obtained from the other four bridge models.

2.5.2 Validation Cases

The remaining bridges analyzed included the following in addition to steel multi-girder bridges with geometric parameters beyond those of the parametric study presented earlier:

- Two-girder continuous steel girder bridges with both cast-in-place and prestressed deck slabs and very wide (7.68-m) girder spacing,
- A continuous hybrid steel girder bridge,
- Simply-supported and continuous tub-girder bridges, and
- Simply-supported and continuous prestressed bulb-tee girder bridges.

Full effective slab width was obtained for all these cases. Further details on the validation cases appear in Appendix J.

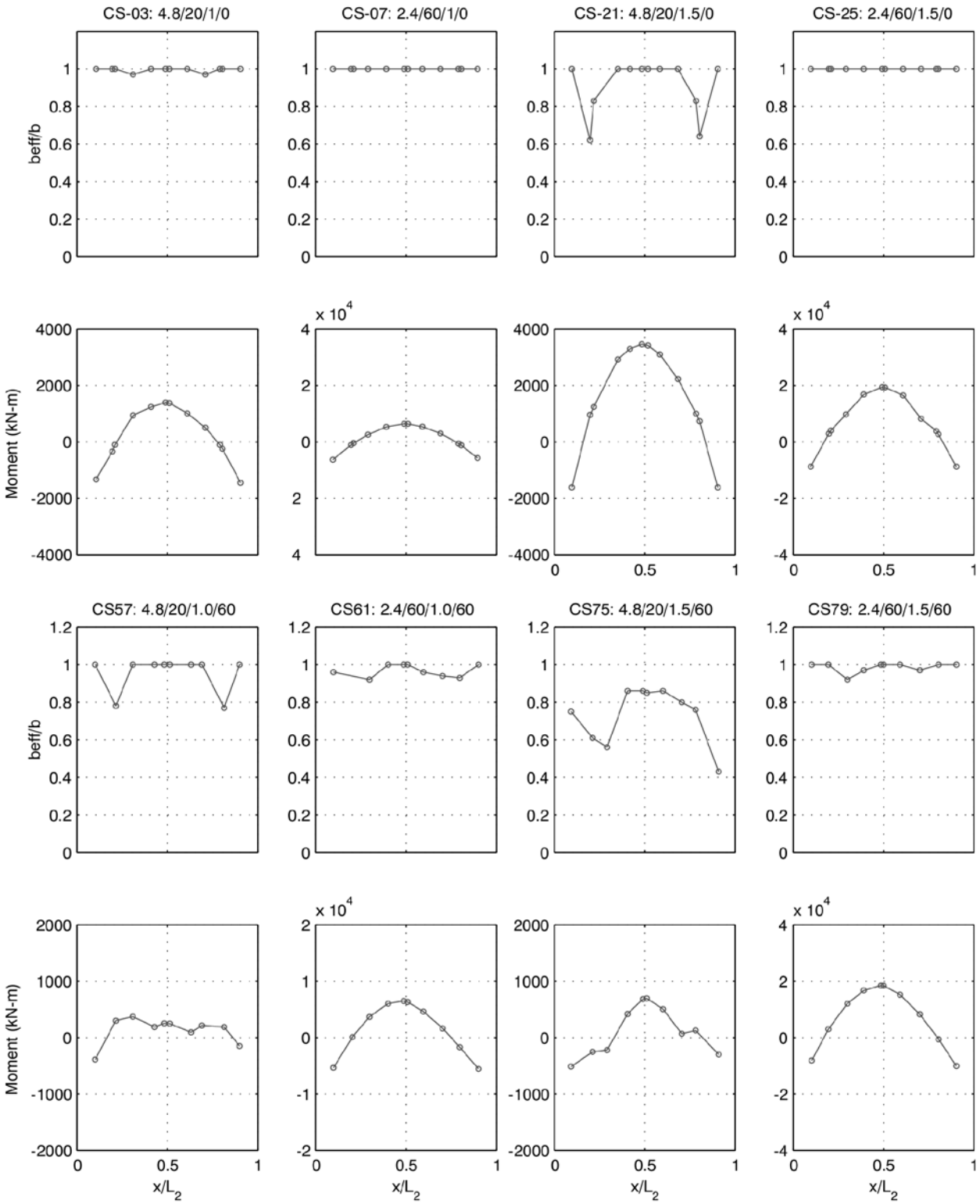

Figure 50. b_{eff}/b and bending moment versus x/L for the multiple-span continuous cases (Span 2 loading, interior girder, positive moment, Service II).

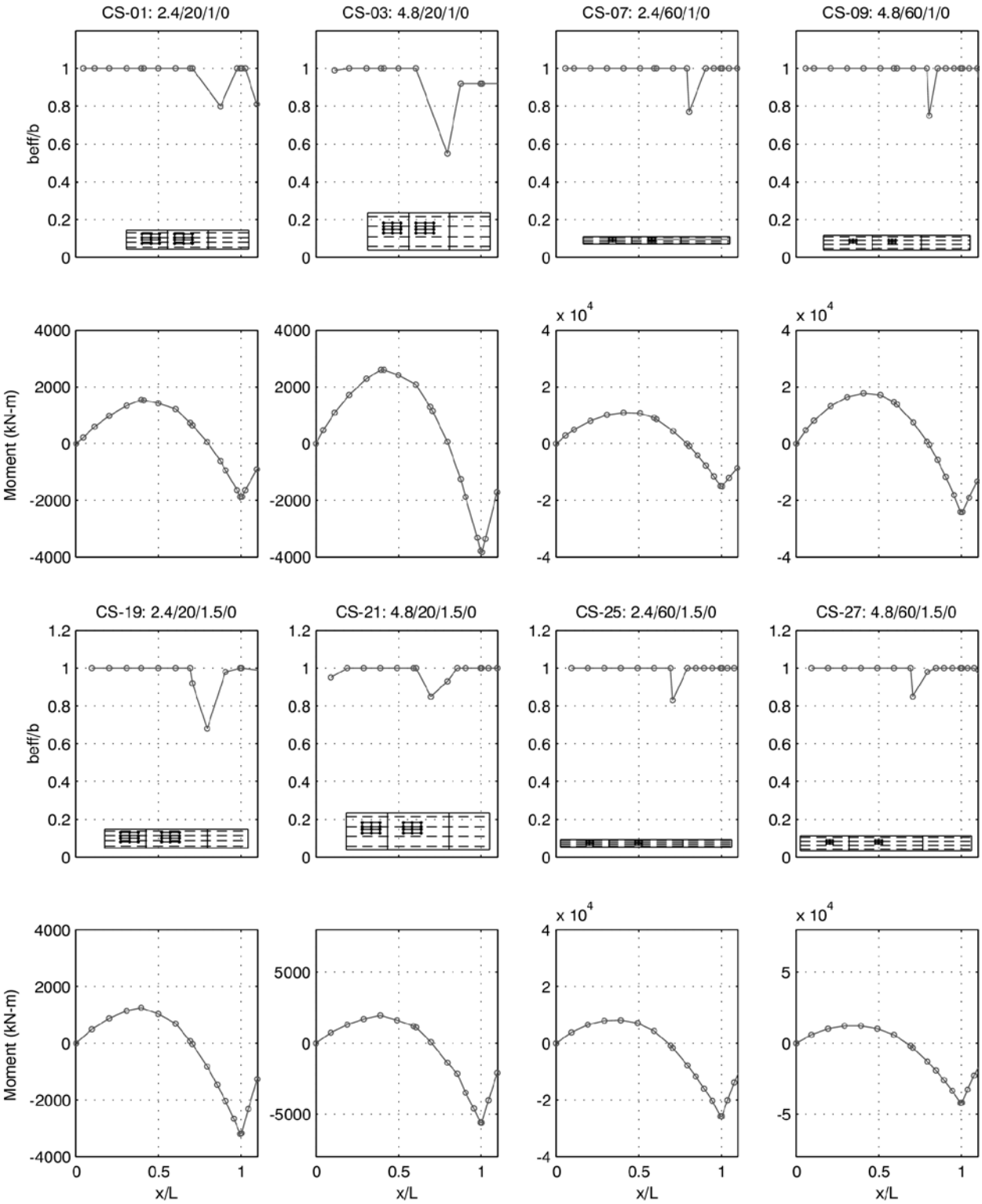

Figure 51. b_{eff}/b and bending moment versus x/L for the multiple-span continuous cases (right bridges, interior girder, negative moment, Service II).

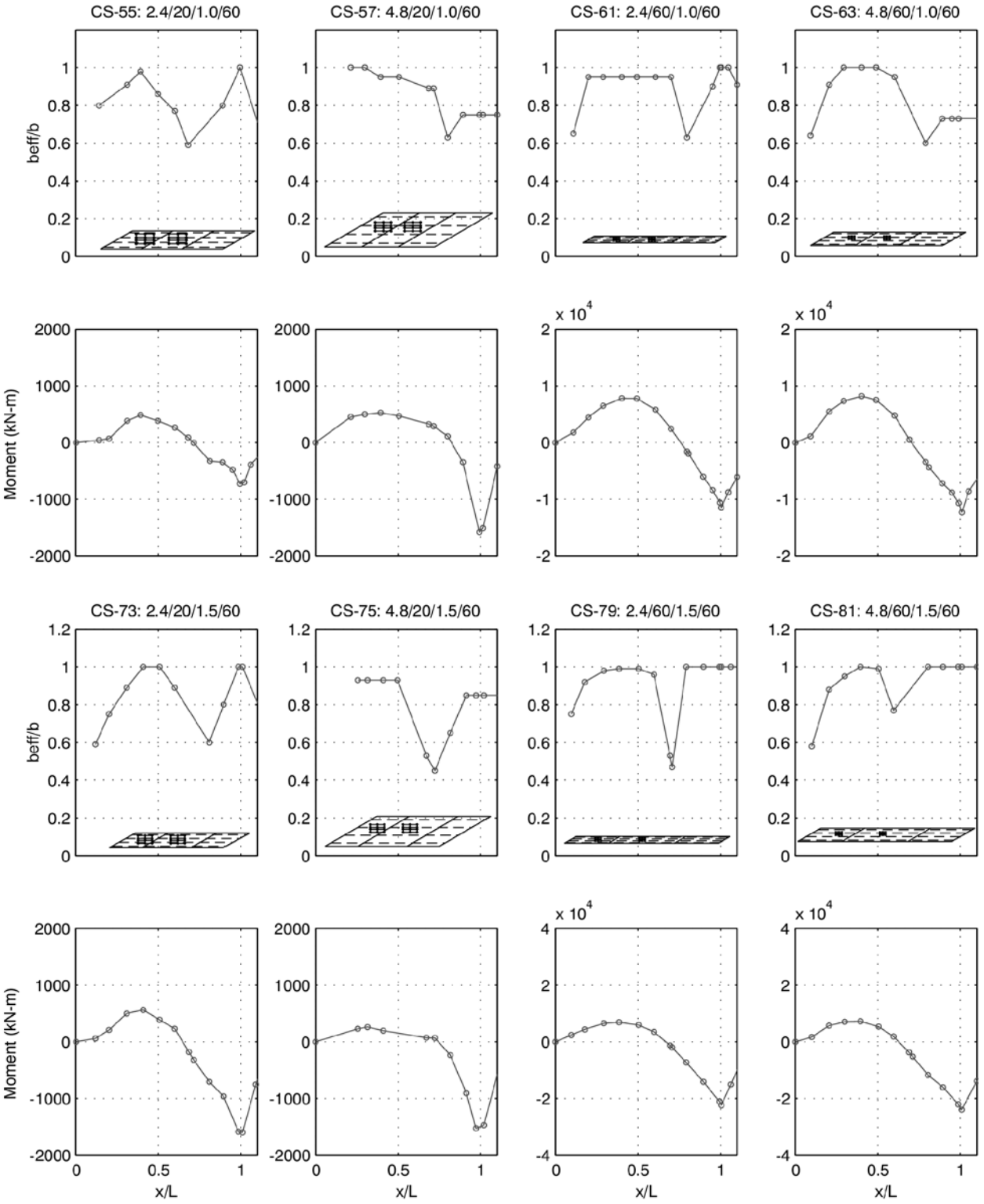

Figure 52. b_{eff}/b and bending moment versus x/L for the multiple-span continuous cases (skewed bridges, interior girder, negative moment, Service II).

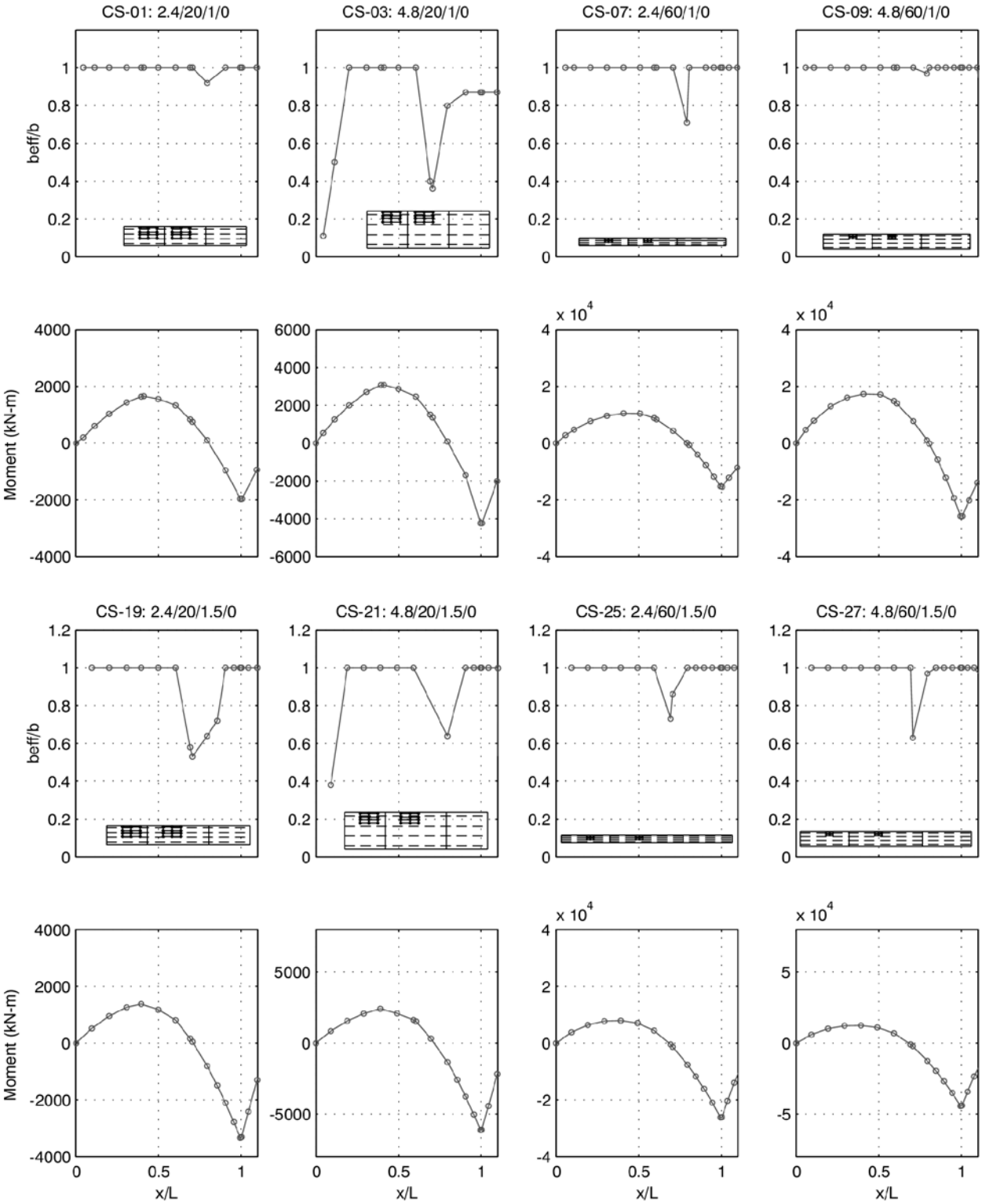

Figure 53. b_{eff}/b and bending moment versus x/L for the multiple-span continuous cases (right bridges, exterior girder, negative moment, Service II).

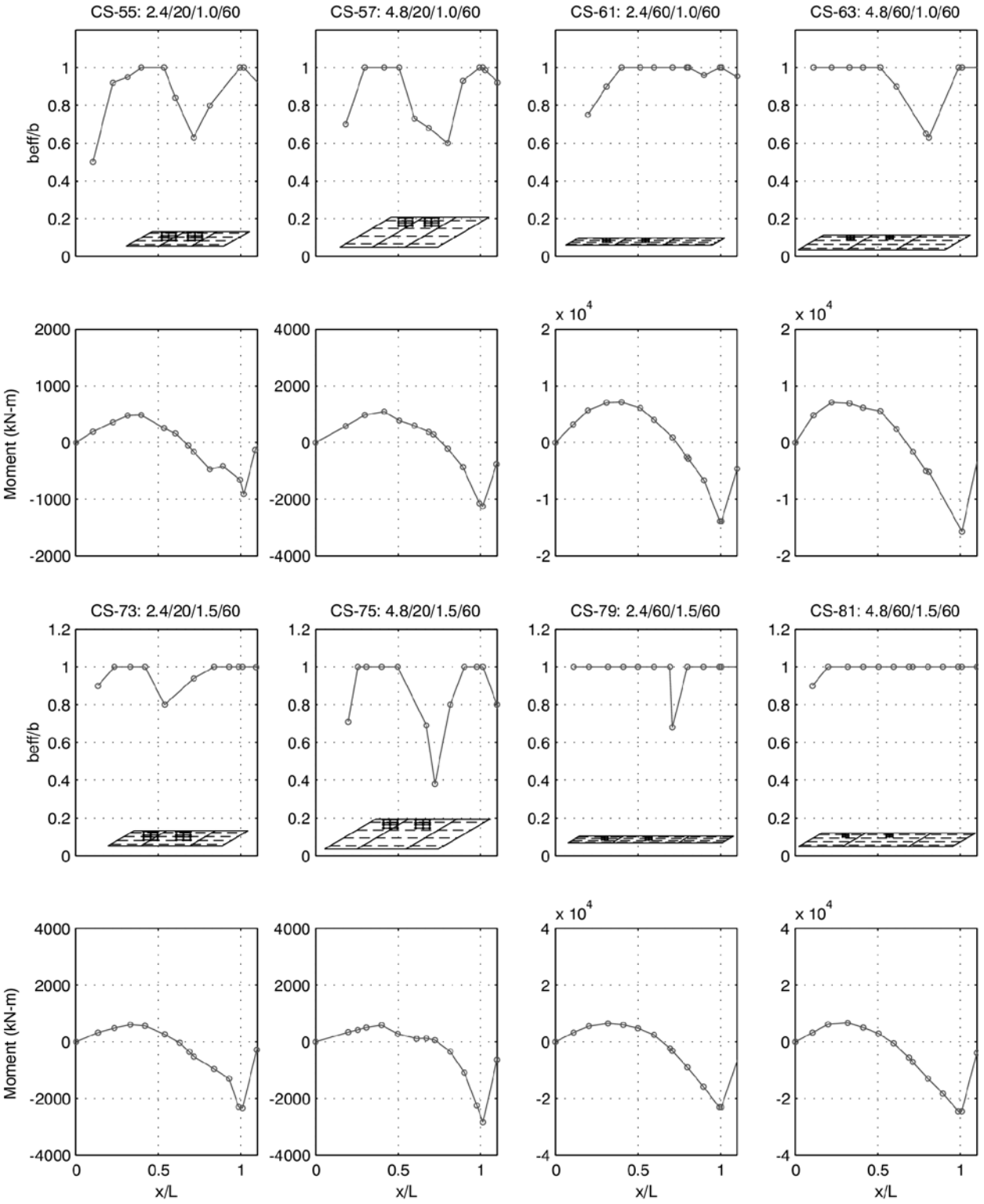

Figure 54. b_{eff}/b and bending moment versus x/L for the multiple-span continuous cases (skewed bridges, exterior girder, negative moment, Service II).

TABLE 9 Effective slab width ratio (b_{eff}/b) for multiple-span continuous bridges (negative moment)

Bridge ID	Interior Girder					Exterior Girder				
	$0.9L_1$	$0.95\ L_1$	$1.0\ L_1$	$0.05\ L_2$	$0.1\ L_2$	$0.9L_1$	$0.95\ L_1$	$1.0\ L_1$	$0.05\ L_2$	$0.1\ L_2$
CS-01	0.90	1.00	1.00	1.00	0.80	1.00	1.00	1.00	1.00	1.00
CS-03	0.92	0.92	0.92	0.92	0.92	0.87	0.87	0.87	0.87	0.87
CS-07	1.00	1.00	1.00	1.00	1.00	1.00	1.00	1.00	1.00	1.00
CS-09	1.00	1.00	1.00	1.00	1.00	1.00	1.00	1.00	1.00	1.00
CS-19	1.00	1.00	1.00	1.00	1.00	1.00	1.00	1.00	1.00	1.00
CS-21	1.00	1.00	1.00	1.00	1.00	1.00	1.00	1.00	1.00	1.00
CS-25	1.00	1.00	1.00	1.00	1.00	1.00	1.00	1.00	1.00	1.00
CS-27	1.00	1.00	1.00	1.00	0.95	1.00	1.00	1.00	1.00	0.95
CS-41	1.00	1.00	1.00	1.00	1.00	1.00	1.00	1.00	1.00	1.00
CS-55	0.80	0.90	1.00	0.80	0.75	0.90	0.95	1.00	0.95	0.90
CS-57	0.75	0.75	0.75	0.75	0.75	0.93	0.97	1.00	1.00	0.90
CS-61	0.80	0.90	1.00	1.00	0.91	0.96	0.98	1.00	1.00	0.90
CS-63	0.70	0.73	0.70	0.73	0.73	0.80	0.90	1.00	1.00	1.00
CS-73	0.80	0.90	1.00	0.90	0.82	1.00	1.00	1.00	1.00	1.00
CS-75	0.85	0.85	0.85	0.85	0.85	1.00	1.00	1.00	0.90	0.80
CS-79	0.94	0.95	0.96	0.95	0.98	1.00	1.00	1.00	1.00	1.00
CS-81	0.97	0.99	1.00	1.00	1.00	1.00	1.00	1.00	1.00	1.00

TABLE 10 Cable-stayed bridges investigated

Bridge ID	Overall Length (m)	Main Span (m)	Edge Girder Spacing (m)	Deck Slab Thickness (mm)
8_8	495	255	16	250
8_15	735	375	30	250
12_8	495	255	16	250
12_15	735	375	30	250
Cooper River	867	471	38.4	240

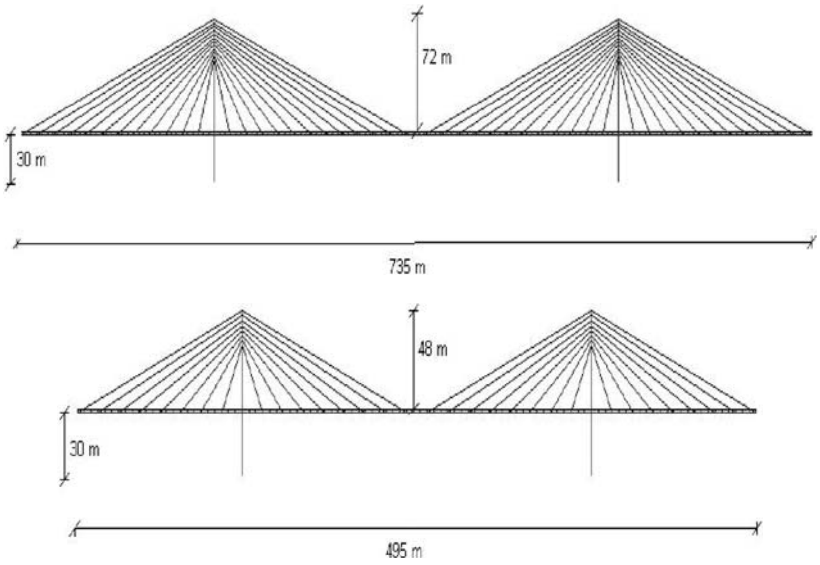

Figure 55. Side views of Bridges 12_8 & 12_15 (total length = 735 m) and Bridges 8_8 & 8_15 (total length = 495 m).

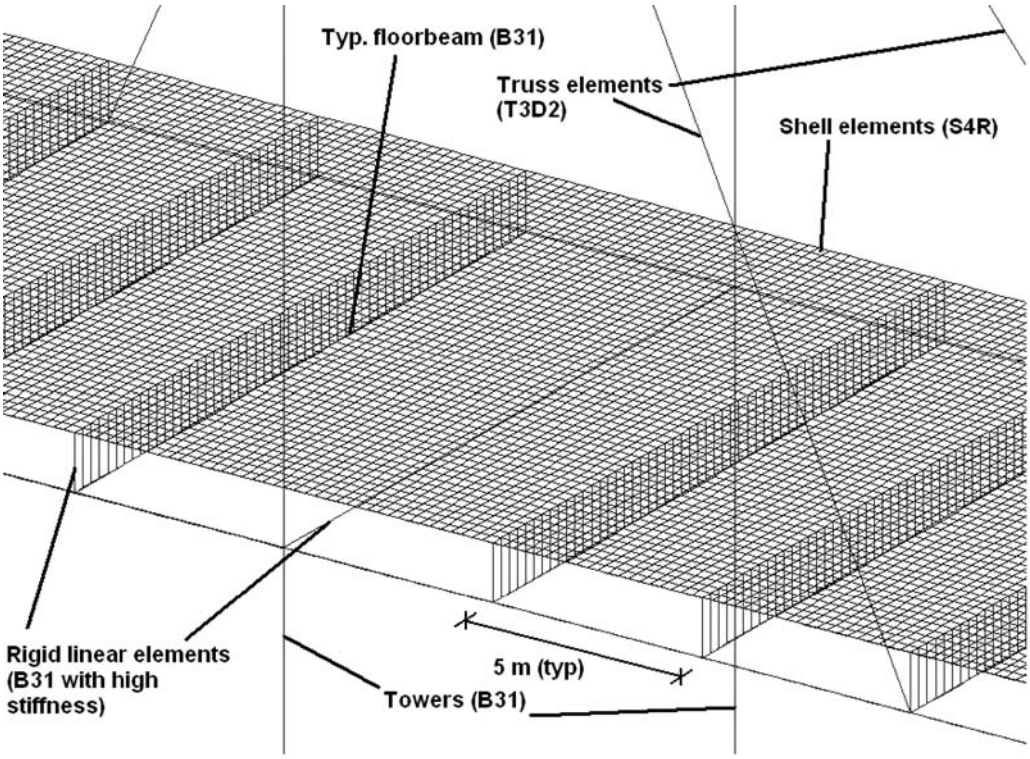

Figure 56. Elements composing the global model; close-up of the area near the cable.

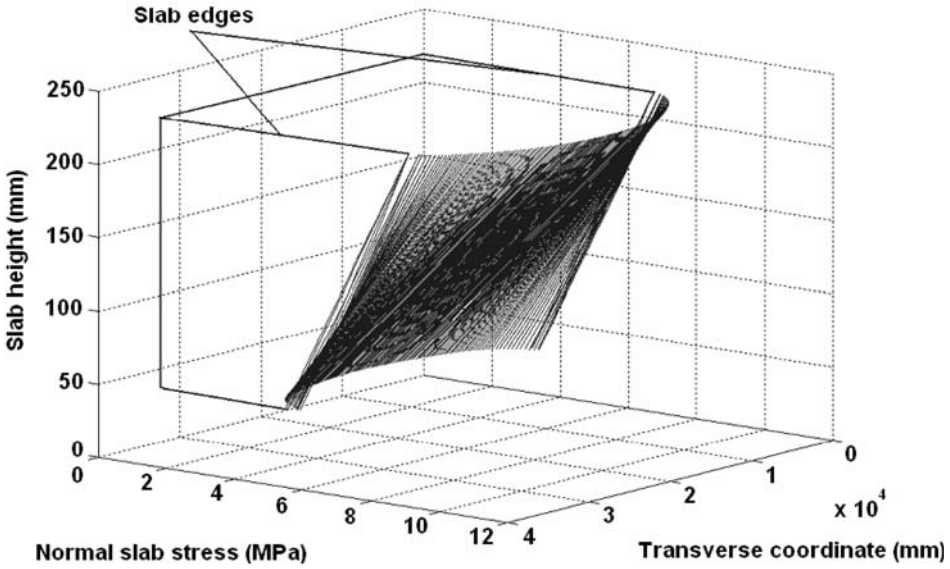

Figure 57. Transverse distribution of normal stresses in the middle of Bridge 12_15 (3-D plot).

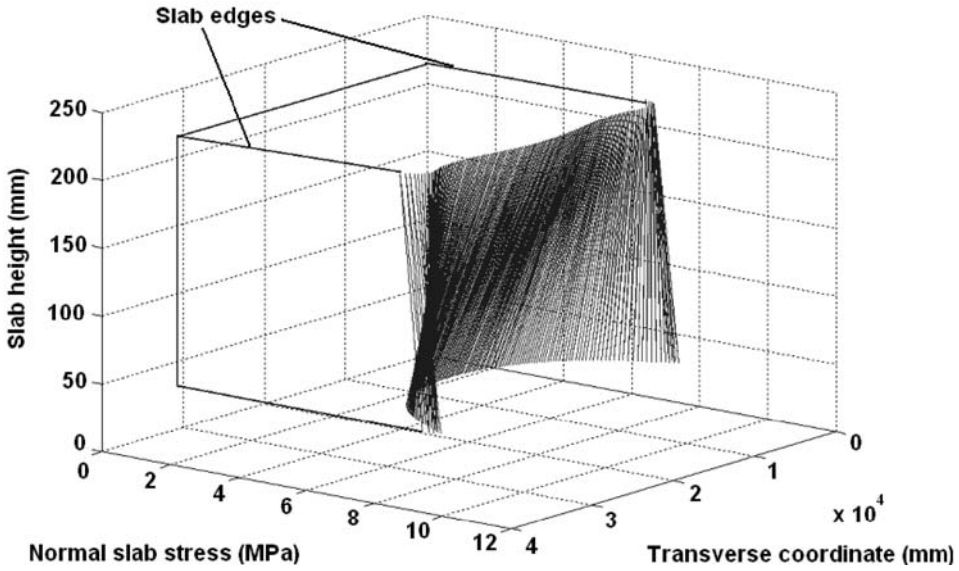

Figure 58. Transverse distribution of normal stresses in the positive moment region close to the support of Bridge 8_15 (3-D plot).

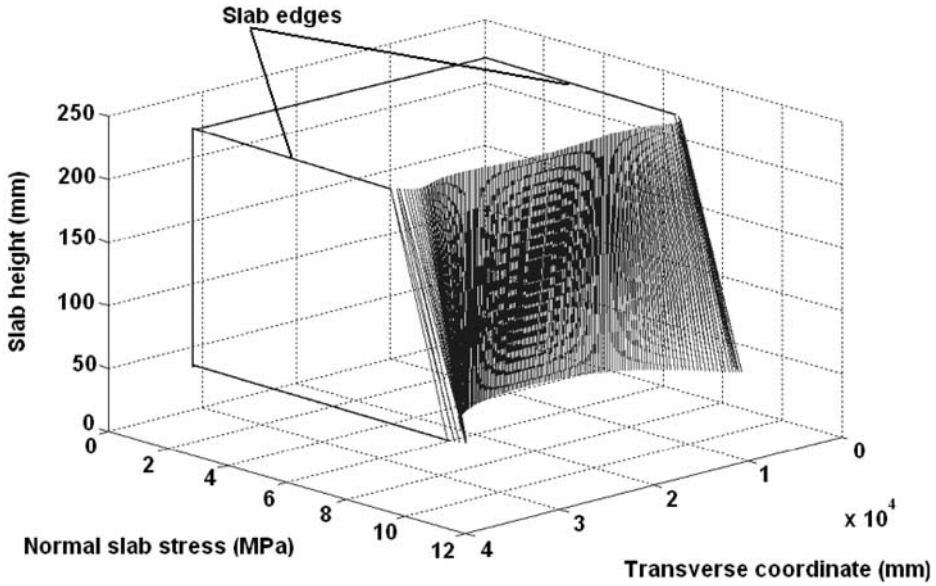

Figure 59. Transverse distribution of normal stresses in the negative moment region close to the support of Bridge 12_15 (3-D plot).

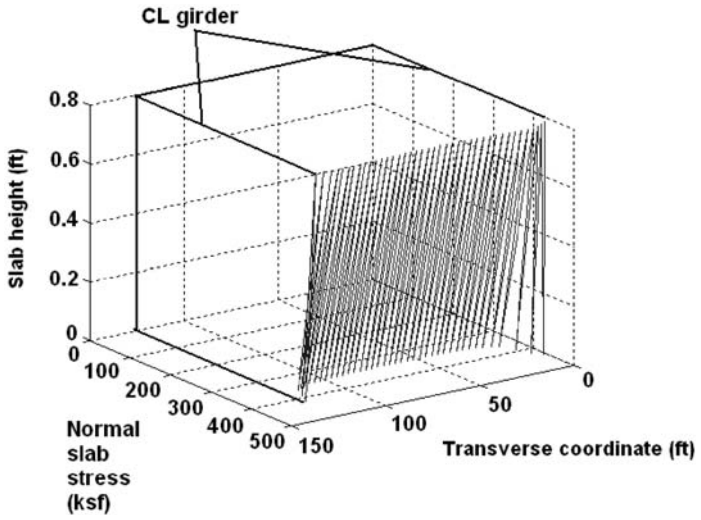

Figure 60. Transverse distribution of normal stresses in the positive moment region close to the support of the Cooper River Bridge (3-D plot).

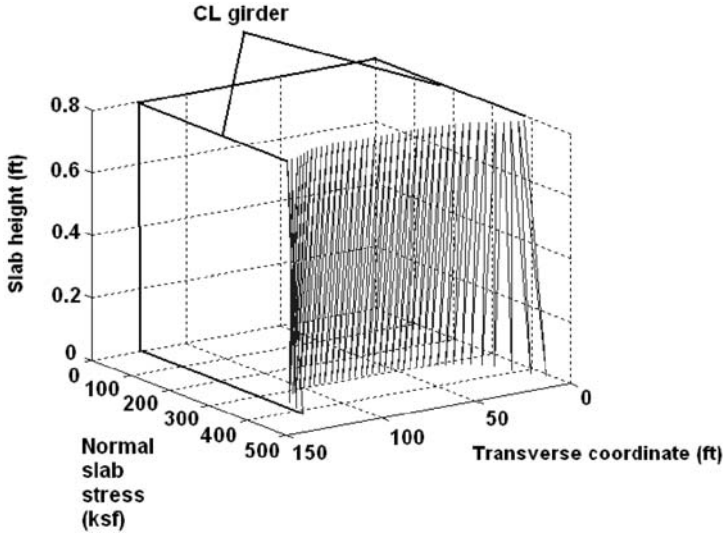

Figure 61. Transverse distribution of normal stresses in the negative moment region close to the support of the Cooper River Bridge (3-D plot).

TABLE 11 Cable-stayed effective width FEM results

Bridge ID	Girder Spacing S (m)	b_{eff}/b		
		Type I Region	Type II Region	Type III Region
8_8	16	1.0	0.95	0.82
8_15	30	1.0	0.95	0.68
12_8	16	1.0	0.99	0.90
12_15	30	1.0	1.0	0.80
Cooper River	38.4	0.99	0.99	0.83

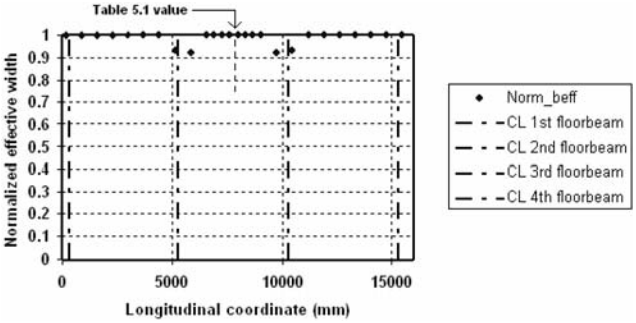

Figure 62. Longitudinal distribution of the normalized effective width for Bridge 8_8 (Region I).

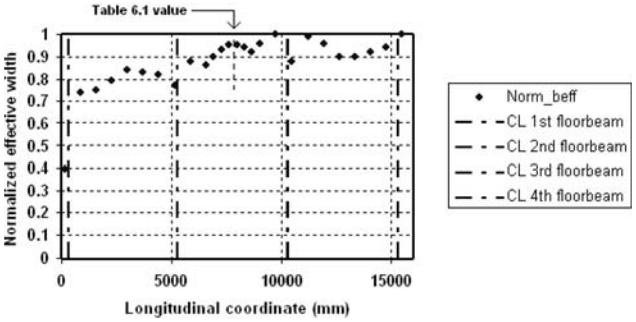

Figure 63. Longitudinal distribution of the normalized effective width for Bridge 8_8 (Region II).

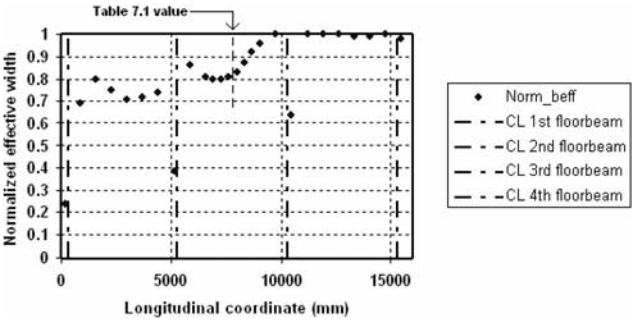

Figure 64. Longitudinal distribution of the normalized effective width for Bridge 8_8 (Region III).

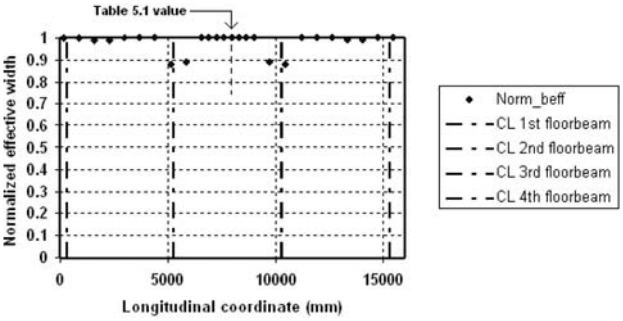

Figure 65. Longitudinal distribution of the normalized effective width for Bridge 12_8 (Region I).

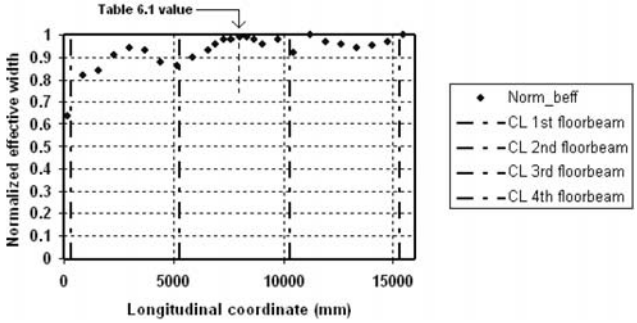

Figure 66. Longitudinal distribution of the normalized effective width for Bridge 12_8 (Region II).

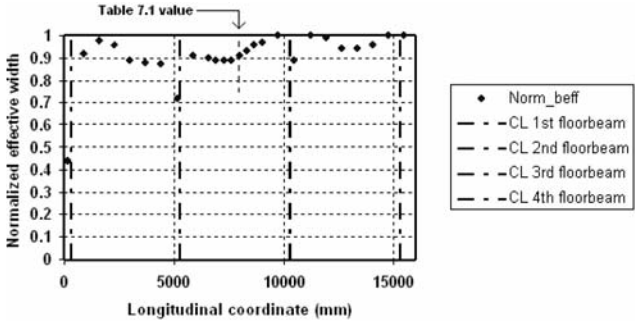

Figure 67. Longitudinal distribution of the normalized effective width for Bridge 12_8 (Region III).

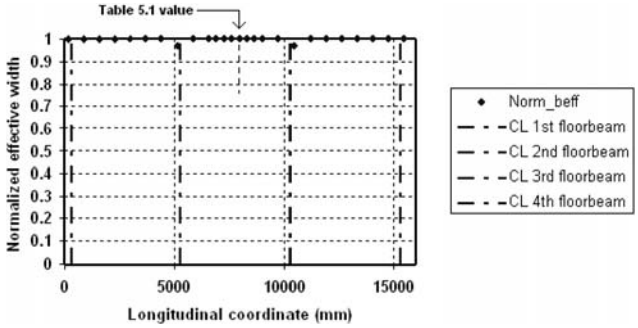

Figure 68. Longitudinal distribution of the normalized effective width for Bridge 8_15 (Region I).

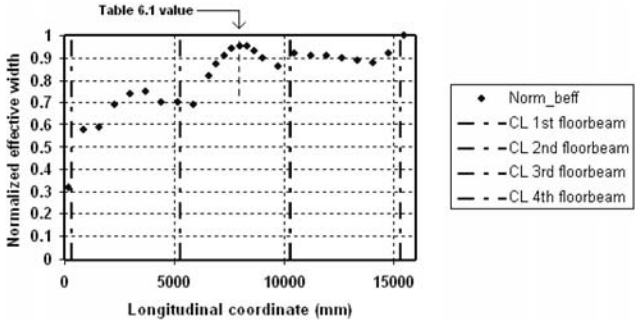

Figure 69. Longitudinal distribution of the normalized effective width for Bridge 8_15 (Region II).

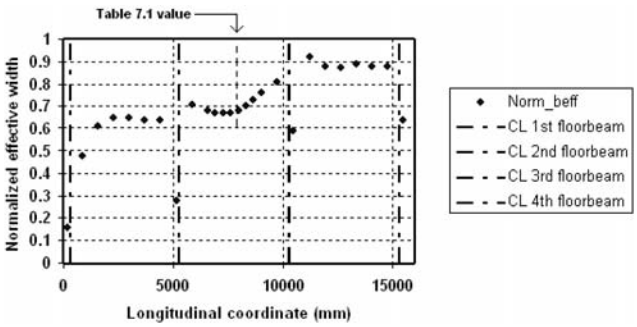

Figure 70. Longitudinal distribution of the normalized effective width for Bridge 8_15 (Region III).

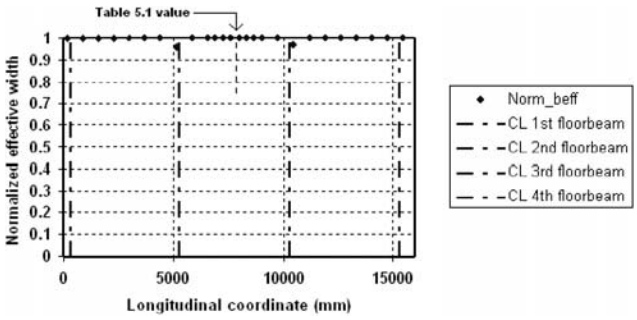

Figure 71. Longitudinal distribution of the normalized effective width for Bridge 12_15 (Region I).

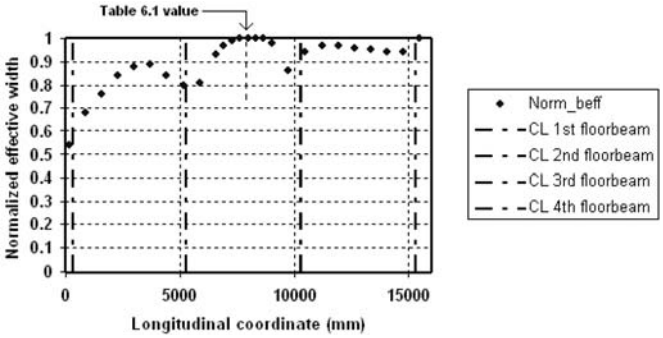

Figure 72. Longitudinal distribution of the normalized effective width for Bridge 12_15 (Region II).

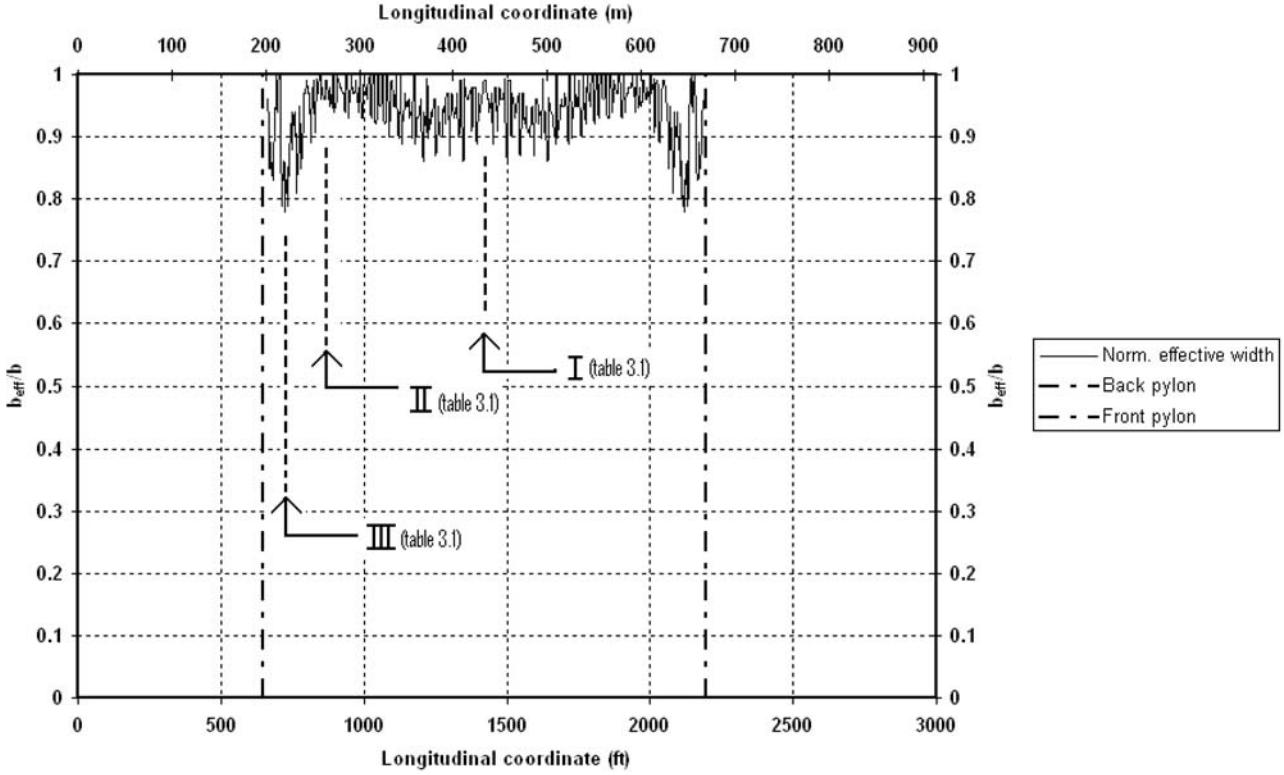

Figure 73. Longitudinal distribution of the normalized effective width for the main span of the Cooper River Bridge.

CHAPTER 3

INTERPRETATION, APPRAISAL, AND APPLICATIONS

3.1 INTRODUCTION

The objectives of this study were to propose criteria for effective width provide recommended specifications and commentary and provide worked examples illustrating the use of those proposed new criteria. Draft criteria were developed based on applying regression approaches and accounting for the different subsets of the parameters varied in the parametric study described in Chapter 2. Effects of those criteria were assessed, using the Rating Factor (RF) as the measure of effect. Based on the assessment, draft criteria are recommended and illustrated in the context of positive and negative moment region worked examples.

3.2 ASSUMPTIONS AND IMPLICATIONS

Some key, almost paradoxical, assumptions underlie the use of the notion of effective slab width, e.g.,

1. Even with the sophisticated computer-aided analysis available for bridge design in the 21st century, traditional line-girder analysis provides an ongoing useful context for analyzing steel girders acting compositely with concrete decks.
2. Given that the context of analyses based on effective width is single member line-girder analysis, analyses based on effective width are not appropriate for use in situations where a line-girder analysis is insufficient and a system analysis is thus considered necessary.

3.2.1 Some Implications of Line-Girder Analysis Limitations

Beyond line-girder analysis, system analysis is generally considered necessary in the following kinds of situations:

- Highly skewed and curved girder bridge analysis and design,
- After-fracture redundancy and load redistribution analysis where required (e.g., Daniels et al., 1989), and
- Detailed design stages for systems where second-order effects can be important, e.g., cable-stayed bridges.

Given that a simplistic line-girder analysis is insufficient for such situations, the use of idealizations that inherently assume line-girder analysis (such as effective slab width) may be considered questionable at best in these kinds of situations.

3.2.2 Some Implications of Wide Girder Spacing

The 12t limitation clearly can be removed. Given that the challenge to the 12t limitation arises, for typical deck thicknesses, in the context of girder spacings wider than 3 m (10 ft) or so, additional implications of wide girder spacings are also of interest. Some of these implications are as follows:

- The empirical method of deck design is prohibited by AASHTO for use beyond a girder spacing of 4.1 m (13.5 ft.) [AASHTO LRFD S9.7.2.4]. Thus, methods of traditional design, prestressed design, and system analysis of decks that go beyond line-girder analysis (e.g., grillage and finite strip) must be used to design the actual decks. Given that these methods typically go beyond line-girder analysis, some may ask why it should still be permissible to use line-girder analysis for the in-plane analysis of the composite girders supporting the resulting decks.
- The use of the line-girder-oriented distribution factor formulas is prohibited by AASHTO for use beyond a girder spacing of 4.9 m (16.0 ft) [AASHTO LRFD S4.6.2.2].
- The possible interaction of plate bending with in-plane "effective width" behavior increases. This interaction is a possible explanation of the "negative shear lag" evident in some of the cable-stayed bridge analysis results presented in Chapter 2.
- Longitudinal shear forces that get "funneled" into the shear connectors increase. Whether the current AASHTO shear stud design criteria still apply, in HPS and HPC composite combinations, may need to be revisited.

Some of these implications of the use of wider girder spacings in conjunction with high-performance steels and concretes point to the need to re-examine existing AASHTO

design criteria and the limits of their applicability (e.g., shear connector design criteria, limits of applicability of empirical deck design methods, and transverse load distribution factors for line-girder analyses). For this study, it was assumed that current AASHTO criteria for such concerns apply, including skew corrections.

3.3 DESIGN CRITERIA DEVELOPMENT

Candidate design criteria were derived by performing regression analyses based on the b_{eff}/b values extracted from the finite element parametric study in the vicinity of the maximum positive and negative moment sections. Candidate effective slab width criteria for positive moment sections were derived initially from the simple-span cases, while the candidate effective slab width criteria for negative moment sections were derived from the multiple-span continuous cases. The b_{eff}/b values from positive moment sections of the multiple-span continuous cases were used to validate the candidate effective slab width design criteria obtained from the simple-span positive moment cases.

The parameters appearing in the regression equations were indeed the main variables of interest in the parametric study:

- Span length L (exterior span length L_1 in continuous-span bridges),
- Span ratio L_2/L_1 in continuous bridges, where L_2 is the length of the interior span,
- Girder spacing S, and
- Skew angle θ.

Various regression equations were generated for interior and exterior girders (separately and with the data combined) using various subsets of the above set of parameters. These regression equations were generated using the general-purpose statistical software package SPSS. Comparisons between these various equations and the FEM-extracted values of effective width ratio b_{eff}/b are given in Appendix K. For the suite of continuous bridges, candidate criteria (regression equations) appear as most unconservative in the case of the CS-75 bridge, which has a short span length, wide girder spacing, and high skew angle.

Results of bridges from the validation cases described in Appendix J are also compared with the various candidate effective width criteria. The span ratio parameter, L_2/L_1, is found in all cases to have minimal effect. Thus it can be removed entirely from the candidate regression criteria. Sifting through the large set of possible criteria and narrowing the list of candidates down to the criteria proposed subsequently required a sound methodology and rationale that could identify the best design criteria. Accordingly, the approach to select the criteria was based on the results of impact assessment using Process 12-50, which is described next.

3.4 IMPACT ASSESSMENT OF CANDIDATE DESIGN CRITERIA

The 12-50 Process (NCHRP, 2003) was originally used for the validation of bridge software. Other possible uses of this process are to determine whether the proposed code changes accomplish the desired objectives and to prevent problems from arising because of changes made by specification writers. The potential benefit of this process comes from specific test computations on real and derived bridges before implementing specification changes. Because flexural design of the section is the primary focus of interest when considering effective width, the sectional flexural capacity and stress in flanges would be the major parameters in test computations. For this reason, the familiar notion of rating factor (RF) is the measure taken to quantify the effect of proposed changes to effective width provisions.

The 12-50 process was used not only to assess the effects of the final recommended provisions but also to narrow the selection process among various different proposed provisions. The winnowing process was based on balancing the degree of effect against the simplicity of the proposed provisions.

3.4.1 Process 12-50

In the 12-50 process, the bridge analysis and design process is divided into manageable computational domains. Within each of these smaller subdomains, the task is described in parametric form. Therefore, the main procedure in each subdomain involves generation of required data for given input parameters.

Bridges in the test suite are selected and their ratings are calculated on the basis of current and proposed effective flange width provisions. The two corresponding rating factors are compared to investigate the significance of code change at critical sections in each bridge. The method of comparison is based on the percentage difference between two results. The existing and new criteria generate results (e.g., stress and moment) at n points in a girder, which in general are termed as a_i and b_i ($i = 1,2,\ldots, n$). In the present study, the a_i represents a rating factor based on existing effective width criteria, and the b_i represents a rating factor based on proposed new criteria. At each point, the absolute average quantity, m_i, is calculated as

$$m_i = \left| \frac{a_i + b_i}{2} \right|$$

The difference between a_i and b_i can be calculated by two methods. The first method (p_1) uses the absolute average at that point. The second method (p_2) uses the maximum absolute average, M, for the calculation:

$$M = \max_{i=1,\ldots,n}\left(m_i\right)$$
$$p_1(\%) = \frac{\left|a_i - b_i\right|}{m_i} \times 100$$
$$p_2(\%) = \frac{\left|a_i - b_i\right|}{m_i} \times 100$$

Therefore, if p_1 or p_2 is larger than the threshold acceptable percentage (p_{allow}), then the two results are concluded as different.

Comparisons based on p_1 are tallied in Appendix L. These tallies show that p_1 values based on full width are very close to p_1 values based on more accurate (and more complex) candidate formulations for effective width. These tallies also show that all effects are rather minimal except for a few wide-girder spacing configurations in negative moment regions.

3.4.2 Rating Factor in LRFR

The general expression for rating factor in LRFR is as follows:

$$RF_{LRFR} = \frac{C - \gamma_{DC} DC - \gamma_{DW} DW \pm \gamma_p P}{\gamma_L LL\left(1 + IM\right)}$$

where

C	capacity ($C = \phi_C \phi_s \phi \times R$: Strength limit state, $C = f_R$: Service limit state)
f_R	allowable stress specified in the LRFD code
R	nominal member resistance
DC	dead-load effect due to structural components and attachments
DW	dead-load effect due to wearing surface and utilities
P	permanent load other than dead loads
LL	live-load effect
IM	dynamic load allowance
γ_{DC}	LRFD load factor for structural components and attachments
γ_{DW}	LRFD load factor for wearing surfaces and utilities
γ_P	LRFD load factor for permanent loads other than dead loads (1.0)
γ_L	evaluation live-load factor
ϕ_C	condition factor
ϕ_S	system factor
ϕ	LRFD resistance factor

Thus, when the Service II limit state is applied, the following equation will be used:

$$RF_{LRFR} = \frac{C - 1.0 \times DC - 1.0 \times DW}{1.3 \times LL\left(1 + IM\right)}$$

For the Strength I limit state, inventory-based load factors are used with $\phi_C = 1.0$ and $\phi_S = 1.0$. Therefore, the resulting equation is

$$RF_{LRFR} = \frac{C - 1.25 \times DC - 1.5 \times DW}{1.75 \times LL\left(1 + IM\right)}$$

The effective flange width of a composite girder increases as stress at the section increases. This is the rationale for developing proposed provisions based on the service limit state at the positive moment section. Consequently, Service II limit state based rating values are used for impact assessment, in particular, at positive moment sections. This section is generally designed as a compact section, and stress of the bottom flange at the Service II limit state typically governs the design. For the design of negative moment sections, generally noncompact sections are used. Therefore, stress developed for the Strength I limit state governs the design of negative moment sections.

Rating factors for positive moment sections are calculated using MathCad worksheets developed for design of the bridges (Appendix O). For negative moment sections, the OPIS program is used in which BRASS-GIRDER (AASHTO, 2004) performs the actual analyses.

3.4.3 Positive Moment Regions

Eight simple-span bridges were selected for the impact investigation in positive moment regions. Service II rating factors of interior and exterior girders were calculated for five different candidate effective width provisions. Based on calculated p_1 values, the impact in positive moment regions is not significant. The maximum p_1 value for interior girders is 3.5 percent, and the maximum for exterior girders is 2.9 percent—where both these maximum values occur for the full width candidate. That is, more complicated curvefit expressions have less error. Details on these results appear in Appendix L.

3.4.4 Negative Moment Regions

Sixteen bridges were selected for the impact investigation in negative moment regions. Strength I and Service II rating factors were calculated for eight different candidate effective width provisions. Service II rating factors, as in the positive moment region, show minimal impacts as measured by p_1.

But a few of the Strength I based rating factors show significant reductions in p_1. This is the first of two concerns that arise in negative moment regions but have no counterpart in positive moment regions.

At the Strength I limit state, whether the rating factor increases or decreases depends on whether a section that was compact (under the old b_{eff}/b criteria) stays compact (using widened value of b_{eff}/b) or whether it becomes noncompact. Under service conditions, a widened effective width results in an increased rating factor for both compact and noncompact sections. At the Strength I limit state, however, what happens to the rating factor depends on whether the section becomes noncompact only using a widened effective width.

The second concern is whether the section is considered as composite and how that compositeness is provided. These two concerns are described next.

3.4.4.1 Webs Made Noncompact

The impact on a strength-based rating factor is substantial when a web that is compact according to the current AASHTO criteria for effective width becomes noncompact according to the proposed full width for effective width. The reasons for this substantial impact are that

- Compact sections can use the full plastic moment for their nominal moment strength and
- Noncompact sections are limited to an elastic stress distribution as the basis for their nominal moment strength.

Paradoxically, the result is that by adding material (to the effective width), flexural resistance has actually decreased—all because a previously compact section is caused to become noncompact by virtue of the raising of the neutral axis which in turn is caused by the widened effective slab width. This is by far the most significant downside impact of the prospect of having widened effective width. There is no corresponding impact when comparing service rating factors because at service, the stress distribution on the cross section is, of course, always based on elastic analysis.

This downside impact, however, is not considered a compelling reason to avoid changing the effective width criteria. The following reasons exist for proceeding with a liberalized effective width criterion:

- The downside impact occurs only for the bridges in the parametric study that have very wide girder spacings [S = 4.8 m (16 ft)].
- Based on the results of the survey reported in Appendix A, probably no existing bridges in the nationwide inventory have girder spacings that wide as well as composite design in the negative moment region.
- Negative moment regions of plate girder bridges designed according to industry guidelines would normally have noncompact webs anyway.

Thus, there are believed to be few if any existing bridges whose ratings would suddenly be reduced by imposing a wider effective width.

3.4.4.2 To Stud or Not To Stud

Although one of the experimental specimens investigated in this study deliberately omitted the placement of shear connectors in the negative moment region, there are at least the following reasons to install shear studs in the negative moment regions of composite girders:

- To maintain consistent design philosophy and practice regarding "composite" design, and
- To resist transverse seismic loads reliably.

Composite Design Philosophy and Practice. For the slab to be acting (such that part of it can be "effective"), it must be acting compositely with the steel girder. Thus, the fundamental premise of this entire investigation ("Effective Slab Width of Composite Steel Bridge Members") has been that behavior is composite. Designers naturally and properly consider this composite action to be delivered by shear connectors. Conversely, configurations without the shear connectors are naturally and properly considered to be noncomposite. Thus, even to consider the notion of effective slab width in negative moment regions without shear studs makes no sense.

Complicating this issue is the ambiguity of the current AASHTO specifications on whether negative moment regions without continuous shear connectors can be considered to be composite when longitudinal deck reinforcing steel is developed and anchored to clusters of shear connectors in moment inflection regions. The negative moment subassemblage experiment conducted in this study further suggests that composite behavior can be attained in such cases, but it is only *one* specimen.

Transmission of Transverse Seismic Loads. It is critically important that a load path be provided in a steel slab-on-girder bridge that will allow seismic damage to be limited to well-confined plastic hinges in the columns (current AASHTO design philosophy as expressed in Art. 4.6.2.8) or in redundant components of a bridge superstructure such as the end cross frames (NCHRP Project 12-49 design philosophy). In either case, given that the bulk of the superstructure mass is

in the deck, shear studs in the negative moment regions provide an essential element of the required load path (Carden et al., 2003). Concerns about fatigue in the shear stud welds in negative moment regions need not prevent welding to the top flange altogether.

3.4.5 Shear Connector Impact

At first glance, one might expect a wider effective slab width to cause more demands on the shear connectors, in order to develop that wider effective slab. The impact of wider b_{eff} on shear connector layout, however, is surprisingly minimal. The reason for this minimal impact apparently stems from offsetting effects. Shear connectors are designed to resist the longitudinal shear flow and are typically governed by fatigue rather than strength. At the fatigue limit state, elastic analysis is performed, where the longitudinal shear flow is given by the familiar equation VQ/I, where I is the moment of inertia of the short-term composite section and Q is the first moment of the transformed area of the slab. A wider b_{eff} increases both Q and I, thus producing offsetting effects.

Several bridges with wide (4.8 m = 16 ft) girder spacings were investigated regarding their shear connector layout in Appendix L. The most significant impact on shear stud layout was for the longest spans investigated (60 m = 200 ft). Even in this case, however, the required shear stud pitch decreased only 10 percent.

3.5 PROPOSED DESIGN CRITERIA

3.5.1 Slab-on-Girder Bridges

Based on the impact assessment of various candidate effective width criteria according to Process 12-50 principles using Rating Factor as the measure of comparison, the additional accuracy achieved by the more complicated formulations is minimal. Thus, this simple formulation is recommended instead: "for both interior and exterior girders designed to be composite sections, the effective flange width may be assumed equal to the physical flange width." This recommendation should be limited to the parameter range used in the parametric study on which it is based:

- Girder spacing $S \leq 4.8$m (16 ft)
- Span Length $L \leq 60$m (200 ft)
- Skew Angle $\theta \leq 60°$

The skew angle θ here is defined as it is in AASHTO LRFD Chapter 4, such that 0 deg skew is a right bridge alignment. Further discussion of the rationale and justification for this recommendation is provided in Appendix M.

Bridge engineers may encounter situations beyond the range of values investigated in the parametric study. The following brief discussion addresses these situations.

3.5.1.1 Span Length L > 60 m (200 ft)

There is no reason to expect that spans longer than 60 m (200 ft) would not behave similarly to 200 ft spans. The span length limit could be relaxed, since in the parametric study presented herein it was found that the longer the span (or, more accurately, the greater the length/width ratio), the more we can be sure that the full width is effective. The reason for specifying the 60 m (200 ft) span length as a limit is that the parametric study did not consider longer spans.

3.5.1.2 Girder Spacing S > 4.8 m (16 ft)

In the parametric study conducted herein, a small number of cases were analyzed with $S > 4.8$ m (up to $S = 7.6$ m). For those few cases, there was no indication that effective width should be taken as less than full width. However, they were only a few cases.

3.5.1.3 Skew Angle $\theta > 60^o$

In the parametric study, no cases were analyzed with skews greater than 60 degrees. What happened with the 60-degree skews analyzed was that although effective width was typically somewhat less than full width, moments extracted from the FEM model were less than moments that would be predicted by a line-girder analysis (with AASHTO 2004 skew correction factors for the transverse live-load distribution factors). Thus, if the designer assumed full width but also used line-girder analysis, there were offsetting errors. The small impact of these offsetting errors on rating factor were such that they allowed use of full effective width. Presumably, such offsetting errors could reasonably be expected for skews greater than 60 degrees. Of course, if the ongoing NCHRP Project 12-62 develops more significant skew correction factors for the AASHTO LRFD transverse live-load distribution factors, then there may not be such offsetting effects.

3.5.2 Cable-Stayed Bridges

In light of the results tallied in Table 11 for the first four analyzed cable-stayed bridges and the longitudinal variation of effective slab width seen in Figures 62 through 72, a reasonable and conservative lower bound set of effective width values for cable-stayed bridges may be summarized as follows:

- 0.90 for regions away from the towers, and
- 0.70 for regions close to the towers.

The above values are suitably conservative for the verification case (Cooper River Bridge) as illustrated in Figure 73. For Cooper River as in Byers' bridges, there was high normalized effective width (close or equal to 1) in most regions away from the towers and a bit lower (but still high—higher than 0.70) in regions close to the pylons.

The above values are recommended for use in cable-stayed bridges with the characteristics of those analyzed in this work. This means that they address bridges with the following characteristics:

- Semi-harp cable pattern with two planes of cables;
- Relatively thin concrete slab (approximate thickness 240 to 250 mm, 9.5 to 10 in.);
- Cable spacing approximately 10 percent of the back span length; and
- Floorbeam spacing approximately one-third of the cable spacing.

3.6 IMPLEMENTATION EXAMPLE

Two worked examples of design calculations based on AASHTO LRFD provisions were prepared to illustrate use of the proposed new effective width criteria based on full width. One of these was in the positive moment region of a continuous hybrid girder, while the other was in the negative moment region of a hybrid girder. Both examples are provided in Appendix O.

Table 12 summarizes flexural performance ratios associated with the limit state checks that are influenced by the effective width. By "flexural performance ratio" is meant the ratio of applied bending stress (or moment) to resisting bending stress (or moment) capacity, at applicable limit states. The last column of the table lists the performance ratios for the current 12t limited effective width provision in the code. Given that the example bridge has a girder spacing of 3.69 m (12 ft $1^1/_4$ in.), the proposed full-width adds approximately 1 m to the effective width of the slab specified by current AASHTO LRFD provisions, in both the positive and negative moment regions.

The effect of this increase in effective width can be assessed by comparing the last two columns of the table, which were both computed for the same trial steel section. Overall, the comparison suggests that the effect of the increase in effective width for this example is minimal—safety margins are increased, but only slightly. The example suggests that for such a girder spacing, it is likely that no designer would make any changes to flange and web plate sizes based on the liberalized effective width. Interestingly, even the web bend-buckling performance ratio is not adversely affected in the negative moment region. Evidently, the increase in the moment of inertia I (which reduces the applied web stress f_{crw}) more than offsets the increase in the depth of the compression portion of the web D_c (which reduces the web bend-buckling strength F_{crw}).

3.7 SUMMARY

The full width being proposed here for composite bridge members subject to the limits of the parametric study ($S \leq 4.8$ m, $L \leq 60$m, $\theta \leq 60°$) is in fact the most liberal of all effective width provisions in all known international codes. This proposal is based on an extensive and systematic investigation of bridge finite element models that are more sophisticated than the models upon which other codes are based, that are corroborated by experimental results both by others and by the authors, and that explicitly investigate the negative moment region much more extensively than previous researchers have done.

TABLE 12 Flexural performance ratios in worked examples

Limit State	Region	Component	Proposed	Current
Service II	Positive	Top Flange	64.7%	69.1%
		Bottom Flange	92.9%	93.8%
	Negative	Top Flange	55.5%	58.6%
		Bottom Flange	66.3%	67.7%
		Web-Bend-Buck	87.2%	89.0%
Strength I	Positive (Compact)		90.2%	91.3%
	Negative	Top Flange	92.3%	96.7%
		Bottom Flange	95.8%	96.7%

In summary, the process that has been followed in arriving at the proposed full width criteria has involved each of the following:

- Formulating a new definition of effective width which for the first time accounts for the variation of stresses through the deck thickness as well as both moment and force equivalence between the finite element model and the line-girder idealization wherein b_{eff} is used;
- Performing judicious finite element modeling and analysis, using appropriate levels of detail (e.g., approximating "smeared" rather than discrete deck rebar and cracking, yet explicitly representing deck thickness using four brick elements through the thickness);
- Corroborating that finite element modeling approach with experimental data produced by others as well as by the authors;
- Designing a suite of bridges according to industry guidelines to support the parametric study;
- Performing a systematic parametric study of finite element models of these bridges that produced results from which effective widths according to the new definition could be methodically extracted;
- Formulating various candidate criteria for effective width, based on regression analysis, that intentionally span the gamut between simplicity and accuracy;
- Applying Process 12-50 in a systematic assessment of impact of those various candidate criteria in order to recommend which criteria were most appropriate;
- Proposing specific draft code and commentary language for implementing those criteria in AASHTO LRFD Article 4.6.2.6.1, for consideration by the AASHTO Subcommittee on Bridges and Structures; and
- Illustrating the use of the recommended criteria in the form of comprehensive worked design calculation examples.

CHAPTER 4

CONCLUSIONS AND SUGGESTED RESEARCH

4.1 CONCLUSIONS

This study has resulted in the recommendation that full width may be used for effective width in composite steel bridge members for most situations of practical interest. This recommendation was determined to be suitable for the Service as well as Strength limit states, for exterior as well as interior girders, and for skewed as well as right alignments.

The simplicity of this recommendation results from an extensive set of analyses on various bridge configurations culminating in the following two consistently observed trends:

- Full width was typically acting at cross sections where it was most needed, i.e., where moments and hence performance ratios would be highest; in the cases where the effective width was less than full width at such cross sections, that cross section had considerable excess flexural capacity, and
- An extensive "impact analysis" based on Process 12-50 principles revealed that more cumbersome curvefit expressions for effective width, although more accurate, were not significantly so in terms of the governing rating factor (RF) of the bridge investigated.

Based on a limited number of studies of prestressed concrete girder configurations producing similar results, the above simple criterion is thought to be reasonable for such configurations as well.

The very notion of effective width presumes composite behavior. A question addressed in one of the experiments performed herein is whether composite behavior can legitimately be assumed in negative moment regions without continuous shear connectors. It would appear that composite behavior can be attained in negative moment regions, even without shear studs being distributed throughout the negative moment region, as long as the longitudinal reinforcing steel is properly anchored and developed. This observation, however, is based on only a single experimental specimen.

4.2 IMPLEMENTATION PLAN

It is recommended that the AASHTO Subcommittee on Bridges and Structures (SCOBS) consider the draft revisions to Article 4.6.2.6.1 of the LRFD Specifications and Commentary as developed herein. These provisions in LRFD two-column format are provided herein on pp. M-7 and M-8 of Appendix M.

4.3 SUGGESTED RESEARCH

4.3.1 Bridge Types and Geometries Not Considered Herein

1. Tied-arch bridges were not explicitly modeled in the FEM studies performed herein. It is not known how the presence of net tension in the floor system of such bridges will affect the effective width. Various decking options should be considered in this context (e.g., cast-in-place and precast prestressed longitudinally post-tensioned).
2. Curved bridges present another situation of interest. The forthcoming 2005 Interims to the AASHTO LRFD Specifications add curved girder analysis provisions to the curved girder resistance provisions that were in the 3rd Edition of the Specifications in 2004. It is generally agreed that a curved girder bridge should be analyzed as a system, such that line-girder simplifications (where effective width is used) would not apply. Approximate methods, however, are explicitly permitted in the 2005 Interims for use in analyzing curved girder bridges. One such approximate analysis method is the V-Load method. The V-Load method idealizes the curved girder as a straight girder subjected to vertical (V) loads applied at diaphragm locations to complement gravity loads. Engineers using the V-Load method will want to know what value of effective width to use for resisting superimposed dead-load and live-load effects on the composite section. The research reported herein simply does not address that question.
3. A third situation not explicitly investigated herein is where decks are longitudinally prestressed. Such decks would be designed not to crack under service loads. Whether the effective width of such decks remaining uncracked at the critical cross section in negative moment regions extends to the full width is an important question. This question was beyond the scope of

the parametric study conducted herein and should be investigated. Although it is worth mentioning that while investigating the negative moment region prior to cracking, the observation was that an apparent smaller b_{eff} than that of a cracked section whereby the rebars are fully engaged in taking the tensile stresses.

4. A fourth situation involves bridge decks that do not have solid thicknesses that meet or exceed the minimum depth of 175 mm (7 in.) specified in Article 9.7.1.1 of the AASHTO LRFD Specifications. The FEM analyses upon which this report's recommendations are based all presumed solid deck thicknesses meeting or exceeding this minimum depth requirement. Situations with other types of decks are thus not included within the scope of the recommendations and therefore should be investigated independently.
5. The research results presented herein focused primarily on slab-on-girder systems. Whether the effective width provisions for slab-on-girder systems can or should be reconciled with the effective width provisions for segmental prestressed concrete box girders is a reasonable question. Posited another way, for example, why should a deck in a segmental box girder experience shear lag differently than a deck in a tub girder? One would not expect a difference, which means that one would not expect a different criterion for effective width. Yet there was no attempt in the present study to reconcile its results with existing provisions for segmental box girders.

4.3.2 Bridge Types and Geometries Considered Herein

Within the framework of the parametric study and additional cases examined herein, further investigation may be appropriate beyond the range limits adopted in this study, i.e.,

- Girder spacings farther apart than 4.8 m (16 ft), or in fact greater than 3.6 m (12 ft) for prestressed girders,
- Span lengths greater than 60 m (200 ft), and
- Skew angles greater than 60 deg.

Although prestressed concrete girder configurations and cable-stayed bridges were considered in this study, only a few such cases were explicitly examined. Expanding the number of analyses on these types of bridges in order to modify or increase the credibility of the recommendations contained herein for these types of bridges may be desirable.

For cable-stayed bridges, the following are suggested as areas for further research regarding effective width:

- **Live-load placement influence on effective width**: No live load was considered in the present study because the dead load is very large in such structures with respect to live load and because Byers (whose results served as a basis for comparison with ours) did not use live load either. Thus, it would be of interest to investigate the live-load influence on the effective width.
- **Influence of cable tensioning during construction on b_{eff}:** Construction steps were not considered in this work. Investigating their influence on b_{eff} is recommended.
- **Negative shear lag in cable-stayed bridges**: The phenomenon has been observed in various types of structures, and further research on the subject is recommended as far as cable-stayed bridges are concerned.
- **Single versus dual effective width**: A single value of effective width was evaluated herein. Attempts to separate normal stresses into their "axial" and their "flexural" components are also recommended for future research although the difficulty of the task is recognized.
- **Impact assessment in terms of rating factor**: As was done for the more common slab-on-girder cases, it would be of interest to investigate how the proposed values of effective width in cable-stayed bridges affect analysis results as measured by rating factor.
- **A wider range of bridge geometries and cable configuration**: For example, in this project the bridges investigated (other than the Cooper River Bridge) were no more than 30 m (100 ft) wide. It would be of interest to determine values of effective width for additional bridges wider than 30 m and for bridges with different cable patterns, cable spacing, floorbeam spacing, slab thickness, and so forth.

4.3.3 Recommendations Originating from Experimental Investigations

From the experimental studies conducted as part of this research, the following recommendations for further research arise:

- Research is recommended for evaluation of instrumentation used for measuring strain on rebars that are embedded in concrete.
- More extensive study, including evaluation of rebar strains, of intentionally composite versus noncomposite slab-on-girder specimens would be valuable. Ideally the specimens would be multi-girder systems. Investigations and comparisons of global and local composite/noncomposite behaviors would be useful. As mentioned in the literature review, AASHTO is confusing on the point of composite behavior relating to shear stud design. It is recommended that research in this area includes evaluation of situations and/or loading that allow noncomposite beams to be evaluated as composite. Surely the details of the steel-concrete bond surface would be of interest since various conditions exist at that location in the field. Perhaps a FEM model with interface elements

only in the shear stud cluster region would be in order since there was no contact in certain regions of the non-composite specimen during later levels of loading in the experiment. This report presents only comparison of one composite specimen to one noncomposite specimen, so it is unreasonable to assume that the material presented here applies to all conditions.

- Further investigation of crack patterns and how they relate to composite beams versus slip regions of non-composite beams with developed rebar may be useful in developing and verifying refinements to concrete and rebar material modeling assumptions and friction modeling assumptions used in finite element models of slab-on-girder bridges.

REFERENCES

AASHTO (1998). *AASHTO LRFD Bridge Design Specifications.*. 2nd Edition with annual updated interims, Washington, DC.

AASHTO (2003). *Guide Manual for Condition Evaluation and Load and Resistance Factor Rating (LRFR) of Highway Bridges*, Washington, DC.

AASHTO (2004). *AASHTO Bridge Design Specifications*, 3rd Edition, Washington, DC.

Ahn, I.-S., et al. (2004). "Effective Flange Width Provisions for Composite Steel Bridges," *Engineering Structures*, 26[12], pp.1843–1851.

American Society of Civil Engineers (1979). *Structural Design of Tall Steel Buildings*, New York.

ANATECH Corp. (1997). *ANACAP-U Concrete Analysis Program User's Manual*, Version 2.5, San Diego, CA.

ATC/MCEER Joint Venture (2002). *NCHRP Report 472: Comprehensive Specification for the Seismic Designs of Bridges*, Transportation Research Board of The National Academies, Washington, DC.

Byers, D. (1999). *Evaluation of the Effective Slab Width for Composite Cable-Stayed Bridge Design*, Ph. D. Thesis, University of Kansas.

Carden, L.P., et al. (2003). "Composite Action in Steel Girder Bridge Superstructures Subjected to Transverse Earthquake Loading," *Transportation Research Record 1814*, Transportation Research Board of The National Academies, Washington, DC. pp.245–252.

Chen, S.S., et al. (2001). "Effective Slab Width for Composite Steel Bridge Members (NCHRP Project 12-58), Preliminary Draft Interim Report.

Chiewanichakorn, M. (2005). *Intrinsic Method of Effective Flange Width Evaluation for Steel-Concrete Composite Bridges*, Ph.D. Dissertation, University at Buffalo, State University of New York, Buffalo, New York.

Chiewanichakorn, M., et al. (2004). "Effective Flange Width Definition for Steel-Concrete Composite Bridge Girder," *Journal of Structural Engineering*, ASCE.

Daniels, J.H., and Fisher, J.W. (1967). "Static Behavior of Continuous Composite Beams," *Fritz Engineering Laboratory Report No. 324.4*, Department of Civil Engineering, Lehigh University, Bethlehem, PA.

Daniels, J. H., et al. (1989). *NCHRP Report 319: After-Fracture Redundancy in Steel Two-Girder Bridges*, Transportation Research Board of The National Academies, Washington, DC.

Garcia, I., and Daniels, J. H. (1971). "Negative Moment Behavior of Composite Beams," *Fritz Laboratory Report No. 359.4*, Lehigh University, Bethlehem, PA.

Kathol, S., et al. (1995). "Strength Capacity of Steel Girder Bridges," *Final Report NO. RES1 (0099) R469*, Nebraska University, Lincoln.

Moffatt, K.R., and Dowling, P.J. (1978). "British Shear Lag Rules for Composite Girders," *Journal of Structural Division*, ASCE, 104[7], pp.1123–1130.

Michael Baker, Jr., Inc. et al. (2003). *NCHRP Report 485: Bridge Software—Validation Guidelines and Examples*, Transportation Research Board of The National Academies, Washington, DC.

Montgomery, D.C. (2001). *Design and Analysis of Experiments*, 5th Edition, John Wiley & Sons.

Oehlers, D.J., and Coughlan, C.G. (1986). "The Shear Stiffness of Stud Shear Connectors in Composite Beams," *Journal of Constructional Steel Research*, Vol. 6, pp.273–284.

Rashid, Y.R. (1968). "Ultimate Strength Analysis of Prestressed Concrete Pressure Vessels," *Nuclear Engineering and Design*, Vol. 7, pp.334–344.

NOTATIONS

A = area of an equivalent compressive stress block for simple beam theory
b = total slab width
b_{eff} = effective slab width
C_{slab} = total or resultant compressive force in the slab
DC = dead-load effect due to structural components and attachments
DW = dead-load effect due to wearing surface and utilities
f'_c = concrete compressive strength
i = element number
I_{xx} = second moment of inertia
IM = dynamic load allowance
M_{FEM} = bending moment at a specific cross section
L = span length
LL = live-load effect
L_1 = exterior span length
L_2 = interior span length
m_i = absolute average quantity
C = capacity
D_c = depth of the compression portion of the web
f_{crw} = web stress
f_R = allowable stress specified in the LRFD code
p_{allow} = threshold acceptable percentage
p_1 = absolute average percentage
p_2 = maximum absolute average percentage
P = permanent load other than dead loads
Q = first moment of transformed area of the slab
RF_{LRFR} = rating factor based on LRFR provisions
R_n = nominal member resistance
S = girder spacing
S_{top} = elastic section modulus for the extreme compression fiber
t = slab thickness
t_{slab} = slab thickness
V = shear force
z_o = location of resultant compressive force in the slab
γ_{DC} = LRFD load factor for structural components and attachments
γ_{DW} = LRFD load factor for wearing surfaces and utilities
γ_L = evaluation live-load factor
γ_P = LRFD load factor for permanent loads other than dead loads
σ = element longitudinal stress
σ_{max} = maximum compressive stress at the extreme compression fiber of slab
σ_{min} = minimum compressive stress at the bottom of the slab
θ = skew angle
ϕ = LRFD resistance factor
ϕ_C = condition factor
ϕ_S = system factor

APPENDIXES A THROUGH L

Appendixes A through L are provided on the enclosed CD-ROM, *CRP-CD-56.*

APPENDIX M
DRAFT CODE AND COMMENTARY LANGUAGE

M.1 STRATEGIES FOR SELECTING PROPOSED DESIGN PROVISIONS

According to Appendix K, there are several proposed design criteria derived by the regression analyses based on the finite element analysis results from the parametric studies. The rationale for selecting the most appropriate design equations is presented in this appendix. Two critical sections, i.e. positive and negative moments, are considered separately.

M.1.1 Positive Moment Section

In the impact studies (Appendix L), the rating factors (RF) of all bridges were computed using different proposed effective slab width design equations, including the current AASHTO–LRFD Specifications. The absolute average percentage or p_1–value was introduced as the main indicator of impacts from the change of specifications compared to the current code. The p_1–values for the full slab width (Equation K–9) were included.

The results from the impact studies for the positive moment section show insignificant differences among all the proposed design equations, i.e. Equations K–3 to K–9 (full slab width). The largest p_1–value occurs on the interior girder of the SS–21 case but is less than 4% compared to the current AASHTO–LRFD code.

Therefore, the full slab width is recommended to be the proposed design criteria for the positive moment section for compositely designed girders.

M.1.2 Negative Moment Section

The regression analyses performed on the FEM–based effective slab width values for the negative moment section results in several design equations which were presented in Appendix K. There are twelve design equations listed from Equations K–10 to K–21.

In order to choose the most appropriate equation from twelve possible equations, the selection process would be more effective by examining the following categories.

1. Cracked versus Uncracked

From a design perspective, the critical negative moment section is located over the interior support, i.e., at $1.0L_1$. The analysis results show that cracking takes place at this maximum negative moment section at service loads. The FEM–based effective slab width values of the cracked slab section were also used in the regression analyses. In addition, cracking of the slab increases the effective slab width which would shift the location of the neutral axis upward and induce larger compressive stresses in the bottom flange of the girders. There are six candidate design equations investigated for cracked slab sections. Figure M.1 summarizes the chosen equations during the selection process.

2. Interior, Exterior and Both Girders Criteria

The six equations mentioned above consist of two equations for interior girder only, two equations for exterior girder only and two equations derived for both interior and exterior girders. Tables M–2 to M–5 summarize the impact results of continuous bridges in terms of the percentage absolute average which was designated as p_1 in Appendix L. The absolute average values were computed based on the rating factor of bridges with the effective slab width determined by the current AASHTO–LRFD Specifications. Hence, column 2 shows all values of zero for the current AASHTO–LRFD Specifications. Columns 3 and 4 illustrate the absolute average values of the FEM–based effective slab width and the full slab width.

Tables M–2 and M–4 show the impact study results in the negative moment section at the Service II Limit State of the interior and exterior girders, respectively. Column 5 shows the absolute average p_1–values based on Equation K–11 for the interior girder only and Equation K–15 for the exterior girder only. Columns 6 and 7 show p_1–values of Equations K–19 (without L_2/L_1) and K–18 (with L_2/L_1), respectively. The p_1–values indicate insignificant differences among all Equations based on the full slab width criteria.

The Strength I Limit State appears to govern the design of the negative moment section for these bridges. The p_I–values of the interior and exterior girders at the Strength I Limit State are summarized in Tables M–3 and M–5, respectively. These p_I–values indicate that all six design equations can be as unconservative as 47% compared to the current specifications. However, columns 5 to 7 show minor differences among all six equations for all bridges. Thus, having one equation for both interior and exterior girders would not be inaccurate. Therefore, two out of six design equations are chosen in this section (see Table M.1).

3. With Span Ratio and Without Span Ratio

There are only two design equations in this section, i.e. Equations K–18 (with L_2/L_1) and K–19 (without L_2/L_1). Figures M.1(a) and M.1(b) plot the p_I–values when the effective slab width computed using Equations K–18 and K–19, for the interior and exterior girders, respectively. The differences between the two design equations are trivial. Therefore, the span ratio parameter (L_2/L_1) can be disregarded from the design equation for the sake of simplicity. The final proposed design criteria for the negative moment section is Equation K–19 (see Table M.1). Figure M.2 shows a three–dimensional surface and contour plots of Equation K–19 and FEM results. Figure M.2(c) is a contour plot of Equation K–19 on L/S versus b_{eff}/b plane for different skew angles range from 10° to50°. Crosses and circles illustrate FEM results scattering above these straight lines, which indicates that Equation K–19 is more conservative than the actual FEM b_{eff}/b values. Similarly, Figure M.2(d) is a contour plot of Equation K–19 on θ versus b_{eff}/b plane for different L/S values range from 10 to 50. The results obtained from finite element analyses are greater than the values computed by Equation K–19. It is noteworthy that the maximum L/S value in the finite element analyses was 25.

In addition, the absolute average or p_I–values of the full slab width also show minor differences compared to the FEM–based p_I–values, which had been treated as the more accurate values. The largest difference in the p_I–value appears in Table M.3 for the CS–63 case (8.5%). As far as

simplicity is concerned, the full slab width is preferable for the design of the negative moment sections when bridges are considered to be within the range of applicability.

The proposed code language and commentary of the effective slab width are presented in the next section and followed by the proposed modified Section 4.6.2.6 in two--column format for the AASHTO–LRFD Specifications.

M.2 DESIGN SPECIFICATIONS

M.2.1 Effective Flange Width

For both interior and exterior girders designed to be composite sections, the effective flange width may be assumed equal to the physical flange width subject to the following range of applicability.

- $L \leq 60m$
- $S \leq 4.8m$
- $\theta \leq 60^{\circ}$

The slab should be assumed to be cracked when this provision is used in the negative moment regions.

M.2.2 Commentary

The effective flange width provisions were determined by regression analyses applied to results obtained from parametric studies of finite element models and by sensitivity analysis of various candidate regression expressions.

For the negative moment region only, one possible alternative for determining the effective flange width is provided by Equation M–1 and is more accurate,

$$\frac{b_{eff}}{b} = 0.948 + 0.003\left(\frac{L}{S}\right) - 0.001\theta \qquad \text{(M–1)}$$

where

S = girder spacing (m)

L = span length (m)

θ = skew angle (degree)

Equation M–1 was derived by a curve–fit procedure applied to a set of bridges selected by the design of experiment concepts. Combining the results with the impact investigations, a full slab width can be considered as the effective flange width (b_{eff}/b = 1.0), as specified in the design criteria. By comparing the results using the effective flange width obtained from the finite element analyses and a full slab width, the difference can be as high as 8.5%. By using Equation M–1, the difference can be reduced to approximately 5.9% in the worst case investigated (NCHRP 12–58 Project).

Both the full physical flange width provision and Equation M–1 (will be called C4.6.2.6.1–1) were formulated based on finite element models that have slab cracking in the negative moment section under service loads. Thus, in negative moment regions these provisions should be used assuming the slab to be cracked, i.e., the composite section to consist of the beam section and the longitudinal reinforcement within the effective width of the concrete deck.

For bridges with wider girder spacing (up to 7.68m), the design criteria may be considered. However, there were limited number of bridges that were investigated during the parametric studies. Extreme caution must be taken by the designer for the use of the design criteria with the wider girder spacing bridges outside the range of applicability.

SPECIFICATIONS

4.6.2.6 EFFECTIVE FLANGE WIDTH

4.6.2.6.1 General

In the absence of a more refined analysis and/or unless otherwise specified, limits of the width of a concrete deck slab, taken as effective in composite action for determining resistance for all limit states, shall be as specified herein. The calculation of deflections should be based on the full flange width. For the calculation of live load deflections, where required, the provisions of Article 2.5.2.6.2 shall apply.

For beams and girders designed to be composite sections, the effective flange width may be assumed equal to the full flange width subject to the following range of applicability.

- $S \le 4.8m$
- $L \le 60m$
- $\theta \le 60^\circ$

The concrete slab should be assumed to be cracked when this provision is used in the negative moment regions.

~~The effective span length used in calculating effective flange width may be taken as the actual span for simply-supported spans and the distance between points of permanent load inflection for continuous spans, as appropriate for either positive or negative moments.~~

~~For interior beams, the effective flange width may be taken as the least of:~~

- ~~One-quarter of the effective span length;~~
- ~~12.0 times the average depth of the slab, plus the greater of web depth or one-half the width of the top flange of the girder; or~~
- ~~The average spacing of adjacent beams.~~

COMMENTARY

C4.6.2.6.1

Longitudinal stresses in the flanges are spread across the flange and the composite deck slab by in-plane shear stresses. Therefore, the longitudinal stresses are not uniform. The effective flange width is ~~a reduced width~~ **the width** over which the longitudinal stresses are assumed to be uniformly distributed and yet result in the same force as the nonuniform stress distribution would if integrated over the whole width.

Deleted: both

The effective flange width provisions were determined by regression analyses applied to results obtained from parametric studies of finite element models and by sensitivity analysis of various candidate regression expressions.

The bridges investigated in the finite element parametric study had solid deck thicknesses that met or exceeded the minimum depth of 175 mm specified in Article 9.7.1.1.

For the negative moment region only, one possible alternative for determining the effective flange width is provided by Equation 1 and is more accurate,

$$\frac{b_{eff}}{b} = 0.948 + 0.003\left(\frac{L}{S}\right) - 0.001\theta \le 1.0 \qquad \text{(C4.6.2.6.1-1)}$$

where

b = full flange width (m)

S = girder spacing (m)

L = span length (m), the lesser of the two span lengths if the two span lengths differ

Formatted: Indent: Left: 0", Hanging: 0.2"

θ = skew angle (°)

Deleted: Equation 1 was

Deleted: the

These provisions were derived by a curve-fit procedure applied to a set of steel girder bridges selected by design of experiment (DOE) concepts. A limited number of concrete girder configurations were also analyzed, producing similar trends. Combining the results with the impact

investigations, a full slab width can be considered as the effective flange width (b_{eff}/b

Deleted: = 1.0), as specified in the design criteria. By comparing the results using the effective flange width obtained from the finite element

SPECIFICATIONS

~~For exterior beams, the effective flange width may be taken as one-half the effective width of the adjacent interior beam, plus the least of:~~

- ~~One-eighth of the effective span length;~~
- ~~6.0 times the average depth of the slab, plus the greater of one-half the web depth or one-quarter of the width of the top flange of the basic girder; or~~
- ~~The width of the overhang.~~

COMMENTARY

= 1.0), as specified in the design criteria. By comparing the results using the effective flange width obtained from the finite element analyses and a full slab width, the difference can be as high as 8.5%. By using Equation 1, the difference can be reduced to approximately 5.9% in the worst case investigated (NCHRP 12-58 Project).

Both the full physical flange width provision and Equation 1 were formulated based on finite element models that developed slab cracking in the negative moment section under service loads. Thus, in negative moment regions these provisions should be used assuming the slab to be cracked, i.e., the composite section to consist of the beam section and the longitudinal reinforcement within the effective width of the concrete deck.

Deleted: have

The longer spans in the finite element parametric study consistently exhibited full effective width. The reason for listing a limiting span length is that the parametric study did not consider span lengths beyond that limit. Similarly, the DOE portion of the parametric study was limited to configurations with girder spacing ≤ 4.8 m, although full width was found to be effective for one case with girder spacing of 7.6 m.

Formatted: Font: 11 pt, Bold, Lowered by 2 pt

In calculating the effective flange width for closed steel and precast concrete boxes, ~~the distance between the outside of webs at their tops will be used in lieu of the web thickness, and~~ the spacing will be taken as the spacing between the centerlines of boxes.

For open boxes, the effective flange width of each web should be determined as though each web was an individual supporting element.

~~For filled grid, partially filled grid, and for unfilled grid composite with reinforced concrete slab, the "slab depth" used should be the full~~

~~depth of grid and concrete slab, minus a sacrificial depth for grinding, grooving and wear (typically 13 mm).~~

Where a structurally continuous concrete barrier is present and is included in the models used for analysis as permitted in Article 4.5.1, the width of overhang for the purpose of this article may be extended by:

$$\Delta w = \frac{A_b}{2t_s} \qquad \text{(C4.6.2.6.1-2)}$$

where

A_b = cross-sectional area of the barrier (mm^2)

t_s = depth of deck slab (mm)

Table M.1: Selection criteria of the effective slab width for the negative moment section

Stages	Equation Number	Equation
Cracked Section	[K–10]	$\frac{b_{eff}}{b} = 0.74 + 0.004\left(\frac{L_1}{S}\right) - 0.002\theta + 0.155\left(\frac{L_2}{L_1}\right)$
	[K–11]	$\frac{b_{eff}}{b} = 0.933 + 0.004\left(\frac{L_1}{S}\right) - 0.002\theta$
	[K–14]	$\frac{b_{eff}}{b} = 0.885 + 0.002\left(\frac{L_1}{S}\right) - 0.0002\theta + 0.063\left(\frac{L_2}{L_1}\right)$
	[K–15]	$\frac{b_{eff}}{b} = 0.963 + 0.002\left(\frac{L_1}{S}\right) - 0.0002\theta$
	[K–18]	$\frac{b_{eff}}{b} = 0.812 + 0.003\left(\frac{L_1}{S}\right) - 0.001\theta + 0.109\left(\frac{L_2}{L_1}\right)$
	[K–19]	$\frac{b_{eff}}{b} = 0.948 + 0.003\left(\frac{L_1}{S}\right) - 0.001\theta$
Both Girders	[K–18]	$\frac{b_{eff}}{b} = 0.812 + 0.003\left(\frac{L_1}{S}\right) - 0.001\theta + 0.109\left(\frac{L_2}{L_1}\right)$
	[K–19]	$\frac{b_{eff}}{b} = 0.948 + 0.003\left(\frac{L_1}{S}\right) - 0.001\theta$

Without L_2/L_1	[K–19]	$\frac{b_{eff}}{b} = 0.948 + 0.003\left(\frac{L_1}{S}\right) - 0.001\theta$

Table M.2: Impact study of the interior girder, negative moment section (Service II)

Bridge ID	p_1^* % (Service II)					
	AASHTO	FEM	Full Width	[K–11]	[K–19] w/o L_2/L_1	[K–18] with L_2/L_1
CS–01	0.0	-0.06	-0.06	-0.06	-0.06	0.00
CS–03	0.0	0.00	0.05	0.00	0.00	0.00
CS–07	0.0	-0.55	-0.55	-0.55	-0.55	0.00
CS–09	0.0	-0.06	-0.06	-0.06	-0.06	-0.06
CS–19	0.0	-0.06	-0.06	0.00	0.00	-0.06
CS–21	0.0	-0.33	-0.33	-0.33	-0.33	-0.33
CS–25	0.0	0.03	0.03	0.03	0.03	0.03
CS–27	0.0	0.14	0.14	0.14	0.14	0.14
CS–55	0.0	0.00	0.00	0.11	0.05	0.05
CS–57	0.0	0.00	0.18	0.06	0.06	0.06
CS–61	0.0	0.00	0.00	0.00	0.00	0.00
CS–63	0.0	0.00	0.04	0.04	0.04	0.04
CS–73	0.0	-0.06	-0.06	0.06	0.00	0.00
CS–75	0.0	0.11	0.17	0.11	0.11	0.11
CS–79	0.0	0.06	0.06	-0.06	-0.03	0.03
CS–81	0.0	0.32	0.32	0.23	0.27	0.27

* $$p_1(\%) = \frac{(RF - RF_{AASHTO})}{AVERAGE(RF, RF_{AASHTO})} \times 100$$

Table M.3: Impact study of the interior girder, negative moment section (Strength I)

Bridge ID	p_1^* % (Strength I)					
	AASHTO	FEM	Full Width	[K–11]	[K–19] w/o L_2/L_1	[K–18] with L_2/L_1
CS–01	0.0	0.3	0.3	0.9	0.9	0.3
CS–03	0.0	14.1	14.6	14.3	14.3	14.1
CS–07	0.0	0.4	0.4	0.4	0.4	0.1
CS–09	0.0	-45.5	-45.5	-45.9	-45.9	-46.5
CS–19	0.0	1.5	1.5	-7.9	-7.9	1.5
CS–21	0.0	-27.4	-27.4	-30.5	-29.8	-28.1
CS–25	0.0	0.1	0.1	0.1	0.1	0.1
CS–27	0.0	-2.7	-2.7	-2.5	-2.5	-2.7
CS–55	0.0	1.7	1.7	-2.2	-0.8	-1.4
CS–57	0.0	1.5	4.4	2.4	3.0	2.7
CS–61	0.0	-0.2	-0.2	0.2	0.1	0.2
CS–63	0.0	2.1	10.6	6.8	8.0	7.4
CS–73	0.0	0.0	0.0	-1.1	-0.1	0.0
CS–75	0.0	-30.9	-30.1	-30.9	-30.6	-30.4
CS–79	0.0	0.2	0.2	-0.3	-0.1	0.1
CS–81	0.0	-0.2	-0.2	0.3	0.1	0.0

* $$p_1(\%) = \frac{(RF - RF_{AASHTO})}{AVERAGE(RF, RF_{AASHTO})} \times 100$$

Table M.4: Impact study of the exterior girder, negative moment section (Service II)

Bridge ID	p_1^* % (Service II)					
	AASHTO	FEM	Full Width	[K–15]	[K–19] w/o L_2/L_1	[K–18] with L_2/L_1
CS–01	0.0	-0.06	-0.06	-0.06	-0.06	0.00
CS–03	0.0	-0.25	-0.25	-0.25	-0.25	-0.25
CS–07	0.0	0.05	0.05	0.05	0.05	0.00
CS–09	0.0	-0.05	-0.05	-0.05	-0.05	-0.05
CS–19	0.0	0.00	0.00	0.00	0.00	0.00
CS–21	0.0	-0.31	-0.31	-0.31	-0.31	-0.31
CS–25	0.0	0.00	0.00	0.00	0.00	0.00
CS–27	0.0	0.12	0.12	0.12	0.12	0.12
CS–55	0.0	-0.06	-0.06	0.00	0.06	0.06
CS–57	0.0	0.06	0.06	0.00	0.00	-0.06
CS–61	0.0	-0.17	-0.17	-0.17	-0.17	0.00
CS–63	0.0	0.00	0.00	0.00	0.00	0.00
CS–73	0.0	-0.06	-0.06	0.00	0.00	0.00
CS–75	0.0	0.10	0.10	0.05	0.05	0.05
CS–79	0.0	0.04	0.04	0.00	-0.04	0.00
CS–81	0.0	0.33	0.33	0.22	0.16	0.22

* $$p_1(\%) = \frac{(RF - RF_{AASHTO})}{AVERAGE(RF, RF_{AASHTO})} \times 100$$

Table M.5: Impact study of the exterior girder, negative moment section (Strength I)

Bridge ID	p_1^* % (Strength I)					
	AASHTO	FEM	Full Width	[K–15]	[K–19] w/o L_2/L_1	[K–18] with L_2/L_1
CS–01	0.0	0.8	0.8	0.3	0.1	-0.4
CS–03	0.0	-22.9	-14.0	-16.1	-16.7	-18.7
CS–07	0.0	0.1	0.1	0.1	0.1	0.0
CS–09	0.0	-41.0	-41.0	-41.5	-41.5	3.9
CS–19	0.0	0.7	0.7	0.3	0.1	0.7
CS–21	0.0	-26.2	-26.2	-27.9	-28.5	-26.7
CS–25	0.0	0.1	0.1	0.1	0.1	0.1
CS–27	0.0	-2.4	-2.4	-2.3	-2.3	-2.4
CS–55	0.0	-1.7	-1.7	-2.7	-4.1	-4.6
CS–57	0.0	5.8	5.8	5.4	4.9	4.6
CS–61	0.0	-0.6	-0.6	-0.5	-0.4	0.3
CS–63	0.0	4.7	4.7	4.7	4.9	4.4
CS–73	0.0	0.0	0.0	0.0	-0.9	0.1
CS–75	0.0	-27.9	-27.9	-28.1	-28.4	-28.3
CS–79	0.0	0.1	0.1	0.0	-0.1	0.0
CS–81	0.0	-1.2	-1.2	-1.1	-0.9	-1.0

* $$p_1(\%) = \frac{(RF - RF_{AASHTO})}{AVERAGE(RF, RF_{AASHTO})} \times 100$$

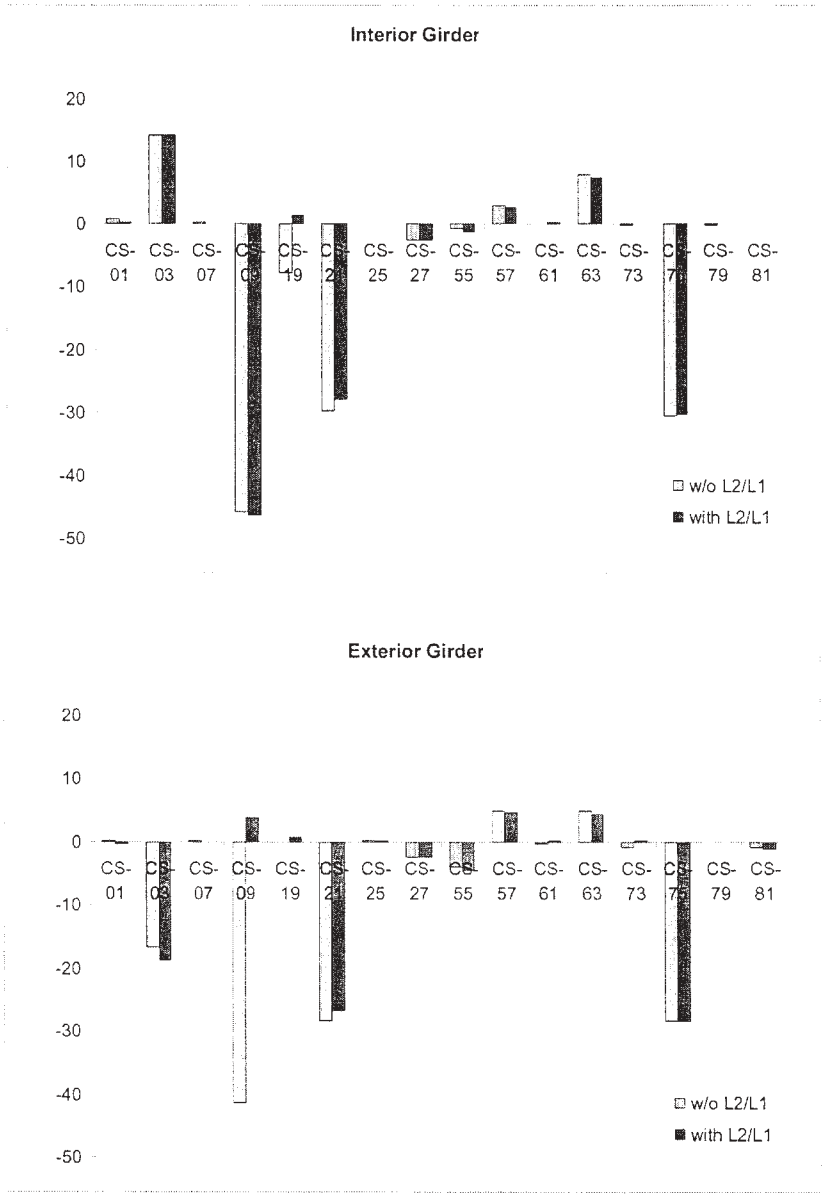

Figure M.1: Comparisons of the absolute average value at Strength I Limit State

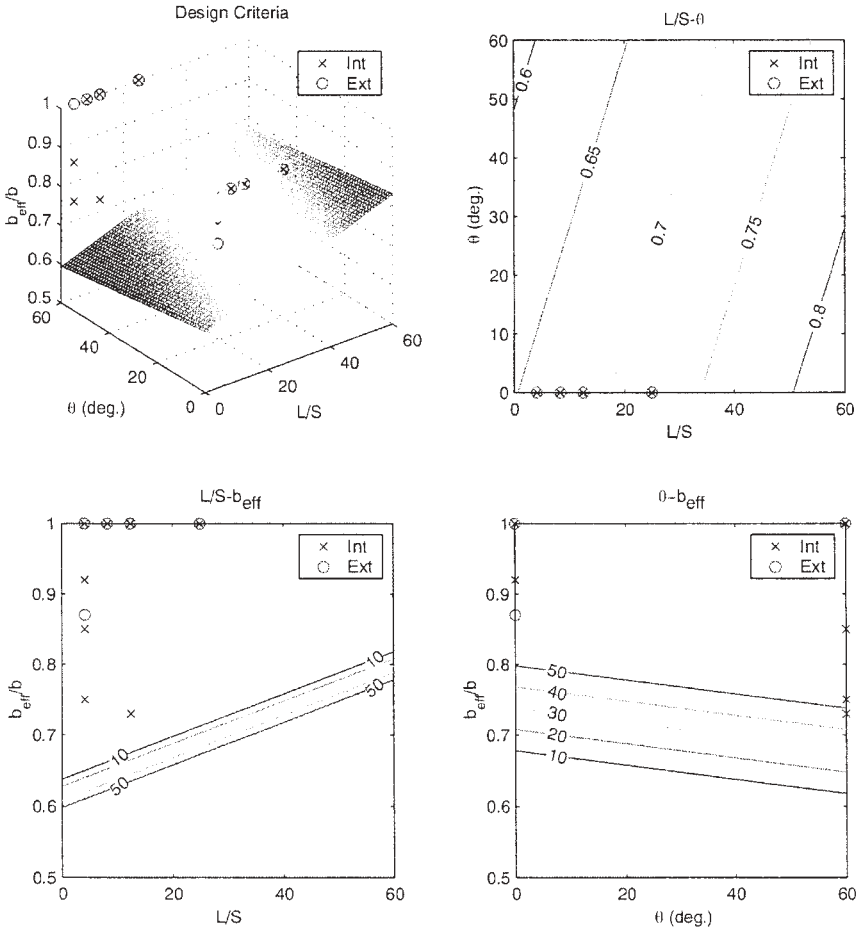

Figure M.2: Three–dimensional plot of the proposed design equation for the negative moment section.

APPENDIX N

Appendix N is provided on the enclosed CD-ROM, *CRP-CD-56.*

APPENDIX O
DESIGN EXAMPLES

Appendix O has not been edited by TRB.

APPENDIX **O**
DESIGN EXAMPLE:
Two-Span Continuous Steel Hybrid Plate Girder Bridge

O.1 Introduction

This example focuses primarily on the design of an interior girder for a two-span continuous superstructure. The interior girder is designed according to the Third Edition of AASHTO LRFD Bridge Design Specification (AASHTO 2004). The specifications are applied in design through a line girder analysis.

O.2 Cross Section Description

The superstructure consists of 5 girders spaced at 3,690 mm spanning a length equal to 40 m measured from girder abutment bearing to pier bearing. The superstructure is offset to an 18 degree skew at both abutments and at the pier. The deck consists of a 200 mm structural thickness with a 40 mm integral wearing surface (IWS). Figure O-1 shows a typical bridge cross section.

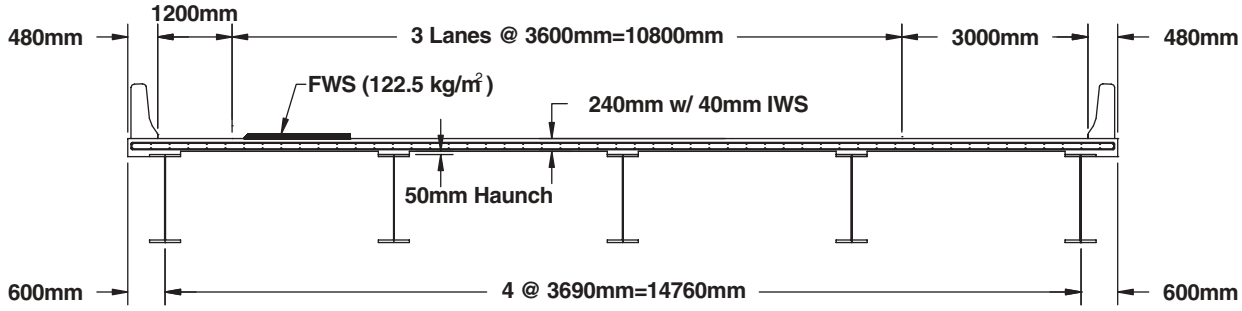

Figure O-1 Typical Bridge Cross Section

O.3 Framing Plan Description

A field splice is located in each of the two spans. The field splice provides a girder length that can be transported and erected easily. The splices are located at a distance of 75 percent of the span length from each abutment bearing point, which is close to the dead load inflection point. The girder is laterally braced at a spacing of 7 meters and 6 meter in the positive and negative moment regions, respectively. The locations of the cross frames avoid interference with the field splice. The cross frames are oriented at 18 degrees, parallel to the skew at the support. If the orientation of the frames exceeds 20 degrees, intermediate cross frames shall be positioned normal to the main members. Figure O-2 shows a framing plan.

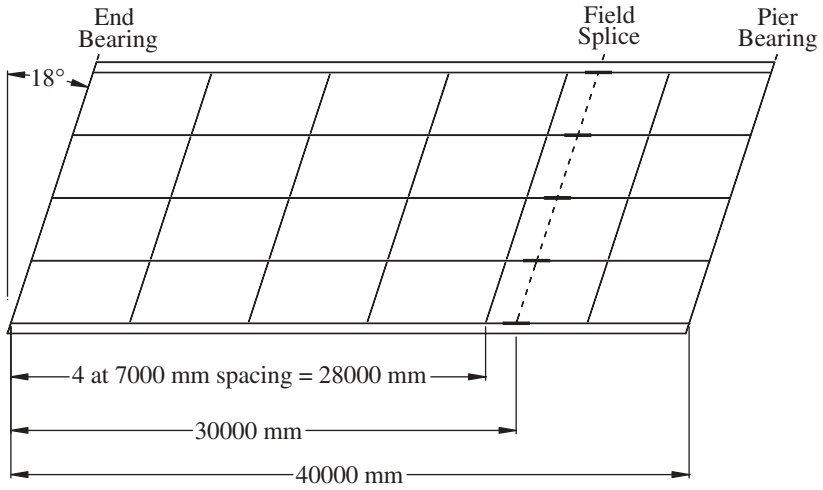

Figure O-2 Bridge Framing Plan

O.4 Material Properties

High performance steel (HPS) flanges were implemented in this design. The entire length of the bottom flange and the top flange in the negative moment regions are designed with HPS following industry guidelines for the most economical configuration (Figure O-3). Each of the I-section structural steels are designed with weathering steel. This design incorporates the following structural steels:

Grade 345W	: Top flange in the positive moment region and the entire web
Grade 485W HPS	: Both flanges in the negative moment regions and the bottom flange in the positive moment region
Grade 420	: Deck reinforcing steel

The concrete compressive strength is 28 MPa with a modular steel-to-concrete ratio, n=8. The deck reinforcing steel has a minimum yield stress of 420 MPa. The deck was designed according to empirical design criteria, which is valid between girders where internal arching can develop.

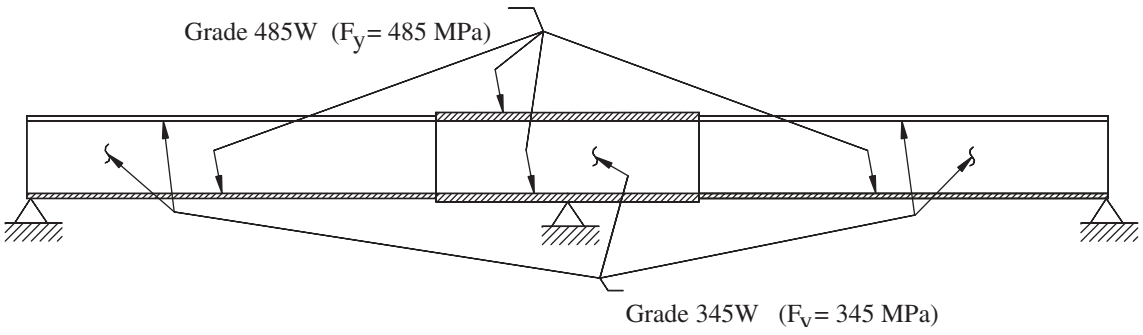

Figure O-3 Hybrid Configuration

O.5 Girder Elevation Description

The elevation view of the interior girder is provided in Figure O-4.

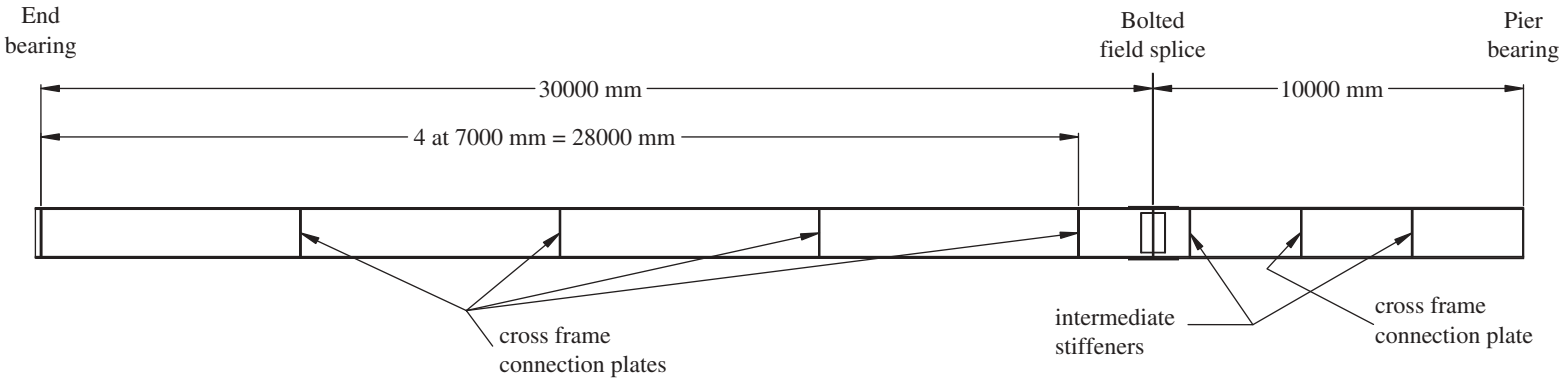

Figure O-4. Elevation View of Interior Girder

O.6 Design Assumptions

- Average daily truck traffic (ADTT) is 2500 with a 75 year design life.
- The concrete haunch is assumed to have no structural contribution to the resistance of the girder and is assumed a constant 50 mm along the entire girder length.
- The plates and girder attachments are assumed to be five percent of the total girder weight.
- The ratio of positive moment stiffness to negative moment stiffness is assumed equal to one in the structural analysis.
- The future wearing surface and parapet loads are assumed to be shared equally by all girders.
- This example assumes no lateral load will be applied to the flanges of interior girders in either the positive or negative moment regions.
- Other design assumptions are stated within the design calculations.

O.7 Notations

Variable [1]	Description
A	Fatigue detail category constant.
A_{10}	Cross-sectional area of number 10 metric bar reinforcement.
A_{16}	Cross-sectional area of number 16 metric bar reinforcement.
A_{19}	Cross-sectional area of number 19 metric bar reinforcement.
$A_{deck.LT}$	Area of structural concrete effective slab for long-term composite section.
$A_{deck.ST}$	Area of structural concrete effective slab for short-term composite section.
ADTT	Average daily truck traffic.
$ADTT_{SL}$	Average daily truck traffic for a single lane.
$A_{f.b}$	Cross-sectional area of bottom flange.
$A_{f.t}$	Cross-sectional area of top flange.
A_{fn}	Area of the flange governed by the variable D_n.
A_g	Cross-sectional area of girder.
A_{g_avg}	Averaged cross-sectional area of the girder in the positive and the negative moment regions.
A_{rb}	Area of the bottom layer of reinforcing steel within the effective slab width.
A_{rt}	Area of the top layer of reinforcing steel within the effective slab width.
$A_{s\_bottom\_min}$	Minimum cross-sectional area of bottom reinforcing steel per unit deck width required in the negative moment region for empirical deck design.
$A_{s\_bottom\_provided}$	Cross-sectional area of bottom reinforcing steel per unit deck width provided in the negative moment region.
$A_{s\_neg\_min}$	Minimum cross-sectional area of reinforcing steel per unit deck width required in the negative moment region for empirical deck design.
$A_{s\_top\_min}$	Minimum cross-sectional area of top reinforcing steel per unit deck width required in the negative moment region for empirical deck design.
$A_{s\_top\_provided}$	Cross-sectional area of top reinforcing steel per unit deck width provided in the negative moment region.
A_{sc}	Cross-sectional area of a shear connector.
A_w	Cross-sectional area of web.
a_{wc}	Ratio of twice the area of the web in compression at the strength limit state to the area of the compression flange. Factor used in the calculation of R_h.
b_{eff}	Structural effective slab width.
$b_{f.b}$	Bottom flange width.
$b_{f.t}$	Top flange width.
C	Ratio of the shear buckling stress to the shear yield strength.
c_1	Skew correction factor variable.
Category	Fatigue detail category.

Variable [1]	Description
C_b	Moment gradient correction factor.
c_{bottom}	Bottom reinforcing steel concrete cover with respect to structural thickness.
CD_i	Factored construction dead load. Applied to the interior girder.
CL	Unfactored construction live load.
CL_i	Factored construction live load. Applied to the interior girder.
C_{rb}	Distance from top of the structural slab to the centroid of the bottom reinforcing steel.
C_{rt}	Distance from top of the structural slab to the centroid of the top reinforcing steel.
c_{top}	Top reinforcing steel concrete cover with respect to structural thickness.
D	Total depth of web excluding flange thickness.
d	Height of girder. Sum of web depth and flange thickness.
$d_{Bot\_Steel\_LT}$	Distance from the elastic neutral axis of the long-term composite girder to the bottom fiber of steel.
$d_{Bot\_Steel\_NC}$	Distance from the elastic neutral axis of the girder cross-section to the bottom fiber of steel.
$d_{Bot\_Steel\_ST}$	Distance from the elastic neutral axis of the short-term composite girder to the bottom fiber of steel.
D_c	Depth of web in compression for the non-composite section in the elastic range.
$DC1_{attachments}$	Unfactored load from plates and attachments. Applied to the girder as a uniform load.
$DC1_e$	Sum of unfactored non-composite section dead loads. Applied to the exterior girder as a uniform load.
$DC1_{girder}$	Unfactored load from the girder self-weight. Applied to the girder as a uniform load.
$DC1_{haunch}$	Unfactored load from the haunch. Applied to the girder a line load.
$DC1_i$	Sum of unfactored non-composite section dead loads. Applied to the interior girder as a uniform load.
$DC1_{sipf}$	Unfactored load from the stay-in-place forms applied to the girder as a uniform load.
$DC1_{slab.e}$	Unfactored load from the exterior girder slab self-weight Applied to the exterior girder as a uniform load.
$DC1_{slab.i}$	Unfactored load from the interior girder slab self-weight. Applied to the interior girder as a uniform load.
D_{cp}	Depth of web in compression at plastic moment.
d_e	Distance from the exterior web of the exterior beam ant the interior edge of the curb or traffic barrier.
$d_{f.b}$	Distance from the bottom of girder to the centroid of the bottom flange.
$d_{f.t}$	Distance from the bottom of girder to the centroid of the top flange.
DFM_1	Moment load distribution factor for one lane loaded case.
$DFM_{1fatigue}$	Moment load distribution factor for fatigue loading case.

Variable [1]	Description
DFM_2	Moment load distribution factor for two lanes loaded case.
DFM_E	Governing skew corrected moment load distribution factor. Applies to the exterior girder.
DFM_{E_F}	Governing skew corrected moment load distribution factor for fatigue loading case. Applies to the exterior girder.
DFM_I	Governing skew corrected moment load distribution factor. Applies to the interior girder.
DFM_{I_F}	Governing skew corrected moment load distribution factor for fatigue loading case. Applies to the interior girder.
DFM_{skew_corr}	Moment load distribution skew correction factor.
DF_n	Nominal fatigue resistance.
DF_{TH}	Constant-amplitude fatigue threshold stress.
DFV_1	Shear load distribution factor for one lane loaded case.
DFV_2	Shear load distribution factor for two lanes loaded case.
DFV_E	Governing skew corrected shear load distribution factor. Applies to the exterior girder.
DFV_{E_F}	Governing skew corrected shear load distribution factor for fatigue loading case. Applies to the exterior girder.
DFV_{E1}	Shear load distribution factor for one lane loaded case calculated using the lever rule. Equal to $DMFLever_1$. Applies to the exterior girder.
DFV_{E2}	Shear load distribution factor for two lanes loaded case. Applies to the exterior girder.
DFV_I	Governing skew corrected shear load distribution factor. Applies to the interior girder.
DFV_{I_F}	Governing skew corrected shear load distribution factor for fatigue loading case. Applies to the interior girder.
DFV_{skew_corr}	Shear load distribution skew correction factor.
D_{M1}	Moment load distribution factor for one lane loaded case including multiple presence factor. Applies to the exterior girder.
D_{M2}	Moment load distribution factor for two lanes loaded case including multiple presence factor. Applies to the exterior girder.
D_{M3}	Moment load distribution factor for three lanes loaded case including multiple presence factor. Applies to the exterior girder.
D_{M4}	Moment load distribution factor for four lanes loaded case including multiple presence factor. Applies to the exterior girder.
$DMFLever_1$	Moment load distribution factor for one lane loaded case with respect to the lever rule. Applies to the exterior girder.
$DMFLever_{1\_f}$	Moment load distribution factor for fatigue loading case with respect to the lever rule. Applies to the exterior girder.
D_n	Minimum of the distances between the non-composite section neutral axis to the top and bottom of the web.
d_o	Stiffener spacing.
D_p	Depth from top of structural slab to the plastic neutral axis of the

Variable [1] .....Description

composite section.

Driving .....Distance to centroid of driving forces with respect to the lever rule.

d_{stud} .....Diameter of shear connector.

D_t.....Depth from top of structural slab to the bottom of the girder.

$d_{Top\_Steel\_LT}$ .....Distance from the elastic neutral axis of the long-term composite girder to the top fiber of steel.

$d_{Top\_Steel\_NC}$.....Distance from the elastic neutral axis of the girder cross-section to the top fiber of steel.

$d_{Top\_Steel\_NC\_avg}$ .....Averaged distance from the elastic neutral axis of the girder cross-section to the top fiber of steel in the positive and negative moment regions.

$d_{Top\_Steel\_ST}$ .....Distance from the elastic neutral axis of the short-term composite girder to the top fiber of steel.

d_w.....Distance from the bottom of girder to the centroid of the web.

e.....Correction factor for moment distribution in an exterior girder.

e_1 .....Correction factor for shear distribution in an exterior girder.

E_c.....Modulus of elasticity of concrete.

e_g .....Distance between the centroid of the non-composite girder and the centroid of the structural deck.

e_{R1}.....Distance between centerline of bridge and first (exterior) design truck.

e_{R2}.....Distance between centerline of bridge and second design truck.

e_{R3}.....Distance between centerline of bridge and third design truck.

e_{R4}.....Distance between centerline of bridge and fourth design truck.

E_s .....Modulus of elasticity of steel.

f'_{c_deck} .....Compressive strength of concrete deck.

f_2.....Stress in compression flange calculated from M_2.

f_{bu}.....Flange bending stress neglecting lateral bending stress.

F_{cr} .....Critical buckling stress.

F_{crw} .....Critical buckling stress of the web.

f_{DC1_cf}.....Stress in the compression flange calculated from unfactored non-composite dead loads.

f_{DC1_tf} .....Stress in the tension flange calculated from unfactored non-composite dead loads.

f_{DC2_cf}.....Stress in the compression flange calculated from unfactored superimposed dead loads.

f_{DC2_tf} .....Stress in the tension flange calculated from unfactored superimposed dead loads.

f_{DW_cf} .....Stress in the compression flange calculated from unfactored wearing surface dead load.

f_{DW_tf}.....Stress in the tension flange calculated from unfactored wearing surface dead load.

f_l .....Flange lateral bending stress.

f_1.....The maximum stress calculated from; 1.) two times f_{mid} minus f_2

Variable [1]	Description
	and 2.) f_o.
$f_{LL\_IM\_cf}$	Stress in the compression flange calculated from unfactored live load plus impact.
$f_{LL\_IM\_tf}$	Stress in the tension flange calculated from unfactored live load plus impact.
f_{mid}	Stress in compression flange calculated from M_{mid}.
F_{nc}	Nominal flexural resistance of the compression flange in terms of stress.
$F_{nc.FLB}$	Nominal flexural resistance with respect to flange lateral buckling in terms of stress.
$F_{nc.LTB}$	Nominal flexural resistance of the compression flange to lateral torsional buckling in terms of stress.
F_{nc_1}	Nominal flexural resistance of the compact compression flange in terms of stress.
F_{nc_2}	Nominal flexural resistance of the noncompact compression flange in terms of stress.
F_{nc_3}	Nominal flexural resistance of the slender compression flange in terms of stress.
f_o	Stress in compression flange calculated from M_o.
$f_{serviceII\_cf}$	Stress in the compression flange calculated using service II load factors.
$f_{serviceII\_tf}$	Stress in the tension flange calculated using service II load factors.
f_{strI_cf}	Stress in the compression flange calculated using strength I load factors.
f_{strI_tf}	Stress in the tension flange calculated using strength I load factors.
F_u	Minimum tensile strength of a shear stud connector.
$F_{y.345}$	Yield stress of steel (50 ksi).
$F_{y.485}$	Yield stress of high performance steel (70 ksi).
F_{yc}	Yield stress of compression flange steel.
F_{yr}	Yield stress of deck reinforcing steel.
$F_{yr.FLB}$	Yield stress of compression flange used to calculate flange lateral buckling resistance.
F_{yt}	Yield stress of tension flange steel.
F_{yw}	Yield stress of web steel.
h_{stud}	Height of shear connector.
I_{deck}	Moment of inertia of the deck about its centroid with respect to the horizontal axis.
$I_{deck.LT}$	Long-term moment of inertia of the deck about its centroid with respect to the horizontal axis.
$I_{f.b}$	Moment of inertia of the bottom flange about its centroid with respect to the horizontal axis.
$I_{f.t}$	Moment of inertia of the top flange about its centroid with respect to the horizontal axis.
I_{LT}	Long-term moment of inertia of the composite section about its

Variable [1]	Description
	centroid with respect to the horizontal axis.
I_{NC}	Moment of inertia of the girder about its centroid with respect to the horizontal axis.
I_{NC_avg}	Averaged moment of inertia of the girder about its centroid with respect to the horizontal axis in the positive and negative moment regions.
I_{ST}	Short-term moment of inertia of the composite section about its centroid with respect to the horizontal axis.
I_w	Moment of inertia of the web about its centroid with respect to the horizontal axis.
I_{yc}	Moment of inertia of the compression flange about its vertical axis.
I_{yt}	Moment of inertia of the tension flange about its vertical axis.
k	Shear buckling coefficient.
K_g	Longitudinal stiffness parameter used in the calculation of load distribution factors.
L_b	Unbraced length.
L_{eff}	Slab effective length based on empirical deck design.
L_p	Lateral bracing limit for flexural capacity governed by plastic bending.
L_{pick}	Length of girder to be erected (picked) for erection and transport.
L_r	Lateral bracing limit for flexural capacity governed by inelastic lateral tosional buckling.
L_{span}	Span length from abutment bearing to pier bearing.
m_1	Multiple presence factor for one lane loaded.
m_2	Multiple presence factor for two lanes loaded.
M_2	Largest moment at either brace point.
m_3	Multiple presence factor for three lanes loaded.
m_4	Multiple presence factor for four lanes loaded.
MAD	Remaining flexural resistance in flange calculated by subtracting stresses due to dead loads factored by the strength I load combination in terms of stress.
M_{DC1}	Moment calculated from unfactored non-composite dead loads.
M_{DC2}	Moment calculated from unfactored superimposed dead loads.
M_{DW}	Moment calculated from unfactored wearing surface dead load.
M_{fat_max}	Maximum stress at point of interest due to fatigue load combination.
M_{fat_min}	Minimum stress at point of interest due to fatigue load combination.
M_{fat_range}	Stress range calculated from M_{fat_min} and M_{fat_max} at point of interest.
min_edge_dist	Minimum shear connecter edge distancespacing.
min_stud_spacing	Minimum center-to-center shear connecter spacing.
M_{LL_IM}	Moment calculated from unfactored live load plus impact.
M_{mid}	Moment calculated at the mid-span of the unbraced region.
M_n	Nominal flexural resistance.
M_o	Moment at brace point opposite to M_2.

Variable [1]	Description
M_p	Plastic moment resistance of composite section.
M_{u_const}	Moment due to factored construction loads.
$M_{u\_strength\_I}$	Factored strength I moment.
M_{yt}	Yield moment of the tension flange.
n	Modular ratio with respect to steel and concrete.
n	Number of stress range cycles per truck.
N	Number of stress cycles during the design life.
N_c	Number of stress cycles on the shear connector during its design life.
n_s	Number of shear connectors in a cross-section.
N_{DL}	Number of design lanes.
N_G	Number of girders.
n_{stud_min}	Minimum number of required shear connectors to satisfy the strength limit state.
Number_Studs	Number of shear connectors provided across the region of interest.
Over_Placement	Factored combined construction live and dead loads. Applies to regions where the wet concrete is in placement.
p	Single lane adjustment factor.
P	The minimum of P_{1p} and P_{2p}.
P_{1p}	Nominal shear force according to the structural deck area.
P_{2p}	Nominal shear force according to the girder area.
P_{br}	Yield force of bottom reinforcing steel within effective slab width.
P_c	Yield force of compression flange.
Pitch	Chosen pitch satisfying the $pitch_{max}$ and $pitch_{min}$ requirements.
$pitch_{max}$	Maximum pitch required satisfying fatigue requirement for shear connector design.
$pitch_{min}$	Minimum pitch for shear connector design.
Previously_Placed	Factored construction dead load including slab weight. Applies to regions where concrete has been placed and live load is no longer present.
P_s	Compressive crushing force of concrete effective slab width.
P_t	Yield force of tension flange.
P_{tr}	Yield force of top reinforcing steel within effective slab width.
P_w	Yield force of web.
Q	First moment of the transformed area of the deck about the short-term neutral axis.
Q_r	Factored shear resistance of an individual shear connector at the strength limit state.
R_1	Moment load distribution factor for one lane loaded case excluding the multiple presence factor.
R_2	Moment load distribution factor for two lanes loaded case excluding the multiple presence factor.
R_3	Moment load distribution factor for three lanes loaded case excluding the multiple presence factor.
R_4	Moment load distribution factor for four lanes loaded case

Variable [1]	**Description**
	excluding the multiple presence factor.
R_b	Load shedding factor for the composite section.
Resisting	Distance to centroid of resisting forces with respect to the lever rule.
R_h	Hybrid factor. A flange stress reduction factor.
r_t	Radius of gyration about the vertical axis.
S	Center to center girder spacing.
$S_{Bot\_Steel\_LT}$	Long-term elastic section modulus of the girder with respect to outer fiber of the bottom flange steel.
$S_{Bot\_Steel\_NC}$	Elastic section modulus of the girder with respect to outer fiber of the bottom flange steel.
$S_{Bot\_Steel\_ST}$	Short-term elastic section modulus of the girder with respect to outer fiber of the bottom flange steel.
$spacing_{bottom\_max}$	Maximum spacing of bottom reinforcing steel based on empirical deck design.
$spacing_{provided}$	Provided reinforcing steel spacing.
$spacing_{top\_max}$	Maximum spacing of top reinforcing steel based on empirical deck design.
$S_{Top\_Steel\_LT}$	Long-term elastic section modulus of the girder with respect to outer fiber of the top flange steel.
$S_{Top\_Steel\_NC}$	Elastic section modulus of the girder with respect to outer fiber of the top flange steel.
$S_{Top\_Steel\_ST}$	Short-term elastic section modulus of the girder with respect to outer fiber of the top flange steel.
s_{truck}	Design truck spacing.
$S_{truck\_parapet}$	Minimum spacing between design truck and parapet.
S_{xt}	Elastic section modulus for the flange calculated according to MAD.
t_{core}	Thickness of deck core with respect to structural thickness.
t_{deck}	Thickness of deck including integral wearing surface.
$t_{f.b}$	Thickness of bottom flange.
$t_{f.t}$	Thickness of top flange.
t_{haunch}	Thickness of haunch.
Transverse_Spacing	The center-to-center transverse shear connector spacing.
t_s	Structural thickness of the deck slab excluding integral wearing surface.
t_w	Thickness of web.
Unplaced	Factored construction dead load excluding slab weight. Applies to regions where concrete has not yet been placed.
V_{cr}	Shear buckling force.
V_{DC1}	Shear calculated from unfactored non-composite dead loads.
V_{DC2}	Shear calculated from unfactored superimposed dead loads.
V_{DW}	Shear calculated from unfactored wearing surface dead load.
V_f	Shear force range calculated from V_{fat_min} and V_{fat_max} used in the

Variable [1]	Description
	design of the shear connectors.
V_{fat_comb}	Shear force range calculated from $V_{fatigue\_min}$ and $V_{fatigue\_max}$ at point of interest.
V_{fat_max}	Maximum shear force at point of interest due to fatigue load combination. Used in the design of the shear connectors.
V_{fat_min}	Minimum shear force at point of interest due to fatigue load combination. Used in the design of the shear connectors.
$V_{fatigue\_max}$	Maximum shear force at point of interest due to fatigue load combination.
$V_{fatigue\_min}$	Minimum shear force at point of interest due to fatigue load combination.
V_p	Plastic shear force.
V_{sr}	Horizontal shear fatigue force range per unit length.
V_{u_const}	Shear calculated from factored construction loads.
w_{bridge}	Width of bridge.
w_{lane}	Width of lane.
w_{oh}	Width of overhang measured from centerline of exterior girder.
w_p	Width of parapet.
$w_{roadway}$	Width of clear roadway.
w_{shdr_lf}	Width of left shoulder.
w_{shdr_rt}	Width of right shoulder.
wt_{conc}	Unit weight of concrete.
wt_{fws}	Unit weight of future wearing surface.
wt_g	Weight of girder per unit length.
w_{truck}	Width of design truck.
wt_{steel}	Unit weight of steel.
x_1	Distance between the centerline of the bridge and the first exterior girder.
x_2	Distance between the centerline of the bridge and the first interior girder.
x_3	Distance between the centerline of the bridge and the second interior girder.
x_4	Distance between the centerline of the bridge and the third interior girder.
x_5	Distance between the centerline of the bridge and the second exterior girder.
X_{ext}	Distance between the centerline of the bridge and the girder of interest.
y_{bar}	Distance to the plastic neutral axis from the top of the girder.
y_{bf}	Distance from the centroid of the bottom flange to the PNA.
y_{deck}	Distance between the centroid of the effective slab and the top of the girder.
Y_{II}	Location of the plastic neutral axis for case II.
y_{rb}	Distance from the centroid of the bottom deck reinforcement to the

Variable [1]	Description
	PNA.
y_{rt}	Distance from the centroid of the top deck reinforcement to the PNA.
y_s	Distance from the centroid of the structural slab to the PNA.
y_{tf}	Distance from the centroid of the top flange to the PNA.
y_w	Distance from the centroid of the web to the PNA.
Z_r	Shear fatigue strength of a shear connector.

Greek Variable [1]	Description
α	Factor for calculation of shear fatigue resistance of a shear connector.
β	Web to flange area ratio used in the calculation of the hybrid factor R_h.
Φ_f	Resistance factor for flexure.
Φ_v	Resistance factor for flexure.
γ_{conc}	Specific gravity of concrete.
$\gamma\Delta f$	Stress at point of interest calculated from M_{fat_range}.
γ_{fws}	Specific gravity of future wearing surface.
λ_f	Slenderness ratio of the compression flange.
λ_{pf}	Slenderness ratio limit for a compact flange.
λ_{rf}	Slenderness ratio limit for a noncompact flange.
λ_{rw}	Slenderness ratio limit for a noncompact web.
η	Load modifier.
η_Δ	Ductility load factor.
η_I	Importance load factor.
η_P	Redundancy load factor.
ρ	Minimum of the ratio of web to compression flange yield stress and 1.

1. Variables having a subscript (n) or (neg) refer to the negative moment region.

O.8 MathCad Worksheet for Bridge Design

DEFINITION OF GEOMETRIC PARAMETERS

General:

$N_G := 5$ number of girders

$N_L := 3$ number of traffic lanes

Lengths:

$L_{span} := 40\ m$ span length

Thicknesses:

$t_{deck} := 240\ mm$ slab thickness w/ IWS

$t_s := 200\ mm$ structural thickness

$t_{haunch} := 50\ mm$ haunch thickness

$c_{top} := 60\ mm$ top reinforcement cover thickness **[S5.12.3]**

$c_{bottom} := 25\ mm$ bottom reinforcement cover thickness **[S5.12.3]**

$t_{core} := t_s - c_{bottom} - c_{top}$ deck core thickness **[C9.7.2.4]**

$t_{core} = 115\,mm$

Widths:

In order to satisfy conditions for empirical deck design the overhang width must be at least 5 times the structural thickness of the slab or 3.0 times the structural thickness of the slab if the parapet is considered structurally continuous. For this design we will assume the parapet as a structural component. Therefore, the overhang width is defined as follows:

$w_{oh} := 3.0 \cdot t_s$ overhang width $w_{oh} = 600\,mm$

$w_{shdr\_lf} := 1.2 \cdot m$ left shoulder width

$w_{shdr\_rt} := 3.0 \cdot m$ right shoulder width

$w_p := 480 \cdot mm$ parapet width

$w_{lane} := 3600 \cdot mm$ lane width

$w_{bridge} := w_{lane} \cdot N_L + w_{shdr\_lf} + w_{shdr\_rt} + w_p \cdot 2$ $w_{bridge} = 15960\,mm$

$w_{roadway} := w_{lane} \cdot N_L + w_{shdr\_lf} + w_{shdr\_rt}$ $w_{roadway} = 15000\,mm$

$S := \dfrac{(w_{bridge} - 2 \cdot w_{oh})}{N_G - 1}$ girder spacing $S = 3690\,mm$

DEFINITION OF MATERIAL PROPERTIES

Concrete Properties:

$f'_{c\_deck} := 28 \cdot MPa$ compressive strength

$= 4$ ksi

$wt_{conc} := 23.56 \cdot \frac{kN}{m^3}$ =150 pcf

$\gamma_{conc} := 2402 \cdot \frac{kg}{m^3}$

$E_c := 0.043 \cdot \left(\frac{\gamma_{conc} \cdot m^3}{kg} \right)^{1.5} \cdot \sqrt{f'_{c\_deck} \cdot MPa}$

$E_c = 26785.9\,MPa$ **[S5.4.2.4-1]**

Steel Properties:

$F_{y.345} := 345 \cdot MPa$ grade 345 steel

$F_{y.485} := 485 \cdot MPa$ grade 485 steel

Future Wearing Surface:

$\gamma_{fws} := 122.5 \frac{kg}{m^2}$ F.W.S. specific gravity

$wt_{fws} := g \cdot \gamma_{fws}$ F.W.S. load

$wt_{fws} = 1.2 \frac{kN}{m^2}$ =25 psf

Steel Reinforcement Properties:

$F_{yr} := 420 \cdot MPa$ =60 ksi yield stress

$E_s := 200000 \cdot MPa$ modulus of elasticity

Steel Decking Properties:

$wt_{sipf} := 718.2 \cdot Pa$ stay-in-place forms

$wt_{steel} := 77 \cdot \frac{kN}{m^3}$ unit weight

Definition of Steel Grade Locations:

Positive Moment Region:

$F_{yc} := F_{y.345}$ $F_{yc} = 345.0\,MPa$ F_{yc} =50 ksi

Yield strength of web in positive moment region:

$F_{yw} := F_{y.345}$ $F_{yw} = 345.0\,MPa$

Yield strength of tension flange in positive moment region:

$F_{yt} := F_{y.485}$ $F_{yt} = 485.0\,MPa$ F_{yt} =70 ksi

Negative Moment Region:

$F_{yc.n} := F_{y.485}$ $F_{yc.n} = 485.0\,MPa$

Yield strength of web in negative moment region:

$F_{yw.n} := F_{y.345}$ $F_{yw.n} = 345.0\,MPa$

Yield strength of tension flange in negative moment region:

$F_{yt.n} := F_{y.485}$ $F_{yt.n} = 485.0\,MPa$

PRELIMINARY PLATE SIZING

Flange Sizing Considerations:

Flange Width Considerations:

- Use minimum of 300 mm in width to allow room for shear studs.
- Consider wider compression flanges for the bottom flange in the negative moment region and top flange in the positive moment region for constructability to increase lateral stability.
- Transition flanges in thickness (not width) at shop welded splices if possible.

Flange Thickness Considerations:

- Provide at least 19 mm in thickness to avoid weld distortion.
- Do not exceed 50 mm for Thermo Mechanical Controlled Processing (TMCP)

Web Sizing Considerations:

- Consider unstiffened webs for span lengths less than 35 m.
- Consider unstiffened webs if the web depth is less than 1300 mm.
- For web depths between 1300-1800 mm subtract 2-3 mm from the unstiffened web design and provided stiffeners as required.
- Provided the thinnest web possible for webs greater than 1800 mm in depth.

Preliminary Flexural Considerations:

Cross-sectional Proportion Limits: **[S6.10.2 '04]**

Web Proportions: **[S6.10.2.1 '04]**

$\frac{D}{t_w} \le 150$ slenderness limit **[S6.10.2.1-1 '04]**

Flange Proportions: **[S6.10.2.2 '04]**

$\frac{b_f}{2 \cdot t_f} \ge 12.0$ compactness limit **[S6.10.2.2-1 '04]**

$b_f \ge \frac{D}{6}$ **[S6.10.2.2-2 '04]**

$t_f \ge 1.1 \cdot t_w$ **[S6.10.2.2-3 '04]**

$0.1 \le \frac{I_{yc}}{I_{yt}} \le 10$ **[S6.10.2.2-4 '04]**

A field splice is located at 0.75 L_{span} for this example. A handling suggestion for shipping and constructability is to provide a minimum flange width as calculated below:

$L_{pick} := 0.75 \cdot L_{span}$ $L_{pick} = 30\,m$ pick length

$b_f := \frac{L_{pick}}{85}$ $b_f = 352.9\,mm$ handling suggestion **[C6.10.3.4-1 '04]**

Trial Depth Selection:

Suggested minimum span-to-depth ratio for a continuous span design:

$D := 0.027 \cdot L_{span}$ $D = 1080\,mm$ **[Table 2.5.2.6.3-1]**

Suggested optimal depth for the hybrid configuration choosen: (Horton, 2002)

$$\frac{L_{span}}{30} = 1333\,mm$$

Summary Trial Girder Dimensions:

	Positive Flexure:		**Negative Flexure:**	
Top flange width:	$b_{f.t} := 400 \cdot mm$	=15.75 in	$b_{f.t.n} := 450 \cdot mm$	=17.72 in
Top flange thickness:	$t_{f.t} := 25 \cdot mm$	= 1 in	$t_{f.t.n} := 40 \cdot mm$	=1.58 in
Bottom flange width:	$b_{f.b} := 400 \cdot mm$	=15.75 in	$b_{f.b.n} := 540 \cdot mm$	=21.26 in
Bottom flange thickness:	$t_{f.b} := 25 \cdot mm$	= 1 in	$t_{f.b.n} := 40 \cdot mm$	=1.58 in
Web depth:	$D := 1300 \cdot mm$	=51.18 in	$D = 1300\,mm$	=51.18 in
Web thickness:	$t_w := 14 \cdot mm$	=0.55 in	$t_{w.n} := 14 \cdot mm$	=0.55 in

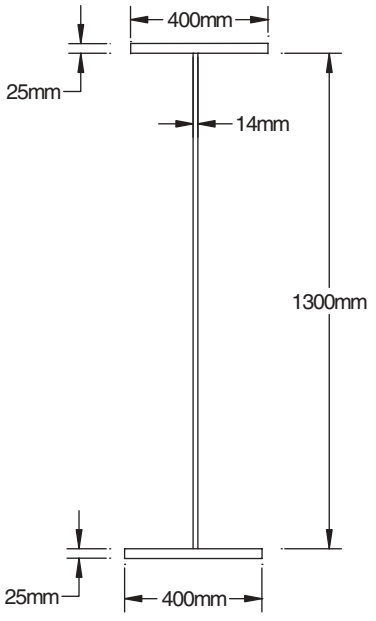

Figure : Cross Section of Interior Girder in Positive Moment Region

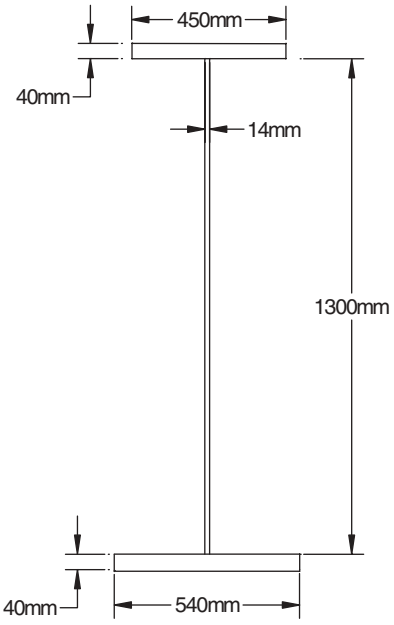

Figure : Cross Section of Interior Girder in Negative Moment Region

NON COMPOSITE SECTION PROPERTIES

Non-Composite Cross-Sectional Properties in the Positive Moment Region:

overall depth: $d := t_{f.t} + D + t_{f.b}$ $d = 1350\,mm$

area of top flange: $A_{f.t} := b_{f.t} \cdot t_{f.t}$ $A_{f.t} = 10000\,mm^2$

area of bottom flange: $A_{f.b} := b_{f.b} \cdot t_{f.b}$ $A_{f.b} = 10000\,mm^2$

area of web: $A_w := D \cdot t_w$ $A_w = 18200\,mm^2$

total area of girder: $A_g := A_{f.t} + A_{f.b} + A_w$ $A_g = 38200\,mm^2$

girder self-weight: $wt_g := A_g \cdot wt_{steel}$ $wt_g = 2.94\,\frac{kN}{m}$

dist. to cent. of top flange: $d_{f.t} := t_{f.b} + D + 0.5 \cdot t_{f.t}$ $d_{f.t} = 1337.5\,mm$

dist. to cent. of bottom flange: $d_{f.b} := 0.5 \cdot t_{f.b}$ $d_{f.b} = 13\,mm$

dist. to cent. of web: $d_w := t_{f.b} + 0.5 \cdot D$ $d_w = 675\,mm$

$$d_{Bot\_Steel\_NC} := \frac{A_{f.t} \cdot d_{f.t} + A_{f.b} \cdot d_{f.b} + A_w \cdot d_w}{A_g} \qquad d_{Bot\_Steel\_NC} = 675\,mm$$

$$d_{Top\_Steel\_NC} := d - d_{Bot\_Steel\_NC} \qquad d_{Top\_Steel\_NC} = 675\,mm$$

$$I_{f.t} := b_{f.t} \cdot \frac{t_{f.t}^3}{12} + A_{f.t} \cdot \left(d_{f.t} - d_{Bot\_Steel\_NC}\right)^2 \qquad I_{f.t} = 4.39 \times 10^9\,mm^4$$

$$I_{f.b} := b_{f.b} \cdot \frac{t_{f.b}^3}{12} + A_{f.b} \cdot \left(d_{Bot\_Steel\_NC} - d_{f.b}\right)^2 \qquad I_{f.b} = 4.39 \times 10^9\,mm^4$$

$$I_w := t_w \cdot \frac{D^3}{12} + A_w \cdot \left(d_w - d_{Bot\_Steel\_NC}\right)^2 \qquad I_w = 2.56 \times 10^9\,mm^4$$

$$I_{NC} := I_{f.t} + I_{f.b} + I_w \qquad I_{NC} = 1.13 \times 10^{10}\,mm^4$$

$$S_{Top\_Steel\_NC} := \frac{I_{NC}}{d_{Top\_Steel\_NC}} \qquad S_{Top\_Steel\_NC} = 1.68 \times 10^7\,mm^3$$

$$S_{Bot\_Steel\_NC} := \frac{I_{NC}}{d_{Bot\_Steel\_NC}} \qquad S_{Bot\_Steel\_NC} = 1.68 \times 10^7\,mm^3$$

Non-Composite Cross Sectional Properties in the Negative Moment Region:

overall depth: $d_n := t_{f.t.n} + D + t_{f.b.n}$ $d_n = 1380\,mm$

area of top flange: $A_{f.t.n} := b_{f.t.n} \cdot t_{f.t.n}$ $A_{f.t.n} = 18000\,mm^2$

area of bottom flange: $A_{f.b.n} := b_{f.b.n} \cdot t_{f.b.n}$ $A_{f.b.n} = 21600\,mm^2$

area of web: $A_{w.n} := D \cdot t_{w.n}$ $A_{w.n} = 18200\,mm^2$

total area of girder: $A_{g.n} := A_{f.t.n} + A_{f.b.n} + A_{w.n}$ $A_{g.n} = 57800\,mm^2$

girder self-weight: $wt_{g.n} := A_{g.n} \cdot wt_{steel}$ $wt_{g.n} = 4.45\,\frac{kN}{m}$

dist. to cent. of top flange: $d_{f.t.n} := t_{f.b.n} + D + 0.5 \cdot t_{f.t.n}$ $d_{f.t.n} = 1360\,mm$

dist. to cent. of bottom flange: $d_{f.b.n} := 0.5 \cdot t_{f.b.n}$ $d_{f.b.n} = 20\,mm$

dist. to cent. of web: $d_{w.n} := t_{f.b.n} + 0.5 \cdot D$ $d_{w.n} = 690\,mm$

$$d_{Bot\_Steel\_NC.n} := \frac{A_{f.t.n} \cdot d_{f.t.n} + A_{f.b.n} \cdot d_{f.b.n} + A_{w.n} \cdot d_{w.n}}{A_{g.n}} \qquad d_{Bot\_Steel\_NC.n} = 648.3\,mm$$

$$d_{Top\_Steel\_NC.n} := d_n - d_{Bot\_Steel\_NC.n} \qquad d_{Top\_Steel\_NC.n} = 731.7\,mm$$

$$I_{f.t.n} := b_{f.t.n} \cdot \frac{t_{f.t.n}^3}{12} + A_{f.t.n} \cdot \left(d_{f.t.n} - d_{Bot\_Steel\_NC.n}\right)^2 \qquad I_{f.t.n} = 9.12 \times 10^9\,mm^4$$

$$I_{f.b.n} := b_{f.b.n} \cdot \frac{t_{f.b.n}^3}{12} + A_{f.b.n} \cdot \left(d_{Bot\_Steel\_NC.n} - d_{f.b.n}\right)^2 \qquad I_{f.b.n} = 8.53 \times 10^9\,mm^4$$

$$I_{w.n} := t_{w.n} \cdot \frac{D^3}{12} + A_{w.n} \cdot \left(d_{w.n} - d_{Bot\_Steel\_NC.n}\right)^2 \qquad I_{w.n} = 2.59 \times 10^9\,mm^4$$

$$I_{NC.n} := I_{f.t.n} + I_{f.b.n} + I_{w.n} \qquad I_{NC.n} = 2.02 \times 10^{10}\,mm^4$$

$$S_{Top\_Steel\_NC.n} := \frac{I_{NC.n}}{d_{Top\_Steel\_NC.n}} \qquad S_{Top\_Steel\_NC.n} = 2.77 \times 10^7\,mm^3$$

$$S_{Bot\_Steel\_NC.n} := \frac{I_{NC.n}}{d_{Bot\_Steel\_NC.n}} \qquad S_{Bot\_Steel\_NC.n} = 3.12 \times 10^7\,mm^3$$

LIVE LOAD GIRDER DISTRIBUTION FACTORS

Interior Beam Moment:

Kg term: **[S4.6.2.2.1-1 '03]**

$$d_{Top\_Steel\_NC\_avg} := \frac{d_{Top\_Steel\_NC} + d_{Top\_Steel\_NC.n}}{2}$$

$$I_{NC\_avg} := \frac{I_{NC} + I_{NC.n}}{2} \qquad I_{NC\_avg} = 1.58 \times 10^{10}\,mm^4$$

$$A_{g\_avg} := \frac{A_g + A_{g.n}}{2} \qquad A_{g\_avg} = 4.8 \times 10^{4}\,mm^2$$

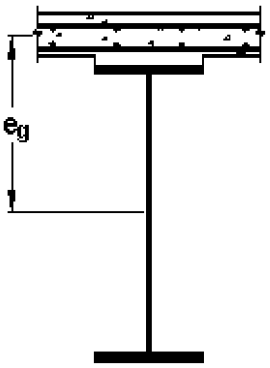

Figure : e_g factor

Distance between C.O.G. of girder and C.O.G. of slab:

$$e_g := d_{Top\_Steel\_NC\_avg} + t_{haunch} + \frac{t_s}{2} \qquad e_g = 853.365\,mm$$

$n := 8$ **[C6.10.1.1.1b '04]**

$$K_g := n\cdot\left(I_{NC\_avg} + A_{g\_avg}\cdot e_g^{\,2}\right) \qquad K_g = 4.06 \times 10^{11}\,mm^4$$

Range of applicability: **[Table S4.6.2.2.2b-1 '03]**

$1100 \le S \le 4900mm$

$110 \le t_s \le 300mm$

$6000 \le L \le 73000mm$

$N_b \ge 4$

$4\ 10^9 \le K_g \le 3\cdot 10^{12} mm^4$

One lane loaded: **[Table S4 .6.2.2.2b-1 '03]**

$$DFM_1 := 0.06 + \left(\frac{S}{4300\cdot mm}\right)^{0.4}\left(\frac{S}{L_{span}}\right)^{0.3}\cdot\left(\frac{K_g}{L_{span}\cdot t_s^{\,3}}\right)^{0.1} \qquad DFM_1 = 0.531$$

Two or more design lanes: **[Table S4 .6.2.2.2b-1 '03]**

$$DFM_2 := 0.075 + \left(\frac{S}{2900\cdot mm}\right)^{0.6}\left(\frac{S}{L_{span}}\right)^{0.2}\cdot\left(\frac{K_g}{L_{span}\cdot t_s^{\,3}}\right)^{0.1} \qquad DFM_2 = 0.81$$

Fatigue factors:

For single-lane loading to be used for fatigue design, remove the multiple presence factor of 1.20.

$$DFM_{1fatigue} := \frac{DFM_1}{1.20} \qquad DFM_{1fatigue} = 0.443$$

Interior Beam Shear: [Table S4 .6.2.2.3a-1 '03]

One lane loaded:

$$DFV_1 := 0.36 + \frac{S}{7600 \cdot mm} \qquad DFV_1 = 0.846$$

Two or more lanes loaded:

$$DFV_2 := 0.20 + \left(\frac{S}{3600 \cdot mm}\right) - \left(\frac{S}{10700 \cdot mm}\right)^{2.0} \qquad DFV_2 = 1.106$$

Exterior Beam Moment: [Table S3 .6.1.1.2-1 '03]

Truck width:

$w_{truck} := 1800 \cdot mm$

Spacing between trucks:

$s_{truck} := 1800 \cdot mm$

Number of design lanes:

$$N_{DL} := \frac{w_{roadway}}{3600 \cdot mm}$$

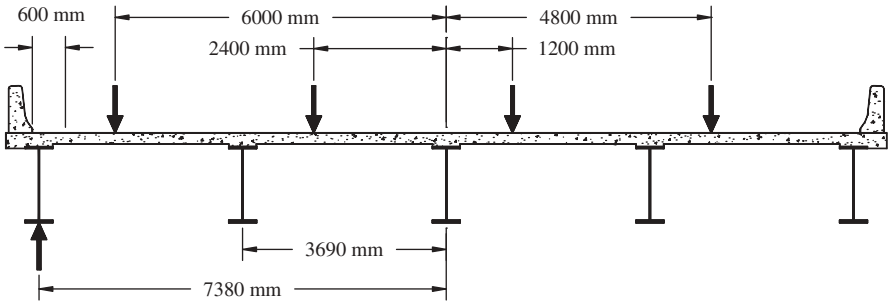

Figure : Position of Truck Reaction for Exterior Girder Distribution Factor

$N_{DL} = 4.2 \qquad N_{DL} := 4$ **[S3.6.1.1.1 '99]**

Spacing Between Parapet and Truck: **[S3.6.1.3.1 '99]**

$S_{truck\_parapet} := 600 \cdot mm$

Truck reaction location from center of bridge:

$$e_{R1} := \frac{w_{roadway}}{2} - S_{truck\_parapet} - \frac{w_{truck}}{2}$$

dist to R1 from CL

$e_{R1} = 6000\,mm$

$$e_{R2} := \frac{w_{roadway}}{2} - S_{truck\_parapet} - w_{truck} - s_{truck} - \frac{w_{truck}}{2}$$

dist to R2 from CL

$e_{R2} = 2400\,mm$

$$e_{R3} := \frac{w_{roadway}}{2} - S_{truck\_parapet} - 2 \cdot w_{truck} - 2 \cdot s_{truck} - \frac{w_{truck}}{2}$$

dist to R3 from CL

$e_{R3} = -1200\,mm$

$$e_{R4} := \frac{w_{roadway}}{2} - S_{truck\_parapet} - 3 \cdot w_{truck} - 3 \cdot s_{truck} - \frac{w_{truck}}{2}$$

dist to R4 from CL

$e_{R4} = -4800\,mm$

Distance between girders and center of bridge:

$x_1 := \frac{w_{bridge}}{2} - w_{oh}$ $\quad x_1 = 7.38\,m$ dist to girder 1 from CL

$x_2 := x_1 - S$ $\quad x_2 = 3.69\,m$ dist to girder 2 from CL

$x_3 := x_2 - S$ $\quad x_3 = 0\,m$ dist to girder 3 from CL

$x_4 := x_3 - S$ $\quad x_4 = -3.69\,m$ dist to girder 4 from CL

$x_5 := x_4 - S$ $\quad x_5 = -7.38\,m$ dist to girder 5 from CL

$X_{ext} := x_1$ $\quad X_{ext} = 7.38\,m$ dist to exterior girder from CL

Multiple Presence Factors:

$m_1 := 1.20$ $\quad m_3 := 0.85$

$m_2 := 1.00$ $\quad m_4 := 0.65$

$$R = \frac{N_L}{N_B} + \frac{X_{ext} \cdot \sum e}{\sum_{N_B} x^2} \qquad \textbf{[C4.6.2.2.2d-1]}$$

One Lane Loaded:

$R_1 := \frac{1}{5} + \frac{X_{ext} \cdot (e_{R1})}{(x_1^2 + x_2^2 + x_3^2 + x_4^2 + x_5^2)}$ $\quad R_1 = 0.53$

$D_{M1} := m_1 \cdot R_1$ $\quad D_{M1} = 0.63$

Two Lanes Loaded:

$R_2 := \frac{2}{5} + \frac{X_{ext} \cdot (e_{R1} + e_{R2})}{(x_1^2 + x_2^2 + x_3^2 + x_4^2 + x_5^2)}$ $\quad R_2 = 0.86$

$D_{M2} := m_2 \cdot R_2$ $\quad D_{M2} = 0.86$

Three Lanes Loaded:

$R_3 := \frac{3}{5} + \frac{X_{ext} \cdot (e_{R1} + e_{R2} + e_{R3})}{(x_1^2 + x_2^2 + x_3^2 + x_4^2 + x_5^2)}$ $\quad R_3 = 0.99$

$D_{M3} := m_3 \cdot R_3$ $\quad D_{M3} = 0.84$

Four Lanes Loaded:

$R_4 := \frac{4}{5} + \frac{X_{ext} \cdot (e_{R1} + e_{R2} + e_{R3} + e_{R4})}{(x_1^2 + x_2^2 + x_3^2 + x_4^2 + x_5^2)}$ $\quad R_4 = 0.93$

$D_{M4} := m_4 \cdot R_4$ $\quad D_{M4} = 0.60$

Exterior Beam Lever Rule:

[Table 4.6.2.2.1-1 '03]

Distance to driving loads:

$$Driving := w_{oh} + S - w_p - S_{truck\_parapet} - \frac{w_{truck}}{2}$$

$Driving = 2310\,mm$

Distance to resisting girder:

$Resisting := S$

$Resisting = 3690\,mm$

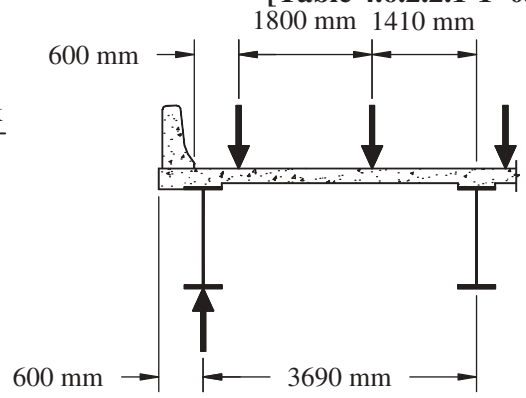

Figure : Position of Truck Tire Reactions for Lever Rule

Distribution Factor Moment:

One Lane Loaded:

$$DMFLever_{1\_f} := \frac{Driving}{Resisting}$$ $DMFLever_{1\_f} = 0.626$

$DMFLever_1 := DMFLever_{1\_f} \cdot 1.20$ $DMFLever_1 = 0.751$

Two or more Lanes Loaded:

$d_e := w_{oh} - w_p$ $d_e = 120\,mm$

$$e := 0.77 + \frac{d_e}{2800 \cdot mm}$$ $e = 0.813$

$DMFLever_2 := e \cdot DFM_2$ $DMFLever_2 = 0.658$

Distribution Factor Shear:

One Lane Loaded: (beam distribution same as moment)

$DFV_{E1} := DMFLever_1$ $DFV_{E1} = 0.751$

Two or more lanes loaded:

$$e_1 := 0.6 + \frac{d_e}{3000 \cdot mm}$$ $e_1 = 0.64$

$DFV_{E2} := e_1 \cdot DFV_2$ $DFV_{E2} = 0.708$

Skew Correction Factors: [S4.6.2.2.2e-1 '03]

If θ is less than 30^o c_1=0.0

If θ is greater than 60^o use $= 60^o$

$\theta := 18 \cdot deg$

$$c_1 := 0.25 \cdot \left(\frac{K_g}{L_{span} \cdot t_s^{\,3}} \right)^{0.25} \cdot \left(\frac{S}{L_{span}} \right)^{0.5} \qquad c_1 = 0.081$$

$$DFM_{skew\_corr} := 1 - c_1 \cdot \tan(\theta)^{1.5} \qquad DFM_{skew\_corr} = 0.985$$

[S4.6.2.2.3c-1 '03]

$$DFV_{skew\_corr} := 1.0 + 0.2 \cdot \left(\frac{L_{span} \cdot t_s^{\,3}}{K_g} \right)^{0.3} \cdot \tan(\theta) \qquad DFV_{skew\_corr} = 1.061$$

Governing Distribution Factors: (skew corrected)

Interior Max:

Moment: $DFM_I := DFM_{skew\_corr} \cdot \max\left(\left(DFM_1 \quad DFM_2 \right) \right)$ $DFM_I = 0.80$

Shear: $DFV_I := DFV_{skew\_corr} \cdot \max\left(\left(DFV_1 \quad DFV_2 \right) \right)$ $DFV_I = 1.17$

Fatigue:

Moment: $DFM_{I\_F} := DFM_{skew\_corr} \cdot DFM_{1fatigue}$ $DFM_{I\_F} = 0.44$

Shear: $DFV_{I\_F} := DFV_{skew\_corr} \cdot DFV_1$ $DFV_{I\_F} = 0.90$

Exterior Max:

Moment: $DFM_E := DFM_{skew\_corr} \cdot \max\left(\begin{pmatrix} D_{M1} & D_{M2} & DMFLever_1 \\ D_{M3} & D_{M4} & DMFLever_2 \end{pmatrix} \right)$ $DFM_E = 0.84$

Shear: $DFV_E := DFV_{skew\_corr} \cdot \max\left(\left(DFV_{E1} \quad DFV_{E2} \right) \right)$ $DFV_E = 0.80$

Fatigue:

Moment: $DFM_{E\_F} := DFM_{skew\_corr} \cdot \max\left(\left(\frac{D_{M1}}{1.2} \quad DMFLever_{1\_f} \right) \right)$ $DFM_{E\_F} = 0.62$

Shear: $DFV_{E\_F} := DFV_{skew\_corr} \cdot DMFLever_{1\_f}$ $DFV_{E\_F} = 0.66$

General Considerations for Limit States

$$\sum \eta_i \cdot \gamma_i \cdot Q_i \le \phi \cdot R_n = R_r \qquad \textbf{[S1.3.2.1-1]}$$

Ductility $\eta_D := 1.00$ **[S1.3.3]**

Redundancy $\eta_R := 1.00$ **[S1.3.4]**

Operational Importance $\eta_I := 1.00$ **[S1.3.5]**

For loads for which a maximum value of gi is appropriate:

$$\eta = \eta_D \cdot \eta_R \cdot \eta_I \ge 0.95 \qquad \eta = 1.00 \qquad \textbf{[S1.3.2.1-2]}$$

For loads for which a minimum value of gi is appropriate:

$$\eta = \frac{1}{\eta_D \cdot \eta_R \cdot \eta_I} \le 1.0 \qquad \eta = 1.00 \qquad \textbf{[S1.3.2.1-3]}$$

DESIGN LOADS

Component Dead Loads:

- DC1 - acts on non-composite section

$DC1_{haunch} := wt_{conc} \cdot \left(b_{f.t} \cdot t_{haunch}\right)$

$DC1_{haunch} = 0.47 \frac{kN}{m}$

$DC1_{sipf} := wt_{sipf} \cdot S$

$DC1_{sipf} = 2.65 \frac{kN}{m}$

$DC1_{girder} := 0.75 \cdot wt_{g} + 0.25 \cdot wt_{g.n}$

$DC1_{girder} = 3.32 \frac{kN}{m}$

$DC1_{attachments} := 5\% \cdot DC1_{girder}$

$DC1_{attachments} = 0.17 \frac{kN}{m}$

Superimposed Component Dead Loads:

- DC2 - acts on long-term composite section
- assumed to be carried equally by all girders

$wt_{p} := 7.2 \cdot \frac{kN}{m}$

$DC2_{p} := \frac{wt_{p}}{N_G} \qquad DC2_{p} = 1.44 \frac{kN}{m}$

Superimposed Component Dead Loads:

- DW - wearing surface load
- acts on long-term composite section
- assumed to be carried equally by all girders

$DW := \frac{wt_{fws} \cdot w_{roadway}}{N_G} \qquad DW = 3.60 \frac{kN}{m}$

Interior Girder Component Dead Load:

$DC1_{slab.i} := wt_{conc} \cdot \left(S \cdot t_{deck}\right)$

$DC1_{slab.i} = 20.86 \frac{kN}{m}$

$DC1_{i} := DC1_{slab.i} + DC1_{haunch} + DC1_{sipf} + DC1_{girder} + DC1_{attachments}$

$DC1_{i} = 27.47 \frac{kN}{m}$

Exterior Girder Component Dead Load:

$DC1_{slab.e} := wt_{conc} \cdot \left[\left[0.5 \cdot S \cdot t_{deck} + w_{oh} \cdot \left(t_{deck} + t_{f.t}\right) \right] \right]$

$DC1_{slab.e} = 14.18 \frac{kN}{m}$

$DC1_{e} := DC1_{slab.e} + DC1_{haunch} + 0.5 \cdot DC1_{sipf} + DC1_{girder} + 0.5 \cdot DC1_{attachments}$

$DC1_{e} = 19.38 \frac{kN}{m}$

EMPIRICAL DECK DESIGN [S9.7.2.1]

Check conditions for use of empirical design method [S9.7.2.2, S9.7.2.4]

The empirical design method may only be used if the following conditions are satisfied:

- Cross frames are used throughout the cross-section at lines of support,
- Supporting components are made of steel and/or concrete,
- Deck is cast in place,
- Deck is of uniform depth (except for haunches over girder flanges),
- Deck is made composite with supporting elements (2 shear connectors min. at 600 mm spacing),
- The ratio of effective length to design depth does not exceed 18.0 and is not less than 6.0,
- Core depth of the slab is not less than 100 mm,
- Minimum depth of slab is not less than 175 mm (excluding sacrificial wearing surface),
- Effective Length does not exceed 4100 mm,
- Overhang beyond the centerline of at least 5.0 times the depth of the slab (this condition also satisfied if the overhang is at least 3.0 times the depth of the slab and a structurally continuous concrete barrier is made composite with the overhang.

Effective length: [S9.7.2.3, S9.7.2.4]

The effective length of slab for purposes of the empirical design method is the distance between flan tips, plus the flange overhang, taken as the distance from the extreme flange tip to the face of the we

$L_{eff} := S - b_{f.t} + \frac{(b_{f.t} - t_w)}{2}$ $L_{eff} = 3483.0\,mm$ $L_{eff} \le 4100mm$ - O.K.

$6 \le \frac{L_{eff}}{t_s} \le 18$ $\frac{L_{eff}}{t_s} = 17.4$ - O.K.

$t_{core} \ge 100mm$ $t_{core} = 115\,mm$ - O.K.

$t_s \ge 175mm$ $t_s = 200\,mm$ - O.K.

This example assumes a structurally continuous parapet

w_{oh} 3.0 t_s $w_{oh} = 600\,mm$ - O.K.

f'_c 28 MPa $f'_{c\_deck} = 28\,MPa$ - O.K.

Selected metric deck reinforcment properties:

$A_{10} := 71mm^2$ $A_{16} := 199mm^2$ $d_{b\_16} := 15.9\ mm$ $A_{19} := 284mm^2$

Reinforcement Requirements - Positive Moment Regions [S9.7.2.5]

The minimum amount of reinforcement in positive moment regions shall be:

For each bottom layer, 0.570 mm^2/mm in both directions

For each top layer, 0.380 mm^2/mm in both directions

Reinforcement shall be Grade 420 or higher and the spacing shall not exceed 450 mm

If the skew exceeds 25 degrees the specified reinforcement in both directions shall be doubled in the zones of the deck. Each end zone shall be taken as the longitudinal distance equal to the effective len the slab specified in Article 9.7.2.3.

Reinforcement bars at bottom (longitudinal and transverse) in positive moment region:

$$spacing_{bottom\_max} := \frac{A_{16}}{0.570\frac{mm^2}{mm}} \qquad spacing_{bottom\_max} = 349\,mm$$

Reinforcement bars at top (longitudinal and transverse) in positive moment region:

$$spacing_{top\_max} := \frac{A_{16}}{0.380\frac{mm^2}{mm}} \qquad spacing_{top\_max} = 524\,mm$$

Use no. 16M bars spaced at 300 mm in the top and bottom layers of reinforcement in both the longitdinal and transverse directions. Spacing is chosen to be consistant with that provided in the negative moment region as determined by the following.

Reinforcement Requirements - Negative Moment Region [S6.10.1.7 '04]

- In negative-flexure regions of any continuous span, the specified minimum longitudinal reinforcement shall not be less than 1% of the total cross-sectional area of the slab.
- The reinforcement shall have a specified minimum yield strength not less than 400 MPa and a size not exceeding no.19 bars to control slab cracking.
- The required longitudinal reinforcement is to be placed within two layers uniformly distributed across the slab width:

  1.) 2/3^{rds} of the specified reinforcement shall be placed in the top layer longitudinally.

  2.) 1/3rd of the specified reinforcement shall be placed in the bottom layer longitudinally.
- The transverse reinforcement need not be any different from that determined from the positive flexure region.

$$A_{s\_neg\_min} := t_s \cdot 0.01\frac{mm}{mm} \qquad A_{s\_neg\_min} = 2.00\frac{mm^2}{mm}$$

Longitudinal reinforcing bars in bottom layer of negative moment region:

$$A_{s\_bottom\_min} := \frac{1}{3}\cdot A_{s\_neg\_min} \qquad A_{s\_bottom\_min} = 0.67\frac{mm^2}{mm}$$

In bottom layer use no. 10M bars spaced at 300 mm alternating with no. 16M bars spaced at 300 mm.

$$spacing_{provided} := 300mm$$

$$A_{s\_bottom\_provided} := \frac{A_{10}}{spacing_{provided}} + \frac{A_{16}}{spacing_{provided}} \qquad A_{s\_bottom\_provided} = 0.90\frac{mm^2}{mm}$$

Longitudinal reinforcing bars in top layer of negative moment region:

$$A_{s\_top\_min} := \frac{2}{3} \cdot A_{s\_neg\_min} \qquad A_{s\_top\_min} = 1.33 \frac{mm^2}{mm}$$

In the top layer use no. 19M bars spaced at 300 mm alternating with no. 16M bars spaced at 300 mm.

$$spacing_{provided} := 300mm$$

$$A_{s\_top\_provided} := \frac{A_{19}}{spacing_{provided}} + \frac{A_{16}}{spacing_{provided}} \qquad A_{s\_top\_provided} = 1.61 \frac{mm^2}{mm}$$

Transverse reinforcing bars in negative moment region:

The transverse steel in both the top and bottom layers is the same as previously determined for the positive moment regions.

The transverse steel in both the top and bottom layers will be no. 16M bars spaced at 300 mm.

DECK REINFORCEMENT SUMMARY:

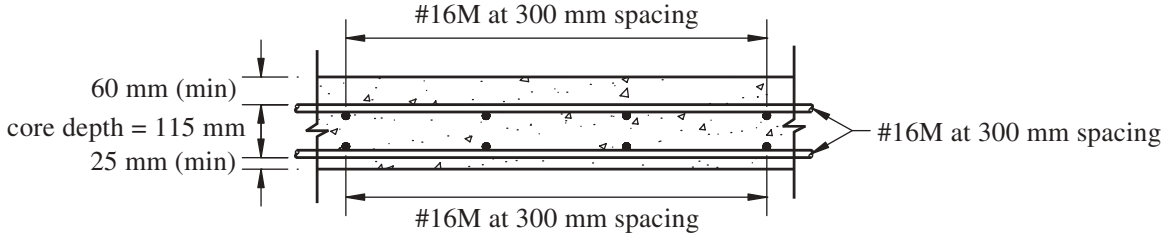

Figure : Positive Moment Region Deck Reinforcement - Emperical Design

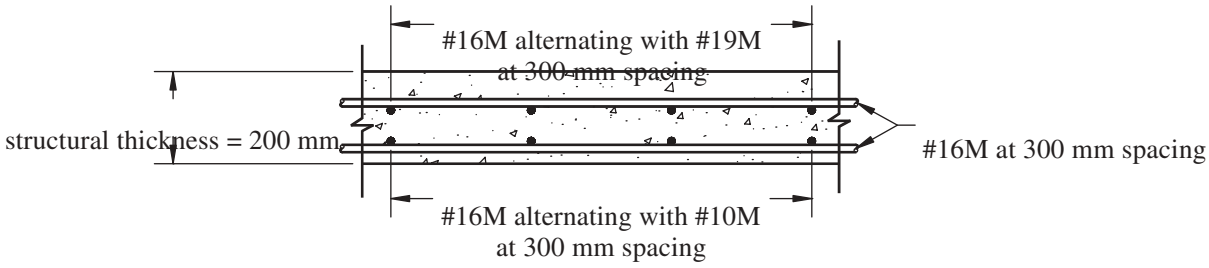

Figure : Negative Moment Region Deck Reinforcement - Emperical Design

COMPOSITE SECTION PROPERTIES

Positive Moment Region:

Short-term composite section: $n := 8$ **[C6.10.1.1.1b]**

For interior beams, the effective flange width may be taken as the least of:

$L_{ext\_eff} := 30m$ $12 \cdot t_s + D = 3.7\,m$ $12 \cdot t_s + \frac{b_{f.t}}{2} = 2.6\,m$ $S = 3.69\,m$

$b_{eff} := S$ $b_{eff} = 3.69 \times 10^3\,mm$ **[Proposed]**

$$A_{deck.ST} := \frac{t_s \cdot b_{eff}}{n} \qquad A_{deck.ST} = 92250\,mm^2$$

$$y_{deck} := t_{haunch} + \frac{t_s}{2} \qquad y_{deck} = 150\,mm$$

$$d_{Bot\_Steel\_ST} := \frac{A_g \cdot d_{Bot\_Steel\_NC} + A_{deck.ST} \cdot (d + y_{deck})}{A_g + A_{deck.ST}}$$

$$d_{Top\_Steel\_ST} := d - d_{Bot\_Steel\_ST}$$

$$I_{deck} := \frac{b_{eff} \cdot t_s^3}{12 \cdot n} \qquad I_{deck} = 3.075 \times 10^8\,mm^4$$

$$I_{ST} := I_{NC} + A_g \cdot (d_{Top\_Steel\_NC} - d_{Top\_Steel\_ST})^2 \ldots + I_{deck} + A_{deck.ST} \cdot (y_{deck} + d_{Top\_Steel\_ST})^2$$

$$S_{Top\_Steel\_ST} := \frac{I_{ST}}{d_{Top\_Steel\_ST}} \qquad S_{Bot\_Steel\_ST} := \frac{I_{ST}}{d_{Bot\_Steel\_ST}}$$

Short-term section properties:

Short-term moment of inertia: $I_{ST} = 3.004 \times 10^{10}\,mm^4$

Short-term distance from top of steel to NA: $d_{Top\_Steel\_ST} = 91.6\,mm$

Short-term distance from bottom of steel to NA: $d_{Bot\_Steel\_ST} = 1258.4\,mm$

Short-term section modulus top section: $S_{Top\_Steel\_ST} = 3.28 \times 10^8\,mm^3$

Short-term section modulus bottom section: $S_{Bot\_Steel\_ST} = 2.387 \times 10^7\,mm^3$

Long-term composite section: $3 \cdot n = 24$ **[S6.10.3.1.1b]**

$$A_{deck.LT} := \frac{t_s \cdot b_{eff}}{3 \cdot n} \qquad A_{deck.LT} = 30750\,mm^2$$

$$d_{Bot\_Steel\_LT} := \frac{A_g \cdot d_{Bot\_Steel\_NC} + A_{deck.LT} \cdot (d + y_{deck})}{A_g + A_{deck.LT}}$$

$$d_{Top\_Steel\_LT} := d - d_{Bot\_Steel\_LT}$$

$$I_{deck.long} := \frac{1}{12} \cdot \frac{b_{eff} \cdot t_s^{\,3}}{3 \cdot n} \qquad I_{deck.long} = 1.025 \times 10^8\,mm^4$$

$$I_{LT} := I_{NC} + A_g \cdot (d_{Top\_Steel\_NC} - d_{Top\_Steel\_LT})^2 \ldots + I_{deck.long} + A_{deck.LT} \cdot (y_{deck} + d_{Top\_Steel\_LT})^2$$

$$S_{Top\_Steel\_LT} := \frac{I_{LT}}{d_{Top\_Steel\_LT}} \qquad S_{Bot\_Steel\_LT} := \frac{I_{LT}}{d_{Bot\_Steel\_LT}}$$

Long-term Section Properties:

Long-term moment of inertia: $I_{LT} = 2.304 \times 10^{10}\,mm^4$

Long-term distance from top of steel to NA: $d_{Top\_Steel\_LT} = 307.1\,mm$

Long-term distance from bottom of steel to NA: $d_{Bot\_Steel\_LT} = 1.0 \times 10^3\,mm$

Long-term section modulus top section: $S_{Top\_Steel\_LT} = 7.503 \times 10^7\,mm^3$

Long-term section modulus bottom section: $S_{Bot\_Steel\_LT} = 2.209 \times 10^7\,mm^3$

Plastic-Moment Capacity for Positive Flexure [Appendix D6.1]

Assumes no net axial force

Section forces:

Rebar area determined by summing the reinforcement area in the deck design section across the effective slab width.

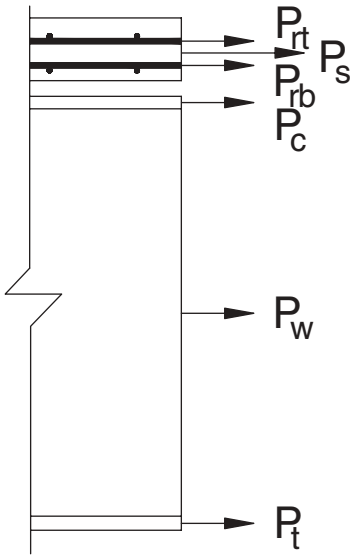

$A_{rt} := \left(\frac{A_{16}}{300 \cdot mm}\right) \cdot b_{eff}$ $A_{rt} = 2447.7\,mm^2$

$A_{rb} := \left(\frac{A_{16}}{300 \cdot mm}\right) \cdot b_{eff}$ $A_{rb} = 2447.7\,mm^2$

$P_{tr} := F_{yr} \cdot A_{rt}$ $P_{tr} = 1.0 \times 10^3\,kN$

$P_s := 0.85 \cdot f'_{c\_deck} \cdot (b_{eff} \cdot t_s)$ $P_s = 17564.4\,kN$

$P_{br} := F_{yr} \cdot A_{rb}$ $P_{br} = 1.0 \times 10^3\,kN$

$P_c := F_{yc} \cdot b_{f.t} \cdot t_{f.t}$ $P_c = 3450.0\,kN$

$P_w := F_{yw} \cdot D \cdot t_w$ $P_w = 6279.0\,kN$

$P_t := F_{yt} \cdot b_{f.b} \cdot t_{f.b}$ $P_t = 4850.0\,kN$

Figure : Plastic Moment Forces

Bottom reinforcement $C_{rb} := t_s - c_{bottom} - d_{b\_16} - \frac{d_{b\_16}}{2}$ $C_{rb} = 151.2\,mm$

Top reinforcement $C_{rt} := c_{top} + d_{b\_16} + \frac{d_{b\_16}}{2}$ $C_{rt} = 83.85\,mm$

Possible Plastic Neutral Axis Locations:

Case I - PNA in web

Case II - PNA in top flange

Case III - PNA in concrete deck, below P_{rb}

Case IV - PNA in concrete deck, at P_{rb}

Case V - PNA in concrete deck, above P_{rb}, below P_{rt}

Case VI - PNA in concrete deck, at P_{rt}

Case VII - PNA in concrete deck, above P_{rt}

Determination of Plastic Neutral Axis **[AASHTO Table D6.1-1]**

$Y_{IV} := C_{rb}$ Case IV - PNA in the Deck

$Y_{IV} = 151.2\,mm$ $t_{f.t} = 25\,mm$ $P_t + P_w + P_c \geq P_s + P_{br} + P_{tr}$

Distance to PNA:

$y_{bar} := Y_{IV}$ From top of the slab $y_{bar} = 151.2\,mm$

Distance from PNA to the bottom flange's NA:

$$y_{bf} := d + t_{haunch} + t_s - \frac{t_{f.b}}{2} - y_{bar} \qquad y_{bf} = 1436.3\,mm$$

Distance from PNA to the web's NA:

$$y_w := 0.5\,D + t_{haunch} + t_s + t_{f.t} - y_{bar} \qquad y_w = 773.9\,mm$$

Distance from PNA to the top flange's NA:

$$y_{tf} := t_{haunch} + t_s + \frac{t_{f.t}}{2} - y_{bar} \qquad y_{tf} = 111.4\,mm$$

Distance from PNA to the bottom reinforcement:

$$y_{rb} := C_{rb} \qquad y_{rb} = 151.2\,mm$$

Distance from PNA to the top reinforcement:

$$y_{rt} := y_{bar} - C_{rt} \qquad y_{rt} = 67.3\,mm$$

Distance from PNA to the slab's NA:

$$y_s := 0.5 \cdot t_s + y_{bar} + t_{haunch} \qquad y_s = 301.1\,mm$$

Plastic moment capacity: (case IV)

$$M_p := \frac{P_s}{2\,t_s} \cdot \left(y_{bar}^{\,2}\right) + \left(P_{tr} \cdot y_{rt} + P_c \cdot y_{tf} + P_w \cdot y_w + P_t \cdot y_{bf}\right)$$

$$M_p = 13281.9\,kN \cdot m$$

Negative Moment Region:

Composite Section:

For interior beams, the effective flange width may be taken as the least of:

$L_{eff\_neg} := 20m \quad 12\ t_s + D = 3.7\,m \quad 12\ t_s + \frac{b_{f.t.n}}{2} = 2.625\,m \quad S = 3.69\,m$ **[S4.6.2.6]**

$b_{eff.n} := S$ $\quad b_{eff.n} = 3.69 \times 10^3\,mm$ **[Proposed]**

$A_{rt.n} := b_{eff.n} \cdot A_{s\_top\_provided}$ $\quad A_{rt.n} = 5940.9\,mm^2$

$A_{rb.n} := b_{eff.n} \cdot A_{s\_bottom\_provided}$ $\quad A_{rb.n} = 3321.0\,mm^2$

$C_{rt.n} := t_{haunch} + t_s - c_{top} - d_{b\_16} - 17.5 \cdot mm$ $\quad C_{rt.n} = 156.6\,mm$

$C_{rb.n} := t_{haunch} + c_{bottom} + d_{b\_16} + 13 \cdot mm$ $\quad C_{rb.n} = 103.9\,mm$

$A_{ft.n} := b_{f.t.n} \cdot t_{f.t.n}$ $\quad A_{ft.n} = 18000.0\,mm^2$

$A_{fb.n} := b_{f.b.n} \cdot t_{f.b.n}$ $\quad A_{fb.n} = 21600.0\,mm^2$

$$d_{Bot\_Steel\_Comp.n} := \frac{\left[\begin{array}{l} A_{ft.n} \cdot \left(d_n - \frac{t_{f.t.n}}{2}\right) + A_{w.n} \cdot \left(t_{f.b.n} + \frac{D}{2}\right) + A_{fb.n} \cdot \left(\frac{t_{f.b.n}}{2}\right) \ldots \\ + \left[A_{rb.n} \cdot \left(d_n + C_{rb.n}\right)\right] + \left[A_{rt.n} \cdot \left(d_n + C_{rt.n}\right)\right] \end{array}\right]}{A_{g.n} + A_{rb.n} + A_{rt.n}}$$

$d_{Top\_Steel\_Comp.n} := d_n - d_{Bot\_Steel\_Comp.n}$

$$I_{Comp.n} := I_{NC.n} + A_{g.n} \cdot \left(d_{Top\_Steel\_NC.n} - d_{Top\_Steel\_Comp.n}\right)^2 \ldots + \left[A_{rb.n} \cdot \left(C_{rb.n} + d_{Top\_Steel\_Comp.n}\right)^2\right] \ldots + \left[A_{rt.n} \cdot \left(C_{rt.n} + d_{Top\_Steel\_Comp.n}\right)^2\right]$$

$$S_{Top\_Steel\_Comp.n} := \frac{I_{Comp.n}}{d_{Top\_Steel\_Comp.n}} \qquad S_{Bot\_Steel\_Comp.n} := \frac{I_{Comp.n}}{d_{Bot\_Steel\_Comp.n}}$$

Bare Steel & Rebar Section Properties (Composite)

Moment of inertia of section: $I_{Comp.n} = 2.628 \times 10^{10}\,mm^4$

Distance from top of steel to NA: $d_{Top\_Steel\_Comp.n} = 611.7\,mm$

Distance from bottom of steel to NA: $d_{Bot\_Steel\_Comp.n} = 768.3\,mm$

Section modulus top section: $S_{Top\_Steel\_Comp.n} = 4.297 \times 10^7\,mm^3$

Section modulus bottom section: $S_{Bot\_Steel\_Comp.n} = 3.421 \times 10^7\,mm^3$

Negative Moment Region:

Composite Section - with deck effective in tension: **[S6.10.4.2.1]**

For members with shear connectors provided throughout their entire length that also satisfy the provisions of Artical 6.10.1.7, flexural stresses caused by service II loads applied to the composite section may be computed using the short-term or long-term composite section, as appropriate.

Short-term composite section for negative flexure:

$$A_{deck.ST.n} := \frac{t_s \cdot b_{eff.n}}{n} \qquad A_{deck.ST.n} = 92250.0\,mm^2$$

$$y_{girder.n} := d_{Top\_Steel\_NC.n} \qquad y_{girder.n} = 731.7\,mm$$

$$y_{deck.n} := t_{haunch} + \frac{t_s}{2} \qquad y_{deck.n} = 150.0\,mm$$

$$d_{Top\_Steel\_ST.n} := \frac{A_{g.n} \cdot y_{girder.n} + A_{deck.ST.n} \cdot y_{deck.n}}{A_{g.n} + A_{deck.ST.n}} \qquad d_{Top\_Steel\_ST.n} = 374.1\,mm$$

$$d_{Bot\_Steel\_ST.n} := d_n - d_{Top\_Steel\_ST.n} \qquad d_{Bot\_Steel\_ST.n} = 1005.9\,mm$$

$$I_{deck.ST.n} := \frac{b_{eff.n} \cdot t_s^{\,3}}{12 \cdot n} \qquad I_{deck.ST.n} = 3.075 \times 10^8\,mm^4$$

$$I_{ST.n} := \left[I_{NC.n} + I_{deck.ST.n} + A_{g.n} \cdot \left(y_{girder.n} - d_{Top\_Steel\_ST.n}\right)^2 \right] \ldots + A_{deck.ST.n} \cdot \left(y_{deck.n} + d_{Top\_Steel\_ST.n}\right)^2$$

$$S_{Top\_Steel\_ST.n} := \frac{I_{ST.n}}{d_{Top\_Steel\_ST.n}} \qquad S_{Bot\_Steel\_ST.n} := \frac{I_{ST.n}}{d_{Bot\_Steel\_ST.n}}$$

Short-term composite section for negative flexure:

Short-term moment of inertia: $I_{ST.n} = 5.328 \times 10^{10}\,mm^4$

Short-term distance from top of steel to NA: $d_{Top\_Steel\_ST.n} = 374.1\,mm$

Short-term distance from bottom of steel to NA: $d_{Bot\_Steel\_ST.n} = 1005.9\,mm$

Short-term section modulus top section: $S_{Top\_Steel\_ST.n} = 1.424 \times 10^8\,mm^3$

Short-term section modulus bottom section: $S_{Bot\_Steel\_ST.n} = 5.297 \times 10^7\,mm^3$

Long-term composite section negative flexure:

$$A_{deck.LT.n} := \frac{t_s \cdot b_{eff.n}}{3\ n} \qquad A_{deck.LT.n} = 30750.0\,mm^2$$

$$d_{Top\_Steel\_LT.n} := \frac{A_{g.n} \cdot y_{girder.n} + A_{deck.LT.n} \cdot y_{deck.n}}{A_{g.n} + A_{deck.LT.n}} \qquad d_{Top\_Steel\_LT.n} = 529.7\,mm$$

$$d_{Bot\_Steel\_LT.n} := d_n \quad d_{Top\_Steel\_ST.n} \qquad d_{Bot\_Steel\_LT.n} = 1005.9\,mm$$

$$I_{deck.LT.n} := \frac{b_{eff.n} \cdot t_s^{\,3}}{12 \cdot n} \qquad I_{deck.LT.n} = 3.075 \times 10^8\,mm^4$$

$$I_{LT.n} := \left[I_{NC.n} + I_{deck.LT.n} + A_{g.n} \cdot \left(y_{girder.n} - d_{Top\_Steel\_LT.n}\right)^2 \right] \ldots + A_{deck.LT.n} \cdot \left(y_{deck.n} + d_{Top\_Steel\_LT.n}\right)^2$$

$$S_{Top\_Steel\_LT.n} := \frac{I_{LT.n}}{d_{Top\_Steel\_LT.n}} \qquad S_{Bot\_Steel\_LT.n} := \frac{I_{LT.n}}{d_{Bot\_Steel\_LT.n}}$$

Long-term composite section negative flexure:

Long-term moment of inertia: $I_{LT.n} = 3.712 \times 10^{10}\,mm^4$

Long-term distance from top of steel to NA: $d_{Top\_Steel\_LT.n} = 529.7\,mm$

Long-term distance from bottom of steel to NA: $d_{Bot\_Steel\_LT.n} = 1005.9\,mm$

Long-term section modulus top section: $S_{Top\_Steel\_LT.n} = 7.007 \times 10^7\,mm^3$

Long-term section modulus bottom section: $S_{Bot\_Steel\_LT.n} = 3.69 \times 10^7\,mm^3$

Plastic Moment Capacity for Negative Flexure [Appendix D6.1]

Section forces:

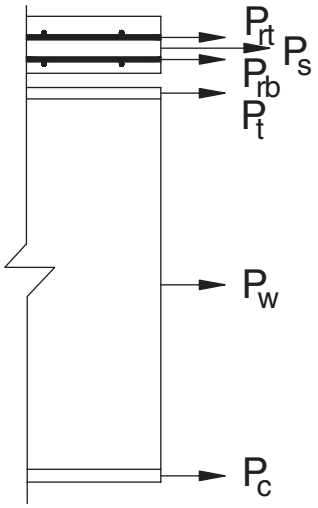

Figure : Plastic Moment Forces

$A_{rt.n} := b_{eff.n} \cdot A_{s\_top\_provided}$ $A_{rt.n} = 5940.9\,mm^2$

$A_{rb.n} := b_{eff.n} \cdot A_{s\_bottom\_provided}$ $A_{rb.n} = 3321.0\,mm^2$

$P_{rt.n} := F_{yr} \cdot A_{rt.n}$ $P_{rt.n} = 2495.2\,kN$

$P_{s.n} := 0 \cdot kN$ $P_{s.n} = 0.0\,kN$

$P_{rb.n} := F_{yr} \cdot A_{rb.n}$ $P_{rb.n} = 1394.8\,kN$

$P_{t.n} := F_{y.485} \cdot t_{f.t.n} \cdot b_{f.t.n}$ $P_{t.n} = 8730.0\,kN$

$P_{w.n} := F_{y.345} \cdot t_{w.n} \cdot D$ $P_{w.n} = 6279.0\,kN$

$P_{c.n} := F_{y.485} \cdot t_{f.b.n} \cdot b_{f.b.n}$ $P_{c.n} = 10476.0\,kN$

$C_{rb.n} := t_{haunch} + c_{bottom} + d_{b\_16} + 13 \cdot mm$ $C_{rb.n} = 103.9\,mm$

$C_{rt.n} := t_{haunch} + t_s - c_{top} - d_{b\_16} - 17.5 \cdot mm$ $C_{rt.n} = 156.6\,mm$

Possible plastic neutral axis locations: Case I - PNA in web
Case II - PNA in top flange

Determination of Plastic Neutral Axis: **[Table D6.1-2]**

Case I - PNA in web $P_{c.n} + P_{w.n} = 16755.0\,kN > P_{t.n} + P_{rb.n} + P_{rt.n} = 12620.0\,kN$

$$y_{bar.n} := \left(\frac{D}{2}\right) \cdot \left(\frac{P_{c.n} - P_{t.n} - P_{rt.n} - P_{rb.n}}{P_{w.n}} + 1\right) \qquad y_{bar.n} = 428.1\,mm$$

Distance from PNA to the bottom flange's NA:

$y_{bf.n} := D + 0.5 \cdot t_{f.b.n} - y_{bar.n}$ $y_{bf.n} = 891.9\,mm$

Distance from PNA to the web's NA:

$y_{w.n} := \left|0.5 \cdot D - y_{bar.n}\right|$ $y_{w.n} = 221.9\,mm$

Distance from PNA to the top flange's NA:

$y_{tf.n} := y_{bar.n} + 0.5 \cdot t_{f.t.n}$ $y_{tf.n} = 448.1\,mm$

Distance from PNA to the bottom reinforcement:

$y_{rb.n} := y_{bar} + t_{f.t.n} + t_{haunch} + c_{bottom} + 1.5 \cdot d_{b\_16}$ $y_{rb.n} = 290.0\,mm$

Distance from PNA to the top reinforcement:

$y_{rt.n} := y_{bar.n} + t_{f.t.n} + t_{haunch} + t_s - c_{top} - 1.5 \cdot d_{b\_16}$ $y_{rt.n} = 634.2\,mm$

Plastic moment capacity: (case I)

[Table D6.1-2]

$$M_{p.n} := \frac{P_{w.n}}{2\,D} \cdot \left[y_{bar.n}^{\,2} + \left(D - y_{bar.n}\right)^2 \right] \ldots + \left(P_{rt.n} \cdot y_{rt.n} + P_{rb.n} \cdot y_{rb.n} + P_{t.n} \cdot y_{tf.n} + P_{c.n} \cdot y_{bf.n}\right) \qquad M_{p.n} = 17521.1\,kN \cdot m$$

I - SECTION FLEXURAL MEMBERS [S6.10 '04]

General: **[S6.10.1 '04]**

All types of I-section flexural members shall be designed as a minimum to satisfy:

The cross section proportion limits specified in Article 6.10.2;
The constructibility requirements specified in Article 6.10.3;
The service limit state requirements specified in Article 6.10.4;
The fatigue and fracture limit state requirements specified in Article 6.10.5;
The strength limit state requirements specified in Article 6.10.6.

This example was organized to consecutively check the Articles listed above for an interior girder only.

Positive Moment Region Cross Section Proportional Limits: [S6.10.2 '04]

WEB PROPORTIONS: [S6.10.2.1 '04]

Web slenderness limit: $\frac{D}{t_w} \le 150$ **[S6.10.2.1.1 '04]**

$$\text{Check\_Web\_Slenderness} := \begin{cases} \text{"OK"} & \text{if } \frac{D}{t_w} \le 150 \\ \text{"Limit not met"} & \text{otherwise} \end{cases}$$

Check_Web_Slenderness= "OK"

- Allows for easier proportioning of the web in preliminary design.
- Satisfies elastic buckling of the web as a column subjected to a radial transverse compression from the curvature of the flanges.
- Allows web-bend-buckling to be disregarded in design of composite sections in positive flexure.

FLANGE PROPORTIONS: [S6.10.2.2 '04]

Flange weld distortion / Compactness limit: $\frac{b_f}{2\,t_f} \le 12.0$ **[S6.10.2.2-1 '04]**

$$\text{Check\_Flange\_Limit} = \begin{cases} \text{"OK"} & \text{if } \max\left(\left(\frac{b_{f.t}}{2\,t_{f.t}} \quad \frac{b_{f.b}}{2\,t_{f.b}}\right)\right) \le 12.0 \\ \text{"Limit not met"} & \text{otherwise} \end{cases}$$

Check_Flange_Limit="OK"

- Limits distortion of flange when welded to the web.
- Local buckling limit.

Web depth to flange width aspect ratio: $b_f \ge \frac{D}{6}$ **[S6.10.2.2-2 '04]**

$$\text{Check\_Flange\_Web\_Limit} = \begin{cases} \text{"OK"} & \text{if } \min\left(\left(b_{f.t} \quad b_{f.b}\right)\right) \ge \frac{D}{6} \\ \text{"Limit not met"} & \text{otherwise} \end{cases}$$

Check_Flange_Web_Limit="OK"

- Controls strength and moment-rotation characteristics of the I-section.
- Ensures stiffened interior web panels to reach requirement for post-buckling shear.

Web shear buckling limit: $t_f \ge 1.1 \cdot t_w$ **[S6.10.2.2-3 '04]**

$$\text{Check\_Shear\_Buckling\_Limit} = \begin{cases} \text{"OK"} & \text{if } \min\left(\left(t_{f.t} \quad t_{f.b}\right)\right) \ge 1.1 \cdot t_w \\ \text{"Limit not met"} & \text{otherwise} \end{cases}$$

Check_Shear_Buckling_Limit="OK"

- Ensures some restraint will be provided by the flanges against web shear buckling.
- Satisfies assumed boundary conditions for web-flange juncture in the web-bend-buckling and compression-flange-local-buckling formulas.

Positive Moment Region Cross Section Proportional Limits: [S6.10.2 '04]

Flange proportion limit: $0.1 \le \frac{I_{yc}}{I_{yt}} \le 10$ **[S6.10.2.2-4 '04]**

Tension Flange: $I_{yt} := \frac{t_{f.b} \cdot b_{f.b}^{3}}{12}$ Compression Flange: $I_{yc} := \frac{t_{f.t} \cdot b_{f.t}^{3}}{12}$

$$\text{Check\_Flange\_Proportion\_Limit} := \begin{cases} \text{"OK"} & \text{if } 0.1 \le \frac{I_{yc}}{I_{yt}} \le 10 \\ \text{"Proportion not within bounds"} & \text{otherwise} \end{cases}$$

Check_Flange_Proportion_Limit="OK"

- Establishes I-section proportional limits in order to ensure validity of equations in specification.
- Ensures more efficient flange proportions and prevents the use of sections that may be particularly difficult to handle during construction.

Negative Moment Region Cross Section Proportional Limits: [S6.10.2 '04]

WEB PROPORTIONS: [S6.10.2.1 '04]

Web slenderness limit: $\frac{D}{t_w} \le 150$ [S6.10.2.1.1-1 '04]

$$Check\_Web\_Slenderness_n := \begin{cases} \text{"OK"} & \text{if } \frac{D}{t_{w.n}} \le 150 \\ \text{"Limit not met"} & \text{otherwise} \end{cases}$$

$Check\_Web\_Slenderness_n = \text{"OK"}$

FLANGE PROPORTIONS: [S6.10.2.2 '04]

Flange weld distortion limit: $\frac{b_f}{2\,t_f} \le 12.0$ [S6.10.2.2-1 '04]

$$Check\_Flange\_Limit_n := \begin{cases} \text{"OK"} & \text{if } \max\left(\left(\frac{b_{f.t.n}}{2\,t_{f.t.n}} \quad \frac{b_{f.b.n}}{2\,t_{f.b.n}}\right)\right) \le 12.0 \\ \text{"Limit not met"} & \text{otherwise} \end{cases}$$

$Check\_Flange\_Limit_n = \text{"OK"}$

Web depth to flange width aspect ratio: $b_f \ge \frac{D}{6}$ [S6.10.2.2-2 '04]

$$Check\_Flange\_Web\_Limit_n := \begin{cases} \text{"OK"} & \text{if } \min\left(\left(b_{f.t.n} \quad b_{f.b.n}\right)\right) \ge \frac{D}{6} \\ \text{"Limit not met"} & \text{otherwise} \end{cases}$$

$Check\_Flange\_Web\_Limit_n = \text{"OK"}$

Web shear buckling limit: $t_f \ge 1.1 \cdot t_w$ [S6.10.2.2-3 '04]

$$Check\_Shear\_Buckling\_Limit_n := \begin{cases} \text{"OK"} & \text{if } \min\left(\left(t_{f.t} \quad t_{f.b}\right)\right) \ge 1.1 \cdot t_w \\ \text{"Limit not met"} & \text{otherwise} \end{cases}$$

$Check\_Shear\_Buckling\_Limit_n = \text{"OK"}$

Flange proportion limit: $0.1 \le \frac{I_{yc}}{I_{yt}} \le 10$ [S6.10.2.2-4 '04]

Tension Flange: $I_{yt.n} := \frac{t_{f.t.n} \cdot b_{f.t.n}^{\,3}}{12}$ Compression Flange: $I_{yc.n} := \frac{t_{f.b.n} \cdot b_{f.b.n}^{\,3}}{12}$

$$Check\_Flange\_Proportion\_Limit_n := \begin{cases} \text{"OK"} & \text{if } 0.1 \le \frac{I_{yc.n}}{I_{yt.n}} \le 10 \\ \text{"Proportion not within bounds"} & \text{otherwise} \end{cases}$$

$Check\_Flange\_Proportion\_Limit_n = \text{"OK"}$

SEVICE LIMIT STATE: Control of Permanent Deflection [S6.10.4 '04]
Positive Moment Region:

Flexure check for top flange steel: $f_f \le 0.95 \cdot R_h \cdot F_{yf}$ **[S6.10.4.2.2-1 '04]**

The compression-flange flexural stresses resulting from unfactored loads are as follows:

$M_{DC1} := 3202 \cdot kN \cdot m$ $\quad f_{DC1\_cf} := \dfrac{M_{DC1}}{S_{Top\_Steel\_NC}}$ $\quad f_{DC1\_cf} = 190.6\,MPa$

$M_{DC2} := 161 \cdot kN \cdot m$ $\quad f_{DC2\_cf} := \dfrac{M_{DC2}}{S_{Top\_Steel\_LT}}$ $\quad f_{DC2\_cf} = 2.1\,MPa$

$M_{DW} := 404 \cdot kN \cdot m$ $\quad f_{DW\_cf} := \dfrac{M_{DW}}{S_{Top\_Steel\_LT}}$ $\quad f_{DW\_cf} = 5.4\,MPa$

$M_{LL\_IM} := 3565 \cdot kN \cdot m$ $\quad f_{LL\_IM\_cf} := \dfrac{M_{LL\_IM}}{S_{Top\_Steel\_ST}}$ $\quad f_{LL\_IM\_cf} = 10.9\,MPa$

Appying Sevice II Factors:

$$f_{serviceII\_cf} := \eta \cdot \left[1.0 \cdot \left(f_{DC1\_cf}\right) + 1.0 \cdot \left(f_{DC2\_cf}\right) + 1.0 \cdot \left(f_{DW\_cf}\right) + 1.3 \cdot \left(f_{LL\_IM\_cf}\right) \right]$$

$f_{serviceII\_cf} = 212.2\,MPa$

Hybrid factor: **[S6.10.1.10.1 '04]**

Because the compression flange in the positive moment regoin is the same yield strength as the web the hybrid factor can be taken as:

$R_h := 1.0$

Flexure check for top flange steel:

$$Check\_Comp\_Flange\_Service\_II := \begin{cases} \text{"OK"} & \text{if } f_{serviceII\_cf} \le 0.95 \cdot R_h \cdot F_{yc} \\ \text{"Permanent deflection limitation exceeded"} & \text{otherwise} \end{cases}$$

Check_Comp_Flange_Service_II = "OK"

$$PR\_Comp\_Flange\_Service\_II := \frac{f_{serviceII\_cf}}{\left(0.95 \cdot R_h \cdot F_{yc}\right)}$$

PR_Comp_Flange_Service_II = 64.7 %

Flexure check for bottom flange steel: $f_f + \frac{1}{2}\cdot f_l \le 0.95\cdot R_h\cdot F_{yf}$ **[S6.10.4.2.2-2 '04]**

The tension-flange flexural stresses resulting from unfactored loads are as follows:

$f_{DC1\_tf} := \frac{M_{DC1}}{S_{Bot\_Steel\_NC}}$ $f_{DC1\_tf} = 190.6\,MPa$

$f_{DC2\_tf} := \frac{M_{DC2}}{S_{Bot\_Steel\_LT}}$ $f_{DC2\_tf} = 7.3\,MPa$

$f_{DW\_tf} := \frac{M_{DW}}{S_{Bot\_Steel\_LT}}$ $f_{DW\_tf} = 18.3\,MPa$

$f_{LL\_IM\_tf} := \frac{M_{LL\_IM}}{S_{Bot\_Steel\_ST}}$ $f_{LL\_IM\_tf} = 149.4\,MPa$

Applying Service II Factors:

$f_{serviceII\_tf} := \eta\cdot\left[1.0\cdot\left(f_{DC1\_tf}\right) + 1.0\cdot\left(f_{DC2\_tf}\right) + 1.0\cdot\left(f_{DW\_tf}\right) + 1.3\cdot\left(f_{LL\_IM\_tf}\right)\right]$

$f_{serviceII\_tf} = 410.3\,MPa$

Flange lateral bending stress: **[S6.10.1.6 '04]**

$f_l := 0\ MPa$

Hybrid factor: **[S6.10.1.10.1 '04]**

$\rho := \min\left(\left(\frac{F_{yw}}{F_{yt}} \quad 1.0\right)\right)$ $\rho = 0.7$

$D_n := d_{Bot\_Steel\_ST} - t_{f.b}$ $D_n = 1233.4\,mm$

$A_{fn} := A_{f.b}$ $A_{fn} = 10000.0\,mm^2$

$\beta := \frac{2\cdot D_n\cdot t_w}{A_{fn}}$ $\beta = 3.454$

$R_h := \frac{12 + \beta\cdot\left(3\rho - \rho^3\right)}{12 + 2\cdot\beta}$ $R_h = 0.96$

Flexure check for bottom flange steel:

Check_Ten_Flange_Service_II:= "OK" if $f_{serviceII\_tf} \le 0.95\cdot R_h\cdot F_{yt}$; "Permanent deflection limitation exceeded" otherwise

Check_Ten_Flange_Service_II = "OK"

$PR\_Ten\_Flange\_Service\_II := \frac{f_{serviceII\_tf}}{\left(0.95\cdot R_h\cdot F_{yt}\right)}$

PR_Ten_Flange_Service_II = 92.9 %

Negative Moment Region:

Flexure check for top flange steel: $f_f \le 0.95 \cdot R_h \cdot F_{yf}$ **[S6.10.4.2.2-2 '04]**

The tension-flange flexural stresses resulting from unfactored loads are as follows:

$M_{DC1.n} := 5592 \cdot kN \cdot m$ $\quad f_{DC1\_tf.n} := \dfrac{M_{DC1.n}}{S_{Top\_Steel\_NC.n}}$ $\quad f_{DC1\_tf.n} = 202.1\,MPa$

$M_{DC2.n} := 288 \cdot kN \cdot m$ $\quad f_{DC2\_tf.n} := \dfrac{M_{DC2.n}}{S_{Top\_Steel\_LT.n}}$ $\quad f_{DC2\_tf.n} = 4.1\,MPa$

$M_{DW.n} := 721 \cdot kN \cdot m$ $\quad f_{DW\_tf.n} := \dfrac{M_{DW.n}}{S_{Top\_Steel\_LT.n}}$ $\quad f_{DW\_tf.n} = 10.3\,MPa$

$M_{LL\_IM.n} := 3854\ kN\ m$ $\quad f_{LL\_IM\_tf.n} := \dfrac{M_{LL\_IM.n}}{S_{Top\_Steel\_ST.n}}$ $\quad f_{LL\_IM\_tf.n} = 27.1\,MPa$

Appying Sevice II Factors:

$f_{serviceII\_tf.n} := \eta \cdot \left(1.0 f_{DC1\_tf.n} + 1.0 f_{DC2\_tf.n} + 1.0 \cdot f_{DW\_tf.n} + 1.3 \cdot f_{LL\_IM\_tf.n}\right)$

$f_{serviceII\_tf.n} = 251.7\,MPa$

Hybrid factor: **[S6.10.1.10.1 '04]**

$\rho := \min\left(\left(\dfrac{F_{yw}}{F_{yt.n}} \quad 1.0\right)\right)$ $\quad \rho = 0.7$

$F_{yt.n.1} := F_{yt.n} \cdot S_{Top\_Steel\_Comp.n}$ $\quad F_{yt.n.2} := F_{yc.n} \cdot S_{Bot\_Steel\_Comp.n}$

$D_n := \begin{cases} \left(d_{Top\_Steel\_Comp.n} - t_{f.t.n}\right) & \text{if } F_{yt.n.1} \le F_{yt.n.2} \\ \left(d_{Bot\_Steel\_Comp.n} - t_{f.b.n}\right) & \text{otherwise} \end{cases}$ $\quad D_n = 728.3\,mm$

$A_{fn} := \begin{cases} A_{f.t.n} & \text{if } D_n = d_{Top\_Steel\_Comp.n} - t_{f.t.n} \\ A_{f.b.n} & \text{otherwise} \end{cases}$ $\quad A_{fn} = 21600.0\,mm^2$

$\beta := \dfrac{2 \cdot D_n \cdot t_{w.n}}{A_{fn}}$ $\quad \beta = 0.94$

$R_h := \dfrac{12 + \beta \cdot \left(3\rho - \rho^3\right)}{12 + 2 \cdot \beta}$ $\quad R_h = 0.98$

Flexure check for top flange steel:

$Check\_Ten\_Flange\_Service\_II_n := \begin{cases} \text{"OK"} & \text{if } f_{serviceII\_tf.n} \le 0.95 \cdot R_h \cdot F_{yt.n} \\ \text{"Permanent deflection limitation exceeded"} & \text{otherwise} \end{cases}$

$Check\_Ten\_Flange\_Service\_II_n = \text{"OK"}$

$PR\_Ten\_Flange\_Service\_II_n := \dfrac{f_{serviceII\_tf.n}}{\left(0.95 \cdot R_h \cdot F_{yt.n}\right)}$ $\quad PR\_Ten\_Flange\_Service\_II_n = 55.5\,\%$

Flexure check for bottom flange steel: $f_f + \frac{1}{2}\cdot f_l \le 0.95\cdot R_h\cdot F_{yf}$ **[S6.10.4.2.2-1 '04]**

The compression-flange flexural stresses resulting from unfactored loads are as follows:

$f_{DC1\_cf.n} := \frac{M_{DC1.n}}{S_{Bot\_Steel\_NC.n}}$ $f_{DC1\_cf.n} = 179.1\,MPa$

$f_{DC2\_cf.n} := \frac{M_{DC2.n}}{S_{Bot\_Steel\_LT.n}}$ $f_{DC2\_cf.n} = 7.8\,MPa$

$f_{DW\_cf.n} := \frac{M_{DW.n}}{S_{Bot\_Steel\_LT.n}}$ $f_{DW\_cf.n} = 19.5\,MPa$

$f_{LL\_IM\_cf.n} := \frac{M_{LL\_IM.n}}{S_{Bot\_Steel\_ST.n}}$ $f_{LL\_IM\_cf.n} = 72.8\,MPa$

Appying Sevice II Factors:

$$f_{serviceII\_cf.n} := \eta\cdot\left[\begin{array}{l}\left[1.0\cdot\left(f_{DC1\_cf.n}\right) + 1.0\cdot\left(f_{DC2\_cf.n}\right)\right] \ ... \\ + 1.0\cdot f_{DW\_cf.n} + 1.3\cdot\left(f_{LL\_IM\_cf.n}\right)\end{array}\right]$$

$f_{serviceII\_cf.n} = 301.0\,MPa$

Flange lateral bending stress: **[S6.10.1.6 '04]**

$f_{l.n} := 0\cdot MPa$

Hybrid factor: **[S6.10.1.10.1 '04]**

$R_h = 0.98$

Flexure check for bottom flange steel:

$$Check\_Comp\_Flange\_Service\_II_n := \left|\begin{array}{l}\text{"OK"} \quad \text{if } f_{serviceII\_cf.n} + \frac{1}{2}\cdot f_{l.n} \le 0.95\cdot R_h\cdot F_{yc.n} \\ \text{"Permanent deflection limitation exceeded" otherwise}\end{array}\right.$$

$Check\_Comp\_Flange\_Service\_II_n = \text{"OK"}$

$PR\_Comp\_Flange\_Service\_II_n := \frac{f_{serviceII\_cf.n}}{\left(0.95\cdot R_h\cdot F_{yc.n}\right)}$

$PR\_Comp\_Flange\_Service\_II_n = 66.3\,\%$

Web Bend Buckling Check: $f_c \le F_{crw}$ **[S6.10.4.2.2-4 '04]**

Flange stress due to service II loads:

$f_{serviceII\_cf.n} = 301.0\,MPa$

$f_{serviceII\_tf.n} = 251.7\,MPa$

$$D_{c.n} := \left(\frac{f_{serviceII\_cf.n}}{\left| f_{serviceII\_cf.n} \right| + f_{serviceII\_tf.n}} \right) \cdot d_n - t_{f.b.n}$$ **[D6.3.1 '04]**

$D_{c.n} = 711.5\,mm$

$$k_n := \frac{9}{\left(\frac{D_{c.n}}{D} \right)^2} \qquad k_n = 30.0$$ **[S6.10.1.9.1-2 '04]**

$$F_{crw.n} := \min\left[\left[\frac{0.9\,E_s\,k_n}{\left(\frac{D}{t_{w.n}} \right)^2} \quad F_{yc.n} \right] \right] \qquad F_{crw.n} = 485.0\,MPa$$ **[S6.10.1.9.1-1 '04]**

$$Check\_Web\_Bend\_Buckling\_Service\_II_n := \begin{cases} \text{"OK"} & \text{if } f_{serviceII\_cf.n} \le F_{crw.n} \\ \text{"Web bend buckling occurs"} & \text{otherwise} \end{cases}$$

$Check\_Web\_Bend\_Buckling\_Service\_II_n = \text{"OK"}$

$$PR\_Web\_Bend\_Buckling\_Service\_II_n := \frac{f_{serviceII\_cf.n}}{F_{crw.n}}$$

$PR\_Web\_Bend\_Buckling\_Service\_II_n = 62.1\%$

STRENGTH LIMIT STATE: [S6.10.6 '04]

Positive Moment Region: [S6.10.7 '04]

COMPACT SECTIONS: [S6.10.7.1 '04]

Sections that satisfy the following requirements shall qualify as compact sections:

- the specified minimum yield strengths of the flanges and web do not exceed 485 MPa,
- the web satisfies the requirement of Article 6.10.2.1.1, and: **[S6.10.7.1.1-1 '04]**
- the section satisfies the slenderness limit: $\frac{2 \cdot D_{cp}}{t_w} \le 3.76 \cdot \sqrt{\frac{E_s}{F_{yc}}}$

Depth of web in compression at the plastic moment: **[D6.3.2 '04]**

$D_{cp} := \max\left(\begin{pmatrix} y_{bar} - t_{f.t} \\ 0\ mm \end{pmatrix}\right)$ $D_{cp} = 126.2\,mm$

$$section := \begin{cases} \text{"Compact"} \text{ if } \left(\frac{2 \cdot D_{cp}}{t_w} \le 3.76 \cdot \sqrt{\frac{E_s}{F_{yc}}}\right) \cdot \left[\max\left(\begin{pmatrix} F_{yc} \\ F_{yt} \end{pmatrix}\right) \le 485\ MPa\right] \cdot \left(\frac{D}{t_w} \le 150\right) \\ \text{"Non-compact"} \text{ otherwise} \end{cases}$$

$section = \text{"Compact"}$

Strength limit state check: $M_u + \frac{1}{3} \cdot f_l \cdot S_{xt} \le \phi_f \cdot M_n$ **[S6.10.7.1.1-2 '04]**

Nominal Flexural Resistance: **[S6.10.7.1.2 '04]**

$D_p := t_s + t_{haunch} + y_{bar}$ $D_p = 401.1\,mm$

$D_t := t_s + t_{haunch} + d$ $D_t = 1600.0\,mm$

$$M_n := \begin{cases} M_p \text{ if } D_p \le 0.1 \cdot D_t \\ M_p \cdot \left[1.07 - 0.7 \cdot \left(\frac{D_p}{D_t}\right)\right] \text{ otherwise} \end{cases}$$

$M_n = 11880.6\,kN \cdot m$ **[S6.10.7.1.2-1 '04]**

[S6.10.7.1.2-2 '04]

In continuous spans, the nominal flexural resistance of the section shall not exceed:

$M_n = 1.3 \cdot R_h \cdot M_y$ **[S6.10.7.1.2-3 '04]**

Hybrid factor: **[S6.10.1.10.1 '04]**

$\rho := \min\left(\left(\frac{F_{yw}}{F_{yt}} \quad 1.0\right)\right)$ $\rho = 0.7$

$D_n := d_{Bot\_Steel\_ST} - t_{f.b}$ $D_n = 1233.4\,mm$

$A_{fn} := A_{f.b}$ $A_{fn} = 10000.0\,mm^2$

$\beta := \frac{2 \cdot D_n \cdot t_{w.n}}{A_{fn}}$ $\beta = 3.454$

$R_h := \frac{12 + \beta \cdot \left(3\rho - \rho^3\right)}{12 + 2 \cdot \beta}$ $R_h = 0.96$

Yield moment bottom flange: **[D6.2 '04]**

$M_{DC1} := 3202 \cdot kN \cdot m$

$M_{DC2} := 161 \cdot kN \cdot m$

$M_{DW} := 404 \cdot kN \cdot m$

$M_{LL\_IM} := 3565 \cdot kN \cdot m$

$F_{yt} = \eta \cdot \left[\left(\frac{1.25 M_{DC1}}{S_{Bot\_Steel\_NC}}\right) + \left(\frac{1.25 M_{DC2} + 1.5 \cdot M_{DW}}{S_{Bot\_Steel\_LT}}\right) + \left(\frac{M_{AD}}{S_{Bot\_Steel\_ST}}\right)\right]$

$M_{AD} := S_{Bot\_Steel\_ST} \cdot \left(\frac{F_{yt}}{\eta} \cdot \frac{1.25 \cdot M_{DC1}}{S_{Bot\_Steel\_NC}} \cdot \frac{1.25 \cdot M_{DC2} + 1.5 \cdot M_{DW}}{S_{Bot\_Steel\_LT}}\right)$

$M_{AD} = 5018.6\,kN \cdot m$

$M_{yt} := \eta \cdot \left(1.25 \cdot M_{DC1} + 1.25 \cdot M_{DC2} + 1.5 \cdot M_{DW} + M_{AD}\right)$

$M_{yt} = 9828.4\,kN \cdot m$

Nominal Flexural Resistance:

$M_n := \min\left(\left(M_p \quad 1.3 \cdot R_h \cdot M_{yt}\right)\right)$ **[S6.10.7.1.2-3 '04]**

$M_n = 12249.6\,kN \cdot m$

Factored moment due to strength I load combination about major axis: **[S6.10.1.6 '04]**

$M_{u\_strength\_I} := 1.25 \cdot M_{DC1} + 1.25 \cdot M_{DC2} + 1.5 \cdot M_{DW} + 1.75 \cdot M_{LL\_IM}$

$M_{u\_strength\_I} = 11048.5\,kN \cdot m$

Flange lateral bending stress: **[S6.10.1.6 '04]**

$f_l := 0 \cdot MPa$

Elastic section modulus for tension flange: **[S6.10.7.1.1 '04]**

$$S_{xt} := \frac{M_{yt}}{F_{yt}} \qquad S_{xt} = 2.0 \times 10^7\, mm^3$$

Resistance factor for flexure:

$\phi_f := 1.0$ **[S6.5.4.2 '04]**

Check Strength I Flexure:

$$Check\_Strength\_I\_Flexure := \begin{cases} \text{"OK"} & \text{if } M_{u\_strength\_I} + \frac{1}{3} \cdot f_l \cdot S_{xt} \le \phi_f \cdot M_n \\ \text{"Flexural resistance failure"} & \text{otherwise} \end{cases}$$ **[S6.10.7.1.1-2 '04]**

$Check\_Strength\_I\_Flexure = \text{"OK"}$

$$PR\_Strength\_I\_Flexure = \frac{M_{u\_strength\_I} + \frac{1}{3} \cdot f_l \cdot S_{xt}}{\phi_f \cdot M_n}$$

$PR\_Strength\_I\_Flexure = 90.2\,\%$

DUCTILITY REQUIREMENT: **[S6.10.7.3 '04]**

$D_p = 401.1\,mm$

$D_t = 1600.0\,mm$

$$Check\_Ductility := \begin{cases} \text{"OK"} & \text{if } D_p \le 0.42 \cdot D_t \\ \text{"Brittle failure"} & \text{otherwise} \end{cases}$$

$Check\_Ductility = \text{"OK"}$ **[S6.10.7.3-1 '04]**

$$PR\_Ductility := \frac{D_p}{(0.42 \cdot D_t)}$$

$PR\_Ductility = 59.7\,\%$

Positive Moment Region: [S6.10.7 '04]

Shear: • The provisions of Article 6.10.9 shall apply. **[S6.10.6.3 '04]**

Shear Resistance: $V_r = \phi_v \cdot V_n$ **[S6.10.9 '04]**

Resistance of unstiffened web in positive moment region: **[S6.10.9.2 '04]**

Plastic shear force:

$V_p := 0.58 \cdot F_{yw} \cdot D \cdot t_w \qquad V_p = 3641.8\,kN$ **[S6.10.9.2-2 '04]**

Shear buckling coefficient for unstiffened condition:

$k := 5$ **[S6.10.9.2 '04]**

$$C := \begin{cases} 1.0 & \text{if } \frac{D}{t_w} < 1.12 \cdot \sqrt{\frac{E_s \cdot k}{F_{yw}}} \\ \left[\frac{1.12}{\left(\frac{D}{t_w}\right)} \cdot \sqrt{\frac{E_s \cdot k}{F_{yw}}}\right] & \text{if } 1.12 \cdot \sqrt{\frac{E_s \cdot k}{F_{yw}}} \le \frac{D}{t_w} \le 1.40 \cdot \sqrt{\frac{E_s \cdot k}{F_{yw}}} \\ \left[\frac{1.57}{\left(\frac{D}{t_w}\right)^2} \cdot \left(\frac{E_s \cdot k}{F_{yw}}\right)\right] & \text{if } \frac{D}{t_w} > 1.40 \cdot \sqrt{\frac{E_s \cdot k}{F_{yw}}} \end{cases}$$

[S6.10.9.3.2-4 '04] **[S6.10.9.3.2-5 '04]** **[S6.10.9.3.2-6 '04]**

$C = 0.53$

Shear buckling resistance:

$V_{cr} := C \cdot V_p \qquad V_{cr} = 1922.1\,kN$ **[S6.10.9.3.3-1 '04]**

Shear resistance of unstiffened web:

$V_{r\_unstiffened} := \phi_v \cdot V_{cr} \qquad V_{r\_unstiffened} = 1922.1\,kN$

End Panel From Abutment: **[S6.10.9.3.3 '04]**

Shear from factored loads at abutment location: $V_{u\_StrengthI} := 1772 \cdot kN$

$$Check\_Shear := \begin{cases} \text{"OK-Unstiffened Design"} & \text{if } V_{u\_StrengthI} \le V_{r\_unstiffened} \\ \text{"Increase shear resistance"} & \text{otherwise} \end{cases}$$

Check_Shear = "OK-Unstiffened Design"

$$PR\_Shear := \frac{V_{u\_StrengthI}}{V_{r\_unstiffened}}$$

PR_Shear = 92.2 %

Negative Moment Region: [S6.10.7 '04]

Sections that satisfy the following requirements shall qualify as compact sections:

- the specified minimum yield strengths of the flanges and web do not exceed 485 MPa,
- the web satisfies the requirement of Article 6.10.2.1.1,

and:

- the section satisfies the slenderness limit: $\frac{2 \cdot D_c}{t_w} \le 5.7 \cdot \sqrt{\frac{E_s}{F_{yc.n}}}$ **[S6.10.7.1.1-1 '04]**

Depth of web in compression in elastic range: **[D6.3.1 '04]**

The tension-flange flexural stresses with strength I factors applied is:

$M_{DC1.n} := 5718 \cdot kN \cdot m$ $\quad f_{DC1\_tf.n} := \frac{M_{DC1.n}}{S_{Top\_Steel\_NC.n}}$ $\quad f_{DC1\_tf.n} = 206.7\,MPa$

$M_{DC2.n} := 288 \cdot kN \cdot m$ $\quad f_{DC2\_tf.n} := \frac{M_{DC2.n}}{S_{Top\_Steel\_Comp.n}}$ $\quad f_{DC2\_tf.n} = 6.7\,MPa$

$M_{DW.n} := 721 \cdot kN \cdot m$ $\quad f_{DW\_tf.n} := \frac{M_{DW.n}}{S_{Top\_Steel\_Comp.n}}$ $\quad f_{DW\_tf.n} = 16.8\,MPa$

$M_{LL\_IM.n} := 3625 \cdot kN \cdot m$ $\quad f_{LL\_I\_tf.n} := \frac{M_{LL\_IM.n}}{S_{Top\_Steel\_Comp.n}}$ $\quad f_{LL\_I\_tf.n} = 84.4\,MPa$

$f_{strI\_tf.n} := \eta \cdot \left[1.25 \cdot \left(f_{DC1\_tf.n}\right) + 1.25 \cdot \left(f_{DC2\_tf.n}\right) + 1.5 \cdot \left(f_{DW\_tf.n}\right) + 1.75 \cdot \left(f_{LL\_I\_tf.n}\right) \right]$

$f_{strI\_tf.n} = 439.5\,MPa$

The compression-flange flexural stresses with strength I factors applied is:

$f_{DC1\_cf.n} := \frac{M_{DC1.n}}{S_{Bot\_Steel\_NC.n}}$ $\quad f_{DC1\_cf.n} = 183.1\,MPa$

$f_{DC2\_cf.n} := \frac{M_{DC2.n}}{S_{Bot\_Steel\_Comp.n}}$ $\quad f_{DC2\_cf.n} = 8.4\,MPa$

$f_{DW\_cf.n} := \frac{M_{DW.n}}{S_{Bot\_Steel\_Comp.n}}$ $\quad f_{DW\_cf.n} = 21.1\,MPa$

$f_{LL\_I\_cf.n} := \frac{M_{LL\_IM.n}}{S_{Bot\_Steel\_Comp.n}}$ $\quad f_{LL\_I\_cf.n} = 106.0\,MPa$

$$f_{strI\_cf.n} := \eta \cdot \left[1.25 \cdot \left(f_{DC1\_cf.n} \right) + 1.25 \cdot \left(f_{DC2\_cf.n} \right) + 1.5 \cdot \left(f_{DW\_cf.n} \right) + 1.75 \cdot \left(f_{LL\_I\_cf.n} \right) \right]$$

$$f_{strI\_cf.n} = 456.5\,\text{MPa}$$

$$D_{c.n} := \left(\frac{f_{strI\_cf.n}}{\left| f_{strI\_cf.n} \right| + f_{strI\_tf.n}} \right) \cdot d_n - t_{f.b.n} \qquad \textbf{[D6.3.1 '04]}$$

$$D_{c.n} = 663.0\,\text{mm}$$

$$\text{Web\_slenderness:=} \begin{cases} \text{"[6.10.8 '04] or [Optional Appendix A '04]"} & \text{if } \frac{2 \cdot D_{c.n}}{t_{w.n}} \le 5.7 \cdot \sqrt{\frac{E_s}{F_{yc.n}}} \\ \text{"Slender web - [6.10.8 '04]"} & \text{otherwise} \end{cases}$$

Web_slenderness= "[6.10.8 '04] or [Optional Appendix A '04]"

Slenderness ratio of compression flange:

$$\lambda_{f.n} := \frac{b_{f.b.n}}{2 \cdot t_{f.b.n}} \qquad \lambda_{f.n} = 6.8 \qquad \textbf{[S6.10.8.2.2-3 '04]}$$

$$\lambda_{pf.n} := 0.38 \cdot \sqrt{\frac{E_s}{F_{yc.n}}} \qquad \lambda_{pf.n} = 7.7 \qquad \textbf{[S6.10.8.2.2-4 '04]}$$

$$\lambda_{rf.n} := 0.56 \cdot \sqrt{\frac{E_s}{F_{yc.n}}} \qquad \lambda_{rf.n} = 11.4 \qquad \textbf{[S6.10.8.2.2-5 '04]}$$

Load-shedding factor: **[S6.10.1.10.2 '04]**

$$\lambda_{rw.n} := 5.7 \cdot \sqrt{\frac{E_s}{F_{yc.n}}} \qquad \lambda_{rw.n} = 115.7 \qquad \textbf{[S6.10.1.10.2-4 '04]}$$

$$a_{wc} := \frac{2 \cdot D_{c.n} \cdot t_{w.n}}{b_{f.b.n} \cdot t_{f.b.n}} \qquad a_{wc} = 0.9 \qquad \textbf{[S6.10.1.10.2-5 '04]}$$

$$R_b := \begin{cases} 1.0 & \text{if } \frac{2 \cdot D_{c.n}}{t_{w.n}} \le \lambda_{rw.n} \qquad \textbf{[S6.10.1.10.2-2 '04]} \\ \min\left[\left[1 - \left(\frac{a_{wc}}{1200 + 300 \cdot a_{wc}} \right) \cdot \left(\frac{2 \cdot D_{c.n}}{t_{w.n}} - \lambda_{rw.n} \right) \right], 1.0 \right] & \text{otherwise} \qquad \textbf{[S6.10.1.10.2-3 '04]} \end{cases}$$

$$R_b = 1.0$$

Hybrid factor: **[S6.10.1.10.1 '04]**

$$\rho := \min\left(\left(\frac{F_{yw.n}}{F_{yc.n}} \quad 1.0\right)\right) \qquad \rho = 0.71$$

$$M_{yt.n} := F_{yt.n} \cdot S_{Top\_Steel\_Comp.n} \qquad M_{yc.n} := F_{yc.n} \cdot S_{Bot\_Steel\_Comp.n}$$

$$D_n := \begin{cases} \left(d_{Top\_Steel\_Comp.n} - t_{f.t.n}\right) & \text{if } M_{yt.n} \le M_{yc.n} \\ \left(d_{Bot\_Steel\_Comp.n} - t_{f.b.n}\right) & \text{otherwise} \end{cases}$$

$$D_n = 728.3\,\text{mm}$$

$$A_{fn} := \begin{cases} A_{f.t.n} & \text{if } D_n = d_{Bot\_Steel\_Comp.n} - t_{f.t.n} \\ A_{f.b.n} & \text{otherwise} \end{cases} \qquad A_{fn} = 18000.0\,\text{mm}^2$$

$$\beta := \frac{2 \cdot D_n \cdot t_{w.n}}{A_{fn}} \qquad \beta = 1.133$$

$$R_h := \frac{12 + \beta \cdot \left(3\rho - \rho^3\right)}{12 + 2 \cdot \beta} \qquad R_h = 0.98$$

Nominal flexural resistance of the flange to local buckling: **[S6.10.8.2 '04]**

$$F_{yr.n} := \begin{cases} \left(0.7 \cdot F_{yc.n}\right) & \text{if } 0.7 \cdot F_{yc.n} \le F_{yw.n} \\ F_{yw.n} & \text{otherwise} \end{cases}$$ **[S6.10.8.2.2-6 '04]**

$$F_{yr.n} = 339.5\,\text{MPa}$$ **[S6.10.8.2.2-1 '04]**

[S6.10.8.2.2-2 '04]

$$F_{nc.FLB.n} := \begin{cases} \left(R_b \cdot R_h \cdot F_{yc.n}\right) & \text{if } \lambda_{f.n} \le \lambda_{pf.n} \\ \left[\left[1 - \left(1 - \frac{F_{yr.n}}{R_h \cdot F_{yc.n}}\right) \cdot \left(\frac{\lambda_{f.n} - \lambda_{pf.n}}{\lambda_{rf.n} - \lambda_{pf.n}}\right)\right] \cdot R_b \cdot R_h \cdot F_{yc.n}\right] & \text{otherwise} \end{cases}$$

$$F_{nc.FLB.n} = 476.3\,\text{MPa}$$

Lateral torsional buckling resistance: **[S6.10.8.2.3 '04]**

Unbraced length:

$L_{b.n} := 6000mm$

Depth of web in compression for non-composite section in elastic range:

$D_{c.n} := d_{Bot\_Steel\_Comp.n} - t_{f.b.n}$ $D_{c.n} = 728.3\,mm$

Radius of gyration about vertical axis:

$$r_{t.n} := \frac{b_{f.b.n}}{\sqrt{12 \cdot \left(1 + \frac{1}{3} \cdot \frac{D_{c.n} \cdot t_{w.n}}{b_{f.b.n} \cdot t_{f.b.n}}\right)}}$$ $r_{t.n} = 144.9\,mm$ **[S6.10.8.2.3-10 '04]**

Limiting unbraced lengths:

$$L_{p.n} := r_{t.n} \cdot \sqrt{\frac{E_s}{F_{yc.n}}}$$ $L_{p.n} = 2942\,mm$ **[S6.10.8.2.3-4 '04]**

$$L_{r.n} := \pi \cdot r_{t.n} \sqrt{\frac{E_s}{F_{yc.n}}}$$ $L_{r.n} = 9244.1\,mm$ **[S6.10.8.2.3-5 '04]**

Moment gradient factor:

moment at middle of unbraced length:	largest moment at either brace point:	moment at brace point opposite to M_2:
$MDC1_{mid.n} := 3747 \cdot kN \cdot m$	$MDC1_{2.n} := 5592 \cdot kN \cdot m$	$MDC1_{o.n} := 1901 \cdot kN \cdot m$
$MDC2_{mid.n} := 193 \cdot kN \cdot m$	$MDC2_{2.n} := 288 \cdot kN \cdot m$	$MDC2_{o.n} := 98 \cdot kN \cdot m$
$MDW_{mid.n} := 483 \cdot kN \cdot m$	$MDW_{2.n} := 721 \cdot kN \cdot m$	$MDW_{o.n} := 245 \cdot kN \cdot m$
$MLL\_IM_{mid.n} := 2908 \cdot kN \cdot m$	$MLL\_IM_{2.n} := 3854 \cdot kN \cdot m$	$MLL\_IM_{o.n} := 1962 \cdot kN \cdot m$

stress at middle of unbraced length:

$$f_{mid.n} := \frac{1.25 \cdot \left(MDC1_{mid.n} + MDC2_{mid.n}\right) + 1.5 \cdot \left(MDW_{mid.n}\right)}{S_{Bot\_Steel\_NC.n}} + \frac{1.75 \cdot \left(MLL\_IM_{mid.n}\right)}{S_{Bot\_Steel\_Comp.n}}$$

$f_{mid.n} = 329.7\,MPa$

largest stress at either brace point:

$$f_{2.n} := \frac{1.25 \cdot \left(MDC1_{2.n} + MDC2_{2.n}\right) + 1.5 \cdot \left(MDW_{2.n}\right)}{S_{Bot\_Steel\_NC.n}} + \frac{1.75 \cdot \left(MLL\_IM_{2.n}\right)}{S_{Bot\_Steel\_Comp.n}}$$

$f_{2.n} = 467.2\,MPa$

Moment gradient factor:

stress at brace point opposite of f_2

$$f_{o.n} := \frac{1.25\cdot\left(MDC1_{o.n} + MDC2_{o.n}\right) + 1.5\cdot\left(MDW_{o.n}\right)}{S_{Bot\_Steel\_NC.n}} + \frac{1.75\cdot\left(MLL\_IM_{o.n}\right)}{S_{Bot\_Steel\_Comp.n}}$$

$f_{o.n} = 192.2\,MPa$

$f_{1.n} := \max\left(\left(2\ f_{mid.n} - f_{2.n}\quad f_{o.n}\right)\right)$ $\quad f_{1.n} = 192.2\,MPa$ **[S6.10.8.2.3-11 '04]**

$$C_b := \begin{cases} 1.0 & \text{if } \begin{cases} f_{2.n} = 0\cdot MPa \\ \dfrac{f_{mid.n}}{f_{2.n}} \geq 1.0 \end{cases} \\ \left[1.75 - 1.05\cdot\left(\dfrac{f_{1.n}}{f_{2.n}}\right) + 0.3\cdot\left(\dfrac{f_{1.n}}{f_{2.n}}\right)^2\right] & \text{otherwise} \end{cases}$$ **[S6.10.8.2.3-6 '04]** **[S6.10.8.2.3-7 '04]**

$C_b = 1.4$

Elastic lateral torsional buckling stress:

$$F_{cr.n} := \frac{C_b\cdot R_b\cdot\pi^2\cdot E_s}{\left(\dfrac{L_{b.n}}{r_{t.n}}\right)^2}$$ $\quad F_{cr.n} = 1575.8\,MPa$ **[S6.10.8.2.3-8 '04]**

Nominal flexural resistance of the flange to lateral torsional buckling:

1. compact unbraced length:

$F_{nc\_1.n} := \left(R_b\cdot R_h\cdot F_{yc.n}\right)$

$F_{nc\_1.n} = 476.3\,MPa$

2. non compact unbraced length:

$$F_{nc\_2.n} := \min\left[\left[\left[C_b\cdot\left[1 - \left(1 - \frac{F_{yr.n}}{R_h\cdot F_{yc.n}}\right)\cdot\left(\frac{L_{b.n} - L_{p.n}}{L_{r.n} - L_{p.n}}\right)\right]\cdot R_b\cdot R_h\cdot F_{yc.n}\right]\right]\right]$$
$$R_b\cdot R_h\cdot F_{yc.n}$$

$F_{nc\_2.n} = 476.3\,MPa$

3. slender unbraced length:

$$F_{nc\_3.n} := \min\left(\left(\frac{F_{cr.n}}{R_b\cdot R_h\cdot F_{yc.n}}\right)\right)$$

$F_{nc\_3.n} = 476.3\,MPa$

Nominal flexural resistance of the flange to lateral torsional buckling:

$$F_{nc.LTB.n} := \begin{cases} F_{nc\_1.n} & \text{if } L_{b.n} \le L_{p.n} \\ F_{nc\_2.n} & \text{if } \left(L_{p.n} < L_{b.n}\right)\cdot\left(L_{b.n} \le L_{r.n}\right) \\ F_{nc\_3.n} & \text{if } L_{b.n} > L_{r.n} \end{cases}$$

$F_{nc.LTB.n} = 476.3\,\text{MPa}$

$$F_{nc.n} := \min\left(\begin{pmatrix} F_{nc.FLB.n} \\ F_{nc.LTB.n} \end{pmatrix}\right) \qquad F_{nc.n} = 476.3\,\text{MPa}$$

Resistance factor for flexure:

$\phi_f := 1.0$ **[S6.5.4.2 '04]**

Check compression flange buckling:

$$\text{Check\_Comp\_Flange\_StrI}_n := \begin{cases} \text{"OK"} & \text{if } f_{strI\_cf.n} + \frac{1}{3}\cdot f_{l} \le \phi_f\cdot F_{nc.n} \\ \text{"Flexural resistance failure"} & \text{otherwise} \end{cases}$$ **[S6.10.3.2.1-2 '04]**

$\text{Check\_Comp\_Flange\_StrI}_n = \text{"OK"}$

$$\text{PR\_Comp\_Flange\_StrI}_n := \frac{f_{strI\_cf.n} + \frac{1}{3}\cdot f_{l.n}}{\phi_f\cdot F_{nc.n}}$$

$\text{PR\_Comp\_Flange\_StrI}_n = 95.8\,\%$

Discretely Braced Flanges in Tension: **[S6.10.3.2.2 '04]**

Check flange nominal yielding: $f_{bu} + f_l \le \phi_f\cdot R_h\cdot F_{yt}$ **[S6.10.3.2.1-1 '04]**

$$\text{Check\_Ten\_Flange\_Yield\_Str1}_n := \begin{cases} \text{"OK"} & \text{if } f_{strI\_tf.n} + f_{l.n} \le \phi_f\cdot R_h\cdot F_{yt.n} \\ \text{"Tension flange yield occurs"} & \text{otherwise} \end{cases}$$

$\text{Check\_Ten\_Flange\_Yield\_Str1}_n = \text{"OK"}$

$$\text{PR\_Ten\_Flange\_Yield\_Str1}_n := \frac{f_{strI\_tf.n} + f_{l.n}}{\phi_f\cdot R_h\cdot F_{yt.n}}$$

$\text{PR\_Ten\_Flange\_Yield\_Str1}_n = 92.3\,\%$

Negative Moment Region: [S6.10.7 '04]

Shear: The provisions of Article 6.10.9 shall apply. **[S6.10.6.3 '04]**

Shear Resistance: $V_r = \phi_v \cdot V_n$ **[S6.10.9 '04]**

Resistance of unstiffened web in negative moment region: **[S6.10.9.2 '04]**

Plastic shear force:

$V_p := 0.58 \cdot F_{yw.n} \cdot D \cdot t_{w.n}$ $V_p = 3641.8\,\text{kN}$ **[S6.10.9.2-2 '04]**

Shear buckling coefficient for unstiffened condition:

$k := 5$ **[S6.10.9.2 '04]**

$$C := \begin{cases} 1.0 & \text{if } \dfrac{D}{t_{w.n}} < 1.12 \cdot \sqrt{\dfrac{E_s \cdot k}{F_{yw.n}}} \quad \textbf{[S6.10.9.3.2-4 '04]} \\ \left[\dfrac{1.12}{\left(\dfrac{D}{t_{w.n}}\right)} \cdot \sqrt{\dfrac{E_s \cdot k}{F_{yw.n}}}\right] & \text{if } 1.12 \cdot \sqrt{\dfrac{E_s \cdot k}{F_{yw.n}}} \le \dfrac{D}{t_{w.n}} \le 1.40 \cdot \sqrt{\dfrac{E_s \cdot k}{F_{yw.n}}} \quad \textbf{[S6.10.9.3.2-5 '04]} \\ \left[\dfrac{1.57}{\left(\dfrac{D}{t_{w.n}}\right)^2} \cdot \left(\dfrac{E_s \cdot k}{F_{yw.n}}\right)\right] & \text{if } \dfrac{D}{t_{w.n}} > 1.40 \cdot \sqrt{\dfrac{E_s \cdot k}{F_{yw.n}}} \quad \textbf{[S6.10.9.3.2-6 '04]} \end{cases}$$

$C = 0.53$

Shear bucking resistance:

$V_{cr} := C \cdot V_p$ $V_{cr} = 1922.1\,\text{kN}$ **[S6.10.9.3.3-1 '04]**

Shear resistance of unstiffened web:

$V_{r\_unstiffened} := \phi_v \cdot V_{cr}$ $V_{r\_unstiffened} = 1922.1\,\text{kN}$

1st Interior Panel From Pier: **[S6.10.9.3.2 '04]**

Shear from factored loads at pier: $V_{u\_StrengthI} := 2377 \cdot kN$

$$Check\_Shear_n := \begin{cases} \text{"OK-Unstiffened Design"} & \text{if } V_{u\_StrengthI} \le V_{r\_unstiffened} \\ \text{"Increase shear resistance"} & \text{otherwise} \end{cases}$$

$Check\_Shear_n = \text{"Increase shear resistance"}$

Therefore, add a stiffener between pier and 1st cross frame:

Stiffener spacing from pier stiffener: $d_o := 3 \cdot m$

$$k := 5 + \frac{5}{\left(\frac{d_o}{D}\right)^2} \qquad k = 5.9 \qquad \textbf{[S6.10.9.3.2-7 '04]}$$

$$C := \begin{cases} 1.0 & \text{if } \frac{D}{t_{w.n}} < 1.12 \cdot \sqrt{\frac{E_s \cdot k}{F_{yw.n}}} \\ \left[\frac{1.12}{\left(\frac{D}{t_{w.n}}\right)} \cdot \sqrt{\frac{E_s \cdot k}{F_{yw.n}}}\right] & \text{if } 1.12 \cdot \sqrt{\frac{E_s \cdot k}{F_{yw.n}}} \le \frac{D}{t_{w.n}} \le 1.40 \cdot \sqrt{\frac{E_s \cdot k}{F_{yw.n}}} \\ \left[\frac{1.57}{\left(\frac{D}{t_{w.n}}\right)^2} \cdot \left(\frac{E_s \cdot k}{F_{yw.n}}\right)\right] & \text{if } \frac{D}{t_{w.n}} > 1.40 \cdot \sqrt{\frac{E_s \cdot k}{F_{yw.n}}} \end{cases}$$

[S6.10.9.3.2-4 '04] **[S6.10.9.3.2-5 '04]** **[S6.10.9.3.2-6 '04]**

$C = 0.63$

$$V_n := \begin{cases} \left[V_p \cdot \left[C + \frac{0.87 \cdot (1 - C)}{\sqrt{1 + \left(\frac{d_o}{D}\right)^2}}\right]\right] & \text{if } \frac{2 \cdot D \cdot t_{w.n}}{\left(b_{f.t.n} \cdot t_{f.t.n} + b_{f.b.n} \cdot t_{f.b.n}\right)} \le 2.5 \\ \left(C \cdot V_p\right) & \text{otherwise} \end{cases}$$

[S6.10.9.3.2-1 '04] **[S6.10.9.3.2-2 '04]** **[S6.10.9.2-1 '04]**

$V_n = 2753.0\,kN$

$$Check\_Shear\_1st\_Int\_Panel\_Str\_I_n := \begin{cases} \text{"OK"} & \text{if } V_{u\_StrengthI} \le \phi_v \cdot V_n \\ \text{"Increase shear resistance"} & \text{otherwise} \end{cases}$$

$Check\_Shear\_1st\_Int\_Panel\_Str\_I_n = \text{"OK"}$

$$PR\_Shear\_1st\_Int\_Panel\_Str\_I_n := \frac{V_{u\_StrengthI}}{\phi_v \cdot V_n}$$

$PR\_Shear\_1st\_Int\_Panel\_Str\_I_n = 86.3\,\%$

2nd Interior Panel From Pier:

Because the distance between the previous stiffener and the 1st cross frame from the pier is the same, there in no need to check the next panel. The panel will have the same shear resistance with lesser applied design shear force.

3rd Interior Panel From Pier: **[S6.10.9.3.2 '04]**

Shear from factored loads at 6 m from pier: $V_{u\_StrengthI} := 1922 \cdot kN$

Stiffener spacing from 1st cross frame stiffener: $d_o := 3 \cdot m$

$$k := 5 + \frac{5}{\left(\frac{d_o}{D}\right)^2} \qquad k = 5.9 \qquad \textbf{[S6.10.9.3.2-7 '04]}$$

$$C := \begin{cases} 1.0 & \text{if } \frac{D}{t_{w.n}} < 1.12 \cdot \sqrt{\frac{E_s \cdot k}{F_{yw.n}}} \qquad \textbf{[S6.10.9.3.2-4 '04]} \\ \left[\frac{1.12}{\left(\frac{D}{t_{w.n}}\right)} \cdot \sqrt{\frac{E_s \cdot k}{F_{yw.n}}}\right] & \text{if } 1.12 \cdot \sqrt{\frac{E_s \cdot k}{F_{yw.n}}} \le \frac{D}{t_{w.n}} \le 1.40 \cdot \sqrt{\frac{E_s \cdot k}{F_{yw.n}}} \qquad \textbf{[S6.10.9.3.2-5 '04]} \\ \left[\frac{1.57}{\left(\frac{D}{t_{w.n}}\right)^2} \cdot \left(\frac{E_s \cdot k}{F_{yw.n}}\right)\right] & \text{if } \frac{D}{t_{w.n}} > 1.40 \cdot \sqrt{\frac{E_s \cdot k}{F_{yw.n}}} \qquad \textbf{[S6.10.9.3.2-6 '04]} \end{cases}$$

$C = 0.63$

$$V_n := \begin{cases} \left[V_p \cdot \left[C + \frac{0.87 \cdot (1 - C)}{\sqrt{1 + \left(\frac{d_o}{D}\right)^2}}\right]\right] & \text{if } \frac{2 \cdot D \cdot t_{w.n}}{\left(b_{f.t.n} \cdot t_{f.t.n} + b_{f.b.n} \cdot t_{f.b.n}\right)} \le 2.5 \qquad \textbf{[S6.10.9.3.2-1 '04]} \ \textbf{[S6.10.9.3.2-2 '04]} \\ \left(C \cdot V_p\right) & \text{otherwise} \qquad \textbf{[S6.10.9.2-1 '04]} \end{cases}$$

$V_n = 2753.0\,kN$

$$Check\_Shear\_3rd\_Int\_Panel\_Str\_I_n := \begin{cases} \text{"OK"} & \text{if } V_{u\_StrengthI} \le \phi_v \cdot V_n \\ \text{"Increase shear resistance"} & \text{otherwise} \end{cases}$$

$Check\_Shear\_3rd\_Int\_Panel\_Str\_I_n = \text{"OK"}$

$$PR\_Shear\_3rd\_Int\_Panel\_Str\_I_n := \frac{V_{u\_StrengthI}}{\phi_v \cdot V_n}$$

$PR\_Shear\_3rd\_Int\_Panel\_Str\_I_n = 69.8\,\%$

O.9 Summary

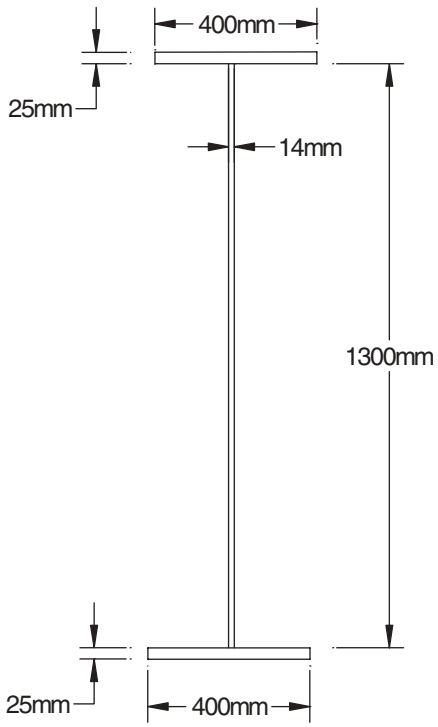

Positive Moment Regions

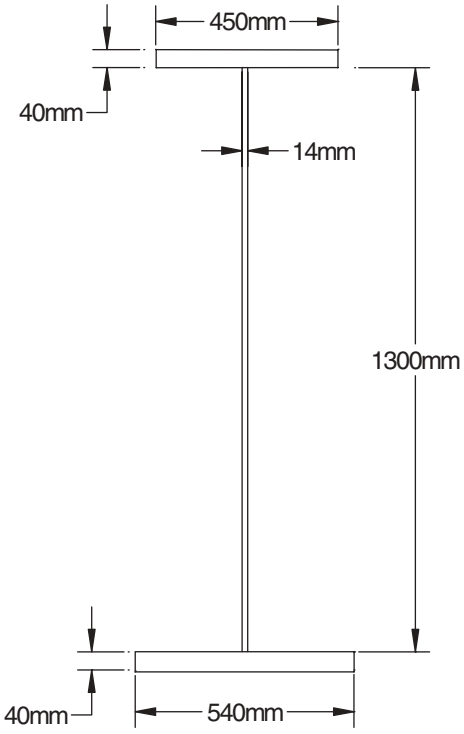

Negative Moment Regions

O.10 Shears and Moments Diagrams

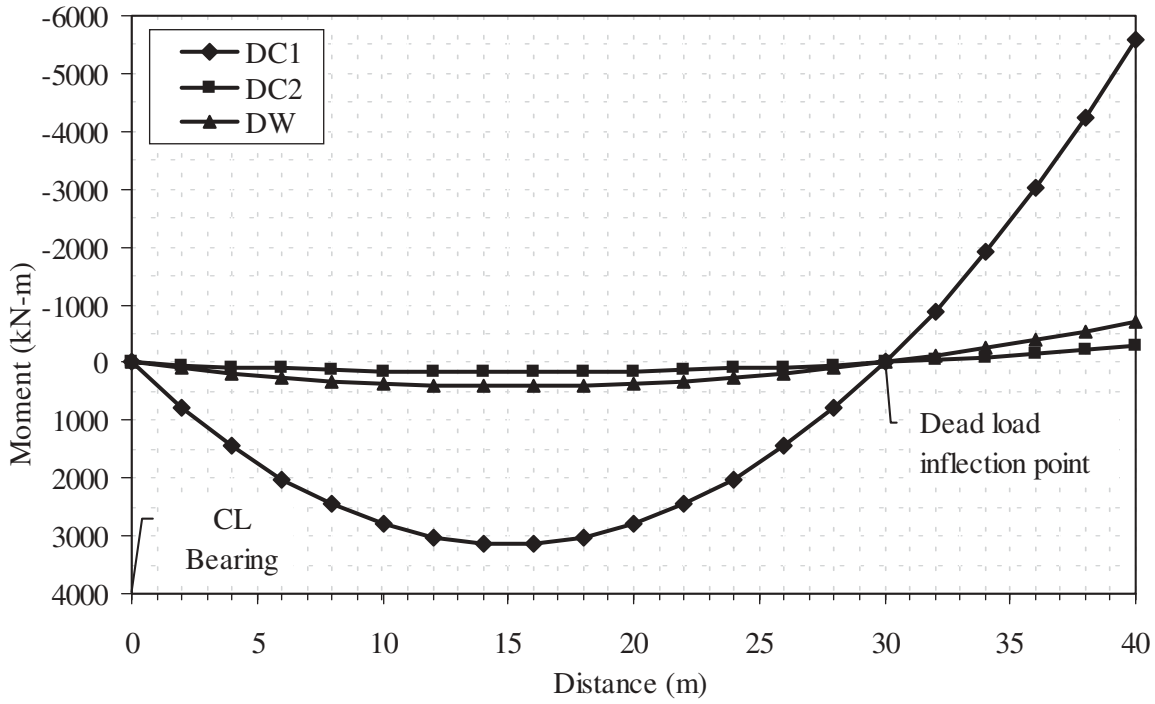

Figure O-5 Moments calculated from unfactored permanent dead loads.

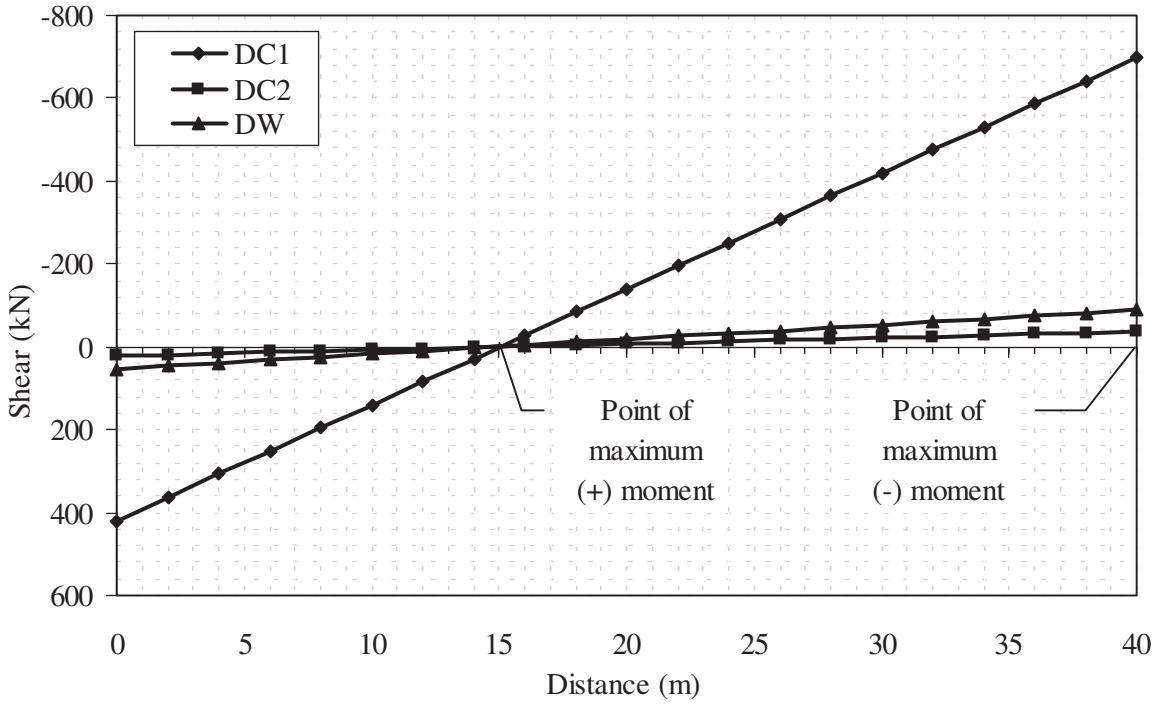

Figure O-6 Shears calculated from unfactored permanent dead loads.

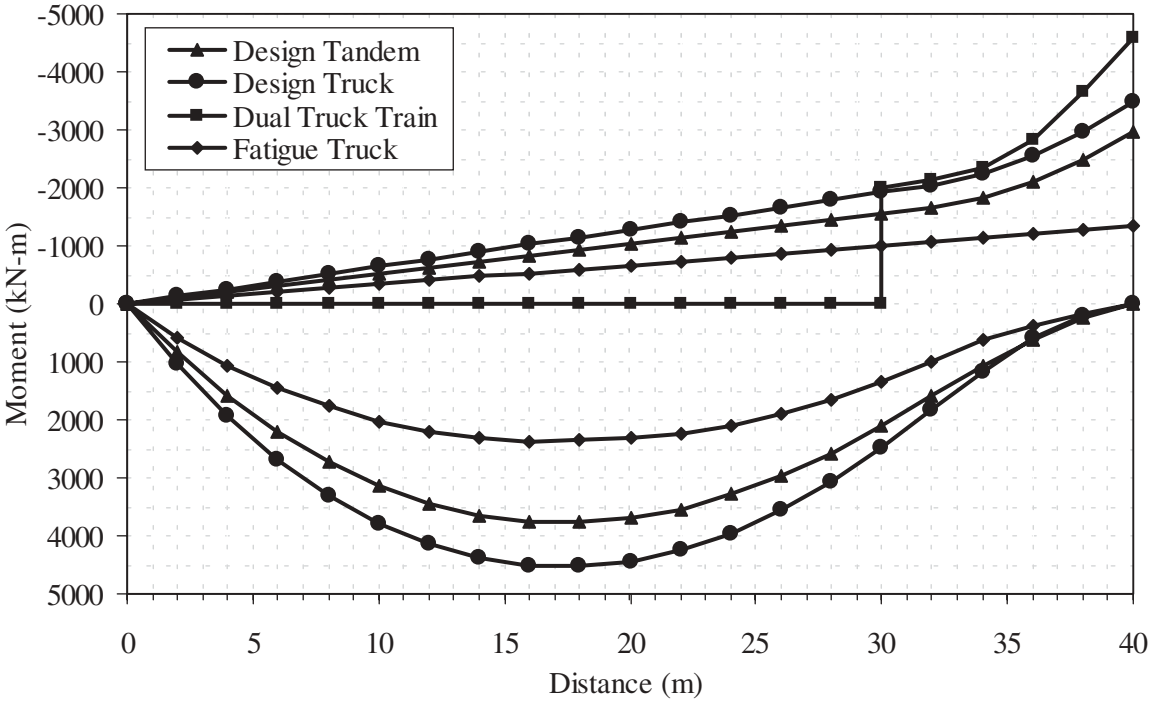

Figure O-7 Moments calculated from unfactored live loads excluding girder distribution factors.

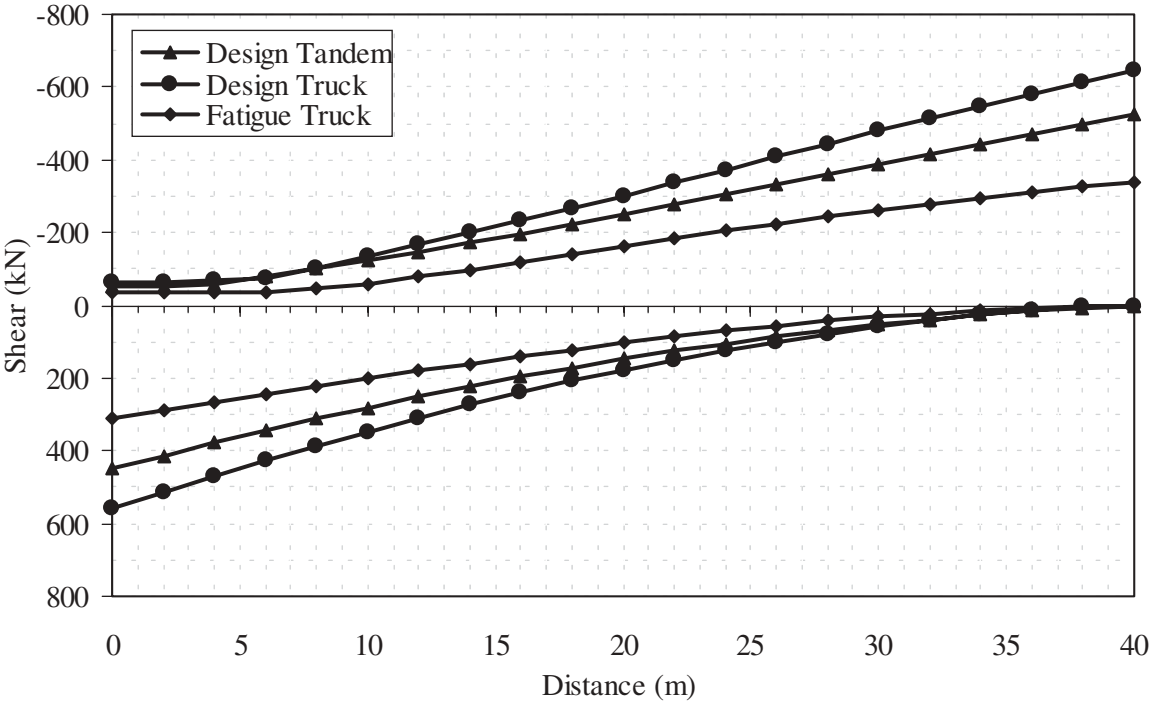

Figure O-8 Shears calculated from unfactored live loads excluding girder distribution factors.

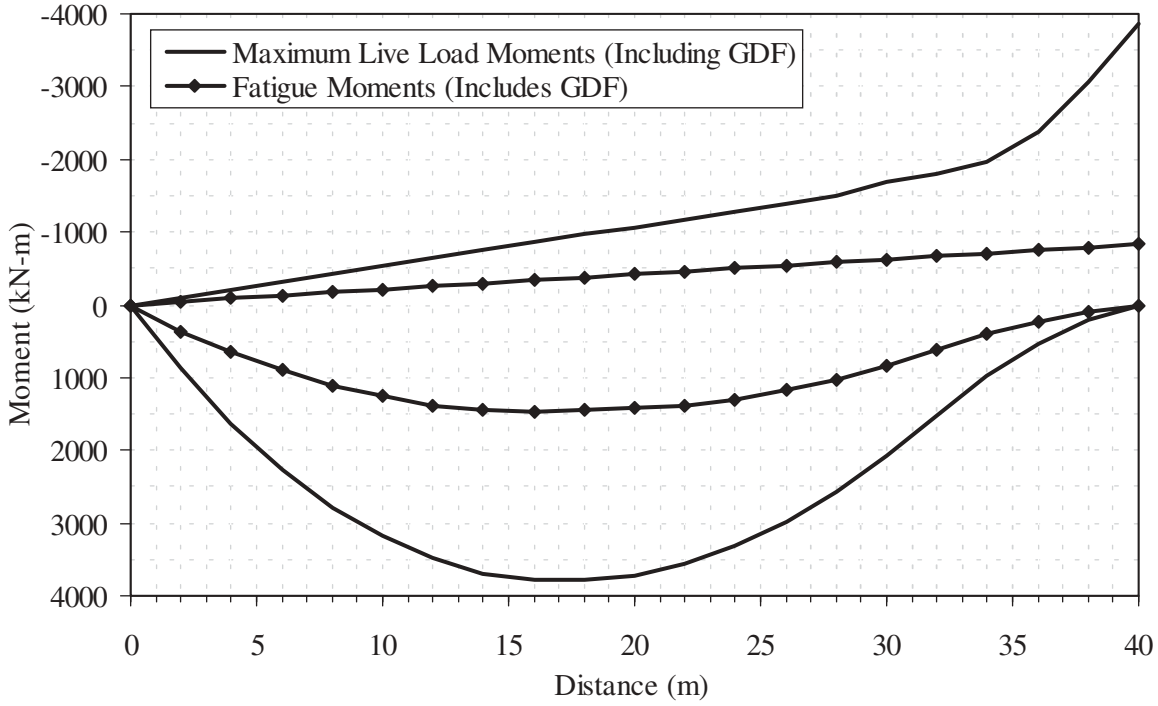

Figure O-9 Maximum moments calculated from unfactored live loads including girder distribution factors.

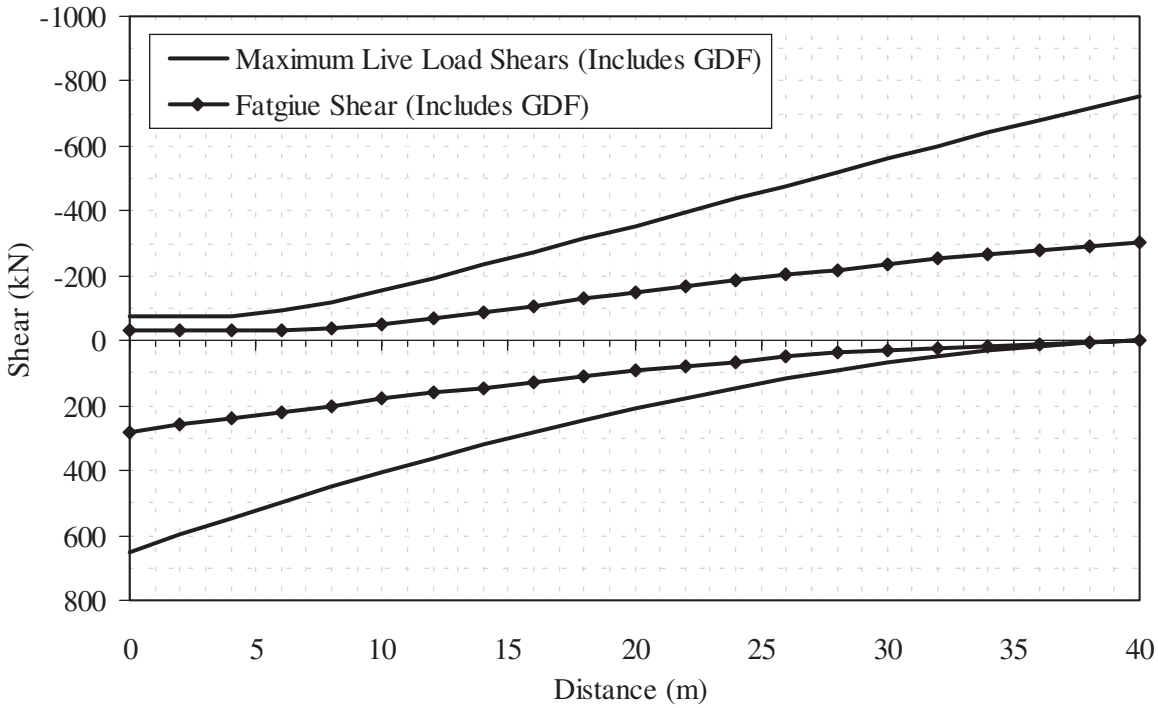

Figure O-10 Maximum shears calculated from unfactored live loads including girder distribution factors.

Abbreviations used without definitions in TRB publications:

AASHO	American Association of State Highway Officials
AASHTO	American Association of State Highway and Transportation Officials
APTA	American Public Transportation Association
ASCE	American Society of Civil Engineers
ASME	American Society of Mechanical Engineers
ASTM	American Society for Testing and Materials
ATA	American Trucking Associations
CTAA	Community Transportation Association of America
CTBSSP	Commercial Truck and Bus Safety Synthesis Program
DHS	Department of Homeland Security
FAA	Federal Aviation Administration
FHWA	Federal Highway Administration
FMCSA	Federal Motor Carrier Safety Administration
FRA	Federal Railroad Administration
FTA	Federal Transit Administration
IEEE	Institute of Electrical and Electronics Engineers
ITE	Institute of Transportation Engineers
NCHRP	National Cooperative Highway Research Program
NCTRP	National Cooperative Transit Research and Development Program
NHTSA	National Highway Traffic Safety Administration
NTSB	National Transportation Safety Board
SAE	Society of Automotive Engineers
TCRP	Transit Cooperative Research Program
TRB	Transportation Research Board
TSA	Transportation Security Administration
U.S.DOT	United States Department of Transportation